

**Picornavirus entry: membrane permeability  
induced by capsid protein VP4**

Anusha Panjwani

Submitted in accordance with the requirements for the degree of  
Doctor of Philosophy

The University of Leeds

School of Molecular and Cellular Biology

September, 2013

The candidate confirms that the work submitted is her own and that appropriate credit has been given where reference has been made to the work of others.

This copy has been supplied on the understanding that it is copyright material and that no quotation from the thesis may be published without proper acknowledgement.

The right of Anusha Panjwani to be identified as Author of this work has been asserted by her in accordance with the Copyright, Designs and Patents Act 1988.

© 2013 The University of Leeds and Anusha Panjwani

## **Acknowledgements**

First and foremost I'd like to thank my supervisor Toby Tuthill for all his support, advice, encouragement and patience throughout the course of my PhD. Thank you for being there to answer my never-ending questions, being my sounding board for ideas, for your confidence in me and always seeing the positive side to things!

I would like to thank my University of Leeds supervisor, Nic Stonehouse for her encouragement and support through the course of my PhD. Terry Jackson for his input and pertinent advice through my PhD will be remembered.

Professor Dave Rowlands for great project and career advice, meals and walks, that made the journey that much more interesting.

Thanks to all members of the Picornavirus structure group and everyone at Pirbright, in particular Joseph, Kyle, Lisa, Lidia, Beatrice for giving me so many fond memories and helping me maintain my sanity especially towards the end of my PhD!

Thank you to Josie for being an amazing friend and housemate.

A big thank you to Professor Jim Hogle and Doreen Hogle for making my visit to Harvard Medical School comfortable, memorable and productive! Thank you to Professor James Chou for giving me the opportunity to work in his lab and my friends and colleagues in Boston Mike, Bill, Mukesh, Sven, Marcello, Florian, Tanxing, Maria for all those useful discussions in the lab and at Starbucks.

My loving thoughts for my parents and my brother for their understanding, encouragement, unconditional warmth and love. Thank you!

## **Abstract**

Non-enveloped viruses such as picornaviruses must penetrate the host cell membrane without the advantage of membrane fusion. This process is thought to involve membrane permeabilisation but the mechanism remains poorly understood.

During picornavirus cell entry, capsid protein VP4 is released from the virus and is implicated in the delivery of the viral genome into the cytoplasm. The studies described in this thesis were undertaken to improve our understanding of the role of VP4 in cell entry. The approach to investigate this used recombinant VP4 and liposome model membranes.

Recombinant VP4 was shown to induce membrane permeability with characteristics similar to that induced by both model pore-forming peptides and infectious virus particles and was influenced by pH, membrane composition and VP4 myristoylation. Chemical crosslinking and dextran release studies demonstrated that VP4 formed a multimeric size-selective membrane pore. The VP4 pore complex was visualised by transmission electron microscopy, which confirmed the multimeric nature of the pore and showed a lumen diameter in agreement with the dextran release studies and consistent with the dimensions required for the passage of viral RNA.

The structure of VP4 reconstituted in membrane-mimetic detergent micelles was analysed by circular dichroism spectroscopy and nuclear magnetic resonance (NMR) spectroscopy. This showed VP4 contained predominantly alpha helical content and the acquired 2D NMR spectrum was typical of a membrane protein.

The membrane permeability induced by synthetic peptides showed that VP4 activity maps to the N-terminal half of VP4. In addition, VP4 activity was enhanced by the presence of a peptide corresponding to the N-terminus of VP1, an additional capsid protein also implicated in cell entry.

These findings present a molecular mechanism for the involvement of VP4 in cell entry and provide a model system which will facilitate exploration of VP4 as a novel antiviral target for the picornavirus family.

# Table of contents

<b>Acknowledgements</b> .....	<b>3</b>
<b>Abstract</b> .....	<b>4</b>
<b>Table of contents</b> .....	<b>5</b>
<b>Table of figures</b> .....	<b>10</b>
<b>Table of tables</b> .....	<b>13</b>
<b>Abbreviations</b> .....	<b>14</b>
<b>Chapter 1 Introduction</b> .....	<b>21</b>
1.1    Introduction .....	22
1.1.1    Clinical features and significance of human rhinovirus, poliovirus and foot-and-mouth disease virus .....	22
1.1.2    Classification of Picornaviruses.....	24
1.2    Genome organisation.....	26
1.3    Polyprotein translation and processing .....	28
1.3.1    Viral proteins.....	29
1.4    Genome replication .....	34
1.5    Picornavirus assembly and structure.....	38
1.5.1    Virus Assembly.....	38
1.5.2    Virus structure.....	41
1.6    Virus cell entry .....	45
1.6.1    Membrane penetration by enveloped viruses .....	46
1.6.2    Membrane penetration by non-enveloped viruses.....	49
1.6.3    Non-enveloped virus capsid proteins facilitating membrane penetration.....	50
1.6.4    Picornavirus entry .....	53
1.7    Aims.....	65
<b>Chapter 2 Materials and Methods</b> .....	<b>66</b>
2.1    General Materials .....	67
2.1.1    Bacterial strains.....	67
2.1.2    Cell lines .....	67

2.1.3	Expression vectors .....	67
2.1.4	Antibodies .....	67
2.1.5	Detergents.....	67
2.1.6	Lipids .....	68
2.2	Manipulation of recombinant DNA.....	68
2.2.1	DNA oligonucleotide primers.....	68
2.2.2	Polymerase chain reaction (PCR).....	68
2.2.3	DNA sequencing.....	69
2.2.4	Restriction digestion of DNA.....	69
2.2.5	Agarose gel electrophoresis.....	70
2.2.6	Gel extraction of DNA .....	70
2.2.7	DNA ligations.....	70
2.2.8	Transformation of chemically competent bacteria .....	70
2.2.9	Bacterial cultures .....	71
2.2.10	Purification of bacterial DNA .....	71
2.2.11	Quantification of DNA.....	72
2.2.12	Bacterial glycerol stocks.....	72
2.3	Protein biochemistry.....	72
2.3.1	Sodium dodecyl sulphate -polyacrylamide gel electrophoresis (SDS-PAGE).....	72
2.3.2	Native polyacrylamide gel electrophoresis (PAGE).....	73
2.3.3	SDS-PAGE fixatives .....	73
2.3.4	Staining methods .....	73
2.3.5	Western blot .....	74
2.3.6	Densitometry analysis of western blots.....	74
2.3.7	Autoradiography .....	75
2.3.8	Chemical crosslinking.....	75
2.3.9	Acetone precipitation .....	75
2.3.10	Measurement of total protein concentration .....	75
2.4	Expression of GST-tagged VP4 in inclusion bodies .....	76

2.5	Isolation of GST-tagged VP4 inclusion bodies.....	76
2.6	Expression of GST-tagged VP4 as soluble protein .....	77
2.7	Purification of GST-tagged soluble protein.....	77
2.8	Expression and purification of His-tagged 3C protease.....	78
2.9	Preparative electrophoresis for isolation of VP4.....	78
2.10	Preparative SDS-PAGE using the prep cell.....	79
2.11	Expression of VP4 and VP4His .....	79
2.12	Purification of VP4His under non-denaturing conditions.....	79
2.13	Purification of VP4His under denaturing conditions .....	80
2.14	Purification of VP4PreGST under denaturing conditions.....	81
2.15	Expression and purification of His-trpLE-VP4 .....	81
2.16	Reconstitution of VP4 and GST-tagged VP4 in detergent micelles.....	82
2.17	Nuclear magnetic resonance (NMR).....	82
2.18	Circular dichroism spectroscopy.....	83
2.19	Transmission electron microscopy .....	83
2.20	Purification of HRV16.....	83
2.21	<sup>35</sup> S-HRV16 labelling and purification.....	84
2.22	Preparation of liposomes.....	84
2.23	Membrane permeability assay .....	85
2.24	FD release assay.....	86
2.25	Liposome floatation assay .....	86
<b>Chapter 3 Expression and purification of recombinant VP4.....</b>		<b>88</b>
3.1	Introduction .....	89
3.2	Purification of recombinant VP4His from GST-tagged VP4 .....	94
3.2.1	Cloning of GST-tagged VP4 from HRV, PV and FMDV.....	94
3.2.2	Expression of GST-tagged VP4 .....	98
3.2.3	Isolation of VP4His from GST-tagged VP4 fusion protein inclusion bodies.....	103
3.2.4	Isolation of VP4His from soluble GST-tagged VP4 .....	108
3.3	Purification of recombinant VP4 and VP4His .....	112

3.3.1	Construction of expression plasmids for VP4 and VP4His .....	112
3.3.2	Expression of VP4 and VP4His .....	115
3.3.3	Purification of HRV VP4His.....	115
3.3.4	Quantification of recombinant VP4His .....	118
3.4	Purification of recombinant VP4 from His-trpLE-VP4.....	122
3.4.1	Cloning of His-trpLE HRV VP4 constructs.....	122
3.5	Purification of native VP4 from HRV16.....	128
3.6	Discussion.....	132
<b>Chapter 4</b>	<b>Characterisation of VP4-induced membrane permeability .....</b>	<b>137</b>
4.1	Introduction .....	138
4.2	Characterisation of VP4-induced membrane permeability .....	143
4.2.1	Recombinant VP4 induces membrane permeability in liposomes .....	143
4.2.2	VP4 mediates concentration-dependent release of carboxyfluorescein from liposomes .....	147
4.2.3	Induction of membrane permeability by VP4 is enhanced by myristoylation and acidic pH conditions .....	148
4.2.4	Membrane permeability induced by VP4 is influenced by membrane composition .....	154
4.2.5	VP4His-induced membrane permeability is not temperature dependent .....	159
4.3	Discussion and future work .....	160
<b>Chapter 5</b>	<b>VP4 forms a size-selective multimeric pore.....</b>	<b>168</b>
5.1	Introduction .....	169
5.2	VP4 forms a pentameric or hexameric multimer .....	170
5.3	VP4 forms a size-selective pore .....	176
5.4	Visualising the VP4-membrane pore complex.....	178
5.5	Discussion and Future Work .....	187
<b>Chapter 6</b>	<b>Structural analysis of VP4: Bioinformatics predictions and characterisation using biophysical techniques .....</b>	<b>192</b>
6.1	Introduction .....	193
6.2	Prediction of VP4 structure and topology .....	197



6.3	Circular dichroism spectroscopy to investigate VP4 secondary structure .....	203
6.4	NMR to investigate VP4 membrane pore complex structure.....	205
6.5	Discussion and future work .....	208
<b>Chapter 7 Towards mapping the function of VP4 and the role of VP1 by use of synthetic peptides .....</b>		<b>212</b>
7.1	Introduction .....	213
7.2	VP4 N-terminus induces more extensive membrane permeability than VP4 C-terminus or VP1 N-terminus peptides .....	214
7.3	VP1N-terminus and VP4 act synergistically to induce membrane permeability .....	218
7.4	Comparison of membrane permeability induced by recombinant VP4 and virus ...	221
7.5	Discussion and future Work.....	223
<b>Chapter 8 Concluding remarks and future perspectives .....</b>		<b>228</b>
8.1	Concluding remarks and future perspectives .....	229
<b>Chapter 9 References.....</b>		<b>232</b>

## Table of figures

Figure 1.1 Phylogentic tree of the picornavirus family.....	25
Figure 1.2 Picornavirus genome organisation and processing pattern. ....	27
Figure 1.3 Cap-independent translation of poliovirus RNA. ....	29
Figure 1.4 Switch from translation to replication. ....	37
Figure 1.5 Structural organisation of the picornavirus capsid. ....	39
Figure 1.6 Picornavirus capsid and pentamer showing the location of capsid proteins. ....	41
Figure 1.7 Binding of the pocket factor into the pocket located at the base of the canyon.....	42
Figure 1.8 Schematic representation of the structure and organisation shared by VP1, VP2 and VP3. ....	43
Figure 1.9 Comparison of picornavirus capsid structures. ....	44
Figure 1.10 The stages of enveloped virus membrane fusion. ....	46
Figure 1.11 Changes in the structure of the HA trimer from neutral pH to acidic pH.....	47
Figure 1.12 Classes of fusion peptides.....	49
Figure 1.13 Schematic representation of receptors used by members of the picornavirus family. ....	55
Figure 1.14 Domain 1 of the receptor binds in the canyon surrounding the fivefold axis. ....	56
Figure 1.15 Models for picornavirus membrane permeabilisation. ....	58
Figure 1.16 The ridge in PV “A” particles comprised of VP1 N-terminus. ....	59
Figure 1.17 Openings at the twofold axis with dimensions consistent with that required for the release of viral RNA.....	62
Figure 1.18 Viral RNA exit site identified at the twofold axis. ....	63
Figure 2.1 Membrane permeability assay. ....	86
Figure 3.1 Schematic of expression constructs used for the generation of recombinant VP4. .	92
Figure 3.2 Schematic of PCR strategy used to generate plasmids encoding GST-tagged VP4. ..	96
Figure 3.3 Restriction digestion products of PCR amplified PV VP4PreGST. ....	97
Figure 3.4 Identification of positive clones for pETPVVP4PreGST.....	98
Figure 3.5 Induction of expression of HRV VP4PreGST. ....	99
Figure 3.6 Comparison of expression levels for GST-tagged VP4 in E.coli pLysS with E.coli rosetta cells.....	101
Figure 3.7 Expression and solubility of optFMDV VP4PreGST.....	102
Figure 3.8 Schematic of purification of VP4His from GST-tagged HRV VP4.....	104
Figure 3.9 His-3C protease elution fractions from nickel affinity chromatography. ....	105
Figure 3.10 Cleavage of GST-tagged HRV VP4 inclusion bodies with 3C or thrombin proteases .....	106
Figure 3.11 Expression and solubility of PV VP4PreGST.....	108

Figure 3.12 Purification of PV VP4PreGST by glutathione affinity chromatography.....	110
Figure 3.13 Release of VP4His from PV VP4PreGST by cleavage with 3C protease. ....	111
Figure 3.14 Schematic of PCR strategy used for the generation of plasmids encoding VP4 and VP4His. ....	113
Figure 3.15 PCR amplified VP4 and VP4His digested with <i>NcoI</i> and <i>XhoI</i> . ....	114
Figure 3.16 Identification of positive pETHRV VP4 and pETHRV VP4His clones by colony screen PCR .....	114
Figure 3.17 Purification of VP4His and $\Delta$ VP4His by nickel affinity chromatography. ....	117
Figure 3.18 Purified VP4His visualised by silver staining. ....	118
Figure 3.19 Quantifying VP4His by comparison with native VP4 from virus (HRV16). ....	120
Figure 3.20 Effect of DMSO on the migration of aprotinin. ....	121
Figure 3.21 PCR amplification products used for the generation of HRV VP4 to be ligated into His-trpLE pMM-LR6 vector.....	123
Figure 3.22 Separation of His-trpLE-VP4 cleavage reaction products by RP-HPLC. ....	125
Figure 3.23 Schematic of purification of VP4 from His-trpLE-VP4. ....	126
Figure 3.24 Molecular weight and purity of purified HRV VP4. ....	127
Figure 3.25 Purification of HRV16.....	129
Figure 3.26 Scintillation counts of fractions obtained from sucrose density gradients containing virus or pre-heated virus particles.....	131
Figure 3.27 Detection of $^{35}\text{S}$ VP4 by autoradiography.....	132
Figure 3.28 Alignment of human rhinovirus, poliovirus and foot-and-mouth disease virus VP4 .....	133
Figure 4.1 HRV VP4His-mediated membrane permeability.....	144
Figure 4.2 PV VP4His-mediated membrane permeability. ....	145
Figure 4.3 Association of VP4His with liposome membranes. ....	146
Figure 4.4 VP4His-induced concentration-dependent CF release from liposomes.....	147
Figure 4.5 Membrane permeability induced by myristoylated and unmyristoylated VP4. ....	148
Figure 4.6 CF fluorescence before and after neutralisation of pH. ....	150
Figure 4.7 Effect of pH and Triton X-100 on CF fluorescence. ....	151
Figure 4.8 Effect of pH and myristoylation on VP4-induced membrane permeability .....	153
Figure 4.9 Effect of cholesterol on VP4His-induced membrane permeability. ....	154
Figure 4.10 Membrane composition of liposomes.....	155
Figure 4.11 VP4His-induced membrane permeability in liposomes mimicking composition of early or late endosomes. ....	156
Figure 4.12 Effect of membrane composition on VP4-induced membrane permeability. ....	157

Figure 4.13 Effect of sphingomyelin and cholesterol in early endosome membrane composition on VP4-induced membrane permeability.....	158
Figure 4.14 Effect of temperature on HRV and VP4His-induced membrane permeability.....	160
Figure 5.1 VP4His forms higher order structures in a favourable environment. ....	172
Figure 5.2 Multimerisation of PV VP4His in the presence or absence of liposomes.....	173
Figure 5.3 Multimerisation of VP4His in the presence or absence of liposomes. ....	175
Figure 5.4 VP4His forms size-selective membrane pores.....	177
Figure 5.5 Reconstitution of VP4 in detergent micelles. ....	182
Figure 5.6 Reconstitution of VP4 in DPC micelles.....	183
Figure 5.7 Reconstitution of VP4ThGST in DPC detergent micelles.....	183
Figure 5.8 Sample optimisation for the visualisation of VP4ThGST oligomeric structures by TEM.....	185
Figure 5.9 Visualisation of VP4ThGST oligomeric structures by TEM.....	186
Figure 6.1 Far UV CD spectra of soluble and membrane proteins. ....	195
Figure 6.2 Helical wheel projection for viral membrane proteins.....	198
Figure 6.3 Bioinformatics predictions for VP4 and p7. ....	200
Figure 6.4 Prediction of VP4 amphipathic helical and $\beta$ -sheet content. ....	201
Figure 6.5 Location of TM domain in VP4.....	202
Figure 6.6 Far UV CD analysis of VP4 reconstituted in detergent micelles. ....	204
Figure 6.7 Overlay of 2D HSQC spectra of $^{15}\text{N}$ -VP4 reconstituted in LMPG or SDS micelles...	208
Figure 7.1 Membrane permeability induced by VP4 and VP1 peptides.....	215
Figure 7.2 Membrane permeability induced by dilution series of VP4 and VP1 peptides.....	216
Figure 7.3 Comparison of membrane permeability induced by VP4 and VP1 peptides, VP4His and $\Delta\text{VP4His}$ .....	217
Figure 7.4 Combined effect of VP4 and VP1 peptides on the induction of membrane permeability.....	219
Figure 7.5 Combined effect of VP4His and VP1 N-terminus peptide on the induction of membrane permeability.....	220
Figure 7.6 HRV and VP4His induced membrane permeability. ....	222

## Table of tables

Table 3.1 VP4 constructs designed for expression of recombinant HRV, PV and FMDV VP4; and the purifications strategies used to purify VP4.....	93
Table 3.2 Table of primers used for the generation of recombinant VP4 constructs for HRV, PV and FMDV .....	95
Table 4.1 Membrane lipids and their structures. ....	142
Table 5.1 Range of detergents used for the optimisation of conditions for the reconstitution of VP4 .....	180

## Abbreviations

$\mu\text{g}/\mu\text{l}$	microgram(s) per microliter
$\mu\text{g}/\text{ml}$	microgram(s) per millilitre
$\mu\text{l}$	microliter(s)
$\mu\text{M}$	micromolar
1D	One dimensional
2D	Two dimensional
A280	absorbance at 280 nm
Å	angstrom(s)
A260	absorbance at 260 nm
ATCC	American type culture collection
BCA	bicinchoninic acid
BEV	bovine enterovirus
BMP	bis(monoacylglycero)phosphate
bp	base pair(s)
BSA	bovine serum albumin
CAR	coxsackie-adenovirus receptor
CD	circular dichroism
CF	carboxyfluorescein
CHAPSO	3-[(3-cholamidopropyl)dimethylammonio]-2-hydroxy-1-propanesulfonate
Chol	cholesterol
CNBr	cyanogen bromide
CPE	cytopathic effect
cpm	counts per minute

cre	cis-active RNA element
cVDPV	circulating vaccine derived polioviruses
D <sub>2</sub> O	distilled water
DAF	decay-accelerating factor
DDM	n-Dodecyl β-D-Maltopyranoside
DFDNB	1,5-difluoro-2,4-dinitrobenzene
DHPC (hepta)	1,2-diheptanoyl- <i>sn</i> -glycero-3-phosphocholine
DHPC (hexa)	1,2-dihexanoyl- <i>sn</i> -glycero-3-phosphocholine
DMA	dimethyl adipimidate
DMPC	1,2-dimyristoyl(d54)- <i>sn</i> -glycero-3-phosphocholine
DMSO	Dimethyl sulfoxide
DNA	deoxyribonucleic acid
dNTP	deoxyribonucleotide(s)
DPC	n-dodecylphosphocholine
DSP	dithiobis (succinimidylpropionate)
DTSSP	dithiobis (sulfosuccinimidylpropionate)
DTT	dithiothreitol
<i>E.coli</i>	<i>Escherichia coli</i>
ECL	electrochemiluminescence
EDTA	Ethylenediaminetetraacetic acid
EMCV	encephalomyocarditis virus
ER	endoplasmic reticulum
ERAV	equine rhinitis A virus
FAST	fusion-associated small transmembrane

FD	Fluorescein isothiocyanate-dextran
FHV	flock house virus
FMD	foot-and-mouth disease
FMDV	foot-and-mouth disease virus
FOS	phosphocholine
g	gram(s)
GA	glutathione agarose
GnHCl	guanidine hydrochloride
gp	glycoprotein
GPI	glycosylphosphatidylinositol
GST	glutathione-S-transferase
HA	haemagglutinin
HAdV	human adenovirus
HAVcr	hepatitis A virus cellular receptor
HCV	hepatitis C virus
HeLa	Henrietta Lacks
HEPES	4-(2-hydroxyethyl)-1-piperazineethanesulfonic acid
His	histidine
HIV	human immunodeficiency virus
HPV	human papilloma virus
hrs	hours
HRV	human rhinovirus
HSG	heparan sulphate glycan
HSQC	heteronuclear single quantum coherence



IB	inclusion bodies
ICAM	intercellular adhesion molecule
Ig	Immunoglobulin
IMAC	immobilised metal ion affinity chromatography
IPTG	Isopropyl $\beta$ -D-1-thiogalactopyranoside
IRES	internal ribosome entry site
Kb	kilobasepairs
KCNE1	Potassium voltage-gated channel subfamily E member 1
kDa	kilodaltons
KOD	kodakaraensis
L	Litre(s)
LAPAO	3-Laurylamido-N,N'-Dimethylpropyl Amine Oxide
LB	luria bertani
LDAO	n-Dodecyl-N,N-Dimethylamine-N-Oxide
LDL	low density lipoprotein
LMPG	14:0 Lyso PG 1-myristoyl-2-hydroxy-sn-glycero-3phospho-(1'-rac-glycerol)
M	molar
MALDI	matrix-assisted laser desorption/ionisation
Mb	myoglobin
mCi	millicurie
MEMSAT	membrane protein structure and topology
MHz	megahertz
min	minute(s)
ml	millilitre(s)

mM	millimolar
MOI	multiplicity of infection
mRNA	messenger RNA
MscL	mechanosensitive channel
ng	nanogram(s)
NHS	N-hydroxysuccinimide
nm	nanometre(s)
NMR	nuclear magnetic resonance
NMT	N-myristoyltransferase
NS	non-structural
o/n	overnight
OD	optical density
OG	octyl $\beta$ -D-glucopyranoside
ORF	open reading frame
PA	L- $\alpha$ -Phosphatidic acid
PABP	poly (A) binding protein
PAGE	polyacrylamide gel electrophoresis
PBS	phosphate buffered saline
PC	L- $\alpha$ -Phosphatidylcholine
PCBP	poly(rC) binding protein
PCR	polymerase chain reaction
PE	L- $\alpha$ -phosphatidylethanolamine
PI	L- $\alpha$ -phosphatidylinositol
POPC	1-Palmitoyl-2-oleoyl- <i>sn</i> -glycero-3-phosphocholine

POPG	1-palmitoyl-2-oleoyl- <i>sn</i> -glycero-3-phosphoglycerol
Pre	3C protease
PTB	polypyrimidine tract-binding protein
PV	poliovirus
PVDF	polyvinyl difluoride
PVR	poliovirus receptor
RDRP	RNA dependent RNA polymerase
RGD	arginine-glycine-aspartic acid
Rhod PE groups	L- $\alpha$ -Phosphatidylethanolamine with lissamine rhodamine B labelled head groups
RNA	ribonucleic acid
RP-HPLC	reverse phase-high pressure liquid chromatography
rpm	revolutions per minute
S	sedimentation coefficient
s/n	supernatant
SCR	short consensus repeat
SDS	sodium dodecyl sulphate
SDS-PAGE	Sodium dodecyl sulphate polyacrylamide gel electrophoresis
sec	second(s)
SM	sphingomyelin
SOC	super Optimal broth with catabolite repression
SV40	simian virus 40
SVM	support vector machine
TAE	Tris-acetate-EDTA
TEM	transmission electron microscopy

Th	thrombin protease
TM	transmembrane
tRNA	transfer ribonucleic acid
U	unit(s)
UTR	untranslated region
UV	ultraviolet
V	volt(s)
v/v	volume/volume
VAPP	vaccine associated paralytic poliomyelitis
VCAM	vascular cell adhesion molecule
VLP	virus like particle
VPg	viral protein genome linked
Vpr	viral protein R
vRNA	viral RNA
w/v	weight/volume
WIN	Winthrop
$\lambda_{em}$	emission wavelength
$\lambda_{ex}$	excitation wavelength

# **Chapter 1**

# **Introduction**

## 1.1 Introduction

The family *Picornaviridae* is composed of small, icosahedral, non-enveloped viruses with a single-stranded, positive sense RNA genome. Many members of the picornavirus family are significant pathogens of humans and livestock. These include foot-and-mouth disease virus, poliovirus, human rhinovirus, enterovirus 71 and hepatitis A virus. These viruses cause diverse diseases such as foot-and-mouth disease, poliomyelitis, the common cold, hand, foot and mouth disease and hepatitis, respectively.

The picornavirus life cycle can be divided into cell entry, translation, replication, assembly and release of virus from the cell. Cell entry involves virus binding to specific receptor(s), endocytosis, host-cell membrane penetration and delivery of the genome to the cytoplasm (the site of replication). Membrane penetration to deliver the viral genome across the membrane is a fundamental step of viral infection, the details of which remain unclear. Intracellular viral RNA replication occurs in the cytoplasm and is initiated by translation of the viral genome to produce the non-structural viral proteins involved in viral genome replication and the structural proteins required for assembly of progeny virus. The virus life cycle involves dynamic interactions with host cell proteins and membranes. A better understanding of these interactions would facilitate the development of improved disease control measures such as better diagnostics, vaccines and antivirals.

The three viruses of relevance to this thesis are human rhinovirus (HRV), poliovirus (PV) and foot-and-mouth disease virus (FMDV), and will be described in more detail in the following sections. In addition to the economic significance of these viruses, recent research has made them good candidates for understanding picornavirus cell entry.

### 1.1.1 Clinical features and significance of human rhinovirus, poliovirus and foot-and-mouth disease virus

#### Human Rhinovirus

Human rhinoviruses (HRV) are causative agents of the most common acute infections in man, the common cold. HRV infections are reported to be responsible for approximately 50% of respiratory tract infections in young adults (Makela *et al.*, 1998). Ninety per cent of children become infected with HRV by the time they are two years old (Blomqvist *et al.*, 2002). HRV infections are also associated with sinusitis, otitis media, chronic obstructive pulmonary disease and exacerbations of asthma (Dougherty and Fahy, 2009). HRV infections can be more

serious and occasionally fatal in certain patient groups such as the immunocompromised and the elderly (Wald *et al.*, 1995). The newly discovered species of HRV C has been reported to be more pathogenic and cause more severe asthmatic attacks compared to the other two existing species of HRV, HRV A and HRV B (Bizzantino *et al.*, 2011). HRV infections are associated with substantial medical complications, morbidity and economic cost. HRV has approximately 100 serotypes (Palmenberg *et al.*, 2009) which make them a difficult target for vaccine design. Antiviral compounds inhibiting viral replication (e.g. a pyridazinamine) and many capsid binding compounds (Winthrop compounds) have been developed but there are as yet no licensed effective antivirals for the common cold.

### **Poliovirus**

Poliovirus (PV) is the causative agent of poliomyelitis. Humans are the only known reservoir of PV which is highly contagious and children in endemic areas become infected by 1 year of age (Alexander *et al.*, 2004). Most PV infections are asymptomatic where viral replication is limited to the alimentary tract. However, when the virus enters the bloodstream and is carried to the central nervous system where it replicates in motor neurons, it causes paralytic poliomyelitis (Nathanson, 2008). Paralytic poliomyelitis is experienced in less than 1% of PV infections. Replication of the virus in the nervous system can result in the loss of muscle function (acute flaccid paralysis) in one or more limbs or reduce breathing capacity and causing difficulty in swallowing (bulbar polio). PV is a significant pathogen of the last century and the huge impact of PV infections on the developed world led to detailed studies of the virus. As a result, PV is biochemically and genetically well characterised and has been used as the model virus in picornavirus research.

PV is the subject of a global eradication programme (the global polio eradication initiative) which has resulted in the interruption of wild poliovirus transmission from most parts of the world. However, poliovirus transmission continues to be prevalent in some developing countries, mainly due to political and logistical reasons resulting in poor accessibility to vaccines.

A live attenuated oral polio vaccine (OPV) and an inactivated polio vaccine (IPV) are both used as part of the vaccination strategy to prevent wild PV transmission. OPV is a powerful public health tool for mass vaccination, however, it has been reported to be genetically unstable which results in accumulation of mutations causing vaccine-associated paralytic poliomyelitis (VAPP) and outbreaks can occur due to circulating vaccine derived polioviruses (cVDPV) (Kew *et al.*, 2005). The ongoing debate over the complete cessation of vaccination is due to the associated risks which may facilitate the re-emergence of PV (e.g. from persistently infected

individuals) in unvaccinated populations. Therefore, there is an urgent need for the development of antivirals which can be used to contain an outbreak, to treat the infected and protect the exposed population, or used to complement IPV administration. Further, efforts to develop a new vaccine which is not reliant on infectious virus, are underway.

### **Foot-and-mouth disease virus**

Foot-and-mouth disease virus (FMDV) infects animals of agricultural and economic importance including cattle, goats, sheep and pigs as well as 70 species of wild animals (Grubman and Baxt, 2004).

Despite being the first virus of vertebrates to be discovered and recognized as a significant disease threatening the cattle industry since the sixteenth century (Mahy, 2005), it continues to adversely affect the world's livestock production. There are seven distinct FMDV serotypes and no cross protection between serotypes. Although, the current conventional FMDV vaccines can prevent clinical disease, they do not provide long-term immunity, thus often requiring frequent revaccination for prophylactic control (Rodriguez and Gay, 2011). Foot-and-mouth disease (FMD) is controlled in disease-free countries by surveillance and strict controls on importation of susceptible animals and animal products. In endemic regions, control measures focus on vaccination, however, in endemic regions FMD is associated with high disease burden and loss of livelihood. The UK suffered an economic loss of over £6 billion from the 2001 FMD outbreak (Mateo et al, 2008), thereby illustrating the significant consequences and economic impact of FMD. International trade embargoes are the main threat to areas free of FMD, mainly the developed countries. Furthermore, FMDV has a significant impact on the developing world. The "stamping out" or slaughter policy followed in the developed world in response to an outbreak cannot be afforded by most developing countries. The significant loss of yield of meat and milk, in combination with the loss of revenue due to strict restrictions on export of animals and animal products to nations free of FMD, makes the control of FMDV of paramount importance (Balinda et al., 2009).

#### **1.1.2 Classification of Picornaviruses**

The picornavirus family consists of 37 species, grouped into 17 genera namely *Aphthovirus*, *Aquamavirus*, *Avihepatovirus*, *Cardiovirus*, *Cosavirus*, *Dicipivirus*, *Enterovirus*, *Erbovirus*, *Hepatovirus*, *Kobuvirus*, *Megrivirus*, *Parechovirus*, *Salivirus*, *Sapelovirus*, *Senecavirus*, *Teschovirus* and *Tremovirus* (Adams and Carstens, 2012; Adams et al., 2013) ([www.picornaviridae.com](http://www.picornaviridae.com)) (Figure 1.1). Further 9 genera have been suggested and will likely



be included into the family of picornaviruses in the near future ([www.picornaviridae.com](http://www.picornaviridae.com)). The classification is based on phylogenetic relationships and genome organisation. Previously used classification methods such as pH stability, receptor usage and host specificity proved to be unreliable factors to establish relationships between viruses to categorise into species or genera, due to the changes in the virus occurring as a result of virus adaptation to changing environments.

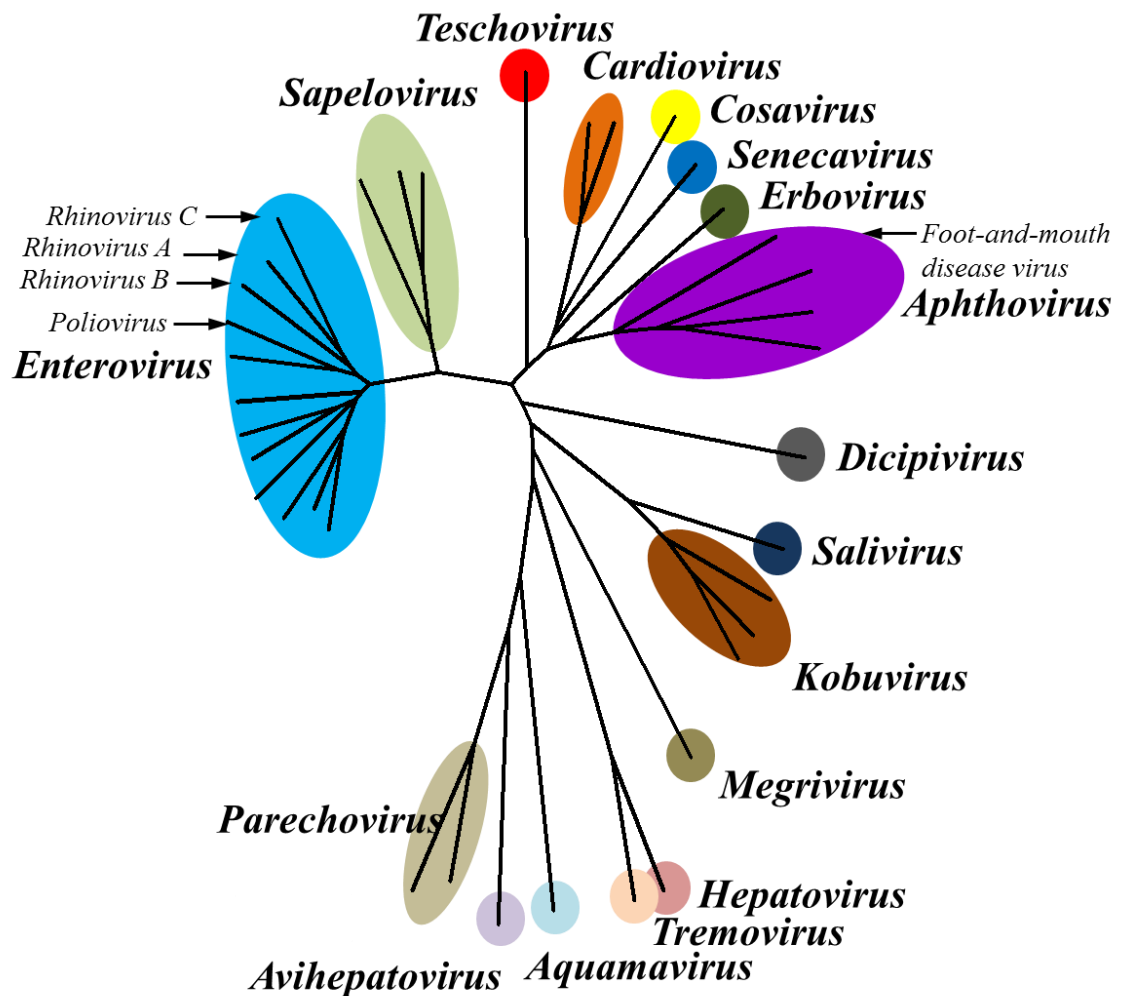


**Figure 1.1 Phylogenetic tree of the picornavirus family.**

The picornavirus family consists of 17 genera and 37 species. Black arrows indicate human rhinovirus and poliovirus belonging to the *Enterovirus* genus; foot-and-mouth disease virus belonging to the *Aphthovirus* genus. Figure kindly provided by Nick Knowles, The Pirbright Institute.

## 1.2 Genome organisation

The basic genome organisation of picornaviruses is conserved and shown in Figure 1.2. Although, genus and species specific differences exist, they are confined to limited regions of the genome. These differences are discussed below. Picornavirus genomes range in length from approximately 7,032 nucleotides of avian encephalomyelitis virus (Marvil *et al.*, 1999) to 8,828 nucleotides of equine rhinitis B virus (Ehrenfeld *et al.*, 2010). The genome normally consists of 3 major regions: the 5' untranslated region (UTR), a single open reading frame (ORF) and the 3'UTR. However, canine picodistovirus is a recently identified member of the *Picornaviridae* which has two ORFs (Adams *et al.*, 2013). The first IRES is located at the 5' UTR and the second IRES between VP1 and 2A. The first ORF contains the P1 region and the second contains the P2 and P3 regions (Woo *et al.*, 2012).

The proteins encoded by the genome take their names based on their sequential locations in the polyprotein (Figure 1.2). The ORF is flanked by UTR located upstream at the 5' and downstream at the 3' end of the genome. The 5' terminal sequence, invariably a UU sequence, is covalently linked to a small protein, viral protein genome-linked (VPg). In enteroviruses (e.g. PV) the viral RNA (vRNA) then folds into a clover leaf shaped secondary structure element while that of aphthoviruses (e.g. FMDV) folds to form the S-fragment which is a long stem loop structure (Bunch *et al.*, 1994; Newton *et al.*, 1985). The PV clover leaf binds multiple cellular and viral proteins, mediating circularisation of the genome necessary for negative strand synthesis and replication (Toyoda *et al.*, 2007). The function of the FMDV S-fragment is not established but it has been suggested to play a role in genome replication (as reviewed in Grubman and Baxt, 2004). A cis-active RNA element (CRE) has been identified in a number of picornaviruses and is present at varying locations such as in the 5' UTR in FMDV, the capsid encoding region (P1) in HRV14 and 2C encoding region in PV (Goodfellow *et al.*, 2003). The CRE is required for the uridylylation of VPg and is essential for the synthesis of plus strand RNA (Steil and Barton, 2009) (section 1.4).

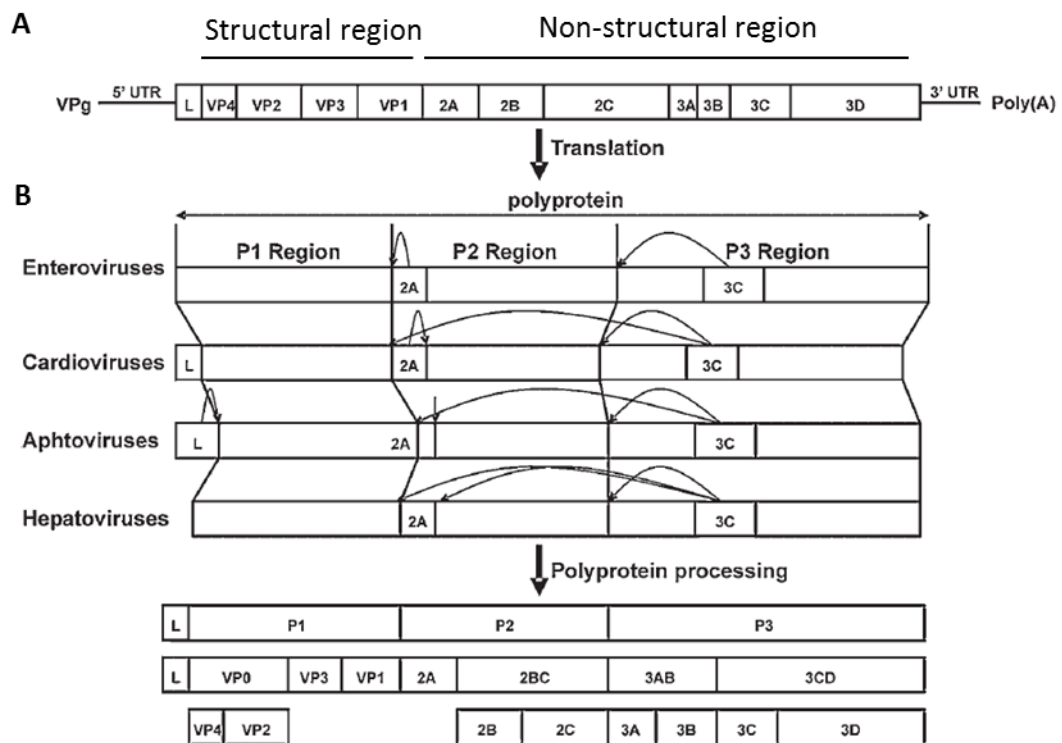


**Figure 1.2 Picornavirus genome organisation and processing pattern.**

**A.** The viral genome flanked by the 3' and 5' untranslated regions. The viral protein genome-linked protein at the 5' end and poly(A) tail at the 3' end. The regions encoding for viral proteins are indicated. **B.** Patterns of polyprotein processing followed in enteroviruses, cardioviruses, aphthoviruses and hepatoviruses. The sources of cleavage activity indicated by the curved arrows (2A and 3C/ 3CD proteases). Figure adapted from (De Palma *et al.*, 2008).

The 5' UTR also contains an internal ribosome entry site (IRES) which directs cap-independent translation of the viral polyprotein (section 1.3). Some picornaviruses such as aphthoviruses and cardioviruses have a Leader protein (L) encoded at the 5' of the P1 region. Other picornaviruses including the enteroviruses and hepatoviruses do not have the L protein. Most picornavirus ORFs have one AUG initiation codon but that of aphthoviruses (e.g. FMDV) contain two in-frame AUG initiation codons (Clarke *et al.*, 1985). This leads to the generation of two alternative forms of the Leader protein (L), Lab and Lb which have the same proteolytic activity (section 1.3.1.2). The P1 region encodes the structural proteins 1A, 1B, 1C and 1D (also known as VP4, VP2, VP3 and VP1). The middle region is P2 which contains the non-structural proteins 2A, 2B and 2C. The P3 region encodes the non-structural proteins 3A, 3B (VPg), 3C and 3D (sections 1.3 and 1.4). The 3' UTR is shorter than the 5' UTR and has extensively structured domains including stem-loop structures and a polyA tail. The polyA tail is involved in translation and replication for e.g. binding to the host cellular protein, poly(A) binding protein (PABP), provides interactions to coordinate activities of 5' UTR and 3' UTR during genome translation and replication (Herold and Andino, 2001; Zoll *et al.*, 2009). However, the 3' UTR of HRV and PV was not absolutely required for genome replication (Todd *et al.*, 1997).

### 1.3 Polyprotein translation and processing

Cellular mRNA translation requires recognition of a 5' cap structure by the eIF4F complex. The eIF4F complex consists of eIF4E which binds to the cap, eIF4A which is a helicase and eIF4G which acts as a scaffold protein and interacts with eIF3, eIF4A, eIF4E and coordinates their functions (Gingras *et al.*, 1999; Hellen and Sarnow, 2001). The 40S ribosomal subunit bound to eIF2 and the initiator methionine tRNA is referred to as the 43S complex. This complex associates with eIF3, creating a 48S pre-initiation complex which is recruited to the 5' end of mRNA. This complex and other initiation factors (eIF1, eIF1A, eIF5 and eIF5B) scans along the mRNA in the 5' to 3' direction until it reaches an appropriate start (AUG) codon which is used to initiate translation. When the AUG start codon is recognised, eIF1 is released and a conformational change in the 40S ribosomal subunit occurs which prevents further scanning along mRNA. Mediated by eIF5B, the 60S ribosomal subunit is recruited to the 40S ribosomal subunit, which results in the formation of the 80S ribosome which is competent to begin protein synthesis (Hellen and Sarnow, 2001; Thompson, 2012).

The next part of the viral life cycle, after cell entry when the vRNA is delivered to the cytoplasm, is translation of vRNA to produce a single polyprotein. In contrast to cap-dependent translation mediated by the mRNA 5' cap structure, picornaviruses utilise a cap-independent translation mechanism which involves the binding of ribosomes to the IRES (a complex RNA structure in the 5' UTR). Picornaviruses have evolved ways of interacting with the host cell translation machinery to shut-off cap-dependent translation of host mRNA by cleavage of eIF4G and subvert the host cell machinery to preferentially translate vRNA by a cap-independent mechanism. During infection with aphthoviruses such as FMDV, cleavage of eIF4G is carried out by the viral proteases, Leader and 3C, whereas in other picornaviruses such as poliovirus, human rhinovirus or coxsackievirus, cleavage of eIF4G is carried out by the viral proteases, 2A and 3C (Fitzgerald and Semler, 2011) and (section 1.3.1.2). By employing cap-independent translation pathway, ribosomes bind directly to the IRES and initiate viral RNA translation. Hence, viral RNA translation does not conform to the 5' 7-methyl guanosine cap recognition by eukaryotic initiation factor 4F (eIF4F) complex and ribosome scanning used for cellular mRNA translation (as reviewed in Jackson *et al.*, 1994).

Host cell proteins such as SRp20, poly(rC) binding protein 2 (PCBP2), polypyrimidine tract-binding protein (PTB) and La are involved in vRNA translation. Serine arginine protein 20 (SRp20) is a cellular splicing factor and has been shown to associate with PCBP2 bound to PV RNA, which together function to recruit ribosomes to the vRNA for translation. PTB has been shown to enhance the activity of picoranviral IRESs (Back *et al.*, 2002; Fitzgerald and Semler, 2011) During infection, La is cleaved and the C-terminal region is translocated from the nucleus

to the cytoplasm where it can bind to the 5' UTR and initiate translation. Therefore, the above mentioned host cell factors, as shown in Figure 1.3, enhance RNA translation of picornaviruses (Blyn *et al.*, 1997; Chase and Semler, 2012).

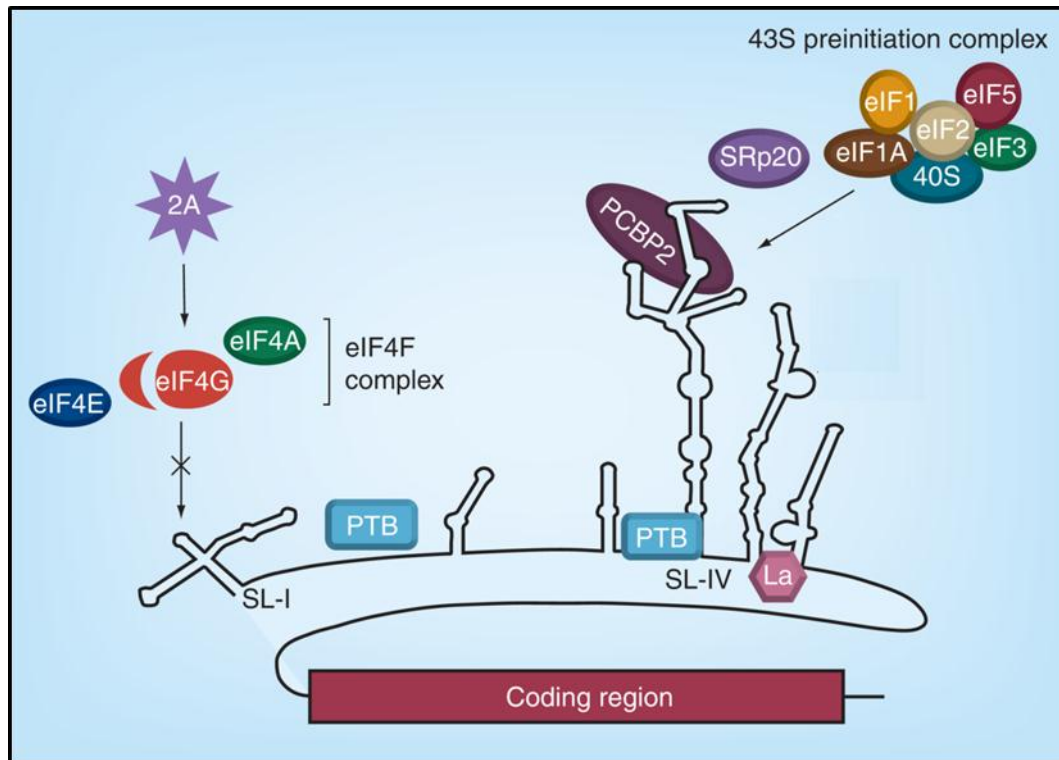


**Figure 1.3 Cap-independent translation of poliovirus RNA.**

The highly structured 5' untranslated region and the lack of a cap at the 5' end prevent cap binding and ribosome scanning. Cap-independent translation is mediated by the disruption of the eIF4F cap-binding complex by the cleavage of eIF4G by 2A protease, the recruitment of the 43S ribosomal subunit to the IRES and recruitment of host cellular proteins such as PTB and La. SL: stem loop, eIF: eukaryotic translation initiation factor, PTB: polypyrimidine tract-binding. Figure adapted from (Chase and Semler, 2012).

### 1.3.1 Viral proteins

The IRES directs translation of the ORF to produce a single polyprotein (section 1.3). The polyprotein is processed by viral proteases to form a number of processing intermediates and mature viral proteins. Processing involves cleavage of the P1 region to produce the capsid proteins; cleavage of P2 and P3 regions by 3CD<sup>pro</sup> (enteroviruses) or 3C<sup>pro</sup> (aphthoviruses) to form the individual non-structural proteins and processing intermediates (e.g. 2BC and 3CD) that are required for viral replication.

#### 1.3.1.1 Structural proteins

Processing of P1 is carried out by 3CD<sup>pro</sup> in enteroviruses (e.g. PV) or 3C<sup>pro</sup> in aphthoviruses (e.g. FMDV). This results in the formation of VP0, VP1 and VP3. VP0 is the precursor of VP2 and

VP4. Picornavirus VP4 has a molecular weight of 7-10 kDa and is present on the inner surface of the capsid. VP4 is myristoylated at the N-terminus, is important for virus infectivity and stability, and has been implicated in potential pore-formation during cell entry of picornaviruses (section 1.6.4.4). VP1, VP2 and VP3 (approximately 30 kDa) are components of the viral capsid that share a similar overall structure (section 1.5.2). VP1 contributes maximum to antigenicity and surface features of the virus. VP2 and VP3 are also present on the surface of the virus capsid. The picornavirus capsid is composed of 60 copies of each of the four structural proteins (section 1.5.2). The assembly and structure of the picornavirus capsid is described in more detail in sections 1.5.1 and 1.5.2.

### 1.3.1.2 Non-structural proteins

The non-structural proteins are encoded by the P2 and P3 regions of the genome (Figure 1.2) and are involved in intracellular virus replication. A number of processing intermediates are also produced which have distinct functions to the final fully processed proteins.

- 2A

The 2A protein of many picornaviruses (e.g. the enteroviruses) is a protease (2A<sup>pro</sup>). During enterovirus translation 2A cleaves at its own N-terminus thereby separating the capsid proteins (encoded by P1) from the non-structural proteins (encoded by P2 and P3). In some other viruses such as aphthoviruses and cardioviruses, 2A does not possess protease activity. Instead, P1 is released from P2/P3 by a different mechanism called ribosomal skipping, where the C terminus of 2A includes a unique amino acid sequence (DxExNPG/P motif) that prevents a peptide bond being formed between the C-terminal glycine of 2A and the N-terminal proline of 2B. This results in the generation of structural proteins as a P1-2A precursor (Donnelly *et al.*, 1997; Donnelly *et al.*, 2001). During capsid assembly, 3C<sup>pro</sup> cleaves 2A to separate it from P1. In hepatoviruses, 2A does not function as a protease (as reviewed in Ryan and Flint, 1997) and the cleavage of P1/2A and 2A/2B is performed by 3C<sup>pro</sup> (Cohen *et al.*, 2002).

PV 2A<sup>pro</sup> also mediates the inhibition of cap-dependent cellular mRNA translation by cleavage of eukaryotic initiation factor 4G (eIF4G) (Krausslich *et al.*, 1987). The other known function of enterovirus 2A is the enhancement of vRNA translation by cleaving the host cell protein p220 (protein of the cap-binding complex), thereby making the cap-binding complex non-functional and inhibiting cap-dependent translation (Hambidge and Sarnow, 1992) (section 1.3).

In enteroviruses, 2A<sup>pro</sup> has folds similar to chymotrypsin like proteases. The structures of 2A<sup>pro</sup> of HRV2 (Petersen *et al.*, 1999) and coxsackievirus B4 (CVB4) (Baxter *et al.*, 2006) have been determined.

- 2B

Picornaviruses replicate their genomes in association with cellular membranes (Gazina *et al.*, 2002; Hsu *et al.*, 2010). For most picornaviruses the precise origin of these membranes is unclear but viruses of the *Enterovirus* genus (e.g. PV and CVB3) are believed to utilise membranes from the early secretory pathway for replication (Hsu *et al.*, 2010; Rust *et al.*, 2001). The 2B proteins of all enteroviruses contain an N-terminal hydrophobic region predicted to form an amphipathic helix with characteristics consistent with those observed in membrane lytic peptides (Shai, 1999). Studies have shown the interaction of the CVB3 2B amphipathic helix with membranes (vanKuppeveld *et al.*, 1996). Coxsackievirus 2B has also been shown to localise to the endoplasmic reticulum and the golgi complex. The membrane binding region of 2B has been proposed to form pores in the golgi and endoplasmic reticulum (ER) membranes, leading to a reduction in Ca<sup>+2</sup> levels in the ER and golgi which may provide conditions required for viral RNA replication (Campanella *et al.*, 2004; Madan *et al.*, 2007; Martinez-Gil *et al.*, 2011; van Kuppeveld *et al.*, 2005).

The 2B protein of aphthoviruses, cardiociruses and hepatoviruses share <20% sequence similarity with enterovirus 2B and do not contain an amphipathic helix. Mechanisms used by 2B of viruses such as encephalomyocarditis virus (EMCV) and FMDV to reduce Ca<sup>+2</sup> levels in the ER are yet to be determined. 2B of hepatoviruses did not appear to have an effect on the Ca<sup>+2</sup> levels in the ER or golgi complex (de Jong *et al.*, 2008).

- 2C

Bioinformatics analysis of PV 2C predicted an amphipathic helical domain at its amino terminus, a nucleotide binding domain in the middle and zinc binding domain at its carboxy terminus (Rodriguez and Carrasco, 1993). Both termini of PV 2C showed RNA binding activity (Teterina *et al.*, 2006). PV 2C is tightly associated with replication complexes (the complex between viral and cellular proteins and membranes required for viral replication) and is therefore, thought to play a role in viral replication (Bienz *et al.*, 1990). PV 2C was also shown to interact with other components of the replication complex, 3A, 3AB (Yin *et al.*, 2007) and the clover leaf structure present at the 5' end of viral RNA (Banerjee and Dasgupta, 2001).

Picornavirus 2C is a multifunction protein. For example enterovirus 2C possesses ATPase and GTPase activities (Rodriguez and Carrasco, 1993), and PV 2C has also been implicated

to play a role in viral RNA encapsidation, though the specific domain responsible for this is yet to be defined (Vance *et al.*, 1997).

Expression of PV 2C or 2BC induces formation of membrane vesicle whereas similar proteins in FMDV have not been identified. In contrast FMDV 2B and 2C are involved in blocking the secretory pathway between ER and golgi (section 1.4).

- 3AB and 3A

The 3AB protein is the precursor for 3A and 3B proteins. PV 3AB has been shown to be important for the anchoring of replication complexes to cellular membranes by interacting with the 5' cloverleaf and enhancing the functions of 3CD and 3D<sup>pol</sup> (Hope *et al.*, 1997; Lama *et al.*, 1994; Paul *et al.*, 1994).

The 3A proteins of different picornaviruses such as Aichi virus, bovine kobuvirus, poliovirus, coxsackievirus B3, and human rhinovirus 14 reorganise cellular membranes associated with the golgi (Greninger *et al.*, 2012) and inhibit protein export from ER to golgi (Doedens *et al.*, 1997). FMDV 3A is significantly longer (153 amino acids) than PV 3A (87 amino acids) and does not block the secretory pathway between ER and golgi (Moffat *et al.*, 2005).

- 3B

The 3B protein or Viral protein genome-linked (VPg) is a small protein (21 to 23 amino acids), covalently linked to the 5' end of the viral genome (Ambros and Baltimore, 1978). Uridylylated VPg functions as a primer for viral RNA synthesis (Andino *et al.*, 1999) (described in section 1.4). The genome of aphthoviruses are unique, in that, they encode for three sequential copies of 3B (Forss and Schaller, 1982). The biological significance of three copies of VPg is not known. It is not clear if 3A or 3C (as 3AB and 3BC) is the donor of VPg for replication. Due to the abundance of 3AB in the infected cell, 3A was thought to be the source of VPg but recent evidence showed that 3BC and 3BCD are likely donors of VPg with 3C serving as a stimulatory factor for 3Dpol in the VPg uridylylation reaction (Pathak *et al.*, 2008).

- 3C

The 3C protein (3C<sup>pro</sup>) is a cysteine protease with chymotrypsin like folds. The structure of 3C is known for a few picornaviruses such as FMDV (Birtley *et al.*, 2005), PV (Mosimann *et al.*, 1997) and HRV14 (Matthews *et al.*, 1994). 3CD in PV and 3C in FMDV, cleaves the viral polyprotein at the 2C/3A junction to release the P3 region. In aphthoviruses, cardioviruses



and hepatoviruses, 3C also cleaves at the N-terminus of 2A to release P1 from 2A (Figure 1.2).

PV 3C cleavage of transcription factors prevents host cell transcription and degradation of PABP by 3C has been shown to inhibit cap-dependent cellular RNA translation (Joachims *et al.*, 1999). FMDV 3C carries out host cell protein cleavages of eIF4G and eIF4A which affects mRNA transcription and cap-dependent translation (Belsham *et al.*, 2000).

- 3CD

The 3CD protein is an intermediate cleavage product of the P3 region of the polyprotein. It is a precursor to 3C protease (3C<sup>pro</sup>) and viral RNA dependent RNA polymerase (3D<sup>pol</sup>). In enteroviruses, 3CD possesses protease activity but not in aphthoviruses. Viral replication has been shown to depend on 3CD interactions with replication machinery such as 5' cloverleaf, the CRE and 3' UTR (Andino *et al.*, 1990; Gamarnik and Andino, 1998; Goodfellow *et al.*, 2000). PV 3CD cleaves the host cellular protein, PCBP2, which favours the switch from translation to RNA replication (Gamarnik and Andino, 1998; Perera *et al.*, 2007) (section 1.4).

- 3D

The 3D protein is an RNA dependent RNA polymerase (RDRP). The 3D polymerase (3D<sup>pol</sup>) transcribes new viral negative sense complement and uses this to produce new positive sense (genomic) RNA, and therefore plays a key role in genome replication. Like many RDRP, 3D<sup>pol</sup> has a high error rate as it lacks proofreading ability, which is related to the substantial genetic diversity in picornaviruses (Hicks and Duffy, 2011). The structures of 3D<sup>pol</sup> as a free enzyme and in complex with VPg have been determined for a number of viruses and have revealed a common structure which includes three domains referred to as finger, palm and thumb (Kerkvliet *et al.*, 2010).

- Leader protein

The Leader protein is present at the start of the ORF in cardioviruses, aphthoviruses and hepatoviruses (Figure 1.2). In aphthoviruses such as FMDV leader protein possesses protease activity. FMDV Leader protease (L<sup>pro</sup>) is a member of the papain-like family of cysteine proteases and its structure has been determined (Guarne *et al.*, 1998).

L<sup>pro</sup> is translated from two in-frame AUG codons, resulting in Lab<sup>pro</sup> and Lb<sup>pro</sup>, both of which are active during infection. Lab<sup>pro</sup> localises to the nucleus and causes degradation of a subunit of nuclear factor kappa beta (NF-κB), to reduce the host inflammatory response during virus replication. L<sup>pro</sup> co-translationally self cleaves, thereby releasing P1. Upon

release, L<sup>pro</sup> cleaves eIF4G, resulting in the inhibition of capped translation of host cell RNA (Belsham, 2013; Medina *et al.*, 1993). This permits continuation of cap-independent translation of viral RNA.

The cardiovirus L protein such as that of mengovirus and encephalomyocarditis virus does not function as a protease but plays a role in virus translation, inhibition of interferon synthesis and phosphorylation of nucleoporins (Dvorak *et al.*, 2001; Hato *et al.*, 2007). The mechanisms for its functions are not well understood. The leader proteins of viruses in the *Kobuvirus* genus do not share sequence identity with any other picornavirus proteins and their functions remain to be defined (Yamashita *et al.*, 2003).

## 1.4 Genome replication

The purpose of genome replication is the synthesis of new viral RNA to allow increased translation of viral proteins and to provide viral genome for assembly into new virus particles. Picornavirus infection induces the rearrangement of cellular membranes which serve as a scaffold for vRNA replication. Studies with PV suggested such membranes were derived from the endoplasmic reticulum (ER) and golgi (Hsu *et al.*, 2010; Schlegel *et al.*, 1996). In PV, ADP ribosylation factor (Arf) dependent membrane trafficking in the early secretory pathway and coat protein II (COPII) dependent budding of vesicles from the ER were shown to be involved in the formation of replication complexes required for RNA replication (Hsu *et al.*, 2010; Rust *et al.*, 2001) and (as reviewed in Chase and Semler, 2012). Replication complexes facilitate an increase in the local concentration of proteins involved in replication. Also, the association with membranes protects the replicating RNA from cellular enzymatic degradation.

Two significant differences between FMDV and enteroviruses in how they interact with the early secretory pathway suggest they use membranes for replication differently. Firstly, although FMDV and PV both inhibit the secretory pathway they do so by different mechanisms (Moffat *et al.*, 2005; Moffat *et al.*, 2007). PV 3A protein inhibits protein secretion whereas for FMDV secretion is not blocked by 3A but instead by 2B and 2C. FMDV 2B and 2C when expressed individually, do not block protein transport, however, when expressed together as 2B with 2C or as 2BC, an inhibitory effect on protein secretion was observed (Moffat *et al.*, 2005; Moffat *et al.*, 2007). Secondly, PV infection is inhibited by golgi membrane modifying drug such as brefeldin A (BFA) while this reagent does not inhibit FMDV infection (Armer *et al.*, 2008; Cuconati *et al.*, 1998; Gazina *et al.*, 2002; Irurzun *et al.*, 1992). This suggests that in contrast to PV, FMDV modifies cellular membranes for replication in an Arf1 (ADP ribosylation factor) and GBF1 (Guanine Nucleotide Exchange Factor for Arf) independent way.

When sufficient amounts of 3D<sup>pol</sup> and other essential viral replication proteins have been synthesised, the vRNA is copied starting from the 3' end to generate a complementary RNA. This negative strand RNA is in turn used to generate multiple positive stranded RNA molecules which serve as templates for translation or as templates, for negative strand synthesis, or for packaging into virions.

vRNA synthesis is initiated within the membrane-associated replication complex. vRNA is synthesised by the viral RNA-dependent-RNA-polymerase, 3D<sup>pol</sup> (Section 1.3.2). 3D<sup>pol</sup> uses the cre as a template to allow VPg uridylylation, resulting in VPg-pU or VPg-pUpU. The location of cre varies between picornaviruses for e.g. in HRV14 it is located in the coding region for P1, in FMDV it is located in the 5' UTR (Mason *et al.*, 2002) whereas in HRV2 and PV it is located in the coding region encoding for 2A and 2C, respectively (Gerber *et al.*, 2001; Goodfellow *et al.*, 2000; McKnight and Lemon, 1998; Yang *et al.*, 2002). Since the FMDV cre can function in trans, it has been referred to as the 3B uridylylation site (bus). Uridylylated VPg then acts as the primer for vRNA replication by annealing at the poly(A) and becoming elongated into the full length viral RNA by 3D<sup>pol</sup> (Murray and Barton, 2003; Nayak *et al.*, 2006). Unlike other picornaviruses, aphthoviruses (e.g. FMDV) contain three distinct copies of VPg which differ in size and amino acid sequences. All three copies of VPg have been shown to be uridylylated *in vitro* but more efficient uridylylation of the third copy of VPg has been observed (Nayak *et al.*, 2005).

Genome circularisation is thought to be a general mechanism used by positive strand RNA viruses for the initiation of vRNA replication. In picornaviruses, 3CD interacts with the host cellular protein PCBP and binds to the cloverleaf structure present at the 5' of the vRNA. The cellular protein PABP1 binds to the 3' poly (A) tail of the vRNA. The interaction of PABP1 at the 3' end with the proteins at the 5' end leads to the circularisation of the genome. This results in the proximity of 3D<sup>pol</sup> and the poly (A) tail which enables the initiation of negative stranded RNA synthesis (Herold and Andino, 2001). 3C and 3CD inactivate host transcription and may mediate the switch from viral RNA translation to replication. Cleavage of host proteins like PABP and PTB by 3C and PCBP2 by 3C/3CD, contributes to the inhibition of cap-dependent cellular RNA translation. Cleavage of host proteins has been proposed to mediate this switch (Figure 1.4) (Back *et al.*, 2002; Parsley *et al.*, 1997), (as reviewed in Chase and Semler, 2012).

In the nucleus of eukaryotes, transcription is carried out by three different RNA polymerases, RNA polymerase I, II and III (Pol I, II and III). During enterovirus infection (e.g. PV), viral proteases 2A and 3C contribute to the disruption of these RNA polymerases, thereby inhibiting host transcription. During FMDV infection, host transcription is also inhibited but by a different mechanism to that of PV. Histone H3 is a protein that contributes to eukaryotic cell mitotic

progression and regulation (Luo *et al.*, 2010) and FMDV 3C<sup>pro</sup> cleaves histone H3 at its N-terminus. Efficient inhibition of host transcription is essential for efficient replication of viral RNA (as reviewed in Chase and Semler, 2012). Picornavirus infections also result in the disruption of nucleocytoplasmic trafficking of proteins such as PCBP2, PTB and La which accumulate in the cytoplasm as a result of inhibition of their nuclear import. The cytoplasmic accumulation of some host proteins such as SRp20 are utilised by the virus during RNA replication and also viral translation (section 1.3).

Thus, picornaviruses subvert host cell machinery to favour viral RNA replication by cleavage of host cell proteins, disruption of cellular trafficking and overall alteration of the host cell environment. It has been suggested that there are numerous as yet undiscovered host proteins that are utilised by viruses to favour viral genome translation and replication over that of cellular mRNA. Therefore, the complete picture of template switching between translation and replication is yet to be understood.

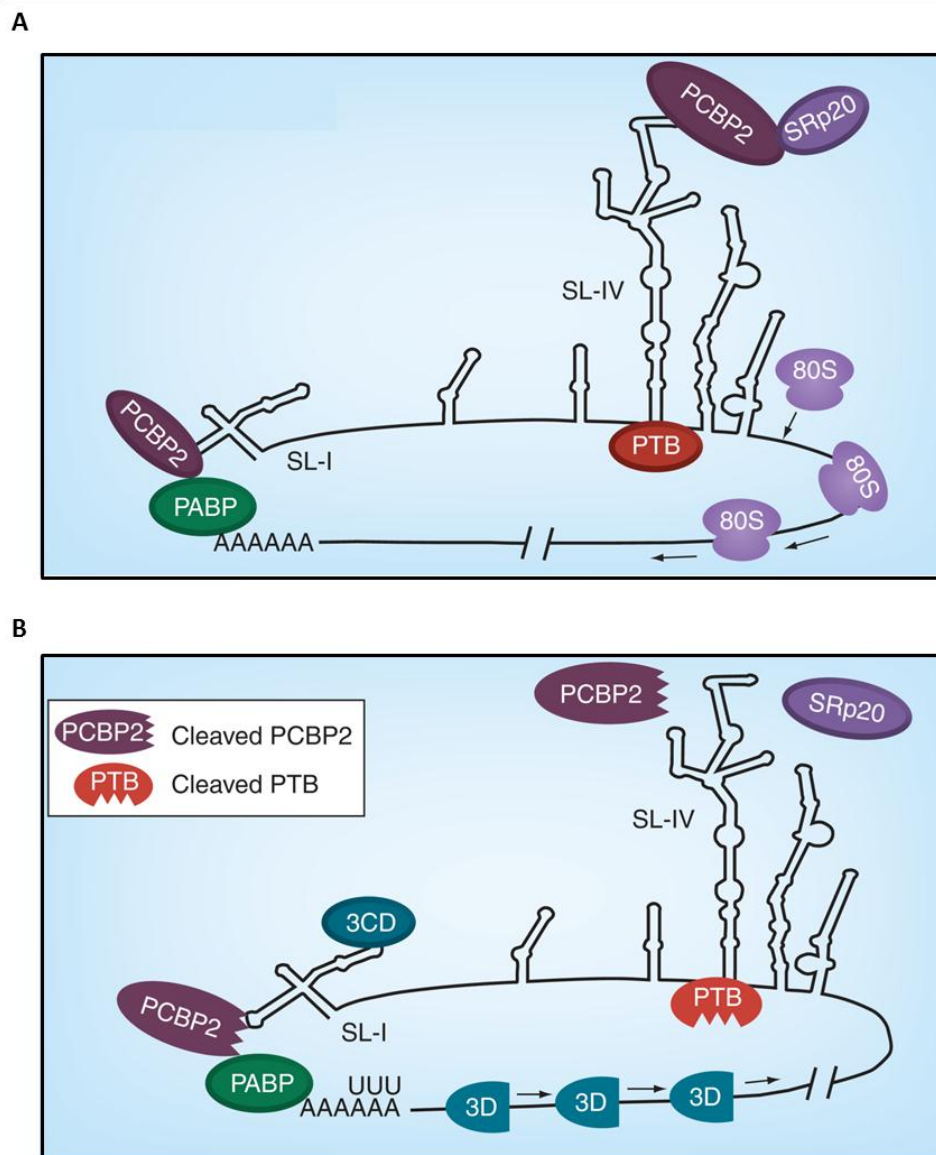


**Figure 1.4 Switch from translation to replication.**

**A.** Viral RNA serves as a template for IRES dependent translation under specific conditions which include recruitment of ribosomal subunit to the IRES and recruitment of host cellular proteins to mediate viral RNA translation. **B.** The specific conditions are altered to favour viral genome to serve as a template for viral RNA replication. Cleavage of PCBP2 and PTB inhibit translation and contribute to the switch from translation to replication. SL: stem loop, PCBP2: poly(rC) binding protein 2, PTB: polypyrimidine tract-binding protein, PABP: poly (A) binding protein, 3D: 3D polymerase, 3CD: 3CD protein, SRp20: serine arginine protein 20. Figure adapted from (Chase and Semler, 2012).

## 1.5 Picornavirus assembly and structure

Picornaviruses are small, non-enveloped RNA viruses with a capsid of icosahedral symmetry. The capsid structures of a number of picornaviruses have been determined by X-ray crystallography. These include HRV2 (Verdaguer *et al.*, 2000), HRV3 (Zhao *et al.*, 1996), HRV14 (Rossmann *et al.*, 1985), HRV16 (Hadfield *et al.*, 1997), PV1 Mahoney (Hogle *et al.*, 1985), PV2 Lansing and PV3 Sabin (Filman *et al.*, 1989), Echovirus 11 (Stuart *et al.*, 2002), FMDV A10 (Fry *et al.*, 2005a) and FMDV SAT1 (Adams *et al.*, 2010). In addition, structures have been determined for assembly intermediates, entry intermediates and virus-receptor complexes at high resolution by X-ray crystallography and at sub-atomic resolution by electron microscopy (Bubeck *et al.*, 2005; Fry *et al.*, 2005b; Hadfield *et al.*, 1999; Lentz and Arnold, 1998; Tuthill *et al.*, 2009; Wien and Hogle, 1995; Zhang *et al.*, 2008). These structures have contributed to the understanding of picornavirus assembly, antigenic variation and host-cell interactions.

### 1.5.1 Virus Assembly

The viral capsid proteins are synthesised as part of a polyprotein which is processed to form the individual capsid proteins (section 1.3). In some picornaviruses, such as enteroviruses, the 2A protease (2A<sup>pro</sup>) autocleaves to release the region encoding the capsid proteins (P1) from the region encoding non-structural proteins (P2 and P3) (Castello *et al.*, 2011). Co-translational cleavage of P1 by 3CD results in VP0 (the capsid protein precursor of VP2 and VP4), VP1 and VP3 (Blair *et al.*, 1993; Marcotte *et al.*, 2007). In aphthoviruses such as FMDV, 3C carries out these cleavages (Birtley *et al.*, 2005). Another important cleavage in FMDV is carried out by the leader protease, the first protein to be produced and which cleaves itself from the structural proteins (as reviewed in Grubman and Baxt, 2004). Enteroviruses do not have a leader protein (Figure 1.2). The function of the structural and non-structural proteins is described in detail in section 1.3.1.

After processing of P1 into VP0, VP1 and VP3 the capsid proteins are unlikely to exist as free individual proteins and rapidly assemble into protomers. Virus particles can be distinguished from each other based on their sedimentation coefficients (S) in a sucrose gradient. Early studies with HRV, PV and EMCV showed that five protomers (6S) assembled to form pentamers (12S), and twelve pentamers self-assembled to form the empty virus particle (80S) (McGregor *et al.*, 1975; McGregor and Rueckert, 1977) (Figure 1.5). The structure of pentamers is not known and has only been inferred from capsid structures. Some picornaviruses naturally form empty particles in the infected cell which are equivalent to the virus but do not contain the vRNA (as reviewed in Putnak and Phillips, 1981). The

sedimentation coefficient of 80S varies slightly for empty capsids of different picornaviruses and depends on the conditions used. The structure of assembled empty capsids have only been determined for PV (Basavappa *et al.*, 1994) and FMDV (Curry *et al.*, 1997; Porta *et al.*, 2013).

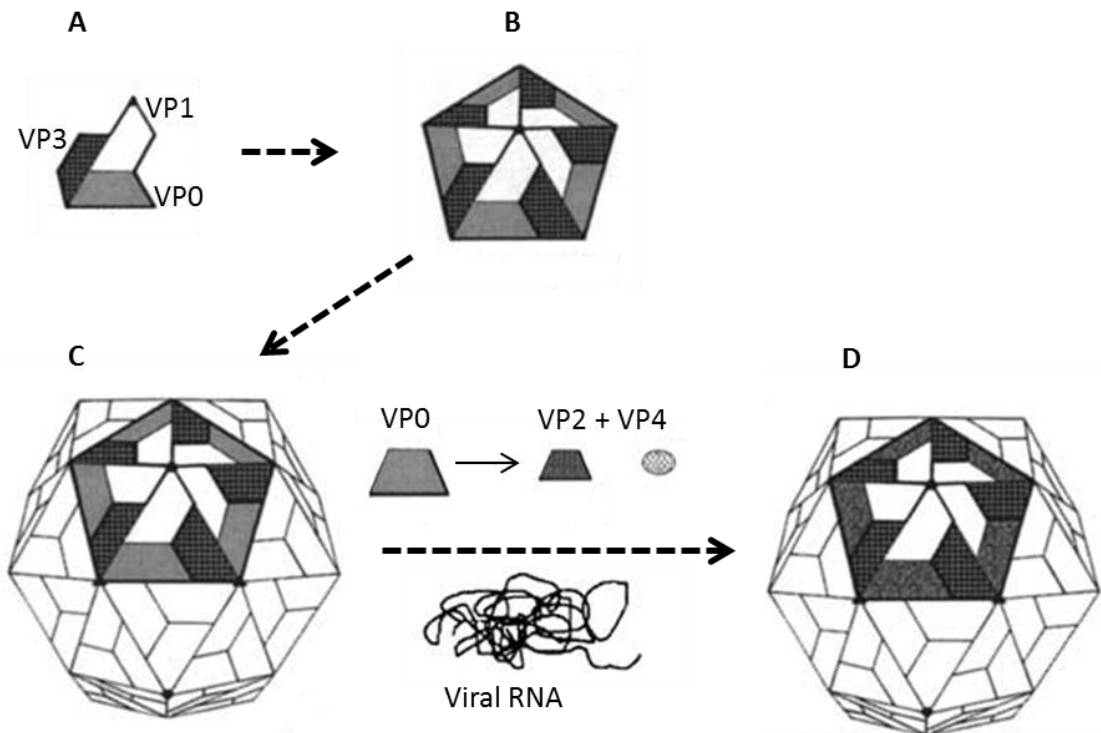


**Figure 1.5 Structural organisation of the picornavirus capsid.**

**A.** Each protomer is comprised of one copy of each of the structural proteins VP0, VP1 and VP3  
**B.** Five protomers assemble to form a pentamer **C.** Twelve pentamers assemble to form an empty capsid with icosahedral symmetry **D.** Encapsidation of RNA cleaves precursor protein VP0 to form VP2 and VP4, forming the mature virus particle. Figure adapted from (Clavijo *et al.*, 2004).

Three theories suggest the possible functions of empty capsids. Empty capsids are thought to be a storage form of pentamers as empty capsids and have been reported to dissociate into pentamers, *in-vitro* (Marongiu *et al.*, 1981; Putnak and Phillips, 1981). Two alternative theories suggest that empty capsids may either be dead-end products when the RNA is limiting or serve as immature particles into which RNA is packaged to form the mature virus particle.

Myristoylation of the capsid precursor protein, VP0, appears to be important for particle assembly in both, native (Marc *et al.*, 1990; Moscufo *et al.*, 1991) and recombinant systems (Abrams *et al.*, 1995; Goodwin *et al.*, 2009). However, myristoylation was shown not to be an absolute requirement for particle assembly (Ansardi *et al.*, 1992). In infected cells, twelve

pentamers assemble to form the empty capsid. As suggested by Rombaut *et al.*, 1991 and demonstrated by Li *et al.*, 2012, pentamers purified from infected cells self-assembled to form empty capsids, in a cell-free system. Capsid assembly was shown to be dependent only on a threshold pentamer concentration, temperature (>24°C) and salt concentration (>500 mM NaCl). However, there is also evidence for other cellular factors including chaperones (e.g. heat shock protein 90) in capsid assembly (Geller *et al.*, 2007; Wang *et al.*, 2013). There may also be a potential role for RNA in the process of capsid assembly as the use of two chemicals, 5-(3,4-dichlorophenyl) methylhydantoin (hydantoin), amino-4,6-dichloropyrimidine (Py 11) and 2-amino-5-(2-sulfamoylphenyl)-1,3,4-thiadiazole (G413), prevented RNA encapsidation and consequently inhibited PV capsid assembly (Verlinden *et al.*, 2000). Only newly synthesised RNA is encapsidated (Baltimore *et al.*, 1966; Nugent *et al.*, 1999) but signals for RNA encapsidation, if present at all, are yet to be identified. Although, a mechanism for capsid assembly has been identified, the nature of the interactions that allow self-assembly to proceed remain to be fully understood.

The structure of native HRV16 showed residues in VP1 and VP2 stacking against RNA bases (section 1.5.2). This was observed across the twofold axes between pentamers (Hadfield *et al.*, 1997). Therefore, interactions between RNA and capsid proteins may play a role in capsid assembly. Similar electron densities representing RNA have been observed in HRV14 (Arnold and Rossmann, 1990), coxsackievirus B3 (Muckelbauer *et al.*, 1995) and PV (Filman *et al.*, 1989).

After RNA encapsidation, maturation cleavage of VP0 into VP2 and VP4 takes place in most picornaviruses except kobuviruses and parechoviruses (Yu *et al.*, 2011) and (as reviewed in Stanway and Hyyppia, 1999). This final stage of assembly permits internal rearrangements of VP2 and VP4 to lock the virus particle into a metastable state which is primed to undergo conformational changes, required to release the viral RNA during infection (Hogle, 2002). The maturation cleavage of VP0 stabilises the virus and is essential for virus infectivity of most picornaviruses such as enteroviruses and aphthoviruses. However, in some aphthoviruses such as FMDV A22, the maturation cleavage of VP0 can occur in the absence of packaged RNA, resulting in the formation of empty particles containing mature forms of VP2 and VP4 (Curry *et al.*, 1997). In PV, the residues forming the VP0 cleavage site are the C-terminal asparagine of VP4 (position 68) and the N-terminal serine of VP2 (position 1) (Ansardi and Morrow, 1995). Mutations of the histidine residue (position 195) of PV VP2, which is present in the vicinity of the VP0 cleavage site, were shown to be lethal as they prevented VP0 cleavage during the final stages of virus assembly (Hindiyeh *et al.*, 1999).



### 1.5.2 Virus structure

The picornavirus capsid is approximately 30 nm in diameter and is composed of sixty copies of each of the four capsid proteins VP1, VP2, VP3 and VP4, arranged with icosahedral symmetry. VP1, VP2 and VP3 form the outer capsid surface while VP4 is distributed on the inner surface of the capsid (Figure 1.6).

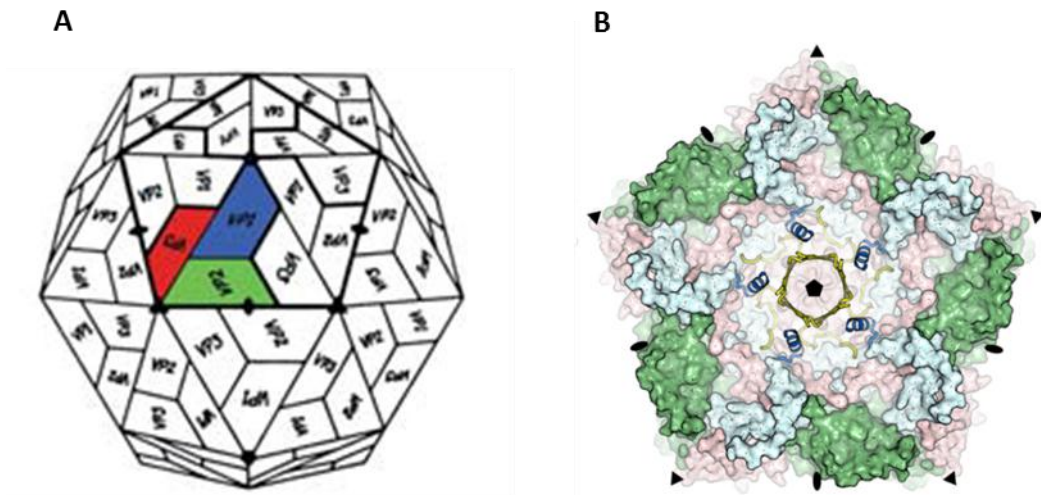


**Figure 1.6 Picornavirus capsid and pentamer showing the location of capsid proteins.**

**A.** Capsid of icosahedral symmetry comprised of VP1 (blue), VP2 (green), VP3 (red) and VP4 (not visible). **B.** A pentamer of icosahedral protomeric units depicting VP1 (blue), VP2 (green) and VP3 (red) forming the surface of the capsid, and VP4 (yellow) which is internal to the capsid. The view is from the inside of a virus. The N-termini of VP1 are depicted as alpha helices (blue). The position of the fivefold (◼), threefold (▲) and twofold (●) icosahedral symmetry axes are shown. Figure adapted from (Tuthill *et al.*, 2009) and (Wang *et al.*, 2012).

VP0 contains the five amino acid myristoylation signal sequence at its N-terminus. Myristoylation of VP0 is a feature of all picornaviruses except for hepatoviruses and parechoviruses. Hepatitis A virus (the only member of the *Hepatitis virus* genus) is unusual as it does not contain a myristoylation signal sequence at the N-terminus of VP0 hence VP0 and VP4 are not myristoylated (as reviewed in Stanway and Hyypia, 1999) also see section 1.5.1. The myristate groups are clustered in a region that locates to the fivefold symmetry axes of the virus. The carbonyl oxygen of the myristate molecules form hydrogen bonds with the hydroxyl groups of threonine (position 28) of adjacent VP4 proteins. Substitution of threonine (position 28) of PV VP4 with different amino acids (valine or serine), resulted in the accumulation of assembly inefficient intermediates, decreased virus infectivity and stability of the assembled mutant; and substitution with some amino acids (glycine or lysine) were lethal and produced non-viable virus particles. Therefore, the interactions between threonine (position 28) in VP4 and the myristate group of the adjacent VP4, were important for virus structure and stability (Moscufo and Chow, 1992).

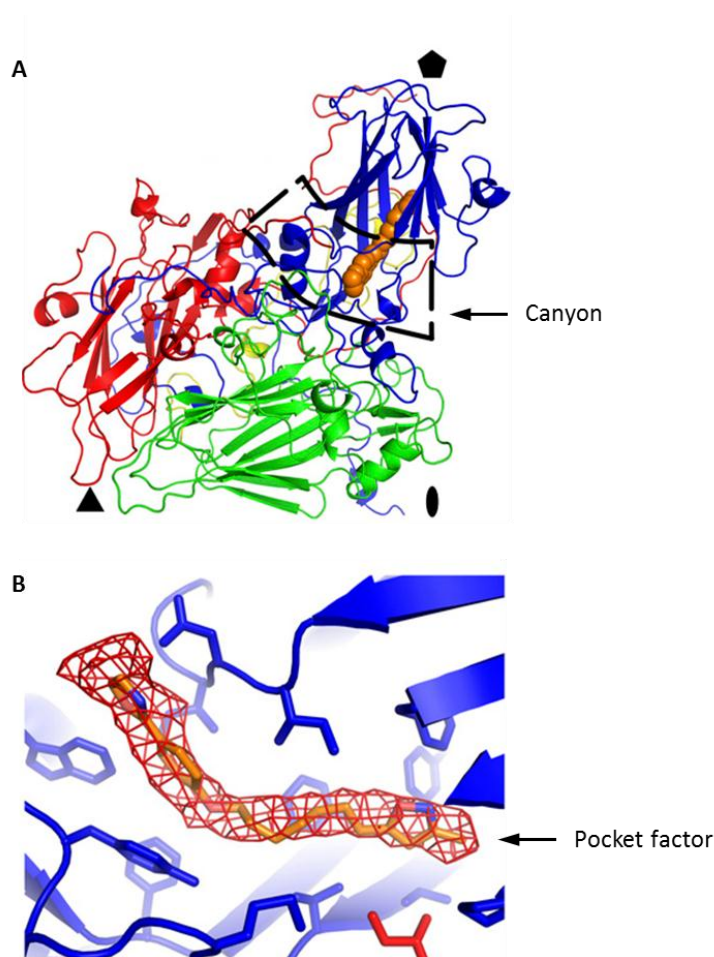


**Figure 1.7 Binding of the pocket factor into the pocket located at the base of the canyon.**

**A.** A capsid protomer depicting VP1 (blue), VP2 (red), VP3 (green) and VP4 (yellow). WIN compound shown as space filling model (orange). The pocket factor and WIN compound share the same binding site in the pocket. **B.** Comparison of pocket factor and WIN compound occupancy in the pocket. Electron density of the pocket factor shown in red and WIN compound model shown in orange. Figure adapted from (Plevka *et al.*, 2013).

The overall capsid structures of members of the picornavirus family are similar (Figure 1.6). One of the defining features of enteroviruses is the canyon which is a depression surrounding the fivefold axis. The canyon is mostly composed of VP1 residues. The base of the canyon forms the binding site for receptors of the immunoglobulin-like superfamily such as the poliovirus receptor (PVR, also called CD155) and intercellular adhesion molecule-1 (ICAM-1) for PV and major group rhinoviruses, respectively (Belnap *et al.*, 2000b; He *et al.*, 2003; Kolatkar *et al.*, 1999; Olson *et al.*, 1993). Cardioviruses such as mengovirus and Theiler's murine encephalomyelitis virus contain a depression similar to the canyon which is not continuous but broken into five deep pits. These pits are also involved in receptor binding (Hertzler *et al.*, 2000; Luo *et al.*, 1987). In contrast, the receptor binding site for minor group rhinoviruses such as HRV2 is a small star shaped dome on the fivefold axis and not the base of the canyon (Hewat *et al.*, 2000). The majority of enteroviruses, contain a pocket factor which is present below the floor of the canyon and contributes to virus particle stability (Plevka *et al.*, 2013)

(Figure 1.7). The X-ray crystal structure for bovine enterovirus (BEV) showed the pocket contained electron density which was modelled to be myristic acid. The release of the pocket factor is a necessary prerequisite for virus uncoating (as reviewed in Smyth and Martin, 2002). In contrast, aphthoviruses do not contain a canyon and the receptor (integrin) binding site for FMDV is an exposed arginine-glycine-aspartic acid (RGD) motif present on the GH loop of VP1 (Jackson *et al.*, 1997; Mason *et al.*, 1994).

VP1-3 adopt a wedge shaped eight stranded beta-barrel structure (Figure 1.8). The narrow ends of the VP1 beta barrel cluster around the fivefold axis. The narrow ends of the VP2 and VP3 beta barrels alternate around the threefold axis. The beta strands are linked by connecting loops, whose lengths and compositions determine virus surface topology which in turn influences receptor binding and antigenicity (Hogle *et al.*, 1985) (as reviewed in Tuthill *et al.*, 2010; as reviewed in Wien *et al.*, 1996) The difference in the length of the connecting loops also contributes to the formation of the canyon (in enteroviruses) and capsid thickness which varies between 33 Å for FMDV and 42.5 Å for HRV14 (Acharya *et al.*, 1989; Jackson *et al.*, 2003; Rossmann *et al.*, 1985), (as reviewed in Tuthill *et al.*, 2010). In contrast to enteroviruses where protrusions are formed by the connecting loops at the fivefold, threefold and twofold axis, aphthoviruses such as FMDV have shorter surface loops, resulting in a smooth capsid surface compared to enteroviruses such as PV (Figure 1.9) (Tuthill *et al.*, 2009; Tuthill *et al.*, 2010).

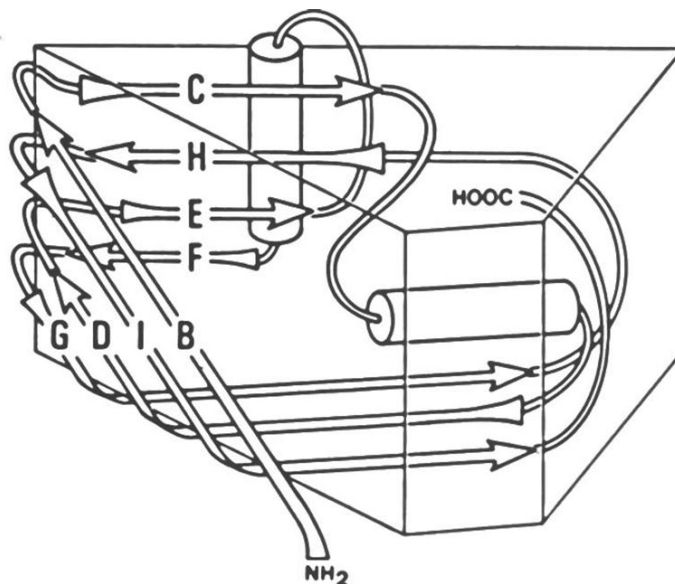


**Figure 1.8 Schematic representation of the structure and organisation shared by VP1, VP2 and VP3.**

A wedge-shaped antiparallel beta barrel comprised of eight strands. Individual beta strands are labelled alphabetically (A-H) and shown as arrows. The cylinders depict the flanking helices. Figure reproduced from (Filman *et al.*, 1989).

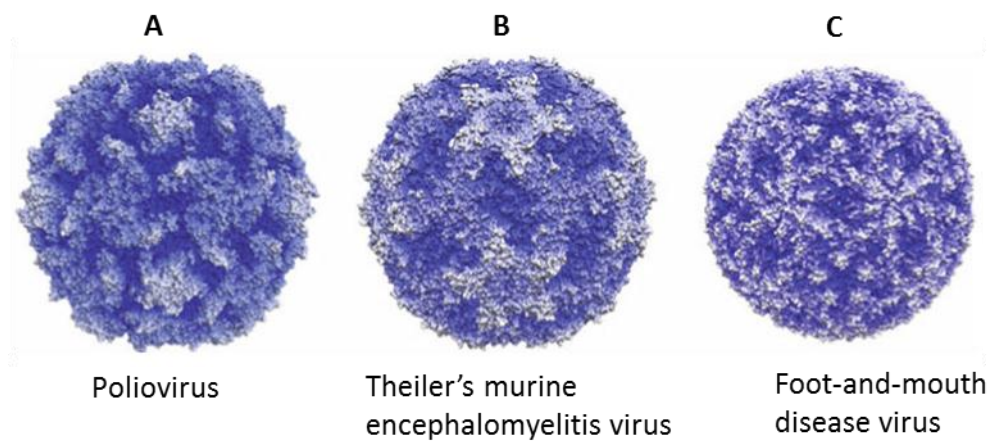


**Figure 1.9 Comparison of picornavirus capsid structures.**

Picornavirus particles represented as radial depth cued images with a colour gradient from innermost surfaces (dark blue) to outermost surfaces (white). **A.** Poliovirus. The canyon surrounding the fivefold axis is clearly identified. **B.** Theiler's murine encephalomyelitis virus. Surface depressions spanning the twofold axis clearly identified. **C.** Foot-and-mouth disease virus with a smooth surface relative to poliovirus and theiler's murine encephalomyelitis virus. Figure adapted from (Tuthill *et al.*, 2010).

In the virus structures determined by X-ray crystallography, portions of the capsid were disordered, suggesting flexibility or multiple adopted conformations. These regions included the N-terminus and central portion of VP4 in most picornaviruses, and the N-terminus of VP2 in some picornaviruses such as FMDV, and N-terminus of VP1 in HRV and PV. In FMDV, the VP1 GH loop is a conformationally flexible loop and was not observed in the crystal structure other than in the chemically reduced FMDV structure (Rowlands *et al.*, 1994). These flexible regions of the capsid proteins are often associated with functions in cell entry (described in section 1.6)

In order for the large size RNA to be contained within the capsid, it has to be tightly packed. The interaction between the vRNA and capsid proteins may play a role in virus assembly. In a structure of PV2, electron densities tentatively assigned to RNA bases appeared to be stacked against the VP4 residues, tyrosine (position 20) and phenylalanine (position 46) (Lentz *et al.*, 1997). In a structure of PV3, electron densities which may correspond to RNA bases appeared to be stacked against tryptophan (position 38) and phenylalanine (position 41) of VP2. Similarly in PV1, RNA bases appeared to be stacked against tryptophan (position 38) and tyrosine (position 41) of VP2 (Filman *et al.*, 1989). Also, the structure of HRV16, revealed the stacking of RNA bases against the tryptophan (position 38) of VP2 and a tentative identification of RNA bases stacking against tyrosine (position 55) of VP1, on the inner surface of the viral capsid (Hadfield *et al.*, 1997). Tryptophan (position 38) is a conserved residue across the picornavirus family (Lentz *et al.*, 1997) and is present in a depression around the threefold axis. Electron

density attributed to RNA was observed stacked against this (tryptophan , position 38) residue. This was reminiscent of the trefoil shaped cluster formed by RNA and bound to the capsid interior of the bean pod mottle virus, a plant icosahedral virus (Chen *et al.*, 1989). Therefore, although RNA is not visible in the above mentioned structures of picornaviruses, the similarity with bean pod mottle virus, suggests the electron density stacked against the capsid proteins is likely to be that of RNA.

## 1.6 Virus cell entry

Viruses are obligate intracellular pathogens and gaining entry into host cells is, therefore, a critical part of the viral life cycle. The initial step in virus entry is the attachment of virus to the cell surface receptor.

PV binds to PVR which is expressed in many cells including those of the small intestine, lung, liver, heart and motor neurons of the spinal cord. Therefore, the neurotropism of PV cannot be explained based solely on the distribution of PVR. The distribution of receptors such as ICAM-1, integrins and decay accelerating factor (DAF) used as receptors by major group HRV, FMDV and the majority of echoviruses, respectively (section 1.6.4.1), suggest that the presence of receptors is not the only factor determining tissue tropism of these viruses. A clear understanding of the relationship between receptor usage and pathogenesis is lacking, partly due the lack of suitable animal models (Evans and Almond, 1998). Some viruses have been shown to use more than one receptor which contributes to virus uptake into the cell. The receptors used will be discussed in more detail in section 1.6.4.1.

After binding of viruses to receptors on the cell surface viruses must enter cells to initiate infection. Most picornaviruses enter the cells using endocytosis and the nature of the endocytic pathway used varies between the viruses. Upon entering the endocytosed vesicle, picornaviruses need to overcome the membrane barrier to gain access to the cytoplasm, without destroying host cell integrity. Enveloped viruses contain an outer membrane (“envelope”) and can enter the cell by a well characterised process of fusion between the viral and host cell membranes. Due to the absence of the membrane layer in non-enveloped viruses, the mechanism used to gain entry into host cells, must be different to enveloped viruses but remains unresolved. The mechanism of membrane permeabilisation by non-enveloped viruses may involve membrane pore formation or disruption.

### 1.6.1 Membrane penetration by enveloped viruses

Enveloped viruses gain entry into host cells by fusion of their membrane with that of the host cell. Proteins, usually glycoproteins (gp), present in the virus envelope catalyse this process. A trigger such as receptor binding or low pH induces conformational changes in an envelope protein which result in the exposure and insertion of a fusion peptide into the host cell membrane. This leads to the mixing of the viral and host cell membrane (hemifusion) and eventually opening of a fusion pore. An overview of this process is shown in Figure 1.10.

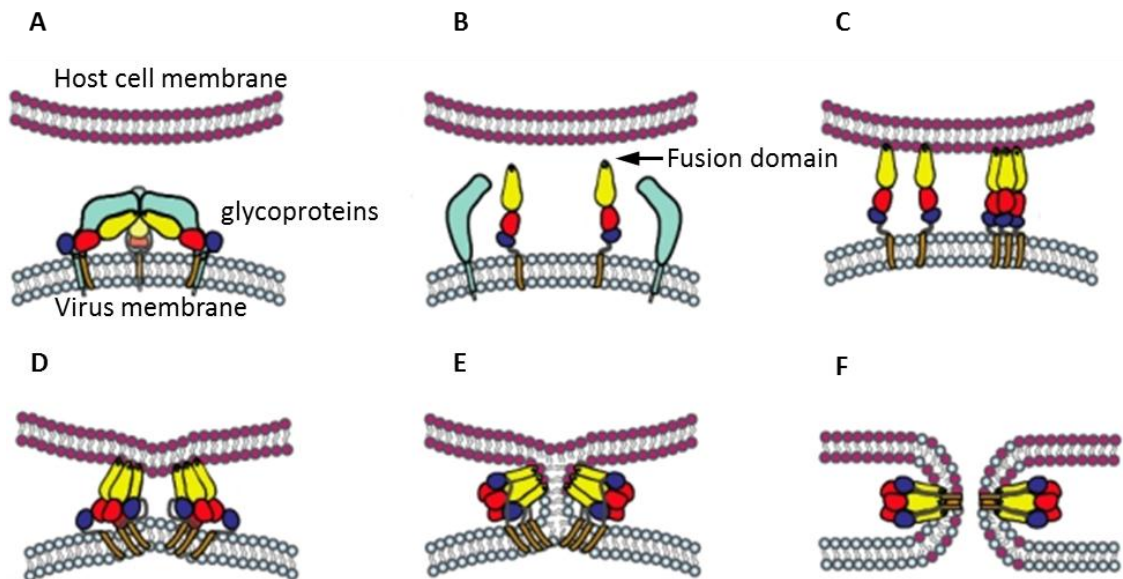


**Figure 1.10 The stages of enveloped virus membrane fusion.**

**A.** Alphavirus particle in pre-fusion state. Virus glycoproteins, virus membrane and host cell membrane are labelled. **B.** Upon exposure to low pH, the glycoproteins dissociate and the fusion domain becomes exposed. **C.** The fusion domain inserts into the host cell membrane. **D.** Distortion of the host cell membrane caused by insertion of the fusion domain. **E.** The virus membrane and host cell membrane merge. This stage is the hemifusion stage. **F.** Complete fusion forms the fusion pore. Figure adapted from (Kielian *et al.*, 2010).

HIV is an enveloped virus, consisting of gp120 and gp41 in its envelope. gp120 binds to its primary cellular receptor, CD4 and then to a co-receptor which induces conformational changes in its structure to expose the N-terminus of gp41 which contains a hydrophobic domain that mediates membrane fusion between virus and host cell membrane (as reviewed in Chan and Kim, 1998) and (as reviewed in Jones *et al.*, 2011). Herpes simplex virus-1 (as reviewed in Spear, 2004) and Sendai virus (Chejanovsky and Loyter, 1985) are other examples where viral glycoproteins fuse directly with the plasma membrane at the cell surface. Other enveloped viruses are endocytosed into acidic compartments (such as endosomes) where the prevailing low pH triggers membrane fusion of the virus and host cell membrane. For example, the influenza gp, haemagglutinin (HA) undergoes conformational changes at low pH which

results in the exposure of hydrophobic fusion peptide that mediates the fusion of viral and host cell membranes (Figure 1.11) (Han *et al.*, 2001).

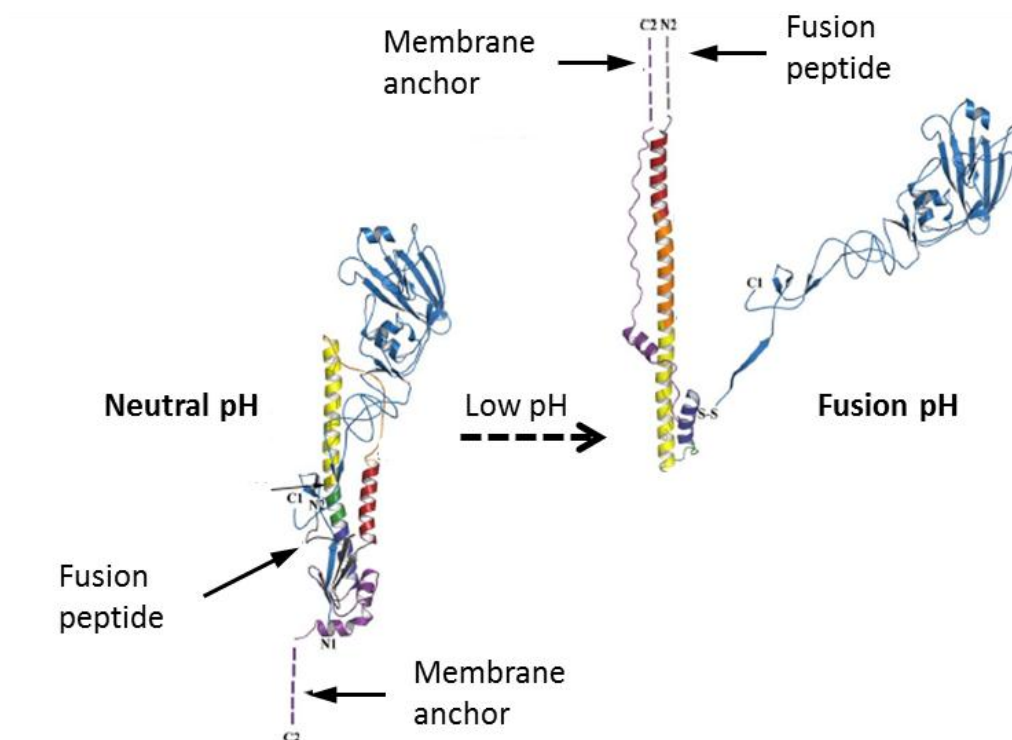


**Figure 1.11 Changes in the structure of the HA trimer from neutral pH to acidic pH.**

HA1 (blue) and HA2 (multi-coloured). The N and C-termini of each chain are labelled. Upon exposure to low pH (fusion pH), HA1 and HA2 are reoriented and refolded. The HA1 membrane distal domains detrimmerise, the fusion peptide becomes relocated to become the N-terminus of the alpha helix and mediates the fusion of viral and host cell membranes. Figure adapted from (Russell *et al.*, 2008).

Viral fusion peptides can, therefore, be classified as either pH dependent or pH independent, based on the trigger required for the activation of the peptides for membrane fusion. Fusion peptides can also be divided into three classes based on their structure and function (Figure 1.12). Class I fusion peptides occur as fusion inactive precursor molecules that undergo proteolytic cleavage to liberate the N-terminus of the fusion peptide necessary to prepare for the fusion of the viral envelope with the target membrane. Fusion can be triggered by low pH and/or receptor binding and results in the extension of an alpha helical coiled coil which pushes the fusion peptide towards the host cell target membrane. All class I fusion peptides contain a heptad repeat-derived six helix bundle structure. Examples of class I fusion peptides include Influenza HA, HIV-1 envelope protein (Env) and paramyxovirus F protein. Class II fusion peptides have an elongated plate-like pre-fusion structure running parallel to the virus envelope. Upon being triggered by the acidic pH, the complex undergoes a conformational

change resulting in the domains near the fusion loops becoming perpendicular to the viral envelope and the target host cell membrane. The fusion loops are brought into close proximity by the reorganization of this complex into trimeric complexes. Unlike the high alpha helical content of class I fusion peptides, the final structure of class II fusion peptides has high beta sheet structure. Examples of class II fusion peptides include dengue virus E and alphavirus E protein. Class III fusion peptides share similarities with both class I and II fusion peptides. They have a pre-fusion native trimeric conformation, an extended conformation enabling viral envelope and target membrane interaction and a hair-pin post fusion structure. A characteristic of this class of fusion peptides is the reversible refolding of the peptides. Therefore, subsequent to the transport through the acidic pH environment which triggers the fusion of the viral envelope with that target host cell membrane, the trimer re-adopts its native conformation. The post-fusion structure is similar to the six-helix bundle structure of class I fusion peptides, but the heptad repeats are absent. Examples of class III fusion peptides include Rhabdovirus G and Baculovirus gp64 (Plempner, 2011).



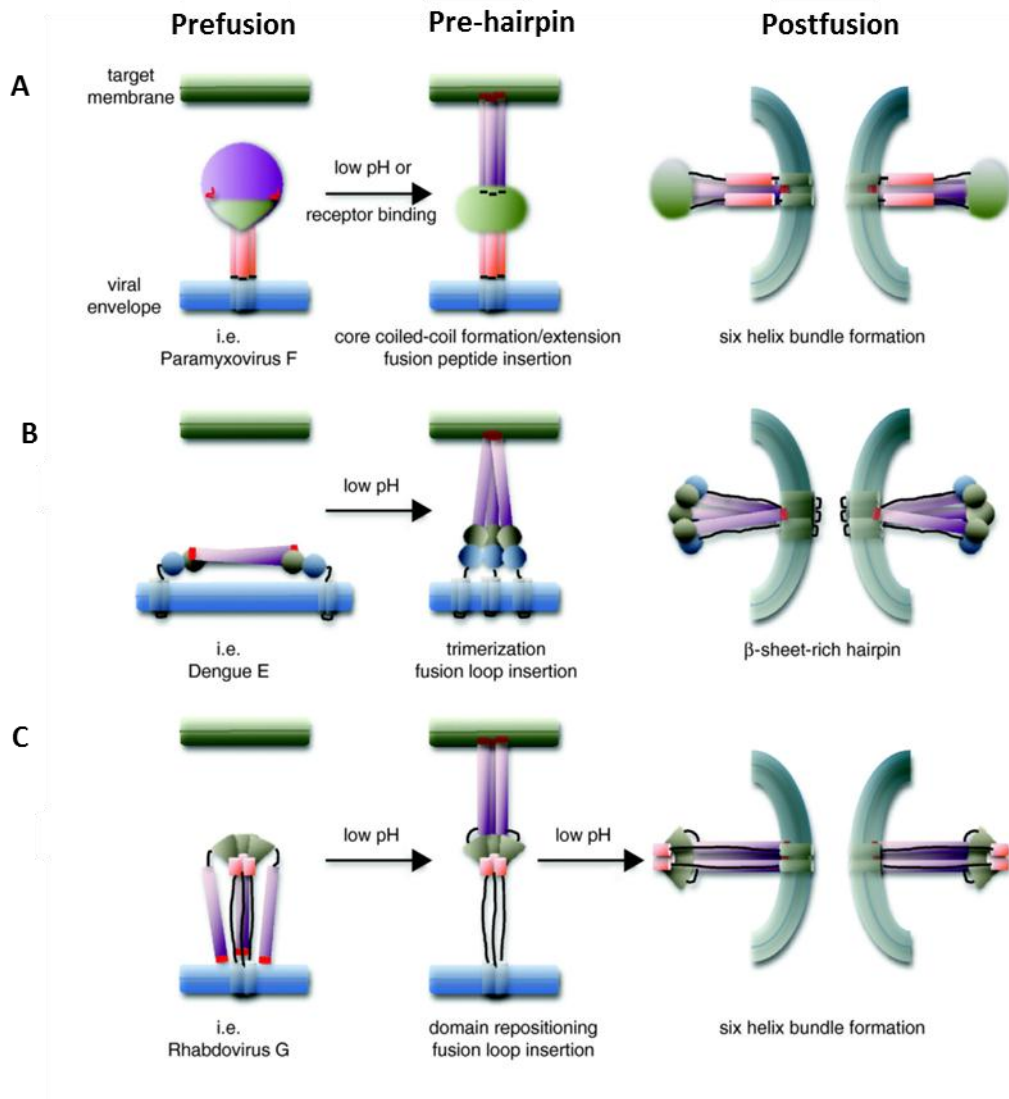


**Figure 1.12 Classes of fusion peptides.**

**A.** Class I fusion peptides. **B.** Class II fusion peptides. **C.** Class III fusion peptides. Prefusion, pre-hairpin and postfusion states are shown in three columns. Triggers for prefusion to pre-hairpin and postfusion are indicated on arrows. Figure reproduced from (Plempner, 2011).

### 1.6.2 Membrane penetration by non-enveloped viruses

Unlike enveloped viruses, which fuse the viral envelope with the cellular membrane, non-enveloped viruses must employ other mechanisms to cross the membrane and gain access to intracellular sites of replication. Non-enveloped viruses can gain entry into the host cell cytoplasm by becoming internalised into an endocytosed vesicle from within which a mechanism of membrane permeabilisation permits delivery of viral genetic material into the cytoplasm.

The virus capsid must be stable to allow environmental survival and transmission between hosts. Paradoxically, they must be sufficiently unstable to allow capsid disassembly during entry. This is achieved by locking the virus in a so-called metastable state. The conformational

changes in the capsid required for virus uncoating (externalisation of VP1 N-terminus and loss of VP4), must be spatiotemporally controlled as the premature release of the viral genome could miss the target replication site and expose the genome to host sensors which may trigger an immune response.

Capsid uncoating can be triggered by engagement with receptors, other host factors, low pH or mechanical stress. PV is an example of a picornavirus where uncoating is triggered by receptor binding whereas in FMDV, also a member of the picornavirus family, uncoating is triggered by low pH. Triggers for PV and FMDV uncoating will be discussed in more detail in section 1.6.4.2. Host factors that play a role in initiating genome release can be receptor binding but also others. Simian virus 40 (SV40) is internalised by lipid raft-mediated endocytosis following virus binding to its cell surface receptor ganglioside GM1. From here the virus is transported to the endoplasmic reticulum (ER), where structural alterations are triggered in the capsid by members of the disulphide isomerase family which facilitate exposure of the membrane permeabilising N-terminal domain of the capsid protein VP2. This results in the release of viral particles into the cytoplasm where they undergo further structural alterations in the capsid, mediating the import of viral genome into the nucleus (Engel *et al.*, 2011) and (as reviewed in Suomalainen and Greber, 2013). Mechanical stress is used by viruses such as human adenovirus (HAdV) to trigger capsid uncoating. HAdV binds to coxsackievirus adenovirus receptor (CAR) via fiber proteins and then engages with integrin receptors. The different motion patterns of CAR and integrins put a mechanical strain on the virus, resulting in the shedding of fibre proteins and exposure of capsid protein VI. The exposure of protein VI is required for the release of virus from the endosome by membrane disruption (Burckhardt *et al.*, 2011; Wiethoff *et al.*, 2005).

### 1.6.3 Non-enveloped virus capsid proteins facilitating membrane penetration

Non-enveloped viruses are metastable and in response to different cues (as described above), undergo conformational changes in their capsids leading to the delivery of the viral genetic material into the cytoplasm. This uncoating process often involves the exposure of proteins from the particle interior to the surface, and mediates membrane permeabilisation which facilitates the transfer of viral genetic material across the membrane.

Membrane permeabilising peptides of different non-enveloped viruses have been reported. The examples of some capsid proteins with membrane permeabilising function facilitating the cell entry process of non-enveloped are discussed here.

- **Reovirus  $\mu$ 1**

Following virus binding to cell receptors, reoviruses are internalised by endocytosis. Partial disassembly of the capsid occurs in the endocytic compartment, resulting in the exposure of the membrane binding protein,  $\mu$ 1, which has been shown to be the principal agent for membrane permeabilisation by reoviruses (Guglielmi *et al.*, 2006; Odegard *et al.*, 2004). Protease cleavage of  $\mu$ 1 leads to the release of the N-terminally myristoylated,  $\mu$ 1N. Studies have shown that the release of  $\mu$ 1N is essential and it directly contributes to membrane permeability mediating reovirus core delivery into the cytoplasm. Synthetic  $\mu$ 1N peptide has been shown to mediate the formation of size-restrictive pores in liposomes. These pores appear too small for the transfer of the core. Therefore, pore formation has been suggested as an initial step towards endosomal disruption. It has been suggested that docking of viral particles onto the pores formed by  $\mu$ 1N, allow the particles to access host cell factors to facilitate widening of the pore for the delivery of cores from the endosome into the cytoplasm. Alternatively, the  $\mu$ 1N concentration in endosomes may itself be high enough to form large pores or that the endosomal membrane is lysed following formation of pores (Chandran *et al.*, 2002; Ivanovic *et al.*, 2008; Zhang *et al.*, 2009).

- **Flock house virus  $\gamma$ 1**

During virus maturation, a capsid precursor protein ( $\alpha$ ) is cleaved to form a small peptide,  $\gamma$ , and other cleavage products. The  $\gamma$  peptide is located on the inner surface of the virus particle. Flock house virus binds its cellular receptors, enters the cell by endocytosis and undergoes conformational changes. The resulting altered particles are sensitive to pH and have lost a proportion of the  $\gamma$  peptide (Walukiewicz *et al.*, 2006). The  $\gamma$  peptide becomes transiently externalised during capsid breathing and irreversibly exposed when the virus particle encounters low pH during entry. The N-terminal 21 residues of  $\gamma$  peptide, have been predicted to form an amphipathic alpha helix and shown to disrupt membranes when synthetically generated (Bong *et al.*, 1999; Bong *et al.*, 2000; Maia *et al.*, 2006). More recent studies using VLPs containing only the amphipathic N-terminal region or that and additional regions of the C-terminus of  $\gamma$  peptide, showed that the N-terminal region of  $\gamma$  peptide was not sufficient to induce membrane permeability. Though the role of the C-terminal region of the  $\gamma$  peptide in entry is as yet undetermined, it was also required for membrane permeabilisation and efficient FHV entry (Banerjee *et al.*, 2009). The findings above demonstrate the crucial role played by flock house virus  $\gamma$  peptide in permeabilising biological membranes during cell entry.

- **Rotavirus VP5\***

For rotavirus infection to be initiated, translocation of the virus particle across the membrane and into the cytoplasm is essential. The proteins VP4 and VP7 are exposed on the surface of the virion (Prasad and Chiu, 1994). The spike protein VP4 is the principal agent for attachment to host cells and membrane penetration (Ludert *et al.*, 1996). Trypsin cleaves VP4 into VP5\* and VP8\*, both of which remain associated with the virion. This cleavage is essential as it primes rotavirus for cell entry. VP5\* was shown to induce size-selective membrane permeability in model membranes (Dowling *et al.*, 2000) whereas membrane permeability was not observed with VP8\* or VP4 (Denisova *et al.*, 1999). The use of monoclonal antibodies against VP5\*, neutralised infectivity and prevented the association with liposomes by VP5\* (Trask *et al.*, 2010). These findings suggested the importance of VP5\* in rotavirus entry and provided a link between uncoating, membrane interaction and rotavirus entry.

- **Adenovirus protein VI**

Adenovirus fiber proteins bind to host cell receptors CAR or CD46 followed by interaction with integrins to initiate virus internalisation via endocytosis (as reviewed in Meier and Greber, 2004). Protein VI is internal to the capsid and released during capsid disassembly within endosomes. The capsid disassembly induced by lowering pH or elevating temperature was required for adenovirus mediated membrane disruption, suggesting that protein VI was necessary for membrane disruption. Protein VI induced pH independent membrane disruption. The amino terminus of protein VI has a predicted amphipathic helical structure and was essential for induction of membrane disruption (Moyer *et al.*, 2011; Wiethoff *et al.*, 2005). Antibodies against protein VI neutralised adenovirus infectivity and reduced membrane permeability induced by adenovirus (Maier *et al.*, 2010). Similar to other non-enveloped viruses, the mechanism of membrane permeabilisation induced by protein VI is not known.

### **Common themes in non-enveloped virus membrane penetration**

Capsid proteins that mediate membrane permeabilisation for the delivery of genetic material across the cellular membrane, share several common features. Non-enveloped virus capsids are stable structures which become metastable upon processing of capsid proteins. During infection, non-enveloped viruses undergo priming which involves conformational changes in the capsid triggered by a range of factors including low pH or receptor binding (section 1.6.2). The conformational changes result in the exposure or release of hydrophobic proteins (or

protein regions) which subsequently mediate interactions with cellular membranes, thereby facilitating the delivery of viral genetic material across the membrane and into the cytoplasm.

From the examples of membrane permeabilising non-enveloped virus proteins described above, it can be gathered that generally, the membrane binding hydrophobic peptide is present on the inner surface of the virion and protected from the external environment. It only becomes exposed when the capsid undergoes conformational changes upon receiving the appropriate trigger in the right environment. For example, membrane permeability is induced by rotaviruses only when capsid conformational changes take place in the presence of membrane. If membranes are added in later to pre-treated virus particles, membrane permeability is not induced (Trask *et al.*, 2010). Uncoating of HRV2 only occurs in the late endosome as it requires the acidic pH to trigger conformational changes necessary to mediate the delivery of the viral genome across the membrane and into the cytoplasm for replication (Prchla *et al.*, 1994). Many of these membrane permeabilising viral proteins are products of precursor proteins and are released as a result of protease cleavage or autocleavage. Membrane binding proteins of non-enveloped viruses are often co or post-translationally modified by the addition of a palmitoyl or myristoyl group at the N-terminus (e.g. N-terminally myristoylated  $\mu$ 1 of reovirus and VP4 of picornaviruses) and predicted to form amphipathic alpha helices.

Therefore, cell entry of non-enveloped viruses appears to follow a common paradigm of viral protein mediated membrane permeabilisation. However, the details of the mechanism of the membrane permeabilisation induced by non-enveloped viruses, remains to be defined.

#### **1.6.4 Picornavirus entry**

Picornaviruses serve as good models to study cell entry of non-enveloped viruses as many members of the picornavirus family can be readily grown in cell culture, many of their receptors are identified and the capsid structures of many resolved. However, defining the mechanism of cell entry used by picornaviruses has been complicated by the expanding and newly identified endocytic pathways and the ability of a given virus to use multiple pathways to gain cell entry. So far, HRV and PV have been used as models to elucidate picornavirus entry.

##### **1.6.4.1 Receptors and endocytosis**

A virus receptor can be defined as a molecule that interacts with the virus particle at the cell surface to promote infection. Receptor interactions allow viruses to attach to cells, provide the signal for cellular processes that internalise the virus particle and in some cases provide a

trigger for conformational changes in the capsid. Picornavirus receptor molecules are structurally diverse. Some picornavirus species such as HRV are classified into different groups based on the receptors used. Major group HRVs bind intracellular adhesion molecule-1 and minor group HRVs bind members of the low density lipoprotein receptor family. Poliovirus bind to poliovirus receptor, also called cluster of differentiation 155 (CD155). Intercellular adhesion molecule-1 (ICAM-1), coxsackievirus-adenovirus receptor (CAR) and poliovirus receptor (PVR) belong to the immunoglobulin (Ig) superfamily. Receptors that do not belong to the Ig superfamily include the low-density lipoprotein receptor (LDLR) which binds minor group HRV, and decay-accelerating factor (DAF) which binds some echoviruses and coxsackie B viruses (Evans and Almond, 1998; Rossmann *et al.*, 2002). A schematic of some of the known picornavirus receptors is shown in Figure 1.13. Poliovirus and major group human rhinovirus binding to receptors are two of the best studied examples. The receptors are anchored to the membrane, single span glycoproteins with three (PVR) or five (ICAM-1) extracellular domains. The amino terminal domain (D1) of the receptors bind into the canyon present around the fivefold axis of HRV and PV (Figure 1.14) (also described in section 1.5.2). Minor group HRVs bind three members of LDLR family: LDLR, very low density lipoprotein receptor (VLDLR) and low density lipoprotein receptor related protein (LRP) (Hofer *et al.*, 1994). The structure of LDLR contains amino terminal repeats, which enables it to make contact with several capsid proteins. Unlike receptor binding at base of the canyon in major group rhinoviruses, LDLRs bind to the star shaped protrusion observed at the fivefold axis (Hewat *et al.*, 2000). Despite the relative similarities in sequence and structure between major and minor group HRVs, they bind to different receptors. This may be due to the differences in charges present at the base of the canyon in major and minor group HRVs (Kolatkar *et al.*, 1999; Vlasak *et al.*, 2003). It is possible that the lack of charge complementarity inhibits binding of minor group HRVs to ICAM-1.

Enteroviruses other than PV often use multiple receptors to mediate cell entry. For example, coxsackie B viruses can infect cells by binding coxsackievirus and adenovirus receptor (CAR) or heparin sulphate proteoglycans. Additionally, DAF functions as an attachment receptor (Bergelson *et al.*, 1997; Shafren *et al.*, 1995; Zautner *et al.*, 2003). Some echoviruses can bind integrin  $\alpha 2\beta 1$  (VLA-2) (Bergelson *et al.*, 1992; Xing *et al.*, 2004) or DAF (Powell *et al.*, 1998; Ward *et al.*, 1994). Enterovirus 71 uses scavenger receptor class B member 2 (SCARB2) (Yamayoshi *et al.*, 2009) and P-selectin glycoprotein (PSGL-1) as receptors (Nishimura and Shimizu, 2009). Field isolates of FMDV have been reported to use a range of RGD binding integrins such as  $\alpha \beta 6$ ,  $\alpha \beta 3$ ,  $\alpha \beta 8$ ,  $\alpha \beta 1$ .  $\alpha \beta 6$  is expressed to high levels on epithelial tissues (site of FMDV infection) and is the predominant receptor used by FMDV isolates to initiate infection *in vivo* (Monaghan *et al.*, 2005). Cell-culture adapted isolates of FMDV were shown to

bind heparan sulphate glycan (HSG), an integrin independent route to initiate infection (Jackson *et al.*, 1996).

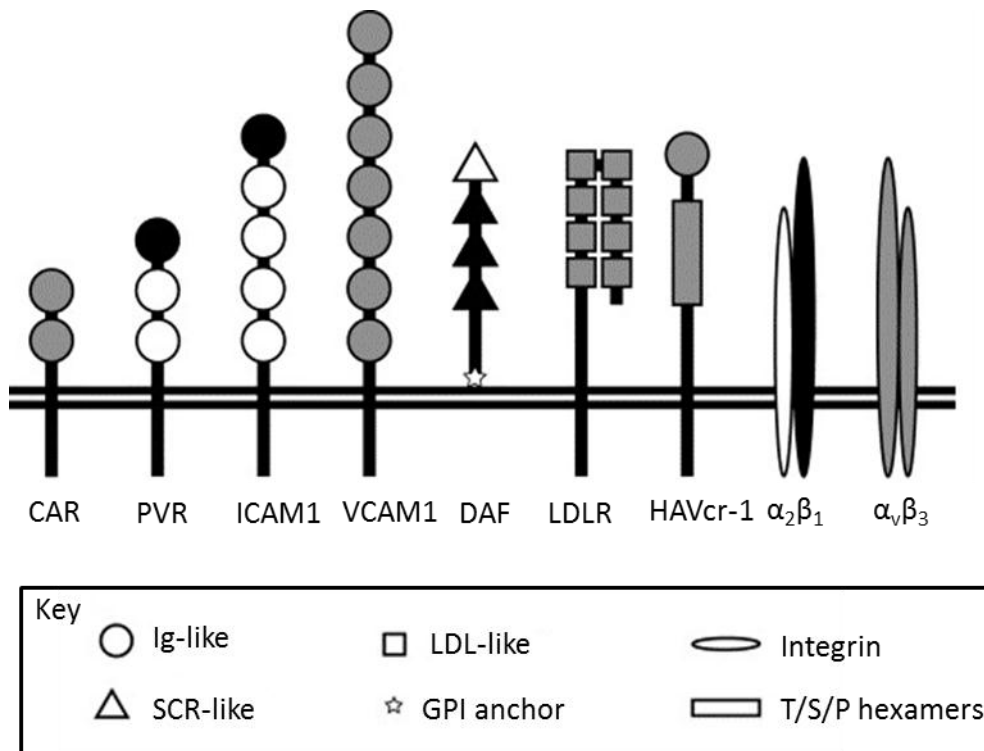


**Figure 1.13 Schematic representation of receptors used by members of the picornavirus family.**

Regions involved in virus binding are shown in black. Regions not known to be involved in virus binding are shown in white. Regions for which no information is available are shown in grey. CAR: coxsackie-adenovirus receptor, DAF: decay-accelerating factor, GPI: glycosylphosphatidylinositol, HAVcr-1: hepatitis cellular receptor type 1, ICAM-1: intracellular adhesion molecule type 1, LDL: low density lipoprotein, LDLR: low density lipoprotein receptor, PVR: poliovirus receptor, SCR: short consensus repeat, T/S/P: threonine/serine/proline, VCAM-1: vascular cell adhesion molecule type 1. Figure reproduced from (Evans and Almond, 1998).

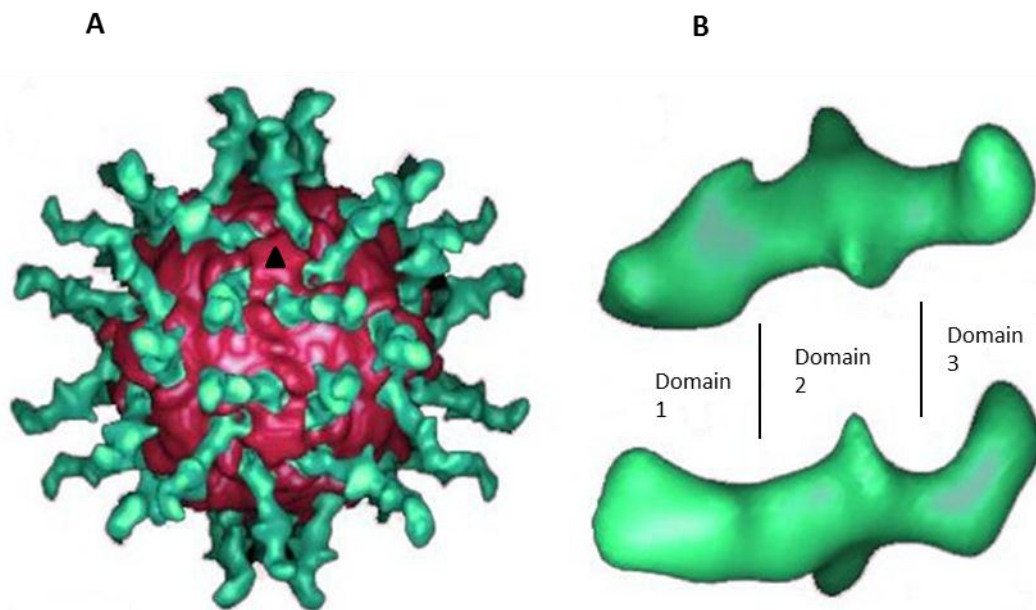


**Figure 1.14 Domain 1 of the receptor binds in the canyon surrounding the fivefold axis.**

**A.** Cryo-EM reconstructions of poliovirus bound to its receptor (PVR). **B.** Two views of a single PVR molecule showing its domains, labeled domain 1, 2 and 3. Domain 1 inserts into the base of the canyon present around the fivefold. The fivefold axis indicated by a black triangle. Figure adapted from (Belnap *et al.*, 2000b).

After binding to cell receptors, many picornaviruses become internalised by endocytosis. For example, after FMDV binds to its cell surface receptors of epithelial cells, FMDV gains entry into the cell by clathrin-dependent endocytic pathway (Berryman *et al.*, 2005), whereas cell-culture adapted FMDV uses caveolin-dependent endocytic pathway (O'Donnell *et al.*, 2008). Upon binding to PVR, PV enters the cell using receptor-mediated endocytosis which is clathrin, caveolin, flotillin and microtubule independent but tyrosine kinase and actin-dependent (Brandenburg *et al.*, 2007). Major and minor group HRVs bind to ICAM-1 or LDLR, respectively and enter the cells via clathrin dependent or independent endocytic pathway or macropinocytosis (Fuchs and Blaas, 2010).

#### 1.6.4.2 Particle alterations and uncoating

In enteroviruses such as PV and HRV, VP4 and the N-terminus of VP1 are internal to the capsid. At physiological temperature these internal capsid proteins are transiently externalised and this phenomenon is referred to as capsid “breathing”. Capsid breathing demonstrates that picornavirus capsids are in a metastable state and ready to undergo conformational rearrangements required for the release of RNA, when the appropriate trigger is received.



The conformational changes in the capsid involve the irreversible externalisation of N-terminus of VP1 and the release of VP4. The conversion of native particle to an altered “A” particle involves the loss of VP4. The “A” particle is characterised by increased hydrophobicity, altered antigenicity and sensitivity to proteases and a lower sedimentation coefficient of 135S relative to the native particle (160S) (Basavappa *et al.*, 1998). The “A” particle is 4% larger than the native particle at the twofold and fivefold axes and 1% larger at the threefold axis. The particle expansion occurs due to structural rearrangements of capsid proteins (Belnap *et al.*, 2000a).

Picornaviruses such as PV, BEV (and most enteroviruses) have a pocket factor present in a hydrophobic pocket formed by VP1 below the floor of the canyon (Figure 1.7). The pocket factor has been suggested to be important for particle stability and its release from the pocket a prerequisite for virus uncoating (Rossmann *et al.*, 2002). Binding sites for the pocket factor and receptors such as ICAM1 and PVR overlap (section 1.5.2). Receptor binding displaces the pocket factor, contributing to conformational changes in the capsid, leading to the release of the viral RNA (Rossmann, 1994). Some compounds such as the Winthrop (WIN) compounds and their derivatives have a strong affinity for the same binding site in the hydrophobic pocket as the pocket factor. Therefore, after the displacement of the pocket factor, WIN compounds bind within the pocket, thereby stabilising the virus and preventing capsid uncoating (Rossmann, 1994) and (as reviewed in Smyth and Martin, 2002).

For some enteroviruses such as PV and HRV3, receptor binding at physiological temperature is sufficient to trigger conformational changes in the capsid. However, for other major group HRVs like HRV16, receptor binding and an acidic pH is required for capsid uncoating (Nurani *et al.*, 2003; Racaniello, 1996). After binding to its receptor, exposure of HRV2 to acidic pH in the endosomal compartments is critical to induce conformational changes in the capsid which subsequently lead to virus uncoating (Prchla *et al.*, 1994).

In contrast to enteroviruses, aphthoviruses are acid labile. As a result of this, FMDV capsids dissociate upon encountering mildly acidic pH in the early endosome. FMDV has been shown to bind and infect cells using receptors other than integrins. Therefore, receptors appear to be required for FMDV binding at the cell surface which helps concentrate the virus, and the acidic pH serves as the trigger for capsid to dissociate, thereby releasing the viral RNA (Mason *et al.*, 1993).

Upon receiving the appropriate trigger such as pH and/or receptor binding, picornaviruses undergo structural rearrangements in the capsid. Enteroviruses such as PV and HRV follow a model of cell entry where the native particle (160S) is converted to an “A” particle (135S) from which RNA release takes place, leaving behind an intact empty capsid (80S) (Figure 1.15A).

However, other picornaviruses such as aphthoviruses do not appear to follow this model of uncoating where RNA release takes place through an intact particle. Instead, aphthoviruses such as FMDV appear to dissociate upon encountering low pH in the early endosome, thereby releasing the viral RNA (Figure 1.15B). In contrast to this existing dogma for aphthovirus uncoating, a recent study showed the detection of an intact but transient empty particle intermediate of the aphthovirus, equine rhinitis A virus (ERAV) (Tuthill *et al.*, 2009). This finding suggested a common model of uncoating involving the formation of an intact intermediate particle by all picornaviruses.

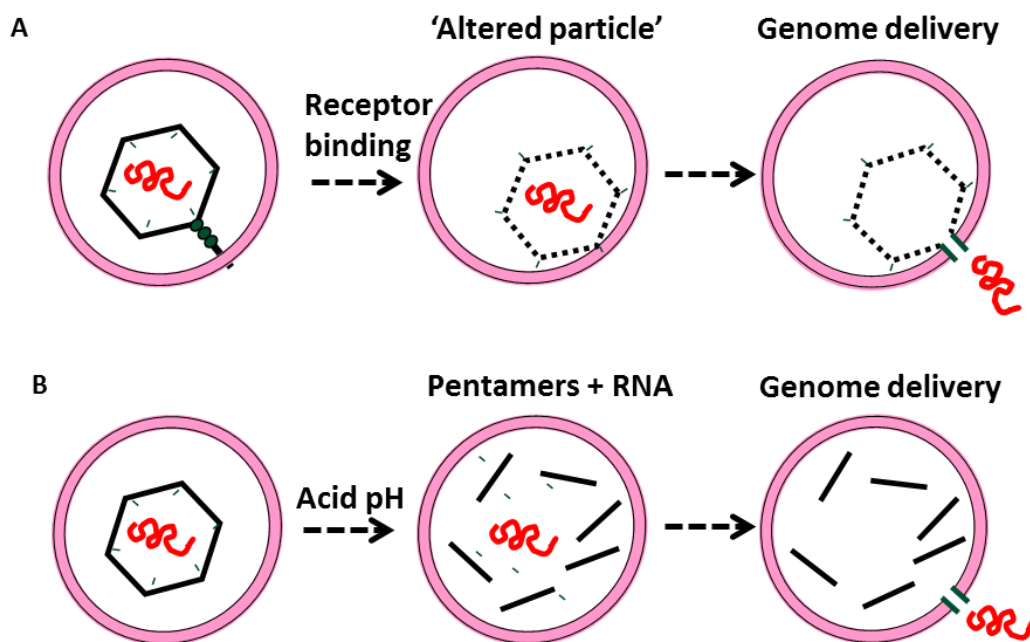


**Figure 1.15 Models for picornavirus membrane permeabilisation.**

**A.** Upon receptor binding, PV capsid undergoes conformational changes, resulting in the exposure of capsid proteins which facilitate delivery of the viral genome through an intact particle. **B.** Upon encountering low pH, the FMDV capsid dissociates to release the viral genome.

PV "A" particles can be formed by heating to 50°C (Curry *et al.*, 1996). It is conceivable that the virus requires high activation energy for capsid conformational changes. The dependence on temperature and activation energy to convert native virus particles to "A" particles in the presence or absence of receptors is different. Studies by Tsang *et al.*, showed that the receptor acts as a catalyst to lower the activation energy required for transition resulting in increased particle conversion from native to "A" particles (Tsang *et al.*, 2001). The activation energy barriers can be lowered by other physiological factors *in vivo* including endosomal acidification

and binding and unbinding metal ions (Garriga *et al.*, 2012; Hogle, 2002) and (as reviewed in Mateu, 2011).

The trigger for conversion of “A” particles to empty particles is not known. The overall shape and dimensions of 135S and 80S are similar. Empty capsids are formed after the release of RNA from 135S particles. Therefore, RNA density observed in cryo-EM reconstructions of PV native (160S) and “A” particles (135S) particles was absent in the 80S particles (Belnap *et al.*, 2000a).

Comparison of cryo-EM reconstructions of PV “A” particles with “A” particles from which the first 31 amino acids at the N-terminus of VP1 were proteolytically removed, revealed the VP1 N-terminus was present near the “propeller tip” around the threefold axis. The “ridge” of density connecting the fivefold mesa with the propeller tip was observed in the “A” particle but not in native particle (Figure 1.16). The “ridge”, was modelled as a potential amphipathic helix and N-terminal residues of VP1 have been attributed to the observed ridge density (Bubeck *et al.*, 2005)

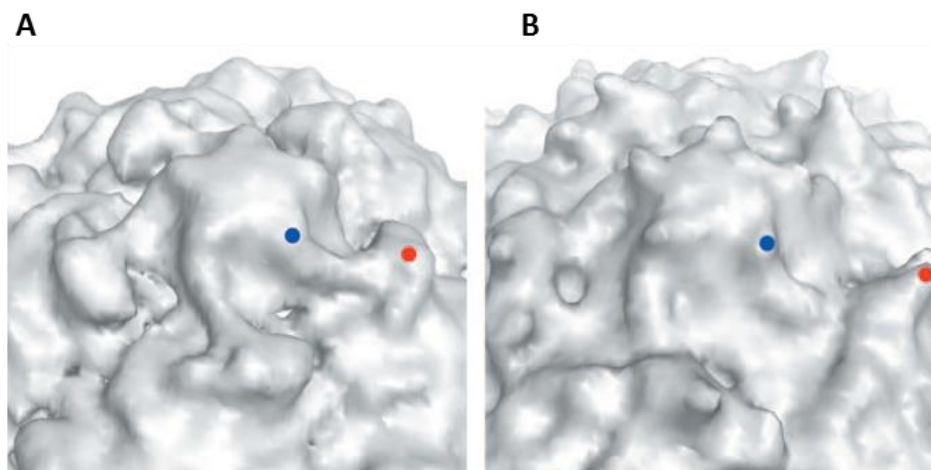


**Figure 1.16 The ridge in PV “A” particles comprised of VP1 N-terminus.**

**A.** Cryo-EM reconstruction of the PV “A” particle showed the linear “ridge” connecting a point on the fivefold mesa (blue dot) with the propeller tip (red dot). **B.** The “ridge” is not observed connecting a point on the fivefold mesa (blue dot) with the propeller tip (red dot) in the native PV particle. Figure reproduced from (Bubeck *et al.*, 2005).

Both native particles and “A” particles were found to be reactive with antibodies raised against peptide corresponding to the N-terminal residues of VP1 (Roivainen *et al.*, 1993). These findings provided evidence for the externalisation of VP1 N-terminal residues in the “A” (135S) particles. The structural rearrangements in VP1 associated with cell entry were determined by 3D reconstructions of cryo-EM images of PV “A” particles bound to antibodies raised against residues of the VP1 N-terminus. Analysis of the antibody binding position in PV native particle breathing state, showed VP1 N-terminal externalisation occurred near the twofold axis (Lin *et*

*al.*, 2012), whereas in the PV “A” particles the VP1 N-terminus was externalised at the propeller tip. This observation suggested that the N-terminus of VP1 is directed to a different exit site during capsid “breathing” and when converted to the “A” particle.

Therefore, there is evidence to show the site of externalisation of VP1 N-terminus, however, the site of release of VP4 is unknown.

#### 1.6.4.3 Site of RNA release

Earlier X-ray crystallographic structures of PV and HRV revealed a solvent filled channel along the fivefold axis and the presence of VP4 and N-terminus of VP1, in close proximity to the fivefold axis, which became externalised during virus entry (Hogle *et al.*, 1985; Rossmann *et al.*, 1985). Displacement of the pocket factor by ICAM-1 binding mediated stronger interactions between ICAM-1 and the binding site which caused structural rearrangements in the vicinity of the pocket, resulting in an opening at the fivefold axis (as reviewed in Rossmann *et al.*, 2000). These observations led to the model of VP1 N-terminus and VP4 externalisation, and RNA egress via the channel present at the fivefold axis. The model proposed five copies of VP1 and VP4 would interact (in an experimentally undefined way) to permeabilise the membrane, possibly by pore formation, which would be contiguous with the solvent channel at the fivefold axis, thus facilitating the RNA egress from the fivefold axis of symmetry (Belnap *et al.*, 2000a; Belnap *et al.*, 2000b; Bubeck *et al.*, 2005; Hadfield *et al.*, 1997; Hewat and Blaas, 2004; Hogle, 2002). However, the dimensions of the openings observed in previous studies (Hewat *et al.*, 2002; Levy *et al.*, 2010; Rossmann *et al.*, 2000), were insufficient to allow RNA egress. The model for picornavirus RNA release has been updated over the last few years.

Comparison of HRV empty capsid and native virus revealed an expansion of the empty particle which involved hinge movements around VP1 pocket causing rearrangements of inter protomer and pentamer interactions which induced openings at the twofold axis (Figure 1.17A, C and E). The dimensions of these observed openings were sufficient to allow RNA egress (Garriga *et al.*, 2012).

The twofold axis being a likely site for RNA exit was also supported by cryo-EM reconstructions of PV capsids caught in the act of releasing RNA from a site at the twofold axis (Figure 1.18). The RNA density footprint was observed at a distance of 20 Å from the twofold axis, immediately above the observed opening at the twofold axis (Figure 1.18C) (Bostina *et al.*, 2011). Also, X-ray crystallographic studies of empty particles of enterovirus 71 (EV71) revealed capsid expansion and openings (8×25 Å) at the twofold axis (Wang *et al.*, 2012), expected to be sufficient to allow the release of viral RNA.

In the case of the openings observed at the twofold of HRV2, the overall negative charge of these openings would facilitate the expulsion of RNA which would be expected to be repulsed by the walls of the openings (Garriga *et al.*, 2012). Therefore, the updated model suggests an opening at the twofold axis as the site for RNA egress. Similar findings of structural rearrangements in different enteroviruses, reinforces the hypothesis that members of the *Enterovirus* genus follow a common theme for capsid uncoating. Other picornaviruses, for example, aphoviruses such as FMDV, dissociate into pentameric capsid subunits as part of the uncoating process. However, there is increasing evidence that even for these viruses, the genome is released from an intact particle prior to the act of dissociation [(Tuthill *et al.*, 2009) and unpublished work at The Pirbright Institute]. Therefore, it is possible that a common theme exists for genome delivery by all picornaviruses.

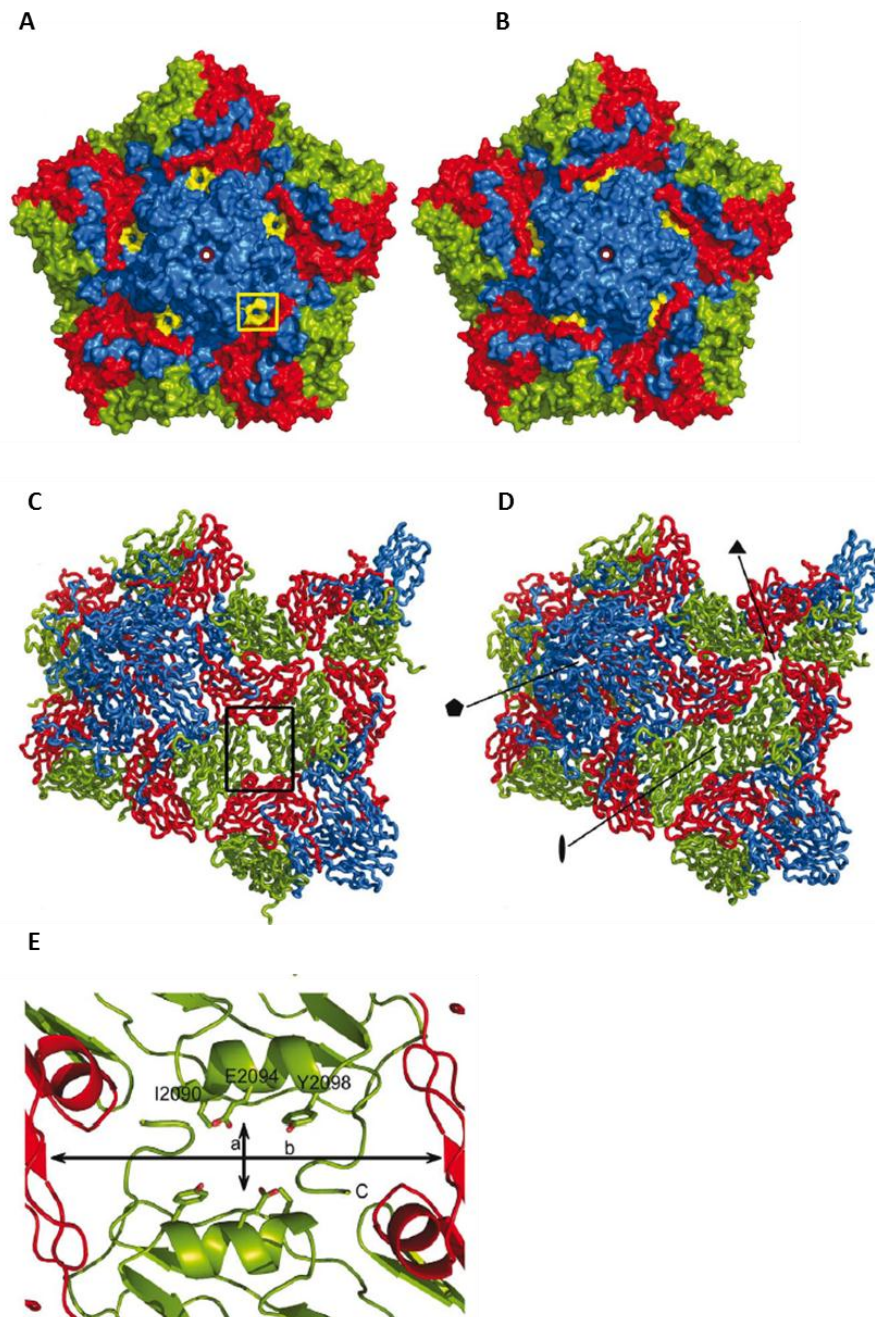


**Figure 1.17** Openings at the twofold axis with dimensions consistent with that required for the release of viral RNA.

**A.** Formation of pores in a pentamer of HRV2 empty particle. The residues forming the outer opening of the pore are highlighted in yellow. One pore is highlighted in a yellow box. **B.** Pore formation not observed in a pentamer of HRV2 native virus particle. The residues highlighted in yellow in panel A are also shown here. **C.** Inter-pentamer contacts of empty capsid depicted as ribbons. An opening in the interface of pentamers (highlighted by a black box) is observed. **D.** Inter-pentamer contacts of native virus capsid depicted as ribbons. The position of the symmetry axes is indicated. **E.** Close-up view of the opening observed at the twofold axis in the empty capsid in panel C. The lines crossing the cavity correspond to distances of (a) 10.2 Å and (b) 30.5 Å. The side chains of VP2 exposed at the pentamer-pentamer interface are labelled. In panels A-E, VP1 is shown in blue, VP2 in green and VP3 in red. Figure adapted from (Garriga *et al.*, 2012).

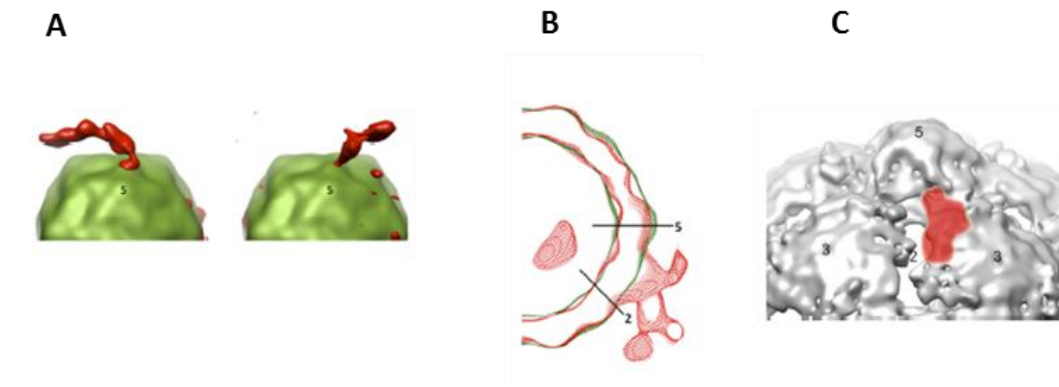


**Figure 1.18 Viral RNA exit site identified at the twofold axis.**

**A.** Surface representation of two virus particles caught in the act of genome release. Capsid shown in green and RNA density shown in red. **B.** Virus particles releasing their genomes (red) and the icosahedrally symmetrized average of the reconstructions is superimposed (in green). Twofold and fivefold axes of symmetry are indicated by black lines. **C.** Footprint of the putative RNA density (red), superimposed on a portion of the empty capsid. Axes of symmetry are numbered. At the chosen contour, holes near the twofold axis are evident and partly covered by the putative RNA footprint. Figure adapted from (Bostina *et al.*, 2011).

The formation of an “umbilicus” near the twofold axis of the virus was observed connecting virus particle to membrane, in cryo-electron tomography (cryo-ET) reconstructions of PV “A” particles interacting with liposomes. The umbilicus was formed close to the site of release of RNA and externalisation VP1 N-terminus. Virus particles did not appear to be in direct contact with the membrane but held  $\sim 50$  Å away from the membrane surface (Strauss *et al.*, 2013). This umbilicus may provide a conduit for the passage of RNA, protecting it from RNase in the endosomal environment.

The viral RNA is densely packed inside the capsid and is expected to become unwound and lose some of its secondary structure during release. The loss of secondary structure required by RNA release was demonstrated by the studies showing loss of an intercalating dye upon RNA release from particles (Brandenburg *et al.*, 2007). One possible explanation for the observation, in EM studies, of particles with varying RNA content (Bostina *et al.*, 2011) may be the pausing of RNA release every time a region of more secondary structure is encountered. The potential factors initiating the release of RNA from the capsid are not known but the high concentration of RNA within the particle and low concentration in the cell may serve as a driving force for RNA release. A recent study of HRV2 showed that RNA exit begins with the 3' end which is the less structured end and is followed by the 5' end (Harutyunyan *et al.*, 2013).

#### 1.6.4.4 Evidence for N-terminus of VP1 and VP4 in membrane permeabilisation

At room temperature, both VP4 and the N-terminus of VP1 are enclosed within the virus capsid and become transiently externalised during capsid breathing. When the appropriate trigger is received, the capsid undergoes a conformational change involving the irreversible externalisation of N-terminus of VP1 and the loss of VP4. Both, VP4 and the N-terminus of VP1 have been suggested to play a role in membrane permeabilisation, facilitating the transfer of RNA across the membrane. However, the precise role played by each protein remains to be defined.

Earlier studies showed that the externalised N-terminus of PV VP1 was responsible for binding liposome membranes (Fricks and Hogle, 1990). A synthetic peptide corresponding to the N-terminus of HRV2 VP1 partitioned into and permeabilised membranes. The peptide mediated selective release of FITC labelled dextrans from isolated endosomes. This indicated the formation of size restrictive membrane pores rather than membrane disruption (Prchla *et al.*, 1995). The involvement of VP1 N-terminus in membrane anchoring was shown by the release of membrane associated PV “A” particles upon treatment with V8 protease which specifically cleaved VP1 to release the N-terminal 30 residues (Tuthill *et al.*, 2006). As described previously (section 1.6.4.2), studies using antibodies raised against the N-terminus of PV VP1 showed that they reacted with PV native particles during capsid breathing and PV “A” particles (Roivainen *et al.*, 1993). Antibodies against the N-terminus of VP1 identified the exit site of VP1 N-terminus in native PV particles at the twofold axis and at the propeller tip in the “A” particles. This may suggest that the N-terminus of VP1 is externalised at the twofold axis during capsid breathing and upon receptor binding is moved to the canyon, thereby enlarging the opening at the twofold axis. Either after or concurrent with RNA release from the twofold axis, the N-termini of VP1 move back to the twofold axis (Lin *et al.*, 2012).

The findings demonstrating the membrane binding and permeabilising function of VP4 include the following: PV VP4 has been shown to partition into cellular and liposomal membranes. Mutations at the N-terminus of PV VP4 (threonine at position 28), either delayed or prevented delivery of RNA during infection and the same mutations also affected the electrophysiological properties of ion channels formed by the mutant viral particles in planar lipid membranes (Danthi *et al.*, 2003; Tosteson *et al.*, 2004), indicating VP4 plays a role in facilitating genome delivery across the membrane. VP4 released during conversion of PV 160S to 135S upon binding to receptor decorated liposomes was shown to be associated with membranes (Tuthill *et al.*, 2006) and recombinant VP4 of HRV16 permeabilised membranes without membrane disruption (Davis *et al.*, 2008), indicating the possibility of membrane pore formation. Dimerisation of VP4 at its N-terminus was observed during capsid breathing of HRV16



containing a serine to cysteine mutation in VP4 (Katpally *et al.*, 2009). Also, VP4 is myristoylated at the N-terminus (Chow *et al.*, 1987), and the myristate group is known to target proteins to membranes (described further in section 4.1). These observations suggest that membrane binding and insertion of VP4 may be by its N- terminus.

Despite this information, the role of VP4 in the induction of membrane permeability remains poorly understood. The site of VP4 release from the capsid, demonstration of the terminus of VP4 that is externalised first and the terminus (or if both termini) responsible for membrane insertion to mediate RNA delivery and the mechanism for VP4-mediated membrane permeability are yet to be determined.

## 1.7 Aims

The capsid proteins, VP4 and N-terminus of VP1 have been suggested to contribute to membrane permeability, thereby facilitating the transfer of RNA across the membrane. The precise roles of the capsid proteins in cell entry and the mechanism of induction of membrane permeability are not known. In this thesis, I have investigated membrane permeability induced by capsid protein VP4 using HRV as a model virus and liposomes as model membranes. The overall aim is to further the understanding of the role of VP4 in picornavirus cell entry. To this end, the specific objectives of this project are as follows:

- To develop a system for the expression and purification of recombinant VP4
- To characterise conditions influencing VP4-induced membrane permeability
- To determine the mechanism for induction of membrane permeability
- To map the function of VP4 and investigate the role of VP1 in cell entry
- To explore biophysical approaches for determining the structure of the VP4 membrane pore complex

# **Chapter 2**

# **Materials and Methods**

## 2.1 General Materials

### 2.1.1 Bacterial strains

*Escherichia coli* (*E. coli*) DH5 $\alpha$  (F<sup>-</sup>,  $\Phi$ 80dlacZ $\Delta$ M15, *endA1*, *recA*, *hsdA1*, (rk<sup>-</sup>, mk<sup>+</sup>), *phoA*, *supE44*  $\lambda$ -, *thi-1*, *deoR*, *gyrA96*, *relA1*, ( $\Delta$ *lacZYA-argF*), U169,  $\lambda$ ) were purchased as chemically competent cells from Invitrogen and used for cloning purposes.

*E. coli* BL21(DE3) pLysS were purchased as chemically competent cells from Invitrogen, genotype F<sup>-</sup> *ompT hsdSB* (rB<sup>-</sup>mB<sup>-</sup>) *gal dcm* (DE3) pLysS (Cam<sup>R</sup>) and used for protein expression purposes.

*E. coli* Rosetta-gami B (DE3) pLacI were purchased from Novagen, genotype F-*ompT hsdSB*(rB-mB-) *gal dcm lacY1 ahpC gor522::Tn10 trxB* pRARE (Cam<sup>R</sup>, Kan<sup>R</sup>, Tet<sup>R</sup>) and used to enhance the expression of proteins by supplying tRNAs for rarely used codons. The rare tRNA genes are present on the same plasmids that carry the *lac* repressor genes.

### 2.1.2 Cell lines

Original stock of Hela Ohio cells were obtained from the American Type Culture Collection (ATCC). Lab stocks maintained at a passage number of below 20.

### 2.1.3 Expression vectors

The commercial bacterial expression vectors pET-23a and pET-23d were purchased from Novagen. pET-23a was used to express PV and FMDV VP4 and VP4 fusion proteins and pET-23d was used to express HRV VP4 and VP4 fusion proteins.

Plasmid encoding Hisx9 tag followed by trpLE in the pMM-LR6 vector (a kind gift from Dr. Fu, the Chou Lab) was used for the expression of His-trpLE-VP4 fusion protein.

### 2.1.4 Antibodies

Commercial antibodies used were monoclonal anti-polyhistidine peroxidase conjugate clone His-1 (Sigma Aldrich) (dilution 1:1000), polyclonal sheep anti-HRV VP4 C-terminus and VP4 N-terminus (kind gift from Professor Rowlands, University of Leeds) (dilution 1:1000). The commercial secondary antibody donkey anti-sheep IgG-alkaline phosphatase (Molecular probes, Invitrogen) (dilution 1:2000).

### 2.1.5 Detergents

Sodium-n-dodecyl sulphate (SDS) was purchased from Sigma-Aldrich, 14:0 Lyso PG 1-myristoyl-2-hydroxy-sn-glycero-3-phospho-(1'-rac-glycerol) sodium salt (LMPG), 3-[(3-Cholamidopropyl)dimethylammonio]-2-hydroxy-1-propanesulfonate (CHAPSO), N,N-

dimethyldodecylamine N-oxide (LDAO), dodecylphosphocholine-12 (DPC), n-Nonylphosphocholine (FOS-9), n-Tetradecylphosphocholine (FOS-14), n-octyl- $\beta$ -D-glucopyranoside (OG), 06:0 PC 1,2-dihexanoyl-*sn*-glycero-3-phosphocholine [DHPC (hexa)], 07:0 PC 1,2-diheptanoyl-*sn*-glycero-3-phosphocholine [DHPC (hepta)] , n-dodecyl- $\beta$ -D-maltoside (DDM), 3-Dodecylamido-N,N'-Dimethylpropyl Amine Oxide (LAPAO) were purchased from Affymetrix or Sigma Aldrich.

### 2.1.6 Lipids

The following phospholipids and cholesterol were purchased from Avanti Polar Lipids, as 10 mg/ml solutions in chloroform. Stock solutions were aliquoted using Hamilton glass syringes into glass vials, sealed with parafilm and stored at -20°C.

PA	L- $\alpha$ -Phosphatidic acid (egg, monosodium salt)
PC	L- $\alpha$ -Phosphatidylcholine (egg)
PE	L- $\alpha$ -phosphatidylethanolamine (Brain, Porcine)
Rhod PE	L- $\alpha$ -Phosphatidylethanolamine with lissamine rhodamine B labelled head groups
PI	L- $\alpha$ -phosphatidylinositol (Soy, sodium salt)
SM	Sphingomyelin (Egg, Chicken)
BMP	bis(monooleoylglycero)phosphate (S,R Isomer) (ammonium salt)

## 2.2 Manipulation of recombinant DNA

### 2.2.1 DNA oligonucleotide primers

Primers were supplied by Sigma-Aldrich as lyophilised powders and resuspended in deionised water to a stock concentration of 100  $\mu$ M and stored at -20°C.

### 2.2.2 Polymerase chain reaction (PCR)

#### 2.2.2.1 Preparative PCR

The proof reading KOD hot start DNA polymerase kit (Novagen) was used to amplify the region of interest from HRV, PV or FMDV plasmids. Each PCR reaction contained 0.2 mM dNTPs, 1 mM MgCl<sub>2</sub>, 10 % v/v DMSO, 1 x KOD buffer, 1 Unit (U) KOD polymerase, 2 mM forward primer, 2 mM reverse primer, ~50 ng template DNA and was made up to 50  $\mu$ l with nuclease free water (Sigma-Aldrich). DNA was amplified in a thermal cycler (Eppendorf) and the reactions were heated to 96°C for 15 seconds, followed by 25 cycles of the following steps; denaturation at 95°C for 2 sec, primer extension at 54°C for 2 sec and annealing at 72°C for 2 sec.

### 2.2.2.2 Colony screen PCR

PCR was performed in a total volume of 100  $\mu$ l in a 0.2 ml PCR tube. The reaction contained 0.5  $\mu$ M of appropriate forward and reverse primer, 1x PCR buffer (200 mM Tris-HCl -pH8.4, 500 mM KCl, supplied as 10x concentrate), 0.2 mM of each deoxyribonucleotide triphosphate (dNTPs), 1.5 mM MgCl<sub>2</sub>, 2.5 Units of Taq DNA polymerase (Life technologies Ltd.), nuclease-free water (Millipore) and a single colony picked from a LB agar plate (with appropriate antibiotics). Tubes were incubated in a thermal cycler (Eppendorf) at 98°C for 10 minutes to completely denature the DNA. 25 cycles of the PCR amplification were carried out. Each cycle consisted of 30 sec at 98°C to completely denature template DNA, annealing at 60°C for 30 sec and extension at 72°C for 1 min. This was followed by cooling to and maintaining the reaction at 4°C.

### 2.2.3 DNA sequencing

Template DNA (500 ng) was heated to 96°C for 1 min to completely denature the DNA. PCR was performed in a total volume of 10  $\mu$ l in a 0.2 ml PCR tube. A 10  $\mu$ l reaction mixture typically contained 50 ng of denatured plasmid DNA template, 1.6 pM of forward or reverse primer, 2  $\mu$ l of 5x Big Dye sequencing buffer, 0.25  $\mu$ l of big dye terminator (Big Dye Terminator v3.1 cycle sequencing kit, Applied Biosystems). Typical reactions started with 1 min denaturing at 96°C followed by 25 amplification cycles. Each cycle consisted of 10 sec denaturing at 96°C, 5 sec annealing at 50°C and 4 min extension at 60°C. This was followed by cooling to and maintaining the reaction at 4°C. DNA was sequenced to confirm the sequence and orientation of the insert in each clone. Sequencing was performed in-house with 3730 DNA Analyzer, Applied Biosystems.

### 2.2.4 Restriction digestion of DNA

All restriction enzymes were purchased from New England Biolabs (NEB). Restriction digests were performed under the optimal conditions using the manufacturer's recommended buffer and incubation temperature. 10  $\mu$ g/ml of BSA (supplied at 10 mg/ml) was added where recommended. Diagnostic digests were typically performed in a total volume of 25  $\mu$ l. The reaction contained 0.5-1  $\mu$ g DNA, restriction enzyme at 10 units/ $\mu$ g of DNA, 1x of appropriate supplied 10x reaction buffer and nuclease free water (Millipore). The reaction was mixed thoroughly and incubated for 2 hrs at 37°C. Preparative digests used for subsequent subcloning contained up to 10  $\mu$ g DNA in a total reaction volume of 50-100  $\mu$ l and incubated for 2-3 hrs at 37°C. 1x DNA loading buffer was added to the reaction and the digestion products analysed by agarose gel electrophoresis (section 2.2.5).

### 2.2.5 Agarose gel electrophoresis

Agarose was dissolved in 1x TAE buffer [242 g Tris-base, 57.1 ml glacial acetic acid, 100 ml 0.5 M EDTA, make up to 1 L with D2O (50x)] to 0.8 %-1.5 % (w/v) with careful heating in a microwave. When cooled, ethidium bromide was added to approximately 0.3 µg/ml (using a 10 mg/ml stock in water) and the molten agarose was poured into an electrophoresis gel cast and a comb inserted. The gel was allowed to set and then placed in an electrophoresis tank (Bio-Rad) containing 1x TAE buffer. Samples for electrophoresis were prepared by adding loading dye (NEB) to a final concentration of 1x. 1 Kb and 100 bp DNA markers (NEB) were electrophoresed alongside samples. Gels were subjected to 90 V for 1 hr. Fluorescent DNA bands were visualised on a UV transilluminator (Bio-Rad) and images captured using a Bio-Rad gel documentation system.

### 2.2.6 Gel extraction of DNA

DNA fragments were excised from agarose gel using a sterile scalpel, under preparative UV illumination on a transilluminator (FotoPrepl, Fotodyne). DNA was purified from the gel by following manufacturer's instruction for QIAquick gel extraction microcentrifuge protocol (Qiagen). Briefly, agarose was solubilised, DNA absorbed onto the matrix, washed with high salt and eluted with nuclease free water (Sigma Aldrich). DNA was quantified using the spectrophotometry (Nanodrop 8000, Thermo Scientific) and stored at -20°C.

### 2.2.7 DNA ligations

All ligations were performed in a total reaction of 20 µl. Vector was dephosphorylated using rapid alkaline phosphatase (Roche Applied Science). Digested PCR product and dephosphorylated vector were added at a ratio of 5:1 and 3:1 to 1x T4 DNA ligase buffer, 5 U of T4 DNA ligase (NEB) and nuclease free water (Millipore). The reaction was mixed thoroughly and incubated at 16°C or o/n at room temperature. Some of the ligation reaction was used for transformation of DH5α *E.coli* cells (section 2.2.8).

### 2.2.8 Transformation of chemically competent bacteria

50 µl of chemically-competent DH5α *E.coli* cells were thawed on ice, followed by the addition of 10 µl of the DNA ligation mix (section 2.2.7) and swirled gently to mix. The cells were incubated on ice for 20 min, heat shocked in a 42°C water bath for 45 sec and then returned to ice for 2 min. 500 µl SOC medium (without antibiotics) was added and placed in a shaking incubator for 1 hr at 37°C. The cells were then plated out onto LB agar plates containing the appropriate antibiotic(s) (Kanamycin used at 50 µg/ml and ampicillin at 100 µg/ml). Plates were inverted and incubated o/n at 37°C.

For the transformation of DH5 $\alpha$ , BL21 (DE3) pLysS or Rosetta-gami B (DE3) pLacI *E.coli* cells, with plasmid DNA, 20-50 ng of DNA was used. The transformed cells were recovered and plated as described above.

### **2.2.9 Bacterial cultures**

A single bacterial colony was picked from an LB agar plate and added to 5 ml LB medium containing the appropriate antibiotic(s) (Kanamycin used at 50  $\mu\text{g/ml}$  and ampicillin at 100  $\mu\text{g/ml}$ ). This was carried out under aseptic conditions. The 5 ml culture was incubated o/n with continuous shaking (250 rpm) at 37°C. A sample of the small scale culture (~1 ml) was used to inoculate 250 ml of LB media containing the appropriate antibiotic(s). The large scale culture was incubated o/n with continuous shaking (250 rpm) at 37°C.

### **2.2.10 Purification of bacterial DNA**

Small scale bacterial cultures (5 ml) grown o/n (section 2.2.9) were centrifuged at 4000 x g for 20 min at 4°C and the medium thoroughly removed from the cell pellet. Plasmid DNA was isolated by following the manufacturer's instructions for PureLink Quick Plasmid Miniprep protocol using centrifugation (Invitrogen). In brief, cells were resuspended in cell resuspension buffer (250  $\mu\text{l}$ ), lysed by addition of cell lysis buffer (250  $\mu\text{l}$ ) and incubated at room temperature for 5 min. Cells were then neutralised with neutralisation solution (350  $\mu\text{l}$ ) before centrifugation at 18,000 x g for 10 min. The cleared bacterial lysate was then added to a miniprep column and centrifuged at 17900 x g for 1 min. Wash solution (800  $\mu\text{l}$ ) was applied twice to the column and centrifuged through the column at 18,000 x g. The column was transferred to a sterile 1.5 ml tube and the DNA eluted with 30-50  $\mu\text{l}$  of nuclease free water (Millipore) by centrifugation.

Large scale bacterial cultures (250-500 ml) grown o/n (section 2.2.9) were centrifuged at 6000 x g for 30 min at 4°C and cell pellet harvested. The plasmid DNA was then purified from the pelleted cells using a plasmid maxi kit (Qiagen) by following manufacturer's instructions. In brief, the bacterial pellet was resuspended in buffer P1 (10 ml), lysed by addition of buffer P2 (10 ml) and incubated at room temperature for 5 min. The cell lysate was neutralised with buffer P3 (10 ml), incubated on ice for 20 min and then centrifuged at 20000 x g for 30 min at 4°C. A QIAGEN tip 500 maxiprep column was equilibrated with buffer QBT (10 ml) and the cleared bacterial lysate was allowed to flow through the column by gravity. The column was washed twice with buffer QC (30 ml) and the DNA eluted with elution buffer QF (15 ml). Isopropanol (10.5 ml) was added to the eluted DNA and centrifuged at 15000 x g for 30 min at 4°C. The s/n was decanted from the DNA pellet, which was then washed with 70 % ethanol (5 ml). After a final centrifugation step at 15000 x g for 10 min at 4°C, the ethanol was removed

and the DNA pellet air dried. The air dried pellet so obtained was resuspended in 0.5 ml of nuclease free water (Millipore).

The DNA obtained from miniprep and maxiprep protocols was stored at -20°C.

#### **2.2.11 Quantification of DNA**

The concentration of DNA was determined by using spectrophotometry (Nanodrop 8000, Thermo Scientific). Plasmid DNA (1 µl) was loaded onto the pedestal of the spectrophotometer and absorbance measurements were taken at 260 nm and 280 nm. This was used to automatically determine DNA concentration (based on DNA concentration being proportional to absorbance at 260 nm for a given path length). The ratio of absorbance at 260 nm and 280 nm was used to determine the purity of DNA (peak absorption by nucleic acid is at 260 nm, while peak absorption for contaminating proteins is at 280 nm).

#### **2.2.12 Bacterial glycerol stocks**

Small scale bacterial cultures (1ml) were added to 225 µl of 80% glycerol in a sterile cryovial. The glycerol stock was mixed well and stored at -80°C. Viability of the cells was checked after one week by scraping off some of the frozen stock and streaking onto an LB agar plate containing the appropriate antibiotic(s).

## **2.3 Protein biochemistry**

### **2.3.1 Sodium dodecyl sulphate -polyacrylamide gel electrophoresis (SDS-PAGE)**

For reducing SDS-PAGE, 10% resolving gel [2 ml glycerol, 5 ml Tricine gel buffer (3 M Tris, 3% (w/v) SDS, pH8.45), 3.8 ml 40% acrylamide (Sigma) and made up to 15 ml with D<sub>2</sub>O] and 5% stacking gel (1.5 ml Tricine gel buffer, 0.62 ml 40% acrylamide/bis-acrylamide and made up to 4.1 ml with D<sub>2</sub>O) were prepared. The amounts of 40% T acrylamide were adjusted to 4.7 ml or 6.2 ml for 12% and 16.5% resolving gels, respectively. 0.1% ammonium persulphate (APS) and 0.001% N,N,N',N'-Tetramethylethylenediamine (TEMED) were added to the resolving and stacking gel mix before pipetting into a gel cast. Gel comb of choice was inserted to make the wells. The gels were placed in a miniPROTEAN® Tetra Cell gel electrophoresis tank (Bio-Rad). 1xTricine cathode buffer [1M Tris, 1M Tricine, 0.1% (w/v) SDS (10x)] was added to the inner chamber and Tricine anode buffer (0.2 M Tris, pH8.9) in the outer chamber. All protein samples were loaded with red loading buffer [10% glycerol, 2% (w/v) SDS, 0.01% (w/v) phenol red, 62.5 mM Tris-HCl pH6.8 (NEB) to give a 1x final concentration] and 10 mM Dithiothreitol (DTT). Samples were heated at 96°C for 10 min, loaded into the wells of the gel and subjected



to electrophoresis at room temperature at a constant voltage of 120 V for typically 1 hr. The migration of protein samples was compared with pre-stained molecular weight markers (Precision Plus Protein Dual colour standards, Bio-Rad).

### **2.3.2 Native polyacrylamide gel electrophoresis (PAGE)**

Pre-cast 4-20% Mini-PROTEAN TGX native-PAGE gels (Bio-Rad) were used for the analysis of protein samples under non-reducing and non-denaturing conditions. Samples were mixed with an equal volume of native loading buffer (30% glycerol, 0.05% bromophenol blue, 150 mM Tris-HCl pH 7.0). Samples were not heated prior to loading onto native PAGE. The native gels were placed in a miniPROTEAN® Tetra Cell gel electrophoresis tank and proteins separated using Tris-glycine running buffer (0.025 M Tris base, 0.192 M Glycine, pH8.5) at 4°C at a constant voltage of 80 V for approximately 3 hrs.

### **2.3.3 SDS-PAGE fixatives**

- Trichloroacetic acid fixation  
SDS-PAGE gels were submerged in 12% trichloroacetic acid for 1-3 hrs with gentle agitation at room temperature.
- Formaldehyde fixation  
A solution of 25% ethanol, 15% formalin (formalin is 35% formaldehyde) was prepared. SDS-PAGE gels were submerged in the solution for 1 hr with gentle agitation at room temperature.
- Glutaraldehyde fixation  
SDS-PAGE gels were submerged in 10% glutaraldehyde for 1 hr with gentle agitation at room temperature. Gels were washed twice with D<sub>2</sub>O for 20 min each before staining with Coomassie.

### **2.3.4 Staining methods**

#### **2.3.4.1 Coomassie brilliant blue staining**

Polyacrylamide gels (sections 2.3.1 and 2.3.2) were incubated in Coomassie Brilliant Blue stain (40 % v/v Methanol, 10 % v/v Acetic acid, 0.25 % w/v Coomassie Brilliant Blue R250) overnight at room temperature with continuous rocking. Gels were destained with destaining solution (40 % v/v methanol, 10 % v/v acetic acid) until protein bands became visible.

#### **2.3.4.2 Silver staining**

**Polyacrylamide gels** (sections 2.3.1 and 2.3.2) were stained with silver stain (Thermo Scientific) according to the manufacturer's instructions.

### 2.3.4.3 Other stains

**Polyacrylamide gels** (sections 2.3.1 and 2.3.2) were stained with other stains:

- Copper chloride ( $\text{CuCl}_2$ ) negative stain: The gel was rinsed in  $\text{D}_2\text{O}$  for 1 min.  $\text{D}_2\text{O}$  was discarded and the gel immersed in 50 ml 0.3 M  $\text{CuCl}_2$  with gentle agitation at room temperature until the protein bands were stained to desired intensity. The solution was discarded and the gel washed in  $\text{D}_2\text{O}$  for 3 min.
- Zinc imidazole negative stain: The gel was rinsed in  $\text{D}_2\text{O}$  for 1 min.  $\text{D}_2\text{O}$  was discarded and the gel immersed in 50 ml 0.2 M imidazole for 1 hr. The solution was discarded and gel immersed in 50 ml 0.3 M  $\text{ZnCl}_2$  with gentle agitation at room temperature until the background became dark blue and the transparent protein bands became visible.
- Sypro orange stain: The gel was immersed in 50 ml of 1:5000 dilution of Sypro orange stain (Bio-Rad) in 7.5% (v/v) acetic acid. The tray was covered with foil for 1 hr with gentle agitation at room temperature. The gel was then rinsed with 7.5% (v/v) acetic acid for 30 sec. The gel was placed on a UV light box (BioRad) for imaging.

### 2.3.5 Western blot

After SDS-PAGE, proteins were transferred to polyvinyl difluoride (PVDF) membrane (Immobilon, Millipore) at 90 V for 1 hr in transfer buffer (0.2 M Tris, 20 % v/v methanol). Membranes were blocked for 1 hr at room temperature or o/n at 4°C in blocking buffer [0.1% (v/v) PBS-Tween 20 (PBS-T), 5% (w/v) dried Marvel milk] with continuous rocking. The membrane was incubated with the primary antibody in blocking buffer at the relevant dilution for 1 hr at room temperature, with continuous rocking. The membrane was then washed three times in 0.1% PBS-T, changing the wash once every 20 min. This was followed by incubating the membrane with the secondary antibody in blocking buffer at the relevant dilution for 1 hr at room temperature, with continuous rocking. For horseradish peroxidase (HRP) conjugated primary antibodies, a secondary antibody was not necessary. The membranes were washed as described previously. Excess of PBS-T was removed and the electrochemiluminescence (ECL) solution (Thermo Scientific) pipetted over the membrane. The membrane was transferred to a light-proof cassette and developed manually using CL-XPosure film (Thermo scientific).

### 2.3.6 Densitometry analysis of western blots

Kodak image station 4000r was used to analyse Western blots by densitometry. Rectangular boxes were drawn around the bands to be compared and control area. Densitometry values were generated using the Carestream Molecular Imaging software, Network edition (MI NE). Mean intensity values were used to generate the graphs.

### **2.3.7 Autoradiography**

Following SDS-PAGE, the gel was submerged in destain (40 % v/v methanol , 10 % v/v acetic acid) for 30 min with gentle agitation at room temperature. The destain solution was discarded and gel submerged in enlightening solution (PerkinElmer) for 30 min with gentle agitation at room temperature. The gel was dried using the vacuum at 80°C. The gel was exposed to CL-XPosure film (Thermo Scientific) in a light-proof cassette at -80°C for up to 2 weeks and developed manually.

### **2.3.8 Chemical crosslinking**

#### **2.3.8.1 Chemical crosslinking with DSP**

Rehydrated samples of VP4His were treated with Dithiobis[succinimidyl propionate] (DSP) (Thermo scientific) to final concentration of 0.5 mM or 1 mM, in a total reaction volume of 25 µl. The reaction was incubated for 20 min at 25°C. The reaction was terminated by the addition of 1 M Tris-HCl, pH7.5 to a final concentration of 50 mM, for 15 min at 25°C. If required, cross-linking was reversed by the addition of 50 mM DTT and incubation at 37°C for 30 min.

#### **2.3.8.2 Chemical crosslinking with glutaraldehyde**

Rehydrated samples of VP4His were mixed with 5 µl of 2.3% freshly prepared solution of glutaraldehyde, in a total volume of 25 µl. The reaction was incubated for 5 min at 37°C. The reaction was terminated by the addition of 1 M Tris-HCl, pH8.0, to a final concentration of 50 mM.

### **2.3.9 Acetone precipitation**

Four times the sample volume of acetone (pre-cooled to -20°C) was added, mixed thoroughly on a vortex and incubated for 60 min at -20°C. For smaller proteins, the acetone containing samples were incubated o/n at -20°C. The precipitated protein was collected by centrifugation at 21, 000 x g for 20 min. The precipitated protein was resuspended in the appropriate buffer.

### **2.3.10 Measurement of total protein concentration**

#### **2.3.10.1 Bicinchoninic acid protein assay**

Bicinchoninic acid (BCA) protein assay (Thermo scientific) was used to determine protein concentrations, according to manufacturer's instructions. Briefly, 10 µl of the protein sample (in triplicate) was mixed with the BCA reagents A and B (50:1, reagent A:B), mixed thoroughly and incubated at 37°C for 30 min. The plate was cooled to room temperature before measuring the absorbance at 562 nm using a plate reader. A series of dilutions of known concentrations of BSA were prepared and assayed alongside the protein samples and a

standard curve plotted. The standard curve was used to determine the protein concentration of each unknown sample.

#### **2.3.10.2 Bradford assay**

Bradford assay (Thermo Scientific) was used to determine protein concentrations, according to manufacturer's instructions. Briefly, 300  $\mu$ l of Bradford reagent (coomassie blue G-250) was added to 10  $\mu$ l of the protein sample (in triplicate), mixed thoroughly, incubated at room temperature for 10 min and absorbance measured at 595 nm using a plate reader. A series of dilutions of known concentrations of BSA were prepared and assayed alongside the protein samples and a standard curve plotted. The standard curve was used to determine the protein concentration of each unknown sample.

#### **2.3.10.3 Spectrophotometry**

The concentration of protein was determined by using spectrophotometry (Nanodrop 8000, Thermo Scientific). Protein sample (2  $\mu$ l) was loaded onto the pedestal of the spectrophotometer and absorbance measurement taken at 280 nm.

## **2.4 Expression of GST-tagged VP4 in inclusion bodies**

One colony of *E.coli* BL21 (DE3) pLysS cells transformed (section 2.2.8) with pETVP4PreGST or VP4ThGST was added to 10 ml of LB (100  $\mu$ g/ml of ampicillin) and grown o/n at 37°C with constant shaking at 250 rpm. Where *E.coli* cells were co-transformed with pET-NMT, kanamycin (50  $\mu$ g/ml) and ampicillin (100  $\mu$ g/ml) were added to the media. 5 ml of the o/n culture was added to 500 ml LB (with appropriate antibiotics) and grown at 37°C with constant shaking at 250 rpm to an OD<sub>600</sub> 0.4. Myristic acid was added to a final concentration of 5  $\mu$ g/ml (using a stock solution in methanol) to *E.coli* cells co-transformed with pETNMT. The culture was induced with 1 mM IPTG for 4 hrs at 37°C. The culture was divided into 50 ml, pelleted and stored at -20°C.

## **2.5 Isolation of GST-tagged VP4 inclusion bodies**

Bacterial cell pellets from 50 ml culture volumes (section 2.4) were lysed with 10 ml of cold lysis buffer (20 mM Na<sub>2</sub>HPO<sub>4</sub>, pH7.4, 150 mM NaCl, 1% Triton X-100, 500  $\mu$ g/ml lysozyme and 1x protease inhibitors (Fermentas), incubated at 4°C for 1 hr on a rotational wheel. The sample was sonicated (10 micron amplitude, Misonix Microson) on ice with 30 sec on and 30 sec off x

10 cycles. The lysate was pelleted at 4000 x g for 15 min to remove cell debris. The pellet was resuspended in 2 ml 100 mM ammonium acetate and inclusion bodies pelleted at 4000 x g for 5 min. The inclusion bodies were resuspended and washed with 2 ml washing buffer (10 mM Tris, pH7.4, 100 mM NaCl, 1x protease inhibitors) and pelleted at 4000 x g for 5 min. The pellet was washed three times with 2 ml 0.1% sarkosyl followed by three washes with 2 ml wash buffer. At the final stage, the inclusion body pellet was resuspended in 1 ml wash buffer (without protease inhibitors).

## 2.6 Expression of GST-tagged VP4 as soluble protein

One colony of *E.coli* BL21 (DE3) pLysS cells transformed with pETVP4PreGST or VP4ThGST was added to 10 ml of LB (100 µg/ml of ampicillin) and grown o/n at 37°C with constant shaking at 250 rpm. Where *E.coli* were co-transformed with pET-NMT, kanamycin (50 µg/ml) and ampicillin (100 µg/ml) were added to the media. Myristic acid was added to a final concentration of 5 µg/ml (using a stock solution in methanol) to *E.coli* cells co-transformed with pETNMT.

## 2.7 Purification of GST-tagged soluble protein

3 L of LB (containing appropriate antibiotics) was inoculated with o/n cultures (using a 1/100 dilution) and grown with constant shaking at 250 rpm at 30°C. At OD<sub>600</sub> 0.7, the cultures were induced with 1 mM IPTG. Myristic acid was added to a final concentration of 5 µg/ml (using a stock solution in methanol) to pETNMT co-transformed bacterial cells. The bacterial cultures were induced for 4 hrs at 30°C. The induced bacterial cells were harvested by centrifugation at 4000 x g for 30 min at 4°C. The cell pellet was divided into three and each pellet was resuspended in 15 ml bacterial lysis buffer [20 mM Na<sub>2</sub>HPO<sub>4</sub>, pH7.4, 150 mM NaCl, 1% Triton X-100, 500 µg/ml lysozyme and 1x protease inhibitors (Fermentas)]. The bacterial cells were lysed by sonication (10 micron amplitude, Misonix Microson) on ice with 30 sec on and 30 sec off x 10 cycles. The soluble protein was obtained by centrifugation at 20 000 x g for 30 min at 4°C. The supernatant (s/n) was applied to a pre-packed 1 ml glutathione agarose column (GE healthcare), according to manufacturer's instructions. The column was equilibrated with binding buffer (1x PBS, pH7.3) and the protein containing sample applied onto the column. The column was washed with 15 ml of binding buffer and GST-tagged VP4 was eluted from the column as 1 ml fractions using elution buffer (50 mM Tris-HCl, 10 mM reduced glutathione,

pH8.0). All fractions were analysed by SDS-PAGE and Coomassie staining. After protein elution, the glutathione agarose column was washed with distilled water, followed by 20% ethanol wash. Fractions containing GST-tagged VP4 and minimum contaminants were pooled and dialysed (using a membrane with 10 kDa molecular weight cut off) against liposome buffer (10 mM HEPES, 107 mM NaCl, pH7.4).

## 2.8 Expression and purification of His-tagged 3C protease

*E.coli* BL21 (DE3) cells were transformed (section 2.2.8) with the plasmid encoding His-3C protease (kind gift from Dr. Toshana Foster). A single colony was picked and inoculated into 5 ml of LB broth containing kanamycin (50 µg/ml) and grown o/n with constant shaking at 250 rpm at 37°C. 400 ml of LB was inoculated with o/n culture (1 in 100 dilution) and grown with constant shaking at 250 rpm at 37°C. At OD<sub>600</sub> 0.6, expression was induced with 1mM IPTG for 3 hrs at 37°C. The induced bacterial cells were harvested by centrifugation at 4000 x g for 30 min at 4°C. The pellet was resuspended in 20 ml lysis buffer (500 µg/ml lysozyme, 1 % Triton X-100, 1x protease inhibitors, PBS) followed by sonication on ice with 30 sec on and 30 sec off x 10 cycles. The clarified s/n was obtained by centrifugation at 20 000 x g for 15 min at 4°C, and eluted using 1 ml pre-packed nickel affinity chromatography column (GE Healthcare), according to manufacturer's instructions. Briefly, the column was washed with 5 ml of D<sub>2</sub>O, equilibrated with buffer 1 (20 mM Na<sub>2</sub>HPO<sub>4</sub>, 0.5 M NaCl, 10 mM imidazole), following which 3C protease containing s/n was applied to the column. The column was washed with 3 ml of buffer 1. 3C protease was eluted using an imidazole gradient of 0.01 M, 0.1 M followed by 0.5 M. The eluted fractions were analysed by SDS-PAGE (section 2.3.1) and Coomassie staining (section 2.3.4.1). The fractions containing minimum contaminants were pooled and dialysed into storage buffer (50 mM Tris, pH8, 150 mM NaCl, 10 mM EDTA, 10 mM β-mercaptoethanol and 20 % glycerol), with two o/n buffer changes. 3C protease was stored at -20°C.

## 2.9 Preparative electrophoresis for isolation of VP4

VP4 excised from the gel was put into dialysis tubing (Spectrum Laboratories, Inc.) with 500 µl of elution buffer (150 mM glycine, 20 mM Tris-base, 0.1% sarkosyl), placed in a gel electrophoresis tank containing elution buffer and subjected to electrophoresis at 100 V for 1 hr. The polarity was then reversed for 1 min. The elution buffer containing VP4 was recovered from the dialysis tubing and precipitated using acetone (section 2.3.9).

## 2.10 Preparative SDS-PAGE using the prep cell

SDS-PAGE using prep cell (model 491, Bio-Rad) was used to purify proteins by continuous elution electrophoresis, according to manufacturer's instructions. Briefly, samples were subjected to electrophoresis through a cylindrical gel matrix comprised of 16.5% tris-tricine resolving gel and 5% stacking gel, using tris-tricine gel anode and cathode buffers (section 2.3.1). Electrophoresis was carried out at 40 mA, o/n at 4°C, using an elution rate of 1 ml/min. A fraction collector (Amersham Pharmacia Biotech) was used to collect protein fractions immediately after the dye front eluted from the gel. Proteins eluted based on their molecular weights, with proteins of the lowest molecular weight eluting first followed by proteins of higher molecular weight. Fractions were analysed by SDS-PAGE (section 2.3.1), Coomassie staining (section 2.3.4.1), silver staining (section 2.3.4.2) and western blot (section 2.3.5).

## 2.11 Expression of VP4 and VP4His

One colony of *E.coli* BL21 (DE3) pLysS cells transformed with pETVP4His or pETVP4 was added to 100 ml of LB (100 µg/ml of ampicillin) and grown o/n at 37°C with constant shaking at 250 rpm. Where *E.coli* cells were co-transformed with pETNMT, kanamycin (50 µg/ml) and ampicillin (100 µg/ml) were added to the media. Myristic acid was added to a final concentration of 5 µg/ml (using a stock solution in methanol) to *E.coli* cells co-transformed with pETNMT.

## 2.12 Purification of VP4His under non-denaturing conditions

3 L of LB (containing appropriate antibiotics) was inoculated with o/n cultures (using a 1/100 dilution of cultures described in section 2.11) and grown with constant shaking at 250 rpm at 30°C. At OD<sub>600</sub> 0.7, VP4 His or VP4 expression was induced by the addition of 0.2 mM IPTG for 3 hrs at 30°C. Myristic acid was added to a final concentration of 5 µg/ml (using a stock solution in methanol) to *E.coli* cells co-transformed with pETNMT. The induced bacterial cell pellet was divided into three and each pellet resuspended in 15 ml lysis buffer (20 mM Na<sub>2</sub>HPO<sub>4</sub>, 150 mM NaCl, 500 µg/ml lysozyme, 1% Triton X-100, 1x protease inhibitors). The bacterial cells were lysed by sonication (10 micron amplitude, Misonix Microson) on ice with 30 sec on and 30 sec

off x 10 cycles. The s/n was collected by centrifugation at 1500 x g for 1 hr at 4°C. The s/n was applied to a pre-packed 1 ml nickel affinity chromatography column (GE Healthcare), according to manufacturer's instructions. Briefly, the column was washed with 50 ml of D<sub>2</sub>O and equilibrated with binding buffer (20 mM Na<sub>2</sub>HPO<sub>4</sub>, 150 mM NaCl, 1% Triton X-100, 30 mM imidazole). 30 mM imidazole was added to the VP4His containing sample and applied onto the column. The column was washed with 50 ml of buffer (20 mM Na<sub>2</sub>HPO<sub>4</sub>, 150 mM NaCl, 1% Triton X-100, 30 mM imidazole) and VP4His eluted as 3 ml fractions using an imidazole gradient (150 mM, 250 mM and 0.5 M). The fractions were analysed by SDS-PAGE (section 2.3.1) and Coomassie staining (section 2.3.4.1) and western blot (section 2.3.5).

## 2.13 Purification of VP4His under denaturing conditions

3 L of LB (containing appropriate antibiotics) was inoculated with o/n cultures (using a 1/100 dilution of cultures described in section 2.11) and grown with constant shaking at 250 rpm at 30°C. At OD<sub>600</sub> 0.7, VP4 His or VP4 expression was induced by the addition of 0.2 mM IPTG for 3 hrs at 30°C. Myristic acid was added to a final concentration of 5 µg/ml (using a stock solution in methanol) to *E.coli* cells co-transformed with pETNMT. Bacteria were lysed in denaturing lysis buffer (20 mM Na<sub>2</sub>HPO<sub>4</sub>, 150 mM NaCl, 1% Triton X-100, 7M urea, pH7.5) and sonicated (10 micron amplitude, Misonix Microson) on ice with 30 sec on and 30 sec off x 10 cycles. The clarified supernatant was collected by centrifugation at 1500 x g for 1 hr at 4°C and applied to a pre-packed 1 ml nickel affinity column (GE Healthcare), according to manufacturer's instructions. Briefly, column was washed with 50 ml of D<sub>2</sub>O and equilibrated with binding buffer (20 mM Na<sub>2</sub>HPO<sub>4</sub>, 150 mM NaCl, 1% Triton X-100, 7M urea, 30 mM imidazole, pH7.5). 30 mM imidazole was added to the sample containing VP4His and applied to the column. The column was washed with 50 ml of buffer (20 mM Na<sub>2</sub>HPO<sub>4</sub>, 150 mM NaCl, 1% Triton X-100, 7M urea, 30 mM imidazole, pH7.5) and VP4His eluted as 3 ml fractions using an imidazole gradient (150 mM, 250 mM and 0.5 M). The fractions were analysed by SDS-PAGE (section 2.3.1) and Coomassie staining (section 2.3.4.1) and western blot (section 2.3.5). Fractions containing VP4His with minimal contaminants were pooled and dialysed (using a membrane with 3.5 kDa molecular weight cut off) against a urea gradient of 7 M, 3 M, 1 M urea (in PBS) for 4hrs each at 4°C. This was followed by dialysis against PBS for 4 hrs or o/n at 4°C. The visibly precipitated VP4His was collected by centrifugation at 21, 000 x g, resuspended in DMSO and stored at -20°C.



## 2.14 Purification of VP4PreGST under denaturing conditions

VP4PreGST was purified under denaturing conditions as described for VP4His in section 2.13.

## 2.15 Expression and purification of His-trpLE-VP4

M9 minimal media was used for the expression of isotopically labelled proteins for NMR spectroscopy. 1 L of M9 minimal media (6 g  $\text{Na}_2\text{HPO}_4$ , 3 g  $\text{KH}_2\text{PO}_4$ , 0.5 g NaCl, 1 g  $^{15}\text{N}$ -labelled  $\text{NH}_4\text{Cl}$ ) was sterilised by autoclaving. 2 ml 1M  $\text{MgSO}_4$ , 3 g D-glucose and 100  $\mu\text{l}$  1M  $\text{CaCl}_2$  and kanamycin (50  $\mu\text{g}/\text{ml}$ ) added to the sterilised media.

VP4 (with serine replacing methionine at position 17) was expressed as a C-terminal fusion to trpLE with an N-terminal 9-His-tag in the pMM-LR6 vector (His-trpLE-VP4). VP4 was purified as using the method previously described for M2 of influenza virus (Schnell and Chou, 2008). *E.coli* BL21 (DE3) cells were transformed (section 2.2.8) with the plasmid encoding His-trpLE-VP4 and grown in 1 L M9 minimal media with constant shaking at 250 rpm at 37°C. At  $\text{OD}_{600}$  0.7, expression was induced with 0.5 mM IPTG for 18 hrs with constant shaking at 250 rpm at 37°C. His-trpLE-VP4 expressed into inclusion bodies. Bacterial cells were lysed using 30 ml buffer [50 mM Tris-HCl (pH8.0), 200 mM NaCl] followed by sonication (Branson Sonifier 450) on ice for 5 min with 2 min recovery time x 2 cycles. Inclusion bodies were pelleted by centrifugation at 38,000 x g for 30 min at 4°C. The inclusion body pellet was lysed using 30 ml of inclusion body lysis buffer (6M guanidine chloride, 50 mM Tris-HCl (pH8.0), 200 mM NaCl, 1% Triton X-100) and homogenised using a glass rod. The soluble material was clarified by centrifugation at 38,000 x g (sorvall SS34) for 30 min at 4°C.

Nickel immobilised metal ion affinity chromatography (IMAC) resin (Thermo Scientific) were used to prepare the column for His-tagged protein purification. The column was washed with  $\text{D}_2\text{O}$  and sample containing His-trpLE-VP4 applied to the column. 50 ml of 8 M urea was applied to the column and followed by 10 ml x 3 column washes with  $\text{D}_2\text{O}$ . His-tagged protein eluted was with 70 % formic acid (4 ml x 3).

VP4 was released from the fusion protein by CNBr cleavage by the addition of 2 g CNBr in 70% formic acid for 1 hr at room temperature. The cleavage reaction was dialysed using a membrane with 3.5 kDa molecular weight cut off, against 4 L water for 40 min x 2, at room temperature. The dialysed material (approximately 12 ml) was collected and divided into two. 10 ml of acetonitrile was added to 7.5 ml of dialysed material and lyophilized o/n. The lyophilised material was dissolved in 4 ml 70 % formic acid and applied onto a C18 column (Higgins Analytical Inc.). VP4 separated from His-trpLE-VP4 by reverse phase-high pressure

liquid chromatography (RP-HPLC) (BioRad), using a 0-100 % linear gradient of buffer (buffer A: 25 % acetonitrile, 0.1 % trifluoroacetic acid to buffer B: 25 % isopropanol, 25 % acetonitrile, 0.1 % trifluoroacetic acid). 5 ml x 56 fractions were collected and the peak fractions containing protein identified by Biologic DuoFlow (BioRad) programme were analysed by SDS-PAGE (section 2.3.1), Coomassie staining (section 2.3.4.1) and silver staining (section 2.3.4.2).

## **2.16 Reconstitution of VP4 and GST-tagged VP4 in detergent micelles**

Purified VP4 (0.1 mg) (section 2.14) was lyophilised and used for the studies to optimise VP4 reconstitution in detergent micelles. The process of refolding lyophilised VP4 involved dissolving in 6 M guanidine hydrochloride (GnHCl) and the appropriate detergent at approximately 100 mM, in sodium acetate (pH5.5), sodium phosphate (pH7.0, pH7.5) or HEPES (pH8.0) buffer. This was followed by dialysis using a membrane with 3.5 kDa molecular weight cut off (Thermo scientific), to remove GnHCl. The reconstitution of VP4 in detergent micelles was confirmed by size exclusion chromatography (AKTA purifier, Unicorn manager software) using a Superose 6 10/300 column (GE Healthcare).

VP4PreGST purified as described in section 2.13 was vacuum dried o/n and similarly reconstituted in a range of detergents. The reconstitution of VP4PreGST in detergent micelles was confirmed by size exclusion chromatography using a Superdex, 200 10/300 column (GE Healthcare).

## **2.17 Nuclear magnetic resonance (NMR)**

10 % deuterated water was added to the reconstituted VP4 (section 2.15) and the sample transferred to an NMR tube. The sample was centrifuged gently at the experimental temperature to remove any trapped air. The sample was placed in Agilent 600 MHz or 700 MHz prior to initiating the 1D or 2D heteronuclear single quantum coherence spectroscopy (HSQC) NMR experiment. Data acquisition, processing and analysis was carried out using NMRPipe and NMRDraw by Dr Fu and Dr Brüeschweiler.

## 2.18 Circular dichroism spectroscopy

VP4 reconstituted in detergent micelles (section 2.15) was subjected to circular dichroism using a circular dichroism spectrophotometer (JASCO J-815) and a 1 cm path length cuvette. Samples were scanned from 260 nm to 190 nm with 1 nm band width in a sample chamber, at 25°C. Continuous scanning mode at a scanning speed of 50 nm/min was used. Spectra were background-corrected for light scattering. Five scans were averaged to generate the final CD spectra. CD spectra were plotted using ProFit (Quantum Soft). CD spectra (ellipticity) were converted to mean residue ellipticity according to the formula:

$$[\Theta]_M = M \cdot \Theta \cdot 0.001 / \{(10) \cdot (l) \cdot (c) \cdot (n) \cdot (0.001)\}$$

Where  $[\Theta]_M$  is  $\text{deg cm}^2 \text{ dmol}^{-1}$ , M is the molecular weight of VP4 (7400 g/mol),  $\Theta$  is the measured ellipticity in degrees, l is the path length of the cuvette in centimeters (0.1), c is the protein concentration (mg/ml) and n is the number of amino acids in VP4.

Far UV spectra were deconvoluted with CDSSTR algorithm in the DichroWeb package ([dichroweb.cryst.bbk.ac.uk/html/userguide.shtml](http://dichroweb.cryst.bbk.ac.uk/html/userguide.shtml)) to estimate protein secondary structure content. This was kindly carried out by Dr. Franz Hagn (Harvard Medical School).

## 2.19 Transmission electron microscopy

EM grids bearing a carbon support were glow discharged for 15 sec (EMS 100 glow discharge unit). VP4GST reconstituted in DPC and purified by size exclusion chromatography (section 2.15) was adsorbed onto grids and stained with 0.75 % uranyl formate (pH4.5). Images were collected on a JEOL 1200EX operating at 80kV.

## 2.20 Purification of HRV16

HRV16 was propagated in HeLa Ohio cells in roller bottles (2125  $\text{cm}^2$ , Greiner Bio One) x 20 in the presence of growth media [Dulbecco's modified eagle medium (DMEM)( Invitrogen), 10% foetal calf serum, 2 mM L- glutamine, 100 U/ml penicillin and 100  $\mu\text{g/ml}$  streptomycin. Cells were infected at a multiplicity of infection (MOI) of 0.1 at 37°C and complete cytopathic effect (CPE) was observed at 48 hrs. Infected HeLa Ohio cells were lysed by three freeze/thaw cycles and clarified supernatants concentrated by precipitation o/n with saturated ammonium

sulphate solution (50 % final concentration). The precipitate was harvested by centrifugation at 4000 x g for 1 hr at 4°C. The precipitate was resuspended in 20 ml PBS and 0.1 % NP-40 (Thermo Scientific) and pelleted through a 2 ml cushion of 30% (w/v) sucrose by centrifugation at 140, 000 x g for 2 hrs at 25°C. The pellet was resuspended in 0.5 ml cold PBS, 0.1 % SDS added to it and centrifuged at 4000 x g for 10 min at 12°C. The s/n was loaded onto a sucrose density gradient comprising 15-45 % (w/v) sucrose which was centrifuged at 140, 000 x g for 2 hrs at 12°C. The gradient was fractionated from bottom to top and absorbance at 260 nm ( $A_{260}$ ) was measured to determine the fractions containing HRV16. The purity of HRV16 fractions was determined by SDS-PAGE (section 2.3.1), Coomassie staining (section 2.3.4.1) and silver staining (section 2.3.4.2). The fractions containing sufficient HRV16 and least contaminants were pooled, divided into 100  $\mu$ l aliquots and stored at -80°C.

## 2.21 <sup>35</sup>S-HRV16 labelling and purification

$2 \times 10^7$  HeLa Ohio cells were infected with HRV16 at an MOI of 5 in the presence of growth media [Dulbecco's modified eagle medium (DMEM)( Invitrogen)], 10% foetal calf serum, 2 mM L- glutamine, 100 U/ml penicillin and 100  $\mu$ g/ml streptomycin. After attachment of HRV16 for 30 min at room temperature, cells were incubated at 37°C for 1 hr. The media was discarded and replaced with methionine-free media, supplemented with 5% dialysed foetal calf serum (Gibco, life technologies), 2 mM L-glutamine, 20 mM sterile HEPES, for 3 hrs at 37°C. The infected cells were labelled at 3 hrs post infection by the addition of 1 mCi of <sup>35</sup>S- methionine (Perkin Elmer). Cells were harvested at 11 hrs post-infection and purified as described in section 2.20.

## 2.22 Preparation of liposomes

Liposomes were prepared as previously described (Tuthill *et al.*, 2006) and as follows. Phosphatidic acid, phosphatidylcholine, cholesterol and rhodamine-labelled phosphatidylethanolamine (Avanti Polar Lipids) (molar ratios 44.5:44.5:10:1 respectively) were mixed and dried under a steady stream of argon to form a film. Liposomes were rehydrated in liposome buffer (107 mM NaCl, 10mM HEPES, pH7.5) containing 50 mM carboxyfluorescein (CF), o/n with constant agitation at room temperature. The mini-extruder (Avanti Polar Lipids, Inc.) was assembled, according to manufacturer's instructions and the rehydrated lipid extruded 13 times through the 400 nm-pore-size filter (Avanti Polar Lipids, Inc.). The liposomes were washed three times by centrifugation at 100, 000 x g to remove external CF from liposomes and finally resuspended in 100  $\mu$ l of liposome buffer. The lipid concentration of

liposome preparations was estimated by comparing the level of rhodamine fluorescence in the liposome sample relative to samples of rehydrated lipids of known concentration. Dynamic light scattering (Malvern Zetasizer  $\mu\text{V}$ ) was used to confirm the average diameter (400 nm) and size distribution of the liposomes. Liposomes were also visualised by negative stain (uranyl acetate, pH4.5) TEM (FEI Tecnai, Philips) (section 2.17).

Similarly, liposomes mimicking the composition of early endosomes or late endosomes were prepared. Liposomes mimicking early endosomes were composed of PC, PE, SM and cholesterol (Avanti polar lipids) (molar ratios 40:10:5:45). Liposomes mimicking late endosomes were composed of PC, PE, PI, BMP and cholesterol (Avanti polar lipids) (molar ratios 40:10:10:20:20).

Liposomes containing Fluorescein isothiocyanate (FITC) conjugated dextrans (FD) (Sigma) were prepared in the same way as CF containing liposomes. Except, the lipid film was rehydrated in the presence of 25 mg/ml FD, 107 mM NaCl, 10 mM HEPES, pH 7.5.

## 2.23 Membrane permeability assay

Purified liposomes containing CF or FD (section 2.22) were diluted in liposome buffer (107 mM NaCl, 10mM HEPES, pH7.5) so that the final lipid content was 50  $\mu\text{M}$ . A typical volume of 5  $\mu\text{l}$  of the test samples and controls were placed into the wells of a black, clear bottomed, 96 well plate (Greiner) and liposomes (95 $\mu\text{l}$ ) added to each well. Membrane permeability was detected in real time by the release, unquenching and increase in CF fluorescence. Measurements were taken every 30 sec for 1 hr at  $\lambda_{\text{ex}}$  485 nm/ $\lambda_{\text{em}}$  520 nm (Plate CHAMELEON V, Hidex). All reagents and plasticware were pre-equilibrated to the reaction temperatures of 25°C or 37°C. Initial rates were calculated from the linear slope of lines generated from the initial four data points.

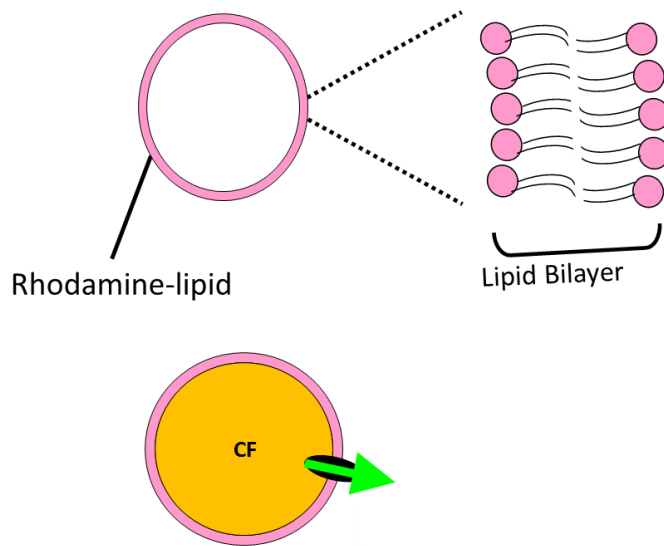


**Figure 2.1 Membrane permeability assay.**

Membrane permeabilisation of carboxyfluorescein containing liposomes results in the release of the dye which becomes unquenched and is read as a signal at  $\lambda_{ex}$  485 nm/ $\lambda_{em}$  520 nm.

## 2.24 FD release assay

Liposomes containing FD were purified as described in section 2.22. Experiments determining real time release of FD could not be carried out due to the low, non-self quenching concentrations of FD used. Therefore, end point fluorescence measurements of liposome free s/n were taken to determine extent of FD release. FD containing liposomes were added to VP4His and control samples, incubated for 30 min at room temperature and centrifuged at 162,000 x g for 30 min at 20°C. The liposome free s/n were collected and transferred to a black, clear bottomed, 96 well plate (Greiner) and readings taken at  $\lambda_{ex}$  485 nm/ $\lambda_{em}$  520 nm. The signal released by the addition of 0.5 % (v/v) Triton X-100 was taken as 100 % and all s/n adjusted to 0.5 % (v/v) Triton X-100 prior to recording fluorescent measurements, to normalise for fluorescence quenching by presence of detergent.

## 2.25 Liposome floatation assay

Purified VP4His (5  $\mu$ M) was added to liposomes (50  $\mu$ M lipid content) in a total volume of 100  $\mu$ l and incubated for 30 min at room temperature. An equal volume of 100  $\mu$ l 40 % w/v ficoll in HEPES, pH7.4 was mixed with the VP4His-liposome reaction so that the final concentration of ficoll was 20 % w/v. The sample was mixed carefully and placed at the bottom

of a 2.2 ml mini-ultracentrifuge tube. This was followed by a layer comprising 1.6 ml of 10 % ficoll w/v followed by a layer of 0.4 ml liposome buffer, pH7.4. This discontinuous gradient was subjected to centrifugation at 33, 000 x g for 1 hr at 25°C. The gradient was fractionated from top to bottom. The pellet was resuspended in 0.1 % SDS. 10 µl of each fraction (and the resuspended pellet) was analysed by SDS-PAGE (section 2.3.1) and anti-His western blot (section 2.3.5). Rhodamine measurements of the fractions were taken at  $\lambda_{ex}$  520 nm/ $\lambda_{em}$  570 nm (Plate CHAMELEON V, Hidex) and used to assess liposome migration in the gradient.

# **Chapter 3**

## **Expression and purification of recombinant VP4**



### 3.1 Introduction

This chapter introduces the rationale for working with recombinant VP4, describes the design and cloning of expression plasmids, strategies devised for expression and purification of recombinant VP4 proteins. In addition, strategies for the purification of native VP4 from virus are described.

VP4 has two functions: as a capsid protein and as a protein which interacts with membranes upon its release from the capsid. VP4 is released from the virus particles during conformational changes which may be triggered by binding to receptors, low pH or elevated temperature (56°C). Released VP4 has been shown to aggregate and deposit as a pellet when dissociated virus was subjected to centrifugation in sucrose gradients (Talbot *et al.*, 1973), VP4 released from the virus particle partitioned into membranes (Danthi *et al.*, 2003; Tuthill *et al.*, 2006), VP4 is myristoylated at its N-terminus and myristoylation is known to target proteins to membranes (section 4.1). Therefore, from the perspective of producing recombinant protein, VP4 was considered as a membrane protein.

Membrane proteins have been purified from natural sources, generated as recombinant proteins or synthesised chemically as short peptides. A range of different expression systems such as the bacteria *E.coli*, yeast *Pichia pastoris* or mammalian and insect cell lines have been used for the generation of recombinant proteins. VP4 constitutes approximately 8 % of the capsid protein (P1) and the limited amounts of native VP4 expected to be purified from virus would be insufficient for the intended functional and structural studies on VP4. Production of recombinant proteins in *E.coli* is quick, relatively inexpensive and facilitates characterisation of the protein in a defined system. Although the use of mammalian cell lines for the expression and purification of VP4 was more relevant, it presented disadvantages of lower production yield and high cost due to complex growth requirements. Therefore, *E.coli* was used for the generation of recombinant VP4 to meet the objectives stated in section 1.7.

Functional and structural studies of recombinant membrane proteins are associated with technical challenges in protein expression, purification and reconstitution due to their hydrophobicity and insolubility (Lin and Guidotti, 2009).

Native VP4 is myristoylated at the N-terminus. Myristoylation is a co-translational modification catalysed by the enzyme N-myristoyltransferase (NMT) involving the covalent attachment of myristic acid to the amino terminal glycine residue of the protein via an amide bond. Myristoylation occurs in numerous eukaryotic cells which express NMT but *E.coli* cells lack endogenous NMT (Farazi *et al.*, 2001; Resh, 1999). Therefore, *E.coli* cells were co-transformed

with a plasmid encoding VP4 and plasmid encoding NMT, to facilitate myristoylation of recombinant VP4 protein.

Studies on VP4 of HRV, PV and FMDV were carried out for reasons including the overall economic significance of all three viruses (section 1.1.1) and the differences in their uncoating mechanisms. Further, PV is the prototype for picornaviruses, genetically and biochemically well studied and was also chosen as one of the viruses in this project due to previous studies on PV VP4 mutations (Threonine at position 28) which were shown to affect RNA delivery into the cytoplasm during infection (Danthi *et al.*, 2003). We wanted to determine if equivalent mutations in HRV and FMDV VP4 had a similar effect on RNA delivery. HRV was chosen for this study due to the availability of an existing system for the expression and purification of GST-tagged HRV VP4 and studies showing VP4-mediated membrane interactions (Davis *et al.*, 2008). FMDV was chosen for this study because FMDV VP4 differs from enterovirus VP4 in size and amino acid composition. Also, FMDV is the subject of extensive research at the Pirbright Institute.

#### **Strategies for the expression and purification of recombinant VP4**

Several approaches were tried for the expression and purification of recombinant VP4 to produce material suitable for use in membrane permeability assays, biochemical studies such as VP4 multimerisation and structural studies including circular dichroism (CD) spectroscopy, transmission electron microscopy (TEM) and nuclear magnetic resonance (NMR) spectroscopy.

VP4 was produced without a tag, with a glutathione S-transferase (GST) or a hexahistidine (His) tag at its C-terminus; or as a His-trpLE fusion at its N-terminus. These constructs are shown in Figure 3.1.

Due to the presence of the myristate group at the N-terminus, myristoylated VP4 could only be produced with tags fused at the C-terminus of VP4. VP4 was therefore expressed with a GST-tag at its C-terminus. The GST-tag offered the advantages of rapidly folding into a stable and soluble form thereby aiding solubility of the fusion protein, and its size (26 kDa) facilitating TEM studies. However, there was concern that the large size of the GST-tag (26 kDa) may influence the activity of VP4 (~8 kDa). Therefore, VP4 with a hexahistidine-tag at its C-terminus was also generated. This protein had the advantage of having a minimal tag but would be more difficult to resolve by TEM due to its small size. The use of fusion tags improves specific binding to matrices and facilitates protein purification but untagged VP4 was desirable for structural studies such as CD and NMR. For the production of untagged protein, VP4 was expressed either directly without a tag or as a fusion to His-trpLE at its N-terminus; in the latter

strategy although VP4 could not be myristoylated, this system provided an established approach for producing high yields of small insoluble proteins. Myristoylated and unmyristoylated forms of recombinant VP4 were expressed and purified for use in functional assays to investigate the influence of myristoylation on the induction of membrane permeability mediated by VP4. The general strategies used for obtaining recombinant VP4 were cleavage of GST-tagged VP4 expressed as soluble protein or in inclusion bodies to release VP4 with a hexahistidine tag; cleavage of His-trpLE-VP4 expressed in inclusion bodies to release untagged VP4; direct expression and purification of His-tagged or untagged VP4. The details of these recombinant VP4 proteins and purification strategies used are summarised in Table (3.1) and will be described in the following sections of this chapter.

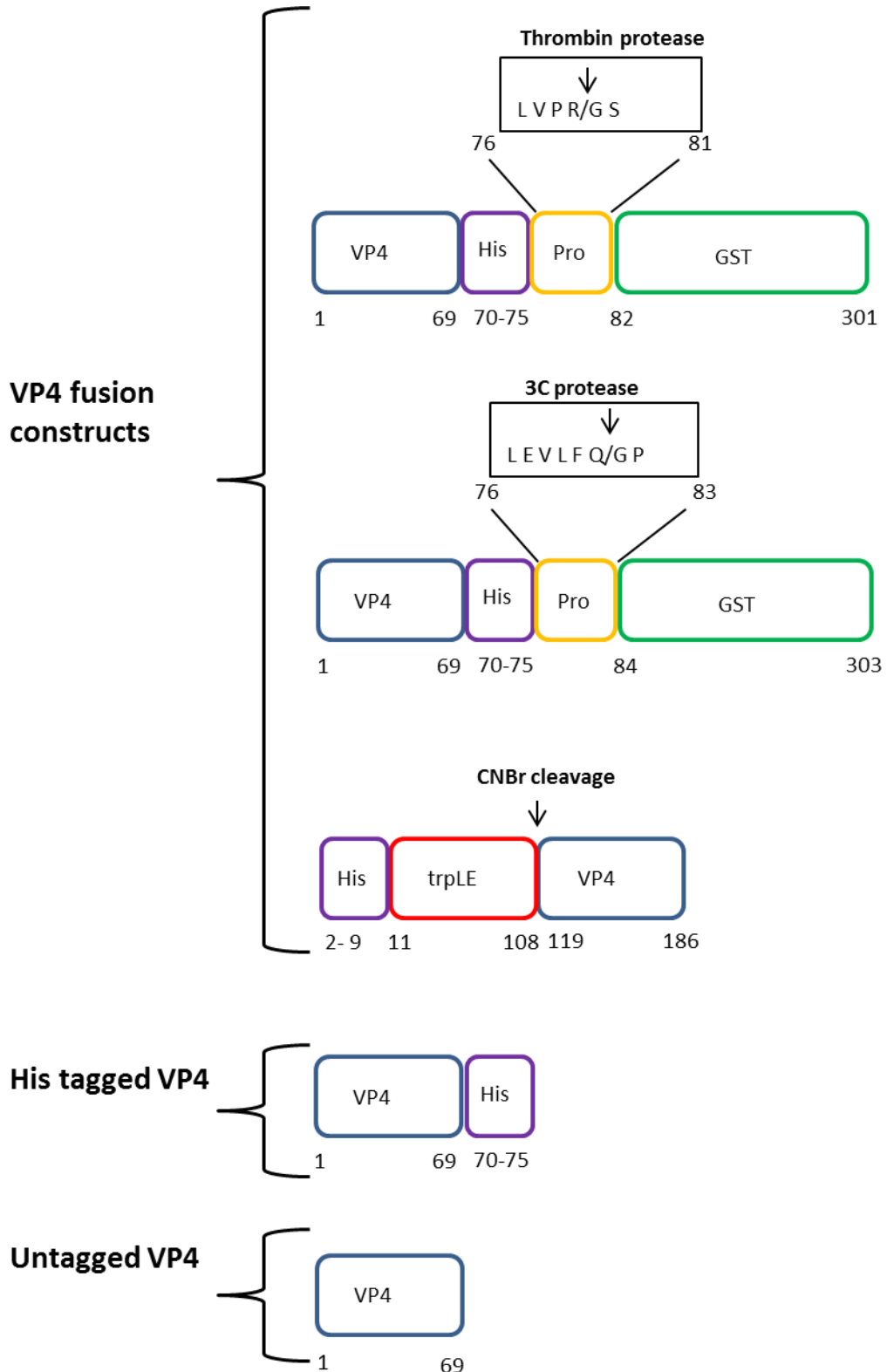


**Figure 3.1 Schematic of expression constructs used for the generation of recombinant VP4.** VP4 constructs were designed to express VP4 protein with a GST or His-tag at its C-terminus or His-trpLE at its N-terminus. VP4 was also directly expressed with a His-tag or as untagged VP4.

**Table 3.1 VP4 constructs designed for expression of recombinant HRV, PV and FMDV VP4; and the purifications strategies used to purify VP4.**

	Name of construct	Cleavage site	Description	Purification procedure
<b>HRV VP4 constructs</b>	<b>HRV VP4</b>	Absent	Direct expression of HRV VP4 as an insoluble protein.	Denaturing conditions, nickel affinity chromatography
	<b>HRV VP4His</b>	Absent	Direct expression of His-tagged HRV VP4 as an insoluble protein.	Denaturing conditions, nickel affinity chromatography
	<b>HRV VP4HisPreGST</b>	3C protease	Expression of GST-tagged HRV VP4 in inclusion bodies or as a soluble protein	Isolation of inclusion bodies, glutathione affinity chromatography. Cleavage of VP4PreGST with 3C protease to release VP4His. VP4His isolated by gel electroelution or prep cell.
	<b>HRV VP4HisThGST</b>	Thrombin protease	Expression of GST-tagged HRV VP4 in inclusion bodies	Purification of inclusion bodies. Cleavage of VP4ThGST with thrombin protease. VP4 isolated by gel electroelution.
	<b>His-trpLE-VP4</b>	Absent	Expression of VP4 as a C-terminal fusion to His-trpLE	Isolation of inclusion bodies, nickel affinity chromatography, CNBr cleavage to release VP4, HPLC
<b>PV VP4 constructs</b>	<b>PV VP4</b>	Absent	Direct expression of PV VP4 as an insoluble protein.	Denaturing conditions, nickel affinity chromatography
	<b>PV VP4His</b>	Absent	Direct expression of His-tagged PV VP4 as an insoluble protein.	Denaturing conditions, nickel affinity chromatography
	<b>PV VP4PreGST</b>	3C protease	Expression of GST-tagged PV VP4 in inclusion bodies or as a soluble protein	Isolation of inclusion bodies, glutathione affinity chromatography. Cleavage of VP4PreGST with 3C protease to release VP4His. VP4His isolated by gel electroelution or prep cell.
	<b>PV VP4ThGST</b>	Thrombin protease	Expression of GST-tagged PV VP4 in inclusion bodies	Purification of inclusion bodies. Cleavage of VP4ThGST with thrombin protease. VP4 isolated by gel electroelution.
<b>FMDV VP4 constructs</b>	<b>FMDV VP4</b>	Absent	Direct expression of FMDV VP4 as an insoluble protein.	Denaturing conditions, nickel affinity chromatography
	<b>FMDV VP4His</b>	Absent	Direct expression of His-tagged FMDV VP4 as an insoluble protein.	Denaturing conditions, nickel affinity chromatography
	<b>FMDV VP4PreGST</b>	3C protease	Expression of GST-tagged FMDV VP4 in inclusion bodies or as a soluble protein	Isolation of inclusion bodies, glutathione affinity chromatography. Cleavage of VP4PreGST with 3C protease to release VP4His. VP4His isolated by gel electroelution or prep cell.
	<b>FMDV VP4ThGST</b>	Thrombin protease	Expression of GST-tagged FMDV VP4 in inclusion bodies	Purification of inclusion bodies. Cleavage of VP4ThGST with thrombin protease. VP4 isolated by gel electroelution.
<b>Codon optimised FMDV VP4 constructs</b>	<b>Opt FMDV VP4</b>	Absent	Direct expression of codon optimised FMDV VP4 as an insoluble protein.	Denaturing conditions, nickel affinity chromatography
	<b>Opt FMDV VP4His</b>	Absent	Direct expression of codon optimised His-tagged FMDV VP4 as an insoluble protein.	Denaturing conditions, nickel affinity chromatography
	<b>Opt FMDV VP4PreGST</b>	3C protease	Expression of codon optimised GST-tagged FMDV VP4 in inclusion bodies or as a soluble protein	Isolation of inclusion bodies, glutathione affinity chromatography. Cleavage of VP4PreGST with 3C protease to release VP4His. VP4His isolated by gel electroelution or prep cell.

## 3.2 Purification of recombinant VP4His from GST-tagged VP4

### 3.2.1 Cloning of GST-tagged VP4 from HRV, PV and FMDV

An existing plasmid expressing HRV16 VP4 with a hexahistidine tag, a thrombin protease cleavage site and a GST-tag fused to its C-terminus (pET23d VP4ThGST) was available from a previous study in the lab (Davis *et al.*, 2008).

In order to generate a plasmid for the expression of GST-tagged PV VP4, nucleotide sequence for VP4 from PV1 Mahoney (pET PV-M) was amplified by PCR (section 2.2.2.1) to produce VP4 with the restriction site *NdeI*, the initiator codon, His-tag and 3C protease sequence, using the appropriate primers (PV VP4\_F and PV VP4/His/Pre\_R, Table 3.2). The GST nucleotide sequence was amplified from the pET23d VP4ThGST construct to produce GST with 3C protease sequence, His-tag, stop codon and the restriction site *XhoI*, using the appropriate primers (His/Pre/GST\_F and GST\_R, Table 3.2). The molecular weight of the amplified PCR products was confirmed by gel electrophoresis using a 1.5 % agarose gel (section 2.2.5). The above obtained PCR products containing the VP4 nucleotide sequence was designed to overlap with the PCR product containing the GST nucleotide sequence to produce the final VP4PreGST product, using the appropriate primers for overlapping PCR (PV VP4\_F and GST\_R). The schematic of this PCR strategy used for the generation of VP4GST is shown in Figure 3.2. FMDV VP4PreGST was generated similarly. HRV VP4PreGST was produced similarly to PV and FMDV constructs except, pET23d was used as the expression vector and *NcoI* was introduced as the restriction site at the N-terminus of VP4. pET23d could not be used for PV and FMDV GST-tagged VP4 constructs due to the presence of *NcoI* restriction site in the sequence, therefore pET23a containing *NdeI* in place of *NcoI* restriction site was used.

Using the same overlapping PCR strategy, constructs encoding PV or FMDV VP4, His-tag, a thrombin cleavage site and flanked by restriction sites *NdeI* and *XhoI* were generated using the appropriate primers. Nucleotide sequences encoding VP4 from PV1 Mahoney (pET PV-M) and FMDV VP4 from FMDV O1K (pT7S3 O1K) were amplified by PCR using appropriate primers (PV VP4\_F and PV VP4/His/Th\_R or FMDV VP4\_F and FMDV VP4/His/Th\_R, Table 3.2). GST was amplified as described above using appropriate primers (His/Th/GST\_F and GST\_R, Table 3.2). Overlapping PCR of the above obtained amplified products was carried out to produce the final VP4ThGST, as described above.

Table 3.2 Table of primers used for the generation of recombinant VP4 constructs for HRV, PV and FMDV

Name	Sequence 5' to 3'	Description of primer
HRV VP4_F	TATACCATGGGCGCTCAAGTATCTAGACAGAATG	Forward primer for amplifying HRV VP4, introducing <i>NcoI</i> and start codon
HRV VP4_R	TATACTCGAGTCAATGTCAGAGTGGGTATGCCTTTCTCCAAC	Reverse primer for amplifying HRV VP4, introducing stop codon and <i>XhoI</i>
HRV VP4His_R	TATACTCGAGTCAATGGTGATGGTGATGGTGTTCAGAGTG	Reverse primer for amplifying HRV VP4, introducing His-tag, stop codon and <i>XhoI</i>
HRV VP4/His/Pre_R	GGGCCCTGGAACAGAACTTCCAGATGGTGATGGTGATGGTGTTCAGAG	Reverse primer for amplifying HRV VP4 with His-tag and introducing 3C protease
His/Pre/GST_F	CATCACCATCACCCTCTGGAAGTCTGTTCAGGGGCCATGTCCCTATACTAG GTTATTGGAAAATTAAGGG	Forward primer for amplifying His-tag and 3C protease, introducing start codon and GST-tag
GST_R	TATACTCGAGTCAATCCGATTTTGGAGG	Reverse primer for amplifying GST-tag, introducing stop codon and <i>XhoI</i>
PV VP4_F	TAGTATACATATGGGTGCTCAGGTTTCATCACAG	Forward primer for amplifying PV VP4, introducing <i>NdeI</i> and start codon
PV VP4_R	TATACTCGAGTCAAGTTAGCATTGGGGCTGTTTTATCAGG	Reverse primer for amplifying PV VP4 and introducing stop codon and <i>XhoI</i>
PV VP4His_R	TATACTCGAGTCAATGGTGATGGTGATGGTGTTCAGCATTGGGGCTGTTTTA TCAGG	Reverse primer for amplifying PV VP4, introducing His-tag, stop codon and <i>XhoI</i>
PV VP4/His/Pre_R	CCCCTGGAACAGAACTTCCAGATGGTGATGGTGATGGTGTTCAGCATTGGGG CTGTTTTATCAGG	Reverse primer for amplifying PV VP4 with His-tag and introducing 3C protease sequence
FMDV VP4_F	TAGTATACATATGGGGCTGGACAATCCAGTCC	Forward primer for amplifying FMDV VP4, introducing <i>NdeI</i> and start codon
FMDV VP4_R	TATACTCGAGTCAAGCGAGAAGAGCGCCGAAAAG	Reverse primer for amplifying FMDV VP4, introducing stop codon and <i>XhoI</i>
FMDV VP4His_R	TATACTCGAGTCAATGGTGATGGTGATGGTGGGCGAGAAGAGCGCCGAAAAG	Reverse primer for amplifying FMDV VP4, introducing His-tag, stop codon and <i>XhoI</i>
FMDV VP4/His/Pre_R	CCCCTGGAACAGAACTTCCAGATGGTGATGGTGATGGTGGGCGAGAAGAGCG CCGAAAAG	Reverse primer for amplifying FMDV VP4 with His-tag and introducing 3C protease sequence
PV VP4His/Th_R	GGATCCACGCGGAACCAGATGGTGATGGTGATGGTGTTCAGCATTGGGGCTG TTTTATCAGG	Reverse primer for amplifying FMDV VP4 with His-tag and introducing thrombin protease sequence
His/Th/GST_F	CATCACCATCACCCTCTGGTCCGCGTGGATCCATGTCCCTATACTAGGTTATT GGAAAATTAAGGG	Forward primer for amplifying His-tag and thrombin protease sequences, introducing start codon and GST-tag
FMDV VP4/His/Th_R	GGATCCACGCGGAACCAGATGGTGATGGTGATGGTGGGCGAGAAGAGCGCCG AAAAG	Reverse primer for amplifying FMDV VP4 with His-tag and introducing thrombin protease sequence
OptFMDV VP4_F	TAGTATACATATGGGTGCAGGCCAAAGCTCTCC	Forward primer for amplifying codon optimised FMDV VP4 and introducing <i>NdeI</i> and start codon
OptFMDV VP4_R	TATACTCGAGTCAATGCCAGCAGTGCACCAAACAG	Reverse primer for amplifying codon optimised FMDV VP4, introducing stop codon and <i>XhoI</i>
OptFMDV VP4His_R	TATACTCGAGTCAATGGTGATGGTGATGGTGTTCAGCAGTG	Reverse primer for amplifying codon optimised FMDV VP4, introducing His-tag, stop codon and <i>XhoI</i>
<i>HindIII</i> VP4_F	GCG CCG AAA GTA CGC GCT AAG CTT GGT ATG GGC GCT CAA GTA TCT AGA CAG AAT	Forward primer for amplifying VP4, introducing MΔS in VP4, <i>HindIII</i> and first few nucleotides of trpLE
VP4 (MΔS)_F	CAC TCA ACA CAA AAT TCT GTG TCA AAT GGA TCC AGC CTC AAT	Forward primer for amplifying VP4 with MΔS
VP4(MΔS)_R	GGA TCC ATT TGA CAC AGA ATT TTG TGT TGA GTG	Reverse primer for amplifying VP4 and introducing MΔS in VP4
<i>BamHI</i> VP4_R	ATATTA GGATCC TCA TTG CAG AGT GGG TAT GCC TTT CTC CAA	Reverse primer for amplifying VP4, introducing stop codon and <i>BamHI</i>

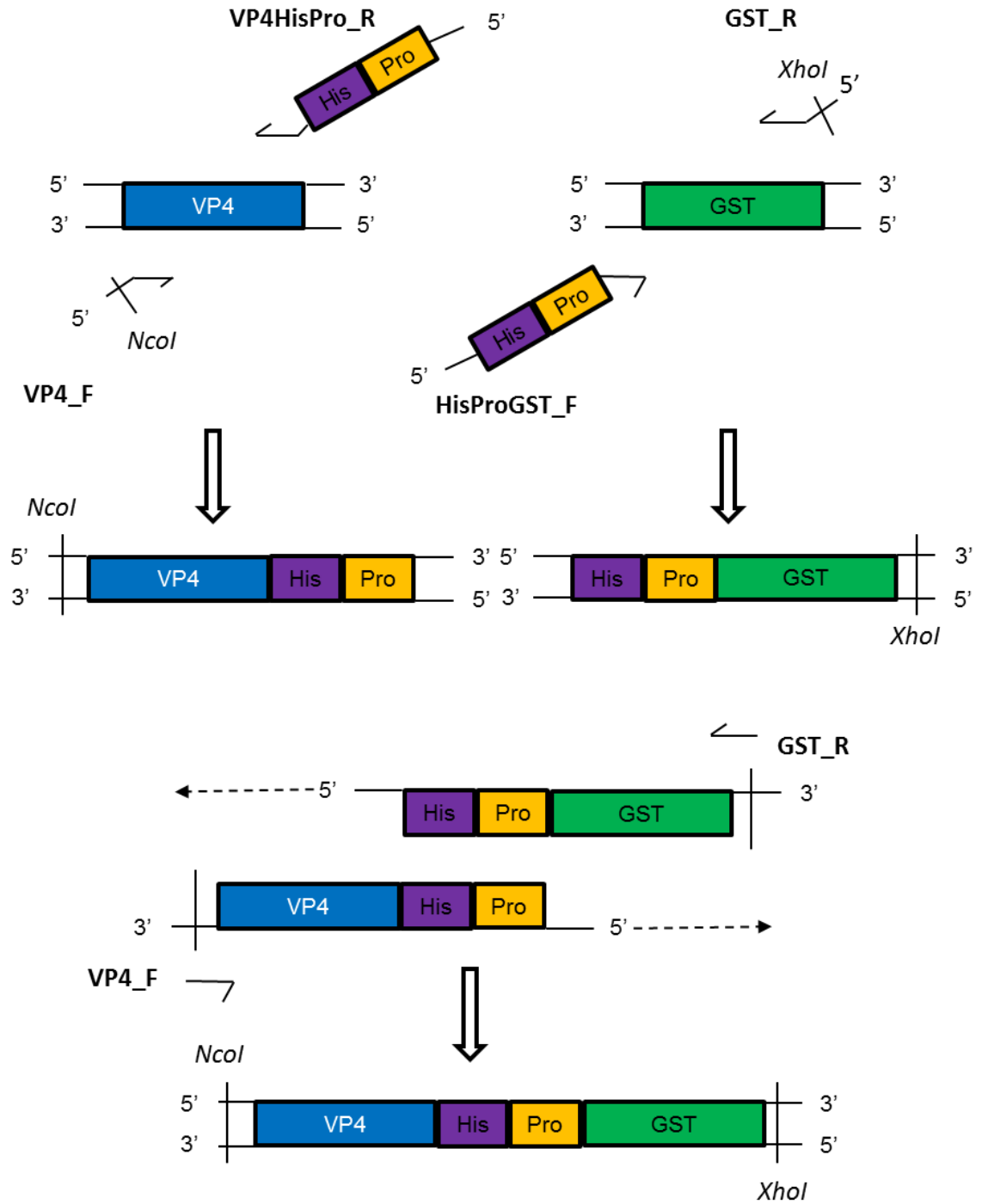


**Figure 3.2 Schematic of PCR strategy used to generate plasmids encoding GST-tagged VP4.**

GST-tagged VP4 plasmid constructs containing either 3C protease (pETVP4PreGST) or thrombin protease coding sequences (pETVP4PreGST) were generated for HRV, PV and FMDV. *NcoI* restriction site was replaced by *NdeI* restriction site in PV and FMDV VP4 constructs. Pro: 3C protease or thrombin protease encoding sequences.



The PCR amplified PV VP4PreGST product was digested with *NdeI* and *XhoI* (section 2.2.4) (Figure 3.3). The digestion product VP4PreGST was gel purified and ligated into *NdeI* and *XhoI* digested pET23a (section 2.2.7). *E.coli* DH5  $\alpha$  cells were transformed with the ligation reaction (section 2.2.8). Colonies were picked, grown in LB media and plasmid DNA purified by miniprep (section 2.2.10). Diagnostic digestion on the miniprep material was carried out with *NdeI* and *XhoI* and positive clones identified by the release of VP4PreGST (920 bp) (Figure 3.4). PCR colony screen (section 2.2.2.2) and sequencing (section 2.2.3) were used to confirm the sequence of the insert. Similarly, PV VP4ThGST, FMDV VP4PreGST, FMDV VP4ThGST DNA clones were generated and sequences confirmed. HRV VP4PreGST was also generated in the same way as explained above, except pET23d vector was used and *NdeI* restriction site was replaced with the *NcoI* restriction site.

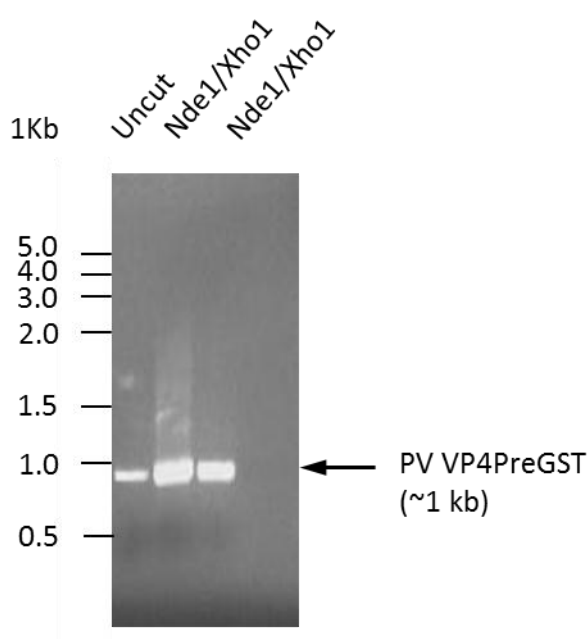


**Figure 3.3 Restriction digestion products of PCR amplified PV VP4PreGST.**

An image of a 1.5 % agarose gel showing PCR amplified PV VP4PreGST digested with the restriction enzymes, *NdeI* and *XhoI*. The digested products were obtained at the expected size of ~1 kb. Uncut PVVP4PreGST was used as a control. The size of molecular weight markers (1Kb ladder) is indicated to the left of the image and was used to confirm the size of the digested product (920 bp).

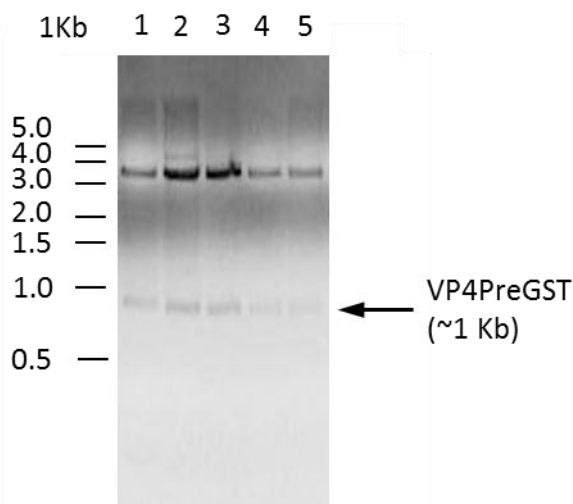


**Figure 3.4 Identification of positive clones for pETPVVP4PreGST.**

An image of a 1.5 % agarose gel showing the products of pETPV VP4PreGST diagnostic digestion with the restriction enzymes, *NdeI* and *XhoI*. Lanes 1-5 show the release of VP4PreGST at the expected size of ~1 kb from pETPVVP4PreGST (~3.5 kb). The size of molecular weight markers (1 Kb ladder) is indicated to the left of the image and was used to confirm the size of the released product (920 bp).

### 3.2.2 Expression of GST-tagged VP4

Myristoylated GST-tagged VP4 was expressed by co-transformation of *E.coli* BL21 (DE3) pLysS cells with plasmids encoding GST-tagged VP4 (VP4ThGST or VP4PreGST) and with a plasmid encoding NMT (section 2.2.8). Cultures (in LB media containing 100 µg/ml ampicillin and 50 µg/ml kanamycin) were grown to OD<sub>600</sub> 0.7 and induced with IPTG. Optimal IPTG concentration used to induce expression and the duration of expression of HRV VP4ThGST had previously been determined in the lab to be 4 hrs post induction of expression with 1 mM IPTG. When expressed at 37°C, expression of GST-tagged VP4 proteins was directed to inclusion bodies whereas expression at 30°C yielded more soluble protein, though a significant proportion was still expressed as insoluble protein.

GST-tagged VP4 proteins contained a His-tag followed by a thrombin protease or HRV14 3C protease cleavage site, followed by the GST-tag (Figure 3.1). VP4His was, therefore, released from the GST-tagged protein by cleavage with thrombin protease or 3C protease. 3C protease was expressed and purified in-house, using established protocols (section 2.8). The use of 3C protease was more economically viable than thrombin protease which was purchased.

HRV VP4PreGST protein expression was induced at 37°C for 4 hrs (section 2.4). Cells were harvested, lysed (section 2.5), proteins separated by SDS-PAGE (section 2.3.1) and stained with Coomassie blue (section 2.3.4.1). High-level expression of HRV VP4GST was demonstrated by

the presence of protein of expected size (approximately 37 kDa) in the induced sample for VP4PreGST but not in the uninduced sample (Figure 3.5).

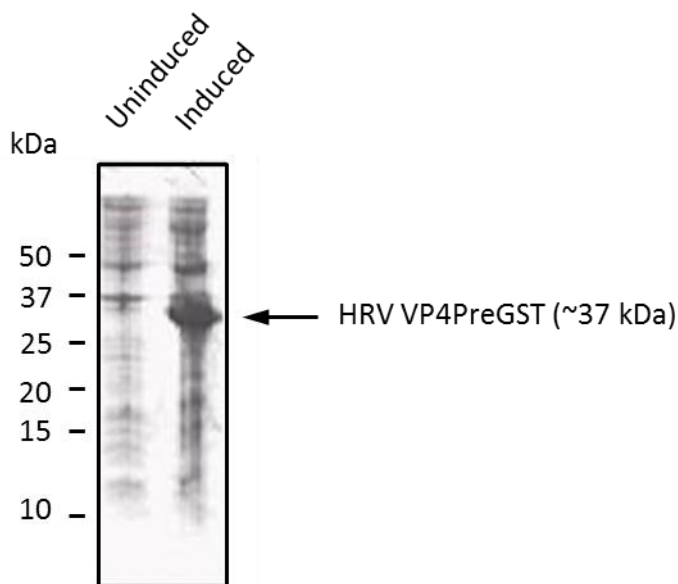


**Figure 3.5 Induction of expression of HRV VP4PreGST.**

Coomassie stained 12 % tris-tricine SDS-PAGE of induced *E. coli* BL21 (DE3) pLysS cells transformed with pETHRV VP4PreGST. Expression of VP4PreGST was observed at ~37 kDa (as indicated by the black arrow). The size of molecular weight markers (kDa) is indicated to the left of the image.

Expression trials for PV and FMDV VP4PreGST and VP4ThGST proteins were carried out at 30°C and 37°C. In contrast to the high-level expression for HRV GST-tagged VP4 proteins detected by SDS-PAGE and Coomassie staining, expression levels at both temperatures tested for PV VP4PreGST and VP4ThGST were very similar and easily observed by anti-His western blot but not by Coomassie staining. The expression levels obtained for FMDV VP4ThGST and VP4PreGST were very low and barely or not detected by anti-His western blot.

Analysis of the expression levels with GST-tagged VP4 from HRV, PV and FMDV showed that HRV had the highest level of expression followed by PV which was followed by very low levels of expression for FMDV.

### 3.2.2.1 Strategies to improve expression levels of GST-tagged fusion proteins

In genomes most amino acids are encoded by two or more synonymous codons. The frequency at which each codon is used differs among genomes. Abundance of transfer RNA (tRNA) in cells reflects the codon bias of its mRNA. Therefore, the abundance of cellular tRNAs

that can read codons determines the translation efficiency of different codons. Codons referred to as “rare” codons are usually translated to a low rate due to low abundance of their cognate tRNAs. “Preferred” codons have high translation efficiency due to the high abundance of their cognate tRNAs. Codon bias implies that genes with abundant codons that are rarely used in *E.coli* are likely to be expressed with low efficiency (Ikemura, 1985; Sharp *et al.*, 1988). Codon optimisation is the exchange of rare codons in an extrinsic gene for more abundant codons without affecting the amino acid sequence of the encoded protein (Chen and Texada, 2006). In order to improve the low or very low levels of expression obtained for PV and FMDV GST-tagged VP4, respectively, the fusion proteins were expressed in *E.coli* Rosetta-gami B (DE3) pLacI cells (section 2.2.8). This strain of *E.coli* has been engineered to supply tRNAs for codons that are “rare” in *E.coli*. These codons are arginine codons AGA, AGG, and CGA, glycine codon GGA, isoleucine codon AUA, leucine codon CUA, and proline codon CCC. *E.coli* Rosetta-gami B (DE3) pLacI cells were transformed with plasmids encoding PV and FMDV GST-tagged VP4 (section 2.2.8) and induced protein expression levels compared with *E.coli* BL21 (DE3) pLysS cells (Figure 3.6).

There was an improved level of expression of PV VP4PreGST in the *E.coli* Rosetta -gami B (DE3) pLacI cells compared to *E.coli* BL21 (DE3) pLysS cells. Levels of PV VP4ThGST protein expression were similar in both strains of *E.coli* as detected by anti-His western blot (Figure 3.6A). In contrast, the levels of FMDV VP4PreGST and VP4THGST expression levels were very low in both strains of *E.coli*, as detected by anti-His western blot (Figure 3.6B). Unsatisfactory yields of VP4 would be expected to be purified with these levels of protein expression.

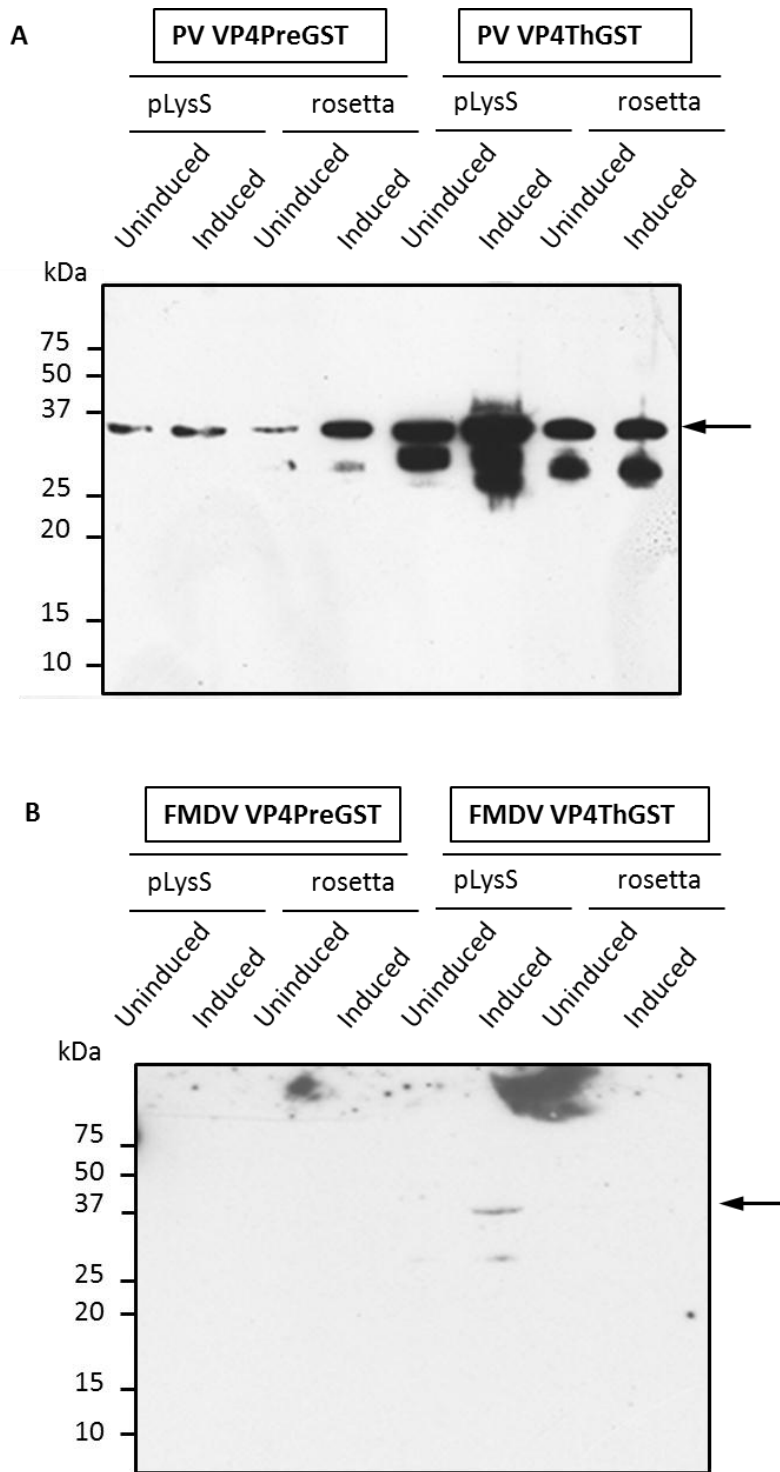


**Figure 3.6 Comparison of expression levels for GST-tagged VP4 in *E.coli* pLysS with *E.coli* rosetta cells.**

Detection of GST-tagged VP4 expression levels by 12 % tris-tricine SDS-PAGE and anti-His western blot. **A.** PV VP4PreGST and VP4ThGST expression levels in *E.coli* pLysS and rosetta cells. **B.** FMDV VP4PreGST and VP4ThGST expression levels in *E.coli* pLysS and rosetta cells. Black arrows in panels A and B indicate expression levels of VP4PreGST and VP4ThGST detected at ~37 kDa. The size of molecular weight markers (kDa) is indicated to the left of the image.

The reasons for very low or undetectable expression levels of GST-tagged FMDV VP4 in *E.coli* Rosetta-gami B (DE3) pLacI cells are not clear. An alternative way to circumvent the problems with rare tRNAs in *E.coli* was to optimise codons from “rare” to “preferred” codons, thereby ensuring a sufficient supply of their cognate tRNAs. A codon optimised sequence encoding FMDV VP4PreGST was commercially synthesised (DNA2.0).

*E.coli* BL21 (DE3) pLysS cells were transformed with the plasmid encoding a codon optimised sequence for FMDV VP4PreGST (optFMDV VP4GST) (section 2.2.8) and expression induced at 30°C and 37°C. Induced cells were harvested 4 hrs post induction, lysed under non-denaturing conditions (section 2.12) and expression levels and solubility of optFMDV VP4GST was analysed by SDS-PAGE (section 2.3.1) and anti-His western blot (section 2.3.5) (Figure 3.7). The level of expression of non-codon optimised HRV VP4His, induced at 30°C was used as a control for comparison with expression levels induced for optFMDV VP4PreGST at 30°C and 37°C (Figure 3.7). Following lysis, optFMDV VP4PreGST was only detected in the total lysate when expressed at 30°C and as insoluble protein when expressed at 37°C. optFMDV VP4PreGST was not detected as soluble protein by anti-His western blot (Figure 3.7). Despite the codon optimisation of FMDV VP4PreGST, the observed expression levels were still low and therefore, not expected to give a sufficient yield of VP4PreGST.

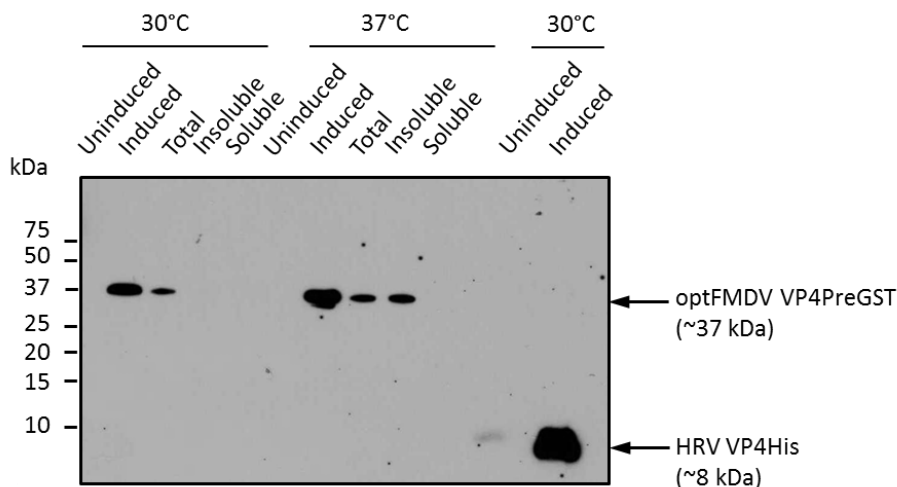


**Figure 3.7 Expression and solubility of optFMDV VP4PreGST.**

Expression and solubility of optFMDVVP4PreGST at 30°C and 37°C, as detected by 16.5 % tris-tricine SDS-PAGE and anti-His western blot. Expression level of HRV VP4His induced at 30°C was used as a control. Black arrow indicates expression levels and solubility of optFMDV VP4PreGST detected at ~37 kDa and expression levels for HRV VP4His detected at ~8 kDa. The size of molecular weight markers (kDa) is indicated to the left of the image.

FMDV VP4 and VP4His were amplified from a sequence encoding FMDV VP4PreGST using appropriate primers (optFMDV VP4\_F and optFMDV VP4\_R ; opt FMDV VP4\_F and optFMDV VP4His\_R, respectively, Table 3.2). However, similar to the observations made before codon optimisation (Figure 3.6B), FMDV VP4 expression levels were very low and not detected by anti-His western blot. Hence, this approach of using codon optimised DNA was not taken further to produce FMDV VP4.

The analysis of expression levels, led to the decision of using GST-tagged HRV VP4 to obtain recombinant VP4 for the intended studies. The following sections discuss the various approaches used to obtain recombinant HRV VP4.

### **3.2.3 Isolation of VP4His from GST-tagged VP4 fusion protein inclusion bodies**

It is well established that high level expression of recombinant proteins in *E.coli* often results in the formation of insoluble aggregates known as inclusion bodies (IB). Previous studies in the lab had shown that expression of VP4ThGST at 37°C yielded protein in IB (section 3.2.2). Small scale studies of VP4PreGST and VP4ThGST expression in *E.coli* BL21 (DE3) pLysS at 37°C and solubility showed the formation of IB. Therefore, large scale cultures expressing VP4PreGST were set up, cell pellets lysed and IB isolated. The purified IB were resuspended in buffer (free of protease inhibitors), aliquoted and stored at -20°C (section 2.5) (Figure 3.8, steps 1-12). A sample of IB (HRV VP4ThGST or HRV VP4PreGST) was analysed by SDS-PAGE (section 2.3.1) and Coomassie staining (section 2.3.4.1).

For the release of VP4His from VP4ThGST IB, cleavage of VP4ThGST with thrombin protease was carried out o/n at 4°C. The cleavage reactions were separated by SDS-PAGE. The gel area in which released VP4 was expected to migrate was excised and protein electroeluted from the gel slice (section 2.9) (Figure 3.8, steps 13-15). Electroeluted VP4His was not detected by Coomassie staining (section 2.3.4.1), silver staining (section 2.3.4.2) or anti-His western blot (section 2.3.5).

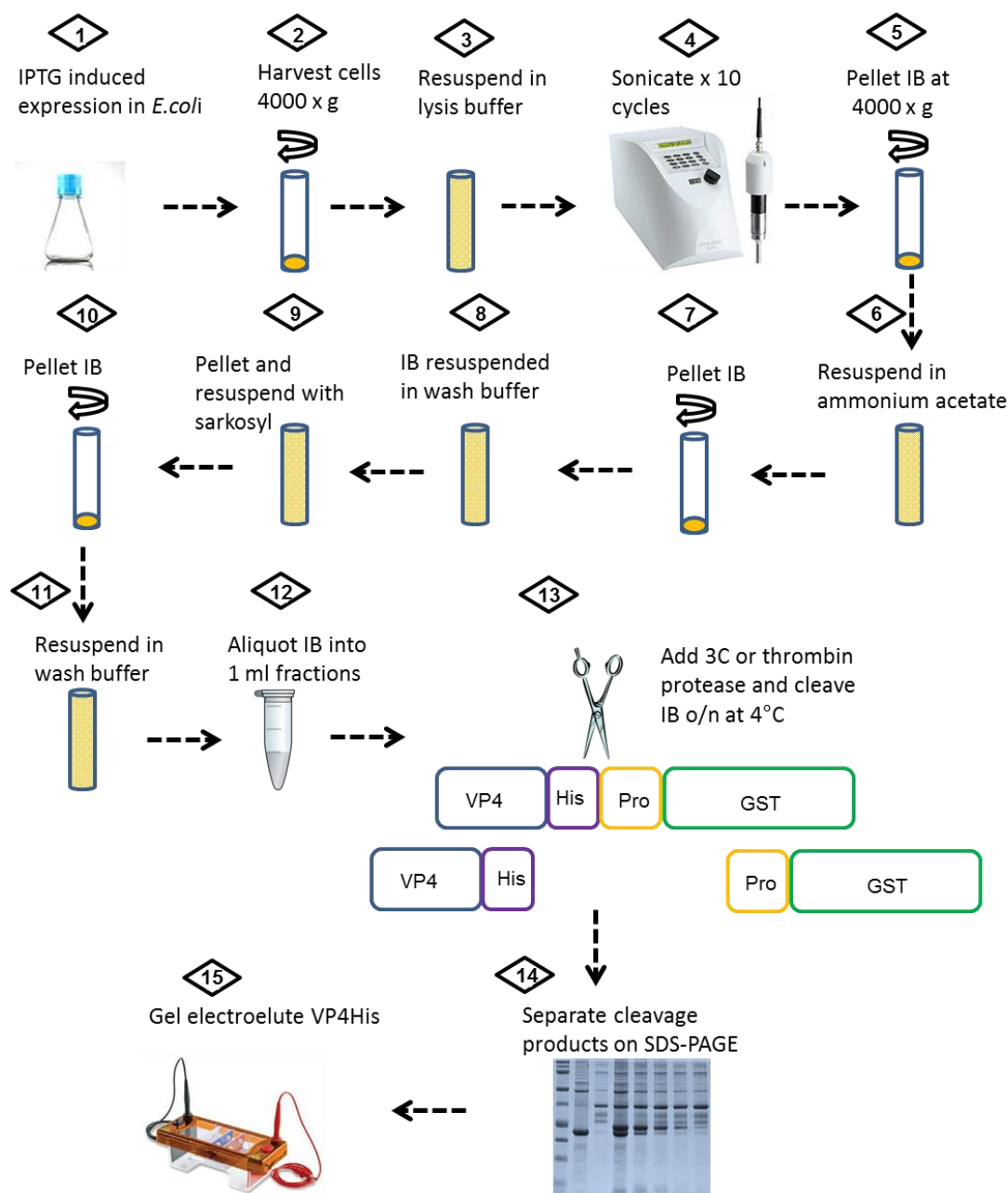


**Figure 3.8 Schematic of purification of VP4His from GST-tagged HRV VP4.**

An overview of the method used for the purification of VP4His from GST-tagged HRV VP4 inclusion bodies is shown in steps 1-15. Briefly, *E.coli* pLysS cells transformed with plasmids encoding GST-tagged VP4. GST-tagged VP4 was expressed in inclusion bodies which were isolated and resuspended in wash buffer (without protease inhibitors). The inclusion bodies were cleaved with 3C protease or thrombin protease for the release of VP4His. The cleavage products were separated by SDS-PAGE, the area where VP4His was expected to migrate to, was excised and VP4His gel electroeluted. Pro: 3C protease or thrombin protease coding sequences, IB: inclusion bodies.



For the release of VP4His from VP4PreGST IB, cleavage of VP4PreGST with 3C protease was carried out. In order to generate 3C protease, *E.coli* BL21 (DE3) pLysS cells were transformed with a plasmid encoding His-tagged 3C protease (pET28b His-3C) (a kind gift from Dr Toshana Foster, University of Leeds). His-3C-protease expression was induced with 1 mM IPTG and cell pellets harvested 3 hrs post induction. His-3C protease was purified by nickel affinity chromatography. The eluted fractions containing 3C protease were resolved by SDS-PAGE (section 2.3.1) and purity determined by Coomassie staining (section 2.3.4.1) (Figure 3.9). The fractions with minimum contaminants were pooled and dialysed into storage buffer and stored at -20°C (section 2.8).

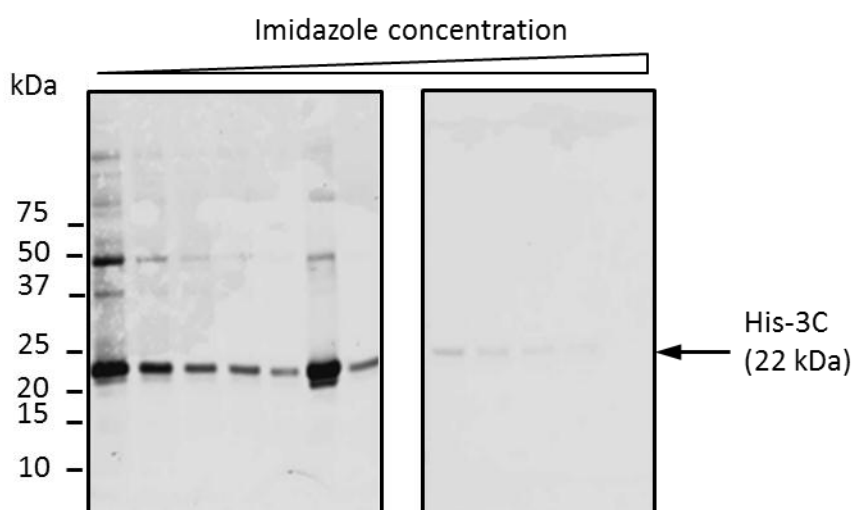


**Figure 3.9 His-3C protease elution fractions from nickel affinity chromatography.**

Fractions containing 3C protease eluted using an increasing imidazole gradient were analysed by 12 % tris-glycine SDS-PAGE and Coomassie staining. Elution fractions were analysed over two separate SDS-PAGE gels. Black arrow indicates observed His-3C protease at 22 kDa. The size of molecular weight markers (kDa) is indicated to the left of the image.

For the release of VP4His from VP4ThGST IB, cleavage of VP4ThGST IB was carried out with thrombin protease (Amersham Biosciences). Twenty units of thrombin protease was added to a standard volume (4 µl) of a standard IB prep or 10 µg of purified 3C protease was added to an excess of IB (50 µl). The cleavage reaction was incubated o/n at 4°C. Cleavage products were separated by SDS-PAGE (section 2.3.1) and analysed by Coomassie staining (section 2.3.4.1) and anti-His western blot (section 2.3.5). Upon cleavage of VP4PreGST or VP4ThGST with 3C or thrombin protease, respectively, the release of VP4His was observed (Figure 3.10). The intensity of appearance of the released GST-tag was directly related to that of VP4His. However, the appearance of the IB, suggested that the cleavage reaction was not going to completion. The small size of VP4His and the poor efficiency of Coomassie stain binding to VP4

possibly contributed to the appearance of VP4 as a protein band of low intensity. Attempts at improving the visualisation of VP4 are discussed in section 3.6.

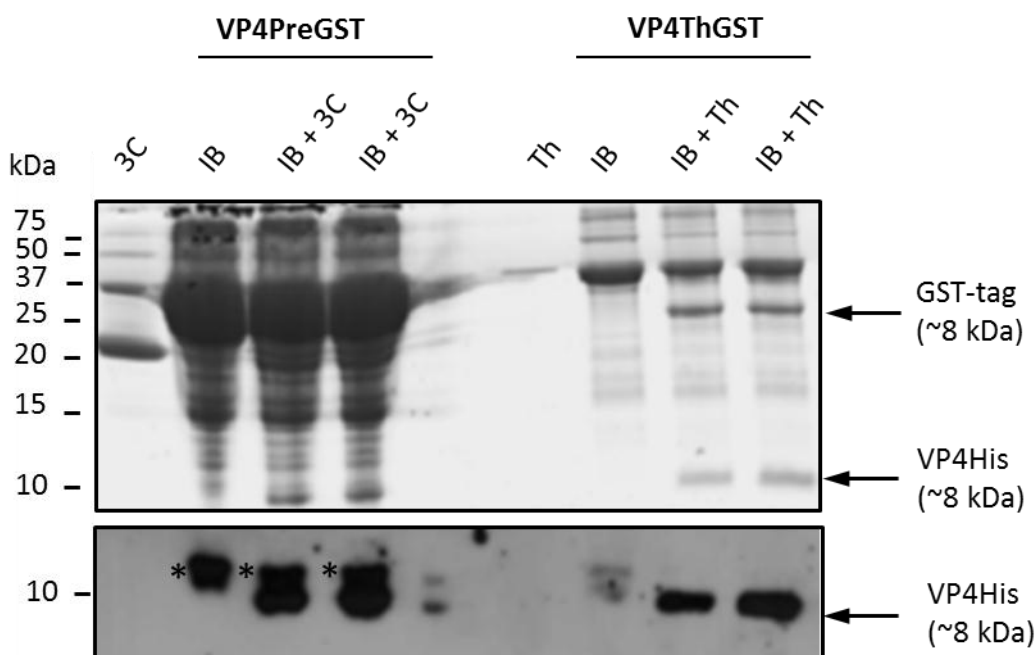


**Figure 3.10 Cleavage of GST-tagged HRV VP4 inclusion bodies with 3C or thrombin proteases.** Release of VP4His by cleavage of HRV VP4PreGST and HRV VP4ThGST inclusion bodies (IB) with 3C protease (3C) or thrombin protease (Th). Cleavage products were analysed by 16.5 % tris-tricine SDS-PAGE and Coomassie staining (top panel) and anti-His western blot (bottom panel). Black arrow indicates released VP4His with expected apparent molecular weight of approximately 8 kDa. The size of molecular weight markers (kDa) is indicated to the left of the image. \* indicates the band detected in HRV VP4PreGST inclusion body (IB) before cleavage.

To attempt purification of VP4His, large scale cleavage reactions were separated by SDS-PAGE (section 2.3.1) and the gel area where VP4His was expected to migrate (~8 kDa) was excised and the protein electroeluted (section 2.9). The electroeluted material was analysed by SDS-PAGE (section 2.3.1) followed by anti-His western blot (section 2.3.5). However, HRV VP4His was not detected.

In order to confirm that the method used to electroelute protein from the gel slice was functional, gel electroelution using a control protein, aprotinin (6.5 kDa) which was of similar size to VP4His, was carried out.

The amount of aprotinin obtained (approximately 1 %) was similar if gel containing aprotinin was excised and aprotinin immediately electroeluted, gel that had been excised, frozen and

then aprotinin electroeluted or gel that had been excised, cut into smaller pieces and then aprotinin electroeluted (section 2.9). The electroeluted material was acetone precipitated (section 2.3.9) and analysed by SDS-PAGE (section 2.3.1) and Coomassie staining (section 2.3.4.1). Majority of the aprotinin was detected by Coomassie staining in the excised gel slice and had not electroeluted. Therefore, electroelution of aprotinin was inefficient. The use of 200 V (84 mA) instead of 100 V for 1 hr, followed by acetone precipitation was found to marginally improve the recovery of aprotinin. The recovered aprotinin was only approximately 5 % of the total input aprotinin. Therefore, suboptimal electroelution and incomplete acetone precipitation contributed to the poor recovery of aprotinin.

The conditions that favoured improved aprotinin recovery were applied to the electroelution of VP4. However, detectable amounts of VP4His were not recovered. This was possibly due to the differences in amino acid composition between aprotinin and VP4, loss of VP4 that occurred during electroelution because of VP4 sticking to the tubing and incomplete acetone precipitation of electroeluted VP4.

A variation on the use of SDS-PAGE to purify VP4His was attempted by using a preparative SDS-PAGE apparatus (Bio-Rad Prep Cell 491). This uses a column of polyacrylamide gel through which proteins are electrophoresed until eluting directly out of the column and into a series of fractions (section 2.10). The high sample capacity enabled multiple cleavage reactions to be loaded and separated by SDS-PAGE. The control protein, aprotinin (1 mg), was first purified to confirm that the prep cell could be used for the purification of small proteins. Following the confirmation of use of the prep cell to purify aprotinin, large scale o/n cleavage reactions of VP4PreGST with 3C protease (25  $\mu$ l IB cleaved with 50  $\mu$ l 3C protease x 10 reactions), were acetone precipitated (section 2.3.9) and loaded onto the prep cell SDS-PAGE column. The use of 3C protease generated in-house was more economically viable than purchased thrombin protease. Hence, 3C protease (instead of thrombin protease) was used for large scale cleavage reactions. The products resulting from 3C protease cleavage of VP4PreGST IB were eluted as 5 ml x 50 fractions. Fractions were acetone precipitated (section 2.3.9) and analysed by SDS-PAGE (section 2.3.1) and anti-His western blot (section 2.3.5). VP4His was not detected in any of the eluted fractions. Possible explanations for the absence of detectable amounts of VP4His included sub-optimal cleavage of VP4PreGST with 3C protease and incomplete acetone precipitation of VP4His present in the prep cell eluted fractions. Furthermore, 1 mg of aprotinin was used as input on the SDS-PAGE column and purification by prep cell recovered approximately 10 % of the total input aprotinin. Therefore, the proof of concept that prep cell could be used for the purification of small proteins was demonstrated with the purification of

aprotinin. This technique could potentially be used for the purification of VP4His but would necessitate a much larger scale IB cleavage prep and high cleavage efficiency with 3C protease.

Despite the above described optimisation steps, insufficient amounts of VP4His were obtained by cleavage of VP4PreGST IB to enable carrying out the intended functional and biochemical assays with VP4His.

### 3.2.4 Isolation of VP4His from soluble GST-tagged VP4

GST-tagged HRV VP4 proteins could be expressed as insoluble protein in IBs (37°C) or as a partially soluble protein (30°C) (section 3.2.2). Expression levels of PV VP4PreGST at 30°C were similar to that observed at 37°C (Figure 3.11).

The approach involving 3C or thrombin protease cleavage of GST-tagged VP4 IB gave limited yields of VP4His (section 3.2.3). Therefore, a different approach using cleavage of soluble VP4PreGST was carried out. Preliminary studies to attempt this used 3C cleavage of soluble PV VP4PreGST. To achieve this, PV VP4PreGST was expressed in *E.coli* BL21 (DE3) pLysS cells at 30°C and the bacterial cell pellet harvested at 4 hrs post induction with 1 mM IPTG. The pellet was lysed by using 1 % Triton X-100 and separated into soluble and insoluble fractions (section 2.7). Analysis of the resulting solubility test fractions (total lysate, insoluble fraction and soluble fraction) by SDS-PAGE (section 2.3.1) and anti-His western blot (section 2.3.5) showed that majority of PV VP4PreGST expressed at 30°C was obtained as soluble protein whereas as at 37°C the majority was insoluble protein (Figure 3.11).

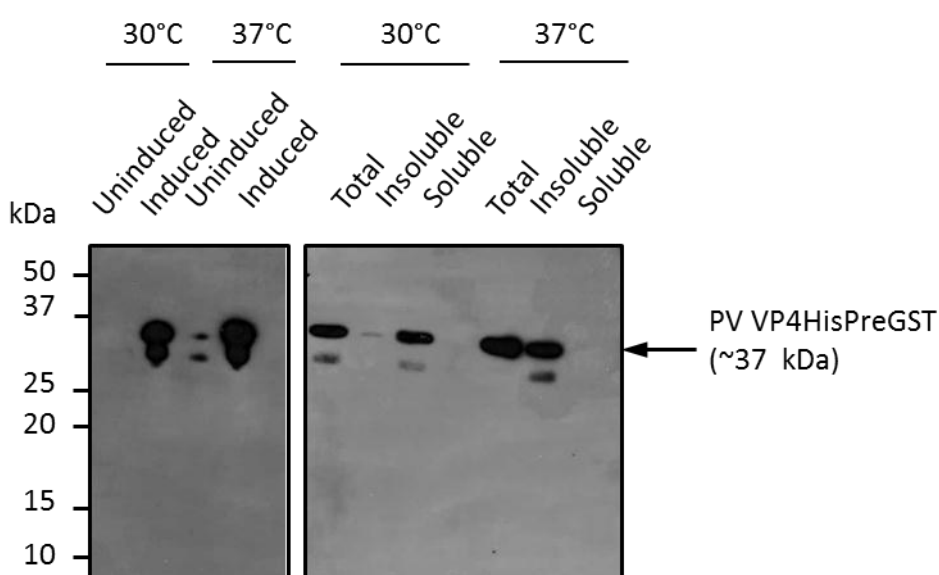
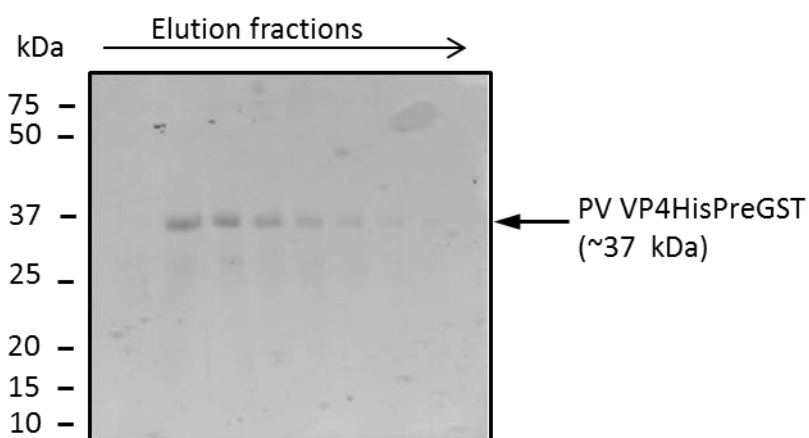


Figure 3.11 Expression and solubility of PV VP4PreGST.

PV VP4PreGST expression and solubility at 30°C and 37°C, as detected by 12 % tris-tricine SDS-PAGE and anti-His western blot. Black arrow indicates PV VP4PreGST detected at ~37 kDa. The size of molecular weight markers (kDa) is indicated to the left of the image.

Soluble PV VP4PreGST was purified using affinity chromatography on an immobilised glutathione agarose column (section 2.7). The eluted fractions were analysed by SDS-PAGE (section 2.3.1) and Coomassie staining (section 2.3.4.1) (Figure 3.12).



**Figure 3.12 Purification of PV VP4PreGST by glutathione affinity chromatography.**

Fractions containing PV VP4PreGST eluted from a glutathione agarose column analysed by 12 % tris-tricine SDS-PAGE and Coomassie staining. Black arrow indicates PV VP4PreGST visualised at ~37 kDa. The size of molecular weight markers (kDa) is indicated to the left of the image.

Fractions containing VP4PreGST with minimum contaminants were pooled and dialysed against 3C protease storage buffer, followed by o/n cleavage with 3C protease in a fivefold dilution series (1  $\mu\text{g}$ - 0.0016  $\mu\text{g}$ ) added to a standard amount of VP4PreGST (0.4  $\mu\text{g}$ ) (concentrations of 3C and VP4PreGST determined by BCA assay). Cleavage products were acetone precipitated and separated by SDS-PAGE (section 2.3.1) and visualised by Coomassie staining (section 2.3.4.1). VP4His released from VP4PreGST was observed after cleavage with 1  $\mu\text{g}$ , 0.2  $\mu\text{g}$ , 0.04  $\mu\text{g}$  3C protease. Released VP4His was not detected when 3C protease was used at a concentration below 0.04  $\mu\text{g}$  (Figure 3.13). The intensity of appearance of released GST-tag was directly related to that of VP4His. The appearance of GST-tag released from VP4PreGST suggested that the cleavage was working better than that inferred from the appearance of the released VP4His. This could possibly be due to the detection problems of VP4 with Coomassie stain (discussed in section 3.6).

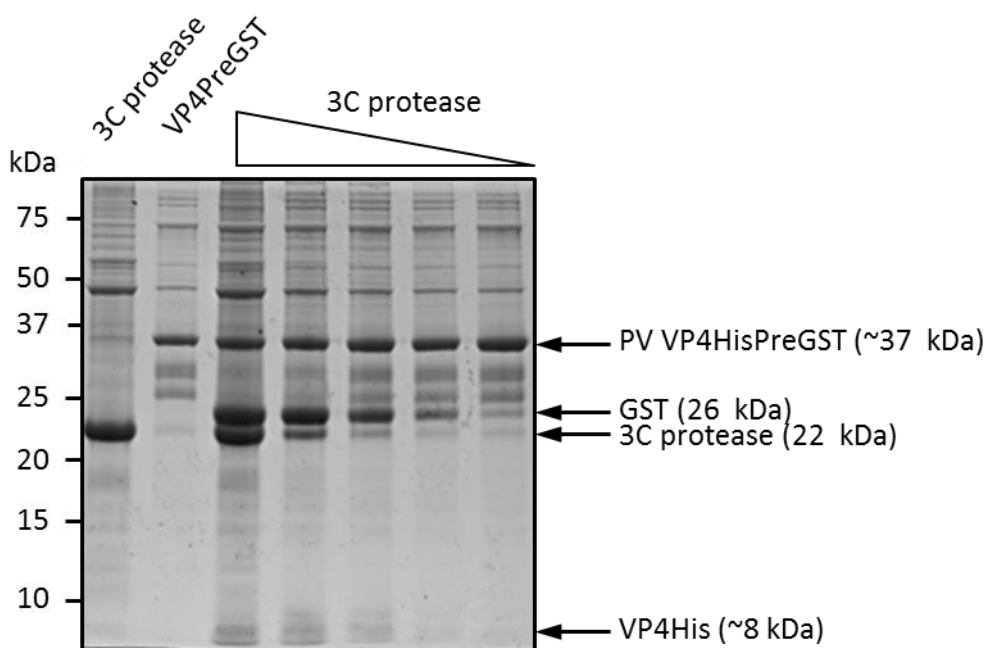


**Figure 3.13 Release of VP4His from PV VP4PreGST by cleavage with 3C protease.**

Soluble PV VP4PreGST cleaved with a dilution series of 3C protease (1  $\mu\text{g}$  - 0.0016  $\mu\text{g}$ ). Cleavage products analysed by 16.5 % tris-tricine SDS-PAGE and Coomassie staining. Black arrows indicate VP4PreGST, GST, 3C protease and VP4His visualised at  $\sim 37$  kDa, 26 kDa, 22 kDa and  $\sim 8$  kDa, respectively. The size of molecular weight markers (kDa) is indicated to the left of the image.

A large scale cleavage reaction (10  $\mu\text{g}$  VP4PreGST and 25  $\mu\text{g}$  of 3C protease) was carried out, acetone precipitated, separated by SDS-PAGE (section 2.3.1), the gel area where VP4His was expected to migrate was excised and gel electroeluted (section 2.9). The electroeluted material was acetone precipitated (section 2.3.9), analysed by SDS-PAGE (section 2.3.1) and anti-His western blot (section 2.3.5). VP4His was not detected.

An alternative method had to be developed due to the limited yields of VP4His obtained using cleavage of VP4GST constructs with 3C or thrombin protease.

### 3.3 Purification of recombinant VP4 and VP4His

#### 3.3.1 Construction of expression plasmids for VP4 and VP4His

Given the limited success of obtaining VP4His from cleavage of GST-tagged VP4 (sections 3.2.3 and 3.2.4), a different strategy of directly expressing and purifying VP4 and VP4His was developed. VP4 had the advantage of being untagged and therefore most similar to native VP4 while the minimal hexahistidine tag present in VP4His facilitated protein purification and detection.

pET23d HRV VP4ThGST was used as template DNA for the PCR amplification of the sequence encoding HRV VP4 and HRV VP4His using the appropriate primers (HRV VP4\_F and HRV VP4\_R or HRV VP4\_F and HRV VP4His\_R, Table 3.2). The schematic of the PCR strategy and the generated PCR products for HRV VP4 and HRV VP4His are shown in Figure 3.14. Similarly, constructs were designed to express VP4 and VP4His from PV and FMDV using the appropriate primers (PV VP4\_F and PV VP4\_R or PV VP4\_F and PV VP4His\_R; FMDV VP4\_F and FMDV VP4\_R or FMDV VP4\_F and FMDV VP4His\_R, Table 3.2), pET23a vector was used instead of pET23d and *NcoI* restriction site was replaced by *NdeI* restriction site.



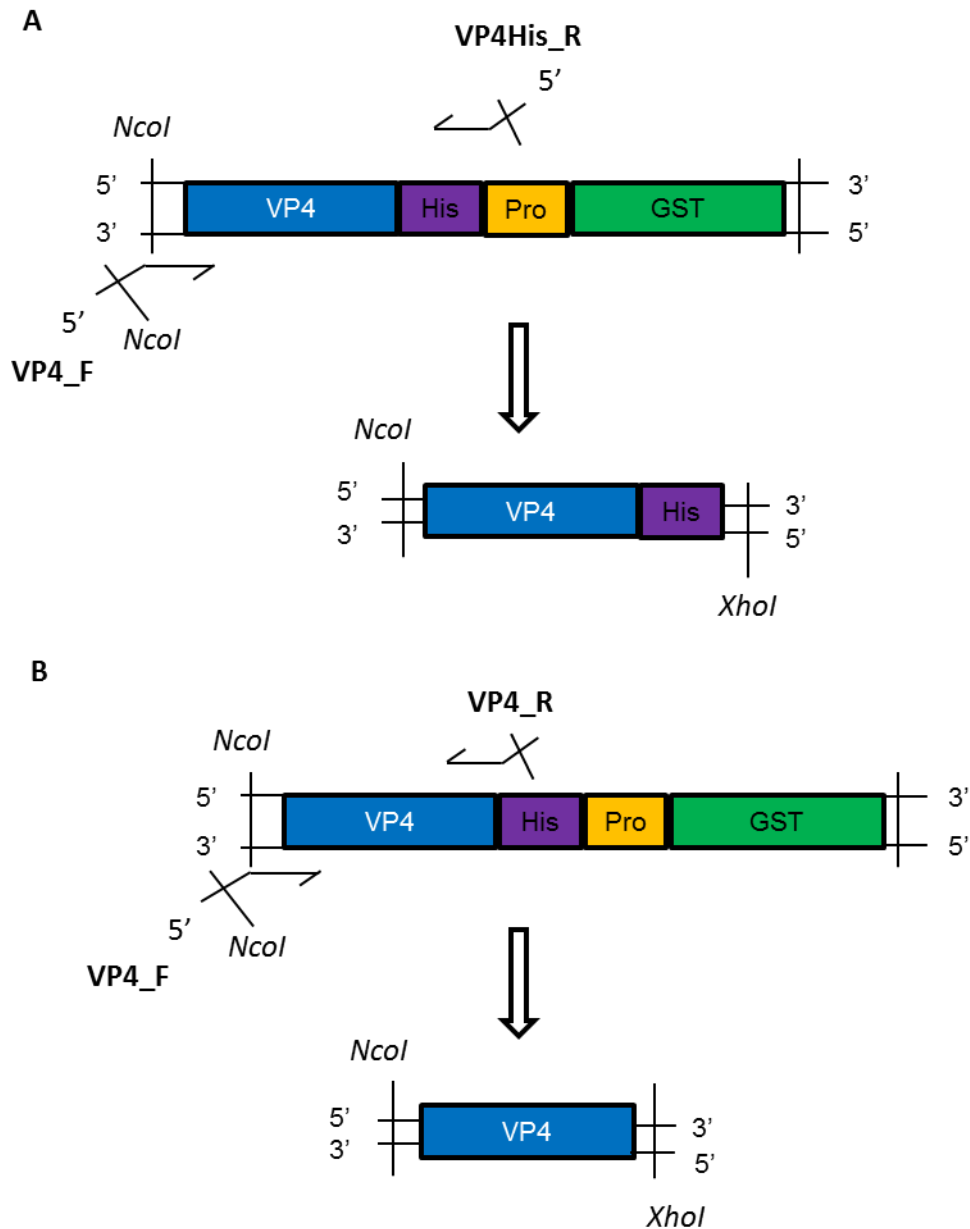


**Figure 3.14 Schematic of PCR strategy used for the generation of plasmids encoding VP4 and VP4His.**

PCR products **A**. VP4His and **B**. VP4 were generated for HRV, PV and FMDV. *NcoI* cleavage site for HRV was replaced by *NdeI* cleavage site in PV and FMDV VP4 plasmid constructs. **Pro: 3C protease or thrombin protease encoding sequences.**

The sizes of PCR products for HRV VP4 and VP4His were confirmed by 1.5 % agarose gel electrophoresis (section 2.2.5) and products digested with *NcoI* and *XhoI* (section 2.2.4) (Figure 3.15). Digestion products were gel purified and ligated into the backbone obtained from *NcoI* and *XhoI* restriction digestion of pETHRV VP4ThGST (sections 2.2.4-2.2.7).

*E.coli* DH5 $\alpha$  cells were transformed with the ligation reactions and positive clones for pETHRV VP4 and pETHRV VP4His identified by colony screen PCR (section 2.2.2.2) using appropriate primers (T7\_P and T7\_T) (Figure 3.16). The sequence of the insert was confirmed by

sequencing (section 2.2.3). Similarly, PV and FMDV VP4 and VP4His constructs were generated and sequences confirmed.

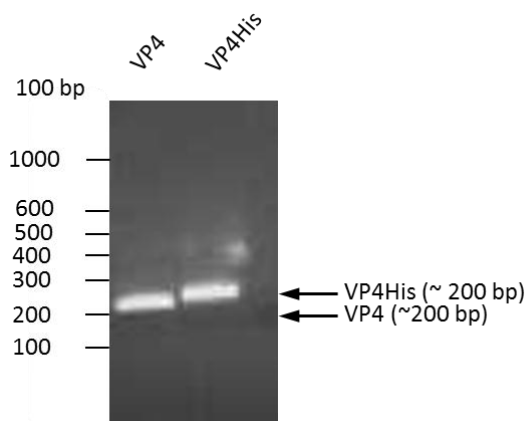


**Figure 3.15 PCR amplified VP4 and VP4His digested with *NcoI* and *XhoI*.**

An image of a preparative 1.5 % agarose gel showing the products of VP4 and VP4His digested with *NcoI* and *XhoI* and observed at ~ 200 bp. The size of molecular weight markers (100 bp ladder) is indicated to the left of the image and was used to confirm the size of the digested products (~200 bp).

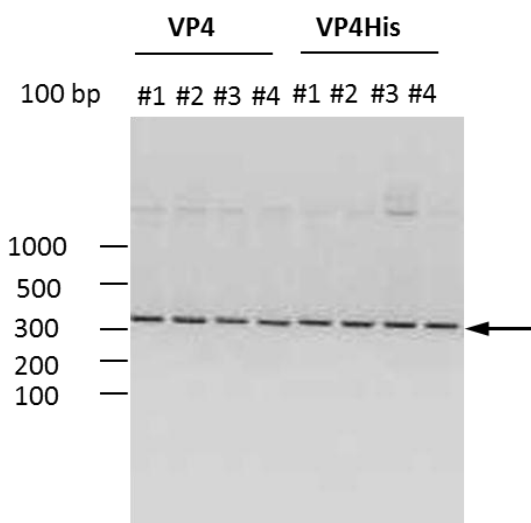


**Figure 3.16 Identification of positive pETHRV VP4 and pETHRV VP4His clones by colony screen PCR.**

An image of a 1.5 % agarose gel showing the identification of positive clones for pETHRV VP4 and pETHRV VP4His by colony screen PCR using T7\_P and T7\_T as primers. Black arrow indicates PCR amplified HRV VP4 or HRV VP4His. The size of molecular weight markers (1Kb ladder) is indicated to the left of the image and was used to confirm the size of the product (~300 bp).

### 3.3.2 Expression of VP4 and VP4His

Expression plasmids generated for VP4 and VP4His, corresponding to VP4 from HRV, PV or FMDV (section 3.3.1) were used to investigate expression levels of VP4 and VP4His. Myristoylated VP4 and VP4His were expressed by co-transformation of *E.coli* pLysS BL21 (DE3) cells with plasmids encoding VP4 (or VP4His) with plasmid encoding NMT (section 2.2.8).

Small scale cultures of transformed *E.coli* BL21 (DE3) pLysS cells were grown at 30°C or 37°C to an OD<sub>600</sub> of 0.7 then induced with IPTG. A range of IPTG concentrations (0.2 mM, 0.5 mM or 1 mM) were tested to induce protein expression and no significant differences were observed. IPTG was used at 0.2 mM for the induction of expression in all future experiments. Samples were collected at 3 hrs post induction and analysed by SDS-PAGE (section 2.3.1), Coomassie staining (section 2.3.4.1) and anti-His western blot (section 2.3.5). Expression levels for HRV VP4His were similar at 30°C and 37°C, detected by Coomassie staining and anti-His western blot. Expression levels for PV VP4His were below the detection limit of Coomassie stain but were easily detected by anti-His western blot. PV VP4His expression levels were higher at 30°C than 37°C. FMDV VP4His expression levels could not be detected at either temperature by Coomassie staining or anti-His western blot.

The induction of expression for untagged VP4 from HRV was detected by Coomassie staining (section 2.3.4.1) and anti-VP4C-terminus western blot (section 2.3.5). The expression levels of PV and FMDV VP4 were too low to be detected by Coomassie staining. The lack of an antibody against VP4 of PV and FMDV prevented the analysis of expression levels of PV and FMDV VP4 by western blot.

On the basis of the observed expression levels, for the production of recombinant VP4 from *E.coli* BL21 (DE3) pLysS cells it was decided to focus on HRV VP4His.

### 3.3.3 Purification of HRV VP4His

Having shown that PV and FMDV VP4 or VP4His were not expressed to sufficient levels, remaining studies used HRV VP4His. The presence of the His-tag facilitated protein purification and identification by western blot.

In order to maximise the yield of purified VP4His, optimisation of purification conditions were carried out. Following induction of VP4His expression in *E.coli* BL21 (DE3) pLysS cells, the bacterial pellet was harvested and lysed under denaturing or non-denaturing conditions. Lysis under non-denaturing conditions (section 2.12) did not give a sufficient yield of purified VP4His as majority of it was insoluble. Therefore, lysis using denaturing conditions was attempted.

Lysis using denaturing conditions is a standard approach to purify recombinant proteins which are expected to be insoluble. The bacterial pellet expressing VP4His was lysed using denaturing conditions (section 2.13). The total lysate was centrifuged to pellet the cell debris and the clarified supernatant applied to nickel affinity chromatography columns. The fractions containing His-tagged proteins were eluted from the column using increasing concentrations of imidazole and analysed by SDS-PAGE, Coomassie staining and anti VP4 C- terminus western blot (section 2.13) (Figure 3.17). Comparison of the two purification conditions showed that a higher yield of VP4His was purified when denaturing conditions were used for protein purification.

The final yield of purified VP4His improved with an increase in urea concentration (3 M, 5 M, 7 M). This was possibly due to increased solubilisation of VP4His. The denaturing conditions with 7 M urea were used for the purification of myristoylated (VP4His) and unmyristoylated VP4His ( $\Delta$ VP4His) (section 2.13). The purified material was dialysed against a stepwise urea gradient and PBS to remove urea. This resulted in VP4His becoming insoluble and therefore precipitating out of solution. The precipitated material was collected and resuspended in DMSO and stored at  $-20^{\circ}\text{C}$  (section 2.13). The high purity of VP4His and  $\Delta$ VP4His was demonstrated by silver stained SDS-PAGE (section 2.3.4.2) (Figure 3.18). The use of polar solvents such as DMSO or methanol are routinely used for resuspending insoluble proteins and are compatible for use in functional assays with model membranes (StGelais *et al.*, 2009; Wetherill *et al.*, 2012). Therefore, VP4His resuspended in DMSO was used in liposome based permeability assays (section 2.23).

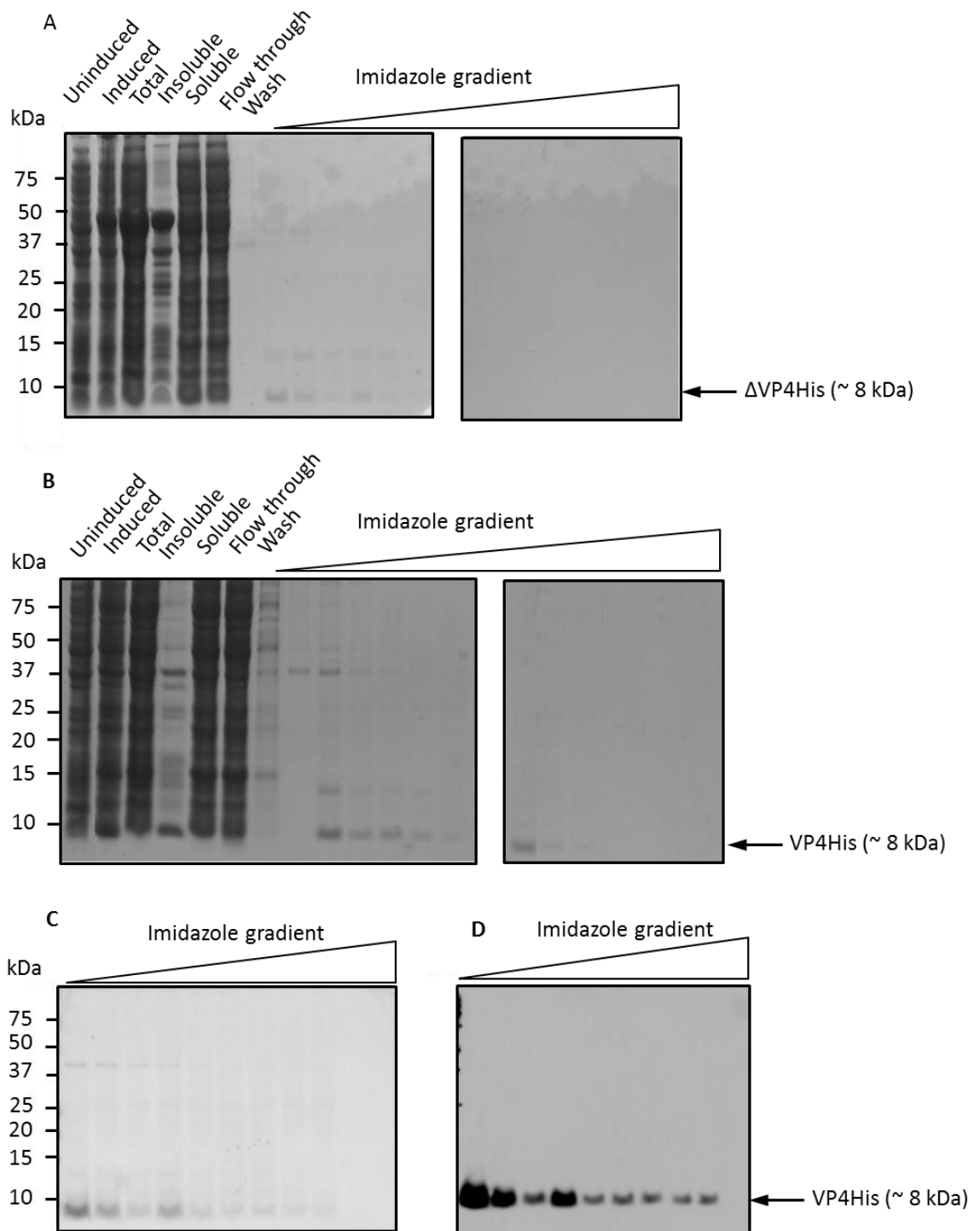


**Figure 3.17 Purification of VP4His and  $\Delta$ VP4His by nickel affinity chromatography.**

**A.** Unmyristoylated VP4His ( $\Delta$ VP4His) and **B.** Myristoylated VP4His (VP4His) eluted from a nickel affinity column using an imidazole gradient and analysed by 16.5 % tris-tricine SDS-PAGE and Coomassie staining. **C.** VP4His fractions eluted from a nickel affinity column using an imidazole gradient and analysed by 16.5 % SDS-PAGE and Coomassie staining or **D.** Same samples as in panel C and analysed by 16.5 % SDS-PAGE and anti-VP4 C-terminus western blot. The size of molecular weight markers (kDa) is indicated to the left of the image.

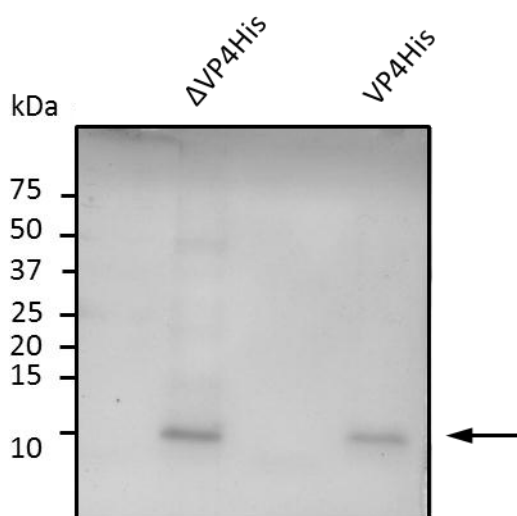


**Figure 3.18 Purified VP4His visualised by silver staining.**

VP4His and  $\Delta$ VP4His precipitate resuspended in DMSO and analysed by 16.5 % tris-tricine SDS-PAGE and silver staining. Black arrow indicates visualised VP4His and  $\Delta$ VP4His at the expected apparent molecular weight of  $\sim$ 8 kDa. The size of molecular weight markers (kDa) is indicated to the left of the image.

### 3.3.4 Quantification of recombinant VP4His

Bradford assay is a standard assay used to determine the concentration of proteins. It is based on the principle that upon binding to protein, the absorbance maximum for an acidic solution of Coomassie brilliant blue (G-250) shifts from 465 nm to 595 nm. Hydrophobic and ionic interactions stabilise the anionic form of the dye which results in a visible colour change. Primarily arginine and to a lesser degree lysine and histidine participate in the binding of the anionic form of the dye. Binding of the anionic species to the aromatic residues (tryptophan, phenylalanine and tyrosine) results in a marginal contribution to the colour change (Compton and Jones, 1985; Georgiou *et al.*, 2008). Due to the small size and lack of desirable amino acid composition of VP4His, the protein concentrations could not be accurately determined by the Bradford assay (section 2.3.10.2).

BCA (bicinchoninic acid) protein assay is another standard assay used to determine the concentration of proteins. The principle of the BCA assay is that  $\text{Cu}^{+2}$  - protein complexes are formed under alkaline conditions, followed by the reduction of  $\text{Cu}^{+2}$  to  $\text{Cu}^{+1}$ . The amino acids cysteine, tryptophan and tyrosine and the peptide bond participate in the reduction of  $\text{Cu}^{+2}$  to  $\text{Cu}^{+1}$ . The extent of reduction is dependent on protein concentration in the sample. BCA forms a purple coloured complex with  $\text{Cu}^{+1}$  under alkaline conditions. This provided the basis for monitoring the reduction of alkaline  $\text{Cu}^{+2}$  by proteins at an absorbance maximum of 562 nm

(Stoscheck, 1990). The BCA assay was not dependent on the same amino acids as Coomassie brilliant blue used in the Bradford assay and was therefore used to determine recombinant VP4 protein concentrations (section 2.3.10.1).

Further, spectrophotometry (Nanodrop 8000) was used to determine the concentration of recombinant VP4 proteins by measuring absorbance at 280 nm (section 2.3.10.3). This was expected to affect the determination of protein concentration due to the presence of aromatic amino acids.

It was important to bear in mind that even though spectrophotometry (Nanodrop) is routinely used for estimating protein concentrations, BSA was used as the default reference set which has an amino acid composition different to VP4, therefore, may influence the measurements of VP4 concentration.

As a result of these above mentioned concerns, concentration of purified VP4His estimated by BCA was confirmed by comparison with native VP4 present in known quantities in purified virus. HRV16 (3 or 1 µg, equivalent to 0.24 or 0.08 µg VP4 respectively) and VP4His (3 µg, 2 µg, 1 µg, 0.5 µg, 0.25 µg) were subjected to SDS-PAGE and visualised by a combination of silver staining (section 2.3.4.2) (Figure 3.19A) and anti-VP4 C-terminus western blot (section 2.3.5) (Figure 3.19B). The migration of native VP4 and VP4His was consistent with their predicted molecular weights of approximately 7.4 kDa and 8.2 kDa, respectively (Figure 3.19).

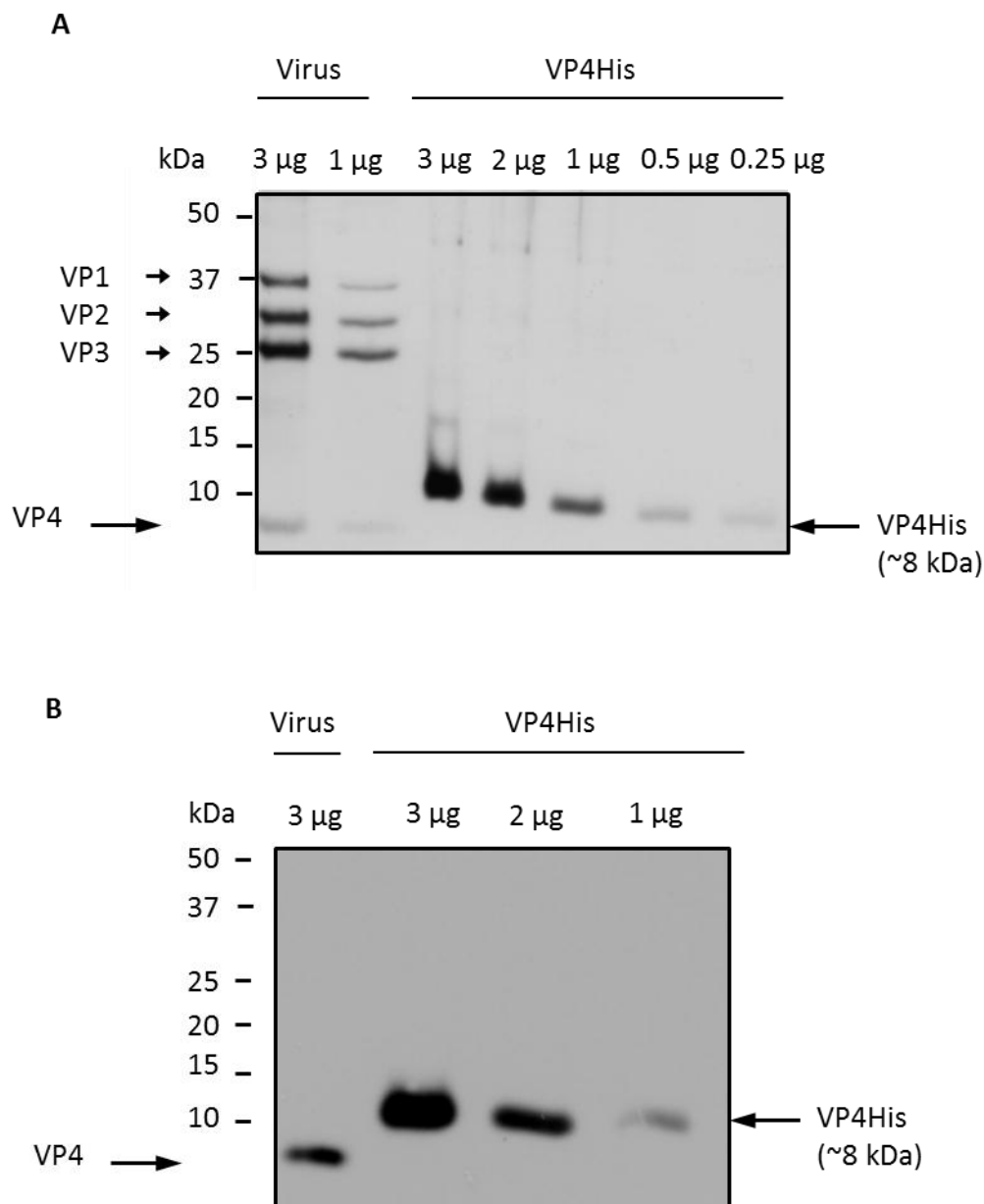


**Figure 3.19 Quantifying VP4His by comparison with native VP4 from virus (HRV16).**

HRV16 and VP4His were subjected to 16.5 % tris-tricine SDS-PAGE and visualised by **A.** silver staining and **B.** anti-VP4 C-terminus western blot. Black arrows on the left indicate the expected position of the viral proteins, VP1, VP2, VP3 and VP4. Black arrows on the right indicate VP4His at the expected size of ~8 kDa. The size of molecular weight markers (kDa) is indicated to the left of the image.

An increase in the amounts DMSO in the sample resulted in slower migration of VP4His. This was shown not to be unique to VP4 as the amounts of DMSO in a sample of aprotinin, affected its migration on SDS-PAGE (Figure 3.20). A dilution series of aprotinin (3 µg - 0.25 µg) was added to a standard volume (16.5 µl) of DMSO or SDS-PAGE loading buffer. In both cases, aprotinin was observed at the expected ~6.5 kDa (Figure 3.20A). However, when a dilution series of aprotinin with correspondingly different amounts of DMSO was subjected to SDS-



PAGE, aprotinin samples containing a higher volume of DMSO migrated slower on SDS-PAGE compared to aprotinin samples containing lower volumes of DMSO (Figure 3.20B). Therefore, the migration of VP4His appeared slower with increasing concentration as a result of the increasing concentration of DMSO in these samples (Figure 3.19).

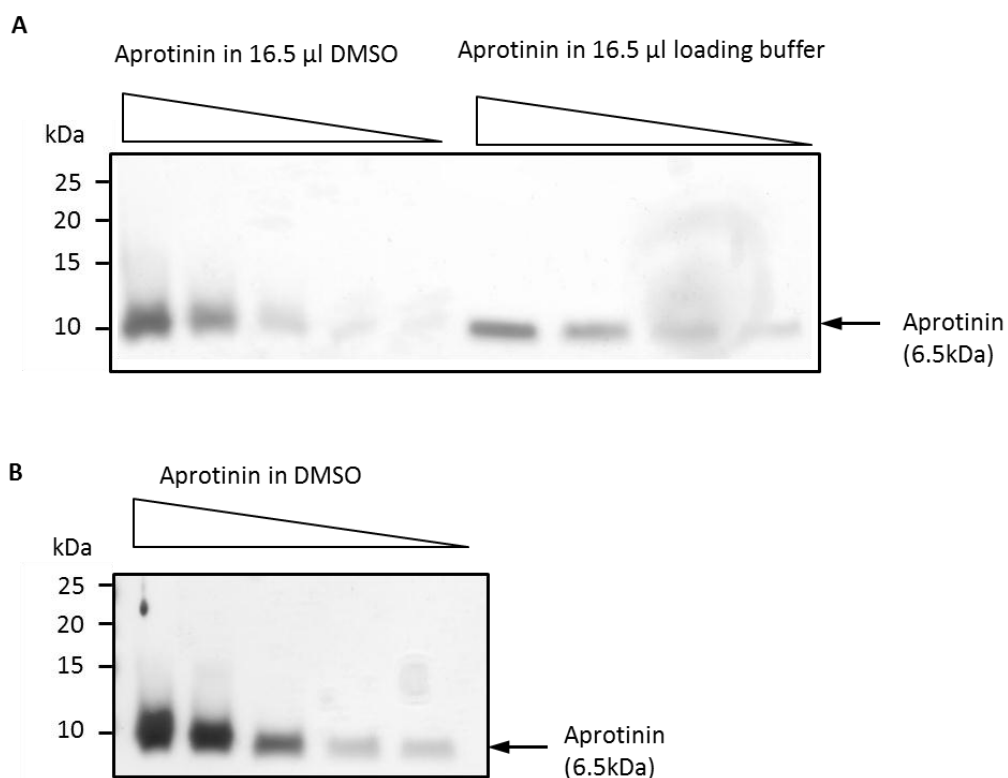


**Figure 3.20 Effect of DMSO on the migration of aprotinin.**

**A.** Dilution series of aprotinin (3, 2, 1, 0.5, 0.25 µg) in a standard volume of 16.5 µl of DMSO or SDS-loading buffer. **B.** Dilution series of aprotinin (3, 2, 1, 0.5, 0.25 µg) in DMSO. Samples in panels A and B were analysed by 16.5 % tris-tricine SDS-PAGE and silver staining. Black arrows indicate aprotinin at the expected size of 6.5 kDa. The size of molecular weight markers (kDa) is indicated to the left of the image.

## 3.4 Purification of recombinant VP4 from His-trpLE-VP4

### 3.4.1 Cloning of His-trpLE HRV VP4 constructs

Although section 3.3 describes the development of an approach for successfully producing VP4His sufficient (approximately 0.16 mg per litre of culture) for the intended biochemical and functional studies, it was desirable to have a higher yield of VP4 to carry out structural studies such as nuclear magnetic resonance (NMR).

The approach for optimisation of recombinant VP4 production, suitable for NMR structural studies, was carried out in collaboration with Professor Chou, Harvard Medical School, USA. A routine approach for the expression and purification of membrane proteins involved the expression of the protein as a C-terminal fusion to His<sub>9</sub> tag followed by trpLE in pMM-LR6 vector (Figure 3.1). VP4 protein expressed as a fusion to His-trpLE (His-trpLE-VP4) formed inclusion bodies. The release of VP4 from His-trpLE-VP4 required cleavage with cyanogen bromide (CNBr) which hydrolyses peptide bonds at the C-terminus of methionine (section 2.15). As methionine residues are sensitive to CNBr cleavage, the methionine at position 17 of VP4 was substituted for serine.

PCR amplification of pETVP4GST template DNA was used for the generation of HRV VP4 (methionine at position 17 substituted with serine), flanked by the restriction sites, *HindIII* and *BamHI* at the 5' and 3' end, respectively. Overlapping PCR was carried out as described for VP4GST (section 3.2.1) except primers *HindIII* VP4\_F and VP4 (MΔS)\_R; VP4 (MΔS)\_F and *BamHI* VP4\_R (Table 3.2) were used to obtain intermediate PCR products. Overlapping PCR was carried out with *HindIII* VP4\_F and *BamHI* VP4\_R (Table 3.2). The resulting PCR products were analysed by 1 % agarose gel electrophoresis (Figure 3.21).

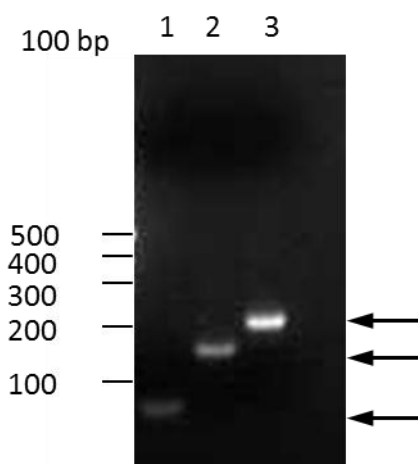


**Figure 3.21 PCR amplification products used for the generation of HRV VP4 to be ligated into His-trpLE pMM-LR6 vector.**

Lane 1: PCR amplification product of HRV VP4 using primers *HindIII* VP4\_F and VP4 ( $\Delta$ S)\_R; Lane 2: PCR amplification product of HRV VP4 using primers VP4 ( $\Delta$ S)\_F and *Bam*HI VP4\_R; Lane 3: PCR amplification product of HRV VP4 using primers *HindIII* VP4\_F and *Bam*HI VP4\_R. Black arrows indicates PCR amplified products at the expected sizes. 100 bp ladder was used to confirm the size of the PCR amplified products. The size of molecular weight markers (100 bp ladder) is indicated to the left of the image and was used to confirm the size of the PCR amplified products.

The final PCR product (Lane 3, Figure 3.21) was digested with restriction enzymes, *HindIII* and *Bam*HI. The digested product was gel purified (section 2.2.6) and ligated into *HindIII* and *Bam*HI digested pMM-LR6 His-trpLE (kindly provided by Bill Qingshan Fu, Chou lab). *E.coli* DH5 $\alpha$  cells were transformed with the plasmid encoding His-trpLE-VP4 (section 2.2.8). A few colonies were picked and grown in LB media overnight. Positive clones containing the correct sequence of the insert were confirmed by sequencing (Sanger sequencing, Genomics Core facilities, Harvard Medical School).

### 3.4.2 Expression of His-trpLEVP4

Small scale expression trials were carried out to determine the optimal conditions for expression of His-trpLE-VP4. Small scale LB cultures of *E.coli* BL21 (DE3) cells (NEB) transformed with plasmids encoding His-trpLE-VP4 were grown at 18°C, 25°C or 37°C to OD<sub>600</sub> 0.7 and induced with 0.5 mM IPTG for 3 hrs or o/n. The induced cells were harvested and expression levels compared by SDS-PAGE (section 2.3.1) and Coomassie staining (section 2.3.4.1). The levels of expression for His-trpLE-VP4 were highest when induced o/n at 37°C. The levels of expression for His-trpLE-VP4 at the other temperatures and time points were comparatively lower as visualised by SDS-PAGE and Coomassie staining. The expression levels

for His-trpLE-VP4 at 37°C were lower than those observed with HRV VP4PreGST and VP4ThGST at 37°C (section 3.2.2) but only marginally higher than expression levels of HRV VP4His at 30°C (section 3.3.2). Therefore, conditions of inducing expression o/n at 37°C were used to generate His-trpLE-VP4.

The conditions of temperature (37°C), IPTG concentration (0.5 mM) and duration of induction of expression (o/n) used for expression of His-trpLE-VP4 in LB media were also used for the induction of expression in M9 minimal media (section 2.15). Levels of expression obtained in LB media and M9 minimal media were similar. Addition of <sup>15</sup>N labelled NH<sub>4</sub>Cl to M9 media was used to generate <sup>15</sup>N labelled VP4.

### 3.4.3 Purification of VP4 from His-trpLE-VP4 constructs

Previous experience in the lab (Chou lab, Harvard Medical School) using His-trpLE in the pMM-LR6 vector for expression of membrane proteins, indicated that such proteins formed inclusion bodies (IB). His-trpLE-VP4 protein expression was induced at 37°C and bacterial cells harvested after o/n induction of His-trpLE-VP4 expression (section 3.4.2). Cell pellets were lysed using denaturing conditions and sonication. IB were purified, lysed, debris pelleted, s/n applied to a nickel affinity chromatography column and His-trpLE-VP4 eluted from the column using formic acid. Cleavage of His-trpLE-VP4 with CNBr resulted in the release of VP4. The cleavage products were dialysed against water using a membrane with a 3.5 kDa molecular weight cut off. Dialysis resulted in the precipitation of VP4 and uncleaved His-trpLE-VP4, which were solubilised by the addition of acetonitrile. This solution was lyophilised o/n to obtain the proteins as a dried powder which was dissolved in formic acid and applied to an HPLC column. VP4 was purified from uncleaved fusion protein (His-trpLE-VP4) by RP-HPLC, with increasing concentrations of acetonitrile introduced over a linear 0-100 % gradient to elute the proteins from the column in order of their hydrophobicity (section 2.15). The efficiency of CNBr cleavage of His-trpLE-VP4 resulting in the release of VP4 was 50 %-70 %. The peak fractions containing proteins, identified by readings at A<sub>280</sub> nm (indicated by peak numbers in Figure 3.22) were collected and analysed by SDS-PAGE and Coomassie staining. <sup>15</sup>N labelled VP4 was expressed as a His-trpLE fusion protein (section 3.4.2), purified and analysed as described for unlabelled VP4. A schematic of the purification procedure is shown in Figure 3.23 (section 2.15).

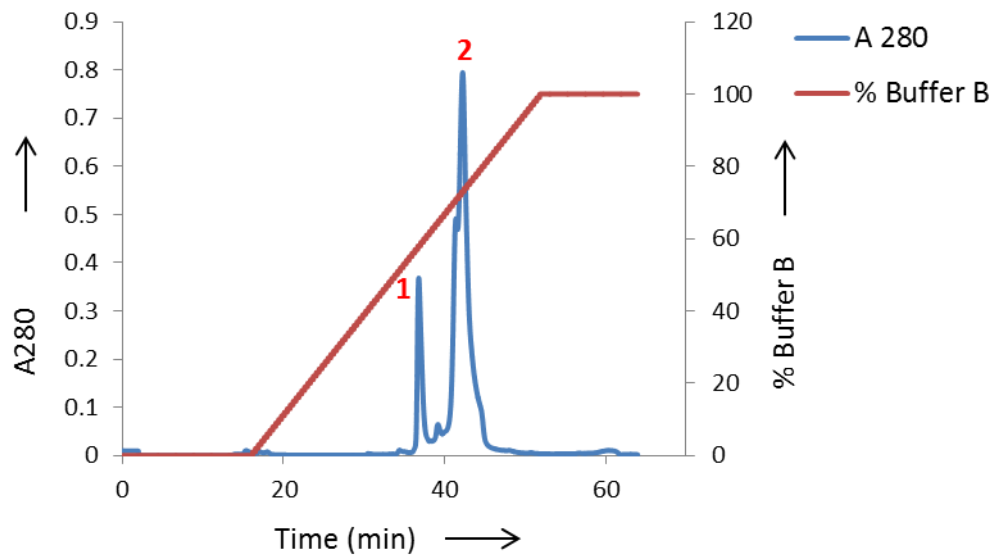


**Figure 3.22 Separation of His-trpLE-VP4 cleavage reaction products by RP-HPLC.**

Fractions containing protein were eluted from a C18 column by a linear acetonitrile gradient shown in red as percentage buffer B. Spectra were recorded at 215 nm and 280 nm. Protein containing fractions appear as peaks which are labelled in red. Peak 1 corresponds to VP4 and Peak 2 corresponds to His-trpLE and His-trpLE-VP4.

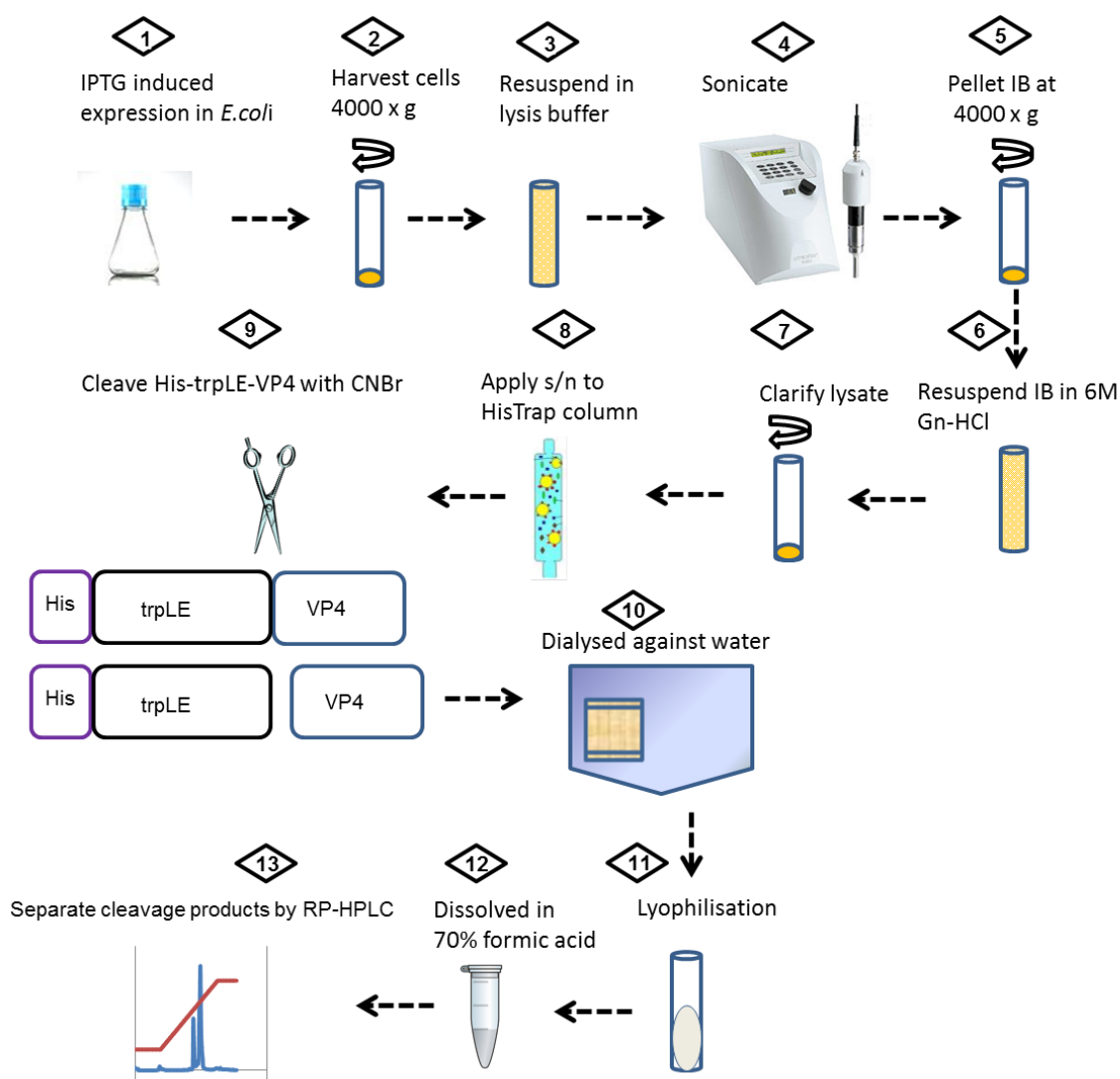


**Figure 3.23 Schematic of purification of VP4 from His-trpLE-VP4.**

An overview of the method used for the purification of VP4 from His-trpLE-VP4 is shown in steps 1-13. Briefly, *E. coli* BL21 (DE3) cells were transformed with plasmids encoding His-trpLE-VP4. His-trpLE-VP4 was expressed in inclusion bodies which were lysed and His-trpLE-VP4 purified by nickel affinity chromatography. VP4 was released from His-trpLE-VP4 by cleaving with CNBr. The lyophilised cleavage products were separated by RP-HPLC. IB: inclusion bodies, RP-HPLC: reverse phase high pressure liquid chromatography

The molecular weight of RP-HPLC purified HRV VP4 was confirmed by matrix-assisted laser desorption/ionization (MALDI) mass spectrometry (carried out at Dana Farber, Harvard Medical School) which showed a molecular mass of 7312.27 Da. This was approximately the expected theoretical molecular weight of 7322 Da (Figure 3.24A). The concentration of VP4 generated by this method was determined by spectrophotometry ( $A_{280}$  nm). Typically 5 mg of VP4 was purified from 1 L of culture and was of high purity as demonstrated by silver stained SDS-PAGE (Figure 3.24B).

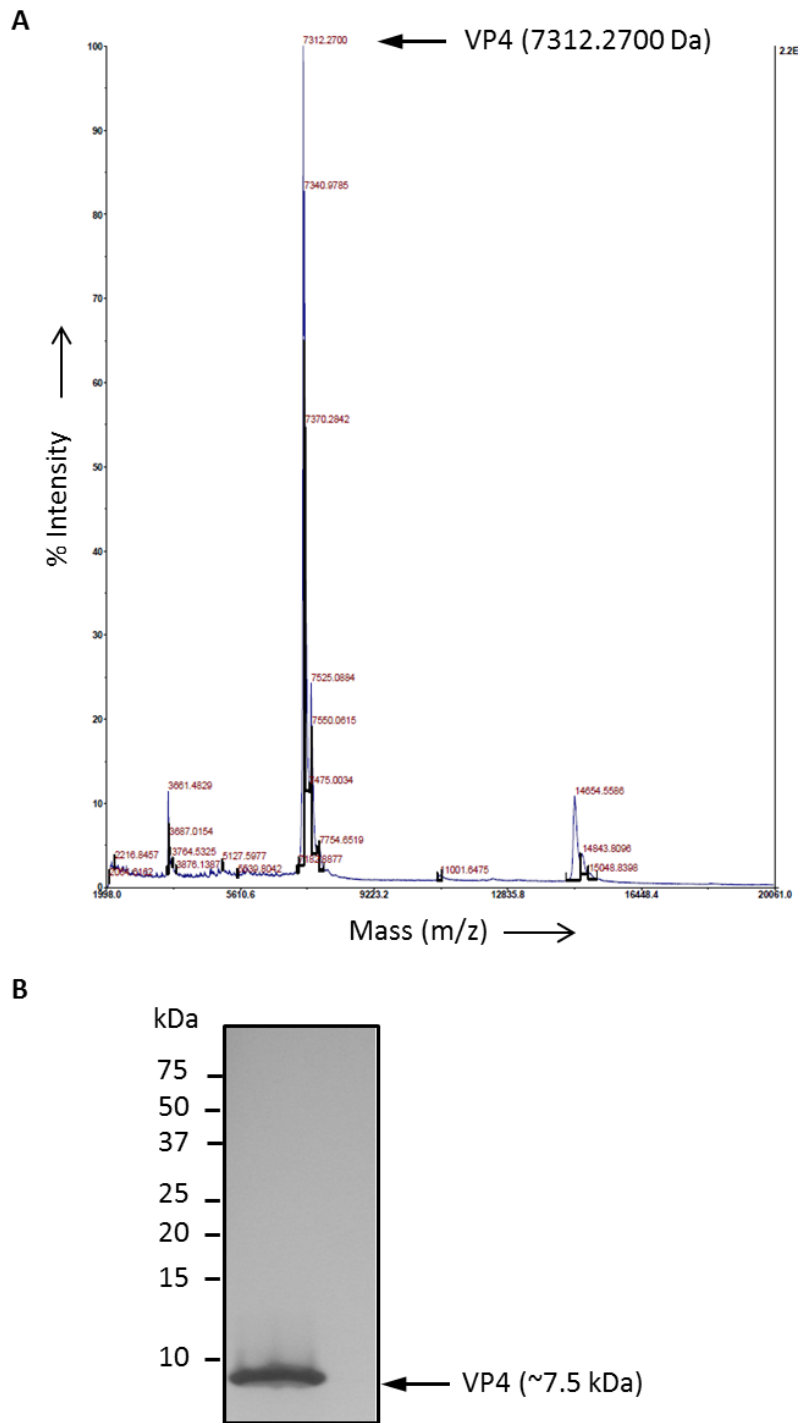


**Figure 3.24 Molecular weight and purity of purified HRV VP4.**

**A.** MALDI mass spectrometric analysis confirming molecular weight of purified HRV VP4. Black arrow indicates the observed VP4 peak at the expected molecular weight (~7000 Da)  
**B.** Purified HRV VP4 visualised by silver stained 16.5 % tris-tricine SDS-PAGE. The size of molecular weight markers (kDa) is indicated to the left of the image.

Therefore, the purification of VP4 from His-trpLE-VP4 gave a much higher yield of VP4 compared to that obtained with the previous strategies of using GST-tagged VP4 as IB or soluble protein and cleavage with 3C or thrombin protease (section 3.2) or by direct expression of VP4His (section 3.3). The purity obtained by this purification method was similar to that observed with direct expression of VP4His and purification under denaturing conditions (section 3.3). However, the yield was significantly higher (~5 mg per litre) and, therefore, this approach was used to generate  $^{15}\text{N}$ -VP4 for NMR structural studies of the VP4 membrane pore complex (described in Chapter 6).

### 3.5 Purification of native VP4 from HRV16

Methods for the production of VP4His and VP4 for functional, biochemical and structural studies were optimised and determined, as described in sections 3.3 and 3.4. It was desirable to include native VP4 from virus for use as a control in the functional studies.

Existing laboratory stocks of HRV16 [derived from the infectious cDNA plasmid (Davis *et al.*, 2008)] were used to infect large scale HeLa Ohio cell cultures. Different MOIs (0.02, 0.1 and 0.5) were tested and the optimal MOI of 0.1 was used to obtain complete CPE at 48 hrs, following which cells were harvested. HRV16 was purified using standard methods (section 2.20). Sucrose gradients were used to purify HRV16 and fractions collected from bottom to top. The fractions were measured at  $A_{260}$  to identify the fractions containing HRV16 (Figure 3.25A). Purified HRV16 was separated by SDS-PAGE (section 2.3.1) and visualised by Coomassie staining (section 2.3.4.1). By comparison with known amounts of BSA on Coomassie stained SDS-PAGE (Figure 3.25B) and measurements taken at  $A_{260}$  nm, concentration of HRV16 was estimated to be 0.15 mg/ml. Approximately 0.6 mg of HRV16 was purified and was of high purity as demonstrated by silver stained (Figure 3.25C).

To make radiolabelled HRV16, the protocol was modified such that cells were metabolically labelled with  $^{35}\text{S}$  methionine to make radiolabelled virus ( $^{35}\text{S}$  HRV16) (section 2.21).



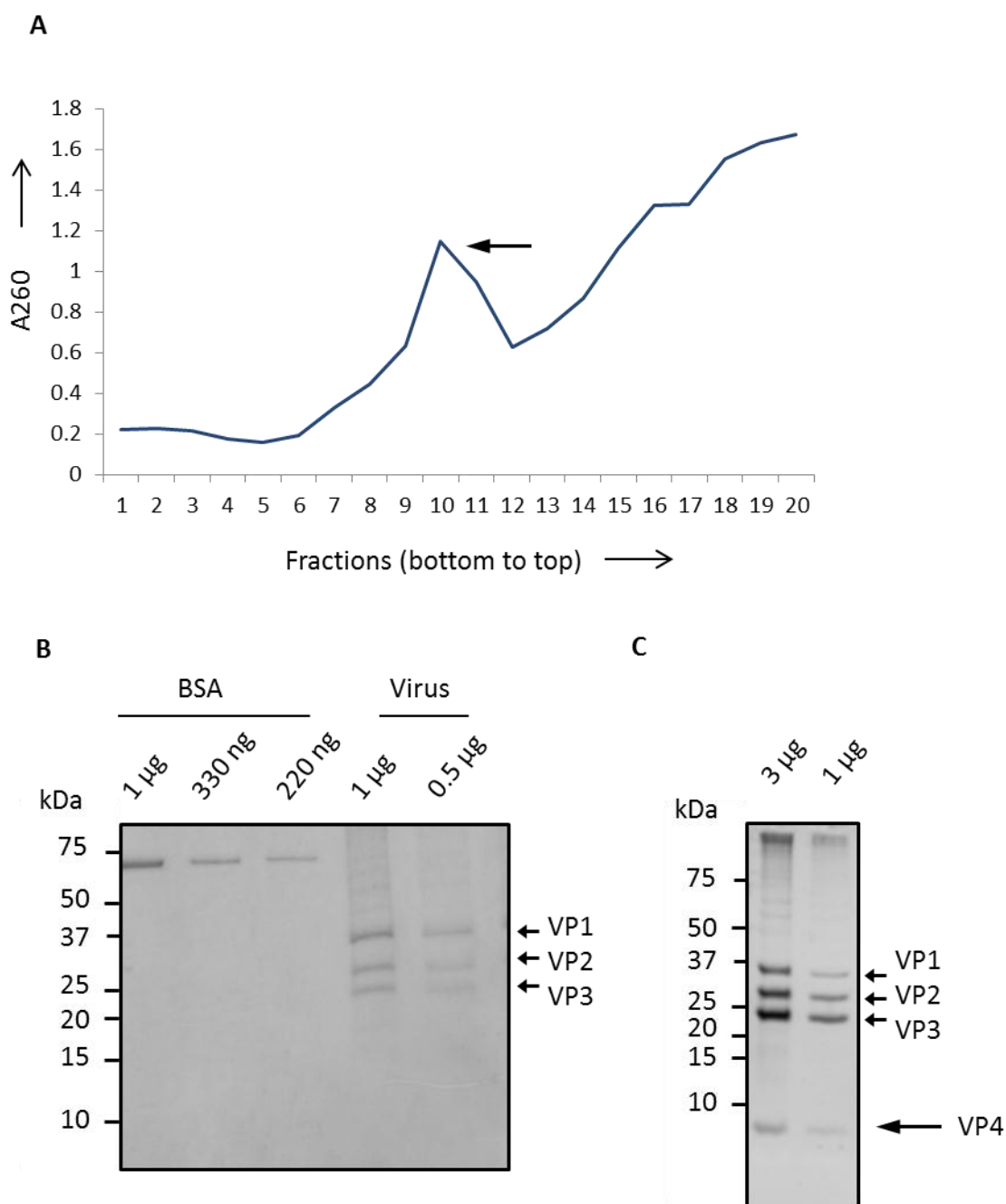


**Figure 3.25 Purification of HRV16.**

**A.** Absorbance measurements at 260 nm of HRV16 sucrose density gradient fractions. Black arrow indicates the fraction containing HRV16. **B.** Coomassie stained 16.5 % tris-tricine SDS-PAGE to estimate the concentration of HRV16 with known concentrations of BSA. Black arrows indicate the expected position of the viral proteins- VP1, VP2, VP3 (VP4 was not observed). **C.** Silver stained 16.5 % tris-tricine SDS-PAGE demonstrating the purity of purified HRV16. Black arrows indicate the expected position of the viral proteins- VP1, VP2, VP3 and VP4. The size of molecular weight markers (kDa) is indicated to the left of the image in panels B and C.

VP4 is released from HRV during uncoating, a process that can be triggered *in vitro* by heating at 60°C. Released VP4 was thought likely to be insoluble, based on findings in this study and a previous report showing that VP4 indeed precipitated upon release and that this could be used to facilitate the separation of VP4 from virus (Talbot *et al.*, 1973). Therefore, the isolation of VP4 from heated virus particles was investigated.

<sup>35</sup>S HRV16 and pre-heated <sup>35</sup>S HRV16 (60°C for 10 min) were analysed on a 15-45 % sucrose gradient. The gradient was fractionated from bottom to top. In order to include material that may have precipitated, the pellet was resuspended in SDS-loading buffer and included in the analysis. The position of radiolabelled virus particles was determined by reading a proportion of each fraction and the pellet on a scintillation counter. Particle alterations are often characterised by their sedimentation coefficients (S) in a sucrose gradient. The sedimentation coefficient of HRV16 is 150S and that of its empty particle is 80S. As expected, pre-heating of HRV16 yielded empty particles (80S), as depicted by the observed shift in particle sedimentation relative to the native virus particle (150S) (Figure 3.26). The fraction containing 150S (fraction number 12, Figure 3.26) was different to that containing 80S (fraction number 16, Figure 3.26). Given the insoluble nature of VP4, it was expected to be in the pellet following sucrose density gradient purification of the pre-heated HRV16 sample. The scintillation counts per minute (cpm) of the fractions and pellet revealed a signal in the pellet (Figure 3.26) of the gradient containing the particles converted to empty particles. A similar peak was absent in the pellet of the gradient containing virus particles.

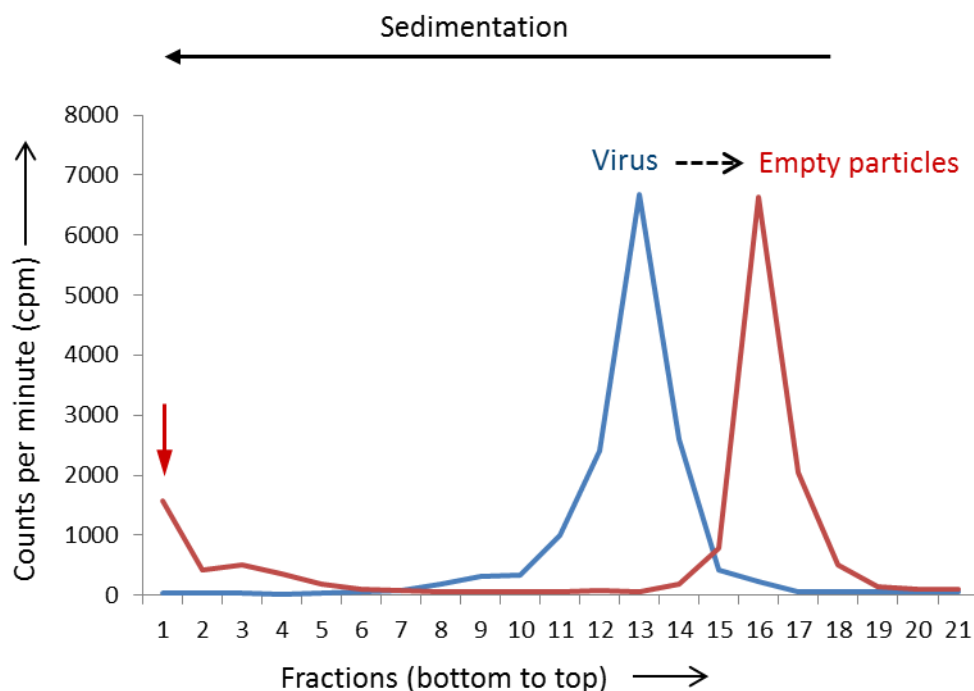


**Figure 3.26 Scintillation counts of fractions obtained from sucrose density gradients containing virus or pre-heated virus particles.**

Virus (blue) and empty particles (red) were obtained at the expected positions in the sucrose density gradient. The pellets of gradients containing virus particles and pre-heated virus particles were resuspended and counts per minute determined. A signal, indicated by the red arrow, in the pellet of the gradient containing pre-heated particles was observed.

In order to investigate if the signal observed in the pellet (red arrow, Figure 3.26) was due to VP4, the pellet was analysed by SDS-PAGE and autoradiography (section 2.3.7). Purified native HRV16 (0.5  $\mu$ g, 3  $\mu$ g), gradient fractions containing empty particles (fraction number 16, Figure 3.26) and fractions from the top of the gradient which were expected to be free of particles (fraction numbers 20 and 21, Figure 3.26), were used as controls to confirm the signal in pellet was that of VP4 (indicated by red arrow, Figure 3.26) by using autoradiography (Figure 3.27). As expected, upon resolving empty particles and purified virus by SDS-PAGE, VP1, VP2 and VP3 were detected in empty particles; and VP1, VP2, VP3 and VP4 were detected in purified virus. The intensity of appearance of the bands for the viral proteins increased with an increase in the amount of empty particles analysed by SDS-PAGE and autoradiography. However, VP4 could only be detected when 3  $\mu$ g of purified virus was analysed by SDS-PAGE and autoradiography (Figure 3.27). It was likely that the signal in the pellet was that of VP4 but the low concentration of VP4 and presence of only two  $^{35}$ S-labelled methionine residues in VP4 contributed to the generation of an insufficient signal that could not be detected by autoradiography. Therefore, the presence of VP4 in the pellet could not be confirmed and was

consistent with previously reported difficulties of detection of VP4 by autoradiography (Danthi *et al.*, 2003). Due to time constraints, this approach was not taken any further.

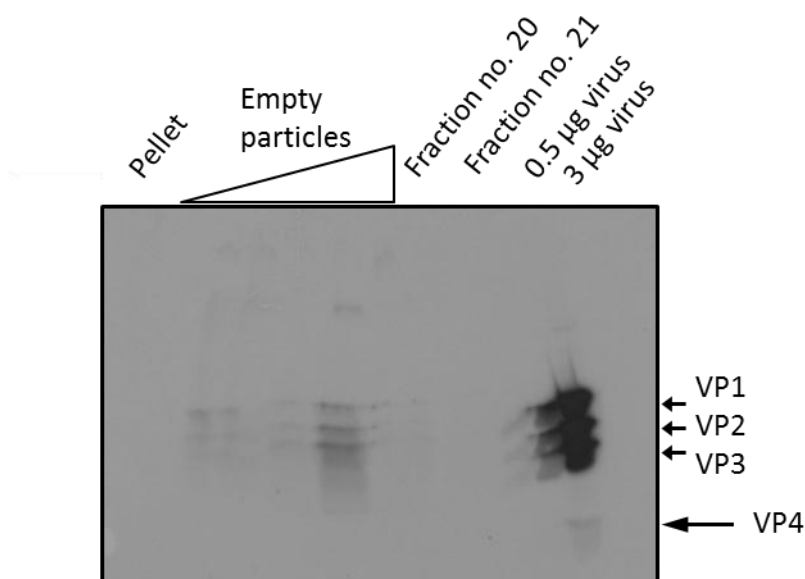


**Figure 3.27 Detection of  $^{35}\text{S}$  VP4 by autoradiography.**

The pellet of the sucrose gradient used to obtain  $^{35}\text{S}$  HRV16 empty particles was analysed by SDS-PAGE and autoradiography. Purified  $^{35}\text{S}$  HRV16 and the fractions of the sucrose density gradient containing  $^{35}\text{S}$  HRV16 empty particles or no particles were used as controls. Black arrows indicate the expected position of the viral proteins, VP1, VP2, VP3 and VP4.

### 3.6 Discussion

Prokaryotic systems have been successfully used for the overexpression and purification of small and hydrophobic membrane proteins. The protein of interest is often fused to tags such as GST (26 kDa) or maltose binding protein (42.5 kDa) to enhance protein solubility and facilitate purification. The aim of this project was to understand the role of VP4 in cell entry, therefore, generation of recombinant VP4 with a small tag or without a tag was considered to be ideal as large tags may affect VP4 function. Native VP4 is myristoylated at the N-terminus and both myristoylated and unmyristoylated recombinant proteins were, therefore, produced in *E.coli*. The requirement for myristoylation meant that VP4 could not be expressed as a fusion protein with a fusion partner at the N-terminus of VP4. Therefore, hexahistidine or GST-tags were fused to the C-terminus of VP4. Attempts were made at purifying VP4His from GST-tagged VP4 or directly expressing and purifying VP4 and VP4His. Purification of VP4His using denaturing conditions generated sufficient yields of VP4His to carry out functional and biochemical assays (described in chapters 4, 5 and 7). HRV VP4 fused to His-trpLE at the N-terminus of VP4 was used to generate a higher yield of unmyristoylated VP4, desirable for

carrying out preliminary structural studies on the VP4 membrane pore complex using NMR (described in chapter 6). HRV VP4ThGST was used to visualise the VP4 membrane pore complex by electron microscopy (Chapter 5).

An established system for the production of myristoylated protein in *E.coli* (Duronio *et al.*, 1990; Matsubara *et al.*, 2005) was used which has previously shown that myristate was added to VP4, as confirmed by mass spectrometry (Davis *et al.*, 2008). Myristoylated and unmyristoylated forms of VP4 were produced in order to investigate the influence of myristoylation on VP4-mediated membrane permeability.

The levels of GST-tagged VP4 expression observed were highest for HRV followed by PV which was followed by very low levels of expression for FMDV. Differences in amino acid composition may have contributed to the differences in expression levels. Although amino acid composition of VP4 from HRV, PV and FMDV are relatively similar (Figure 3.28), there are other factors such as codon bias that could contribute to the differences in observed VP4 expression levels.

```

HRV16 GAQVSRQNVGTHSTQNMVSNGLN-YFNINY-----FKDAASSGASRLDFSQDPSKF 52
PV    GAQVSSQKVGAEHNSNRAYGGSTIN-YTTINY-----YRDSASNAASKQDFSQDPSKF 52
FMDV  GAGQSSPATGSQNSG--NTGSIINNYMQQYQNSMDTQLGDNAISGGSNEGSTDTTSTH 58
      ** * .*:.. .. ** :* * :* * * * ..* . . : : *..

HRV16 TDPVK--DVLEKGIPTLQ----- 68
PV    TEPIK--DVLIKTAPEMLN----- 68
FMDV  TTNTQNNDFWFSKLASSAFSGLFGALLA 85
      * : * : * . :.

```

**Figure 3.28 Alignment of human rhinovirus, poliovirus and foot-and-mouth disease virus VP4.**

VP4 residues are coloured according to their physicochemical properties—small hydrophobic residues (red), acidic residues (blue), basic residues (purple), hydroxyl/sulphydryl/amine residues (green). \* (asterisk) indicates positions which have a single, fully conserved residue. : (colon) indicates conservation between groups of strongly similar properties, . (period) indicates conservation between groups of weakly similar properties. The alignment was obtained by submitting HRV, PV and FMDV VP4 amino acid sequences into the alignment programme <http://www.ebi.ac.uk/Tools/msa/clustalw2>.

Every organism shows codon bias as the codon usage frequency varies between different organisms and between proteins of the same organism. Codon usage is an important factor influencing protein expression (Gustafsson *et al.*, 2004) as major differences in codon usage between *E.coli* and host cells may result in decreased mRNA stability, premature termination of transcription or translation or inhibition of protein synthesis (as reviewed in Angov, 2011). In order to improve PV and FMDV VP4 expression levels, *E.coli* Rosetta-gami B (DE3) cells which supply cognate tRNAs for rarely used codons in *E.coli* were transformed with plasmids

encoding GST-tagged PV or FMDV VP4. This improved expression levels for GST-tagged PV VP4 but not for GST-tagged FMDV VP4 (section 3.2.2.1). For the comparison of the function of VP4 from HRV, PV and FMDV, the expression levels of FMDV VP4 required improvement. Therefore, GST-tagged FMDV VP4 which showed very low levels of expression was selected for an additional strategy of codon optimisation to improve FMDV VP4 expression to a level that could be used to generate FMDV VP4. A codon optimised sequence for expression of FMDV VP4PreGST in *E.coli* was synthesised (DNA2.0). The level of expression with codon optimised FMDV VP4PreGST was improved relative to the non-codon optimised protein, however, expression level was still too low to give a sufficient yield of purified FMDV VP4 for the intended functional and biochemical assays (section 3.2.2.1).

High frequency or clusters of rare codons in the protein being expressed in *E.coli* may contribute to low levels of protein expression. But these are absent in PV and FMDV VP4. Therefore, other factors contributing to low levels expression are currently unclear.

As an alternative to expressing and purifying FMDV VP4, the use of FMDV VP4 synthetic peptide was considered as there is precedence for other pore forming proteins, e.g. HRV2 VP1 N-terminus (Prchla *et al.*, 1995) and Influenza A M2 protein (Ma *et al.*, 2009; Rosenberg and Casarotto, 2010) being used as functional peptides. Several peptide synthesis companies were approached and either considered it unfeasible due to the size and unfavourable amino acid composition of FMDV VP4 (85 residues) or attempted synthesising FMDV VP4 but failed to do so (Peptide Protein Research Ltd).

Overexpression of non-native proteins in *E.coli* often results in the formation of IB. GST-tagged VP4 proteins were expressed in IB. Purifying recombinant proteins from IB can be advantageous as IB consist mainly of the protein of interest, can be easily isolated due to relatively higher density and are resistant to proteases (Debernardezclark and Georgiou, 1991; Singh and Panda, 2005).

VP4His was released from GST-tagged VP4 by cleavage with 3C or thrombin protease. Of the various constructs tested, the highest levels of expression were obtained with HRV, therefore GST-tagged HRV VP4 proteins were used for further large scale cleavage studies. It was clear from the appearance of the products of the cleavage reaction after analysis by SDS-PAGE, that VP4His was being released. Following cleavage of GST-tagged VP4, the presence of the released GST was directly related to the appearance of VP4His. The appearance of GST-tagged VP4 suggested cleavage was incomplete. This was not entirely unexpected as the GST-tagged protein was being expressed in inclusion bodies where the protease cleavage site may not always be accessible (section 3.2.3). However, the observed incomplete cleavage of soluble

GST-tagged VP4 (section 3.2.4) suggested a factor other than the restricted availability of the cleavage site was contributing to the incomplete cleavage. One possible explanation for the incomplete cleavage was the presence of a sub-optimal thrombin cleavage site. Thrombin protease cleaves between arginine and glycine (LVPR/GSMS). Proline at position P2 and arginine at position P3' are required for maximal cleavage efficiency. A recent study showed that mutation of arginine residue at position P3' reduced the cleavage efficiency of thrombin protease (Gallwitz *et al.*, 2012). Therefore, the thrombin protease cleavage sequence in VP4ThGST (LVPR/GSMS) may be sub-optimal.

As an alternative approach for generating recombinant VP4, plasmids encoding VP4 and VP4His were directly expressed (section 3.3), thereby circumventing problems associated with generating VP4His from GST-tagged VP4. The levels of expression of VP4His from different viruses showed the same pattern as GST-tagged VP4 proteins, i.e. HRV VP4His expressed to the highest level followed by PV VP4His followed by very low level expression for FMDV VP4His. Only HRV showed a level of expression sufficient for purification of VP4His with appropriate yield, therefore, all further work described in the following chapters used recombinant VP4 from HRV, unless stated otherwise.

In order to start preliminary studies of the VP4-membrane pore complex using NMR, a higher yield of VP4 than that obtained with expression and purification of VP4His (section 3.3) was necessary. The presence of a myristate group at the N-terminus of VP4 was expected to increase hydrophobicity and tendency to aggregate, thereby raising technical issues with reconstitution of VP4 required for biophysical studies such as CD and NMR. It was, therefore, decided to express and purify unmyristoylated VP4. The expression of VP4 as a fusion protein with His-trpLE was used to purify VP4 for preliminary NMR studies. In contrast to the inefficient cleavage of VP4ThGST and VP4PreGST with thrombin or 3C protease (sections 3.2.3 and 3.2.4), respectively, cleavage of His-trpLE-VP4 with CNBr was efficient (up to 70 %) and contributed to the generation of at least 20 fold higher yield of VP4 compared to VP4His, desirable for NMR studies.

The influence of myristoylation in the ability of VP4 to induce membrane permeability is described in section 4.2.3. Future work should therefore be carried out to optimise the production of myristoylated VP4 to enable a comparative NMR study of the structures of the VP4 membrane pore complex formed by myristoylated and unmyristoylated VP4. This would help gain an understanding of the influence of myristoylation on VP4 structure and membrane pore complex formation.

SDS-PAGE was used to visualise recombinant and native forms of VP4. The signal for VP4 stained with Coomassie stain appeared lower than expected. Therefore, the two potential issues associated with the poor visualisation of VP4 were investigated. The first potential concern was that of inefficient fixation of VP4 and the second of poor staining of VP4 with Coomassie dye.

Fixatives are used to prevent diffusion of proteins and to keep protein bands sharp and resolved in SDS-PAGE. A range of different fixatives were used with the aim of retaining the trapped denatured protein within the polyacrylamide gel matrix, thereby facilitating better protein staining. Different fixatives such as 10 % glutaraldehyde, 15 % formalin and 12 % trichloroacetic acid (section 2.3.3) were investigated. After fixing proteins on SDS-PAGE with one of the above fixatives, VP4His was stained with Coomassie blue. However, the use of the above fixatives did not improve VP4His staining with Coomassie blue.

Coomassie brilliant blue dye binds to basic amino acids such as arginine, lysine and histidine (Tal *et al.*, 1985). HRV VP4 contains approximately 10 % basic amino acids (Rx2, Kx4, Hx1) which may have contributed to the poor binding of Coomassie stain to VP4. Therefore, Coomassie stain (CBR-250) was not ideal for the visualisation of VP4 band. The poor binding of Coomassie stain was also likely to have contributed to the underestimation of VP4 concentration by the Bradford assay (section 3.3.4). Alternative stains including copper chloride, zinc imidazole, sypro orange (section 2.3.4.3) were attempted to improve the visualisation of VP4. Visualisation of VP4 was not significantly improved by any of the above stains compared to VP4 visualised with Coomassie stain.

Silver stain is known to be up to 100 times more sensitive than Coomassie stain. Charged amino acids such as arginine, lysine, glutamic acid, histidine and aspartic acid bind to silver ions, followed by the reduction to free metallic silver which gives the visible image. (Chevallet *et al.*, 2006; Merril *et al.*, 1988; Nielsen and Brown, 1984). HRV VP4 contains the residues Ex2, Dx5, Rx2, Kx4, Hx1 and possibly contributed to the better visualisation of VP4 with silver stain better than with Coomassie stain.

Due to the concerns associated with the visualisation of VP4, it was important to compare recombinant VP4 with native VP4. Recombinant VP4 was quantified by comparison with native VP4, using a combination of silver staining and anti-VP4C western blot (section 3.3.4). Although, silver staining gave an estimate of recombinant VP4 concentration relative to native VP4, it was important to bear in mind the hexahistidine tag in recombinant VP4 was absent in native VP4, which may have influenced silver staining of recombinant VP4.



# **Chapter 4**

## **Characterisation of VP4- induced membrane permeability**

## 4.1 Introduction

### Existing evidence for role of VP1 and VP4 in cell entry

During cell entry by enteroviruses, receptor and/or pH-induced conformational changes result in the conversion of native virus into an altered or “A” particle from which VP4 has been released and in which the N-terminus of VP1 has become externalised (section 1.6.4.2).

Enterovirus “A” particles are hydrophobic and more sensitive to proteases than native particles (Fricks and Hogle, 1990; Hogle, 2002). Comparison of cryoEM structures of PV “A” particles and “A” particles with the N-terminal 31 residues of VP1 proteolytically removed, demonstrated the externalisation of the N-terminus of VP1 which was therefore available for membrane insertion (Bubeck *et al.*, 2005). VP1-mediated membrane interaction of “A” particles was confirmed by similar proteolytic cleavage studies (Tuthill *et al.*, 2006). The interaction between the N-terminus of VP1 with liposome membranes was suggested for tethering of “A” particles to liposome membranes in a receptor independent manner (Tuthill *et al.*, 2006). A recent tomographic study has proposed an “umbilicus” connecting PV capsid to membrane which has been hypothesised to facilitate RNA transfer across the membrane, with the VP1 N-terminus and/or VP4 shielding the RNA from enzymatic degradation (Strauss *et al.*, 2013). Therefore, there is evidence for the role of VP1 N-terminus in facilitating genome delivery, however, the extent and precise role of VP1 N-terminus in genome delivery remains unclear.

Several experimental findings have suggested a role for VP4 in the induction of membrane permeability (described in section 1.6.4.4). These included studies with recombinant GST-tagged VP4 which associated with membranes and induced permeability in intact liposomes (Davis *et al.*, 2008). VP4 released from PV was also shown to be associated with liposome membranes (Tuthill *et al.*, 2006). PV with mutations in VP4 formed channels in lipid bilayers with different electrophysiological properties. The same mutations in VP4 also either delayed or prevented RNA delivery during infection (Danthi *et al.*, 2003; Tosteson *et al.*, 2004). Therefore, these findings indicate that VP4 may be part of a potential channel, facilitating RNA delivery into the cytoplasm.

### Use of liposomes as model membranes

Liposomes are artificially prepared vesicles composed of single or multiple lipid bilayers. Liposomes constitute a valuable model system, permitting experiments to be carried out under a tightly controlled range of conditions. Self-quenching dyes which fluoresce upon dilution when released into the surrounding aqueous buffer can be used to fill liposomes. Real-time monitoring of the fluorescence allows for analysis of dye release and measurement of

membrane permeability induction. To investigate the role of VP4 in cell entry, liposomes comprised of one lipid bilayer were used as model membranes.

The use of liposomes to study membrane permeability is a standard approach. Liposome membrane permeability has been shown to be induced by several small viral proteins including p7 of HCV (StGelais *et al.*, 2007), SH of RSV (Carter *et al.*, 2010; Gan *et al.*, 2008), M2 of IAV (Duff and Ashley, 1992; Vijayvergiya *et al.*, 2004),  $\mu$ 1N of reovirus (Zhang *et al.*, 2009), VP4 of SV40 (Raghava *et al.*, 2011). Liposomes have also been used to study membrane permeability by peptides such as GALA and melittin. Melittin is a well characterised pore-forming peptide and has been shown to mediate the release of carboxyfluorescein (CF) from liposomes (Ladokhin *et al.*, 1997; Schwarz *et al.*, 1992). GALA is a pore-forming peptide that induces membrane permeability by pore formation at pH<6 (Nicol *et al.*, 1996; Nicol *et al.*, 2000; Parente *et al.*, 1990).

Previous experience in the lab involved testing different liposome compositions. This led to the conclusion that PA:PC:cholesterol:rhod-PE (44.5:44.5:10:1) was a robust and stable composition. Therefore, unilamellar vesicles comprised of PA, PC, rhod-PE and cholesterol were used as the composition of choice for model membranes to investigate membrane permeability induction (section 2.22-2.23).

### **Role of protein myristoylation**

Myristoylation at the amino terminus of proteins is a co-translational modification involving the covalent linkage of a saturated C14 fatty acid myristate via an amide bond to the N-terminal glycine of the protein. The enzyme myristoyl CoA: protein-N-myristoyltransferase catalyses the transfer of myristate from myristoyl CoA to the N-terminus of the protein following the removal of methionine by methionine aminopeptidase (Boisson and Meinel, 2003; Frottin *et al.*, 2006; Glueck *et al.*, 2010). Protein myristoylation is known to play a role in several biological functions such as protein structure, stability and membrane interactions. Myristoylated viral proteins include HIV-1 Nef (Matsubara *et al.*, 2005), p14 FAST (fusion associated small transmembrane) protein of reptilian reovirus (Corcoran *et al.*, 2004),  $\mu$ 1 of reoviruses (Odegard *et al.*, 2004).

Although the addition of the myristate group is a lipid anchor modification that is likely to direct proteins to the membrane, a myristate group alone does not always provide enough binding strength to keep the protein anchored to the membrane. Other factors including electrostatic interactions of basic residues with acidic phospholipids can also contribute to the anchorage of proteins to membranes (Murray *et al.*, 1998; Yalovsky *et al.*, 1999).

A precursor protein of several non-enveloped viruses undergoes cleavage to generate a hydrophobic peptide. At the early infection stage, the virus particles undergo conformational

changes in response to cellular triggers such as receptor binding, pH or binding to specific lipid components. This results in the release of the lipophilic peptide which ultimately induces membrane permeability. These peptides are often short, hydrophobic and myristoylated at the N-terminus. Myristoylated proteins of non-enveloped viruses include reovirus  $\mu 1$  and picornavirus VP4 (section 1.6.3). Therefore, cleavage and release or exposure of membrane binding peptides bearing fatty acid modifications such as myristoylation appear to be a conserved feature shared by non-enveloped viruses. This suggests the relevance of myristoylation in the induction of membrane permeability by non-enveloped viruses.

#### **Triggers for conformational changes in rhinoviruses**

For cell entry of rhinoviruses, receptor binding and/or pH may serve as the trigger for entry. For minor group rhinoviruses such as HRV2, low density lipoprotein (LDL) receptors are used to gain cell entry but exposure to low pH is an essential trigger for irreversible structural changes necessary for the transfer of the genome into the cytoplasm for replication (Prchla *et al.*, 1994). For major group rhinoviruses, dependence on pH varies from partial to complete (Bayer *et al.*, 1999; Nurani *et al.*, 2003; Schober *et al.*, 1998). HRV infection of HeLa cells treated with bafilomycin (inhibitor of vacuolar-type H<sup>+</sup>ATPase that raises the endosomal pH to neutral) showed receptor bound HRV16 required a low pH5.5-6.0 environment to uncoat whereas HRV3 uncoated even at pH7.0 (Nurani *et al.*, 2003) (section 1.6.4.1).

#### **Effect of membrane composition on viral membrane protein function**

Phospholipids are the fundamental building blocks of cell membranes. They spontaneously form bilayers in aqueous solutions due to the fatty acid tails which are hydrophobic. Their polar head groups are hydrophilic and are therefore in contact with water. Lipid composition varies between membranes of cellular compartments. The structures and properties of some of the lipid components of membranes are shown in Table 4.1. Early endosomes have a membrane composition similar to plasma membranes with a high percentage of cholesterol. Upon maturation to late endosomes, the lipid composition is modified as there is a decrease in cholesterol and an increase in bis(monoacylglycero)phosphate (BMP) (van Meer *et al.*, 2008). Cholesterol is required for a number of important biological processes such as signal transduction (Maxfield and Wustner, 2002) and regulation of membrane fluidity over a range of temperatures. The fluidity of membranes is known to be reduced in membranes enriched with cholesterol (Bastiaanse *et al.*, 1997). This reduction in fluidity is because the rigid hydrocarbon rings of cholesterol interact with the fatty acid chains of the lipid components of the membrane. On the other hand, the presence of cholesterol in the membrane prevents tight packing of interactions between fatty acid chains, thereby making membranes fluid at lower temperatures. The cholesterol content in plasma membranes is higher than in

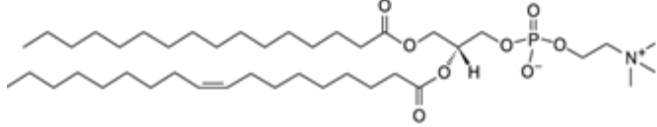
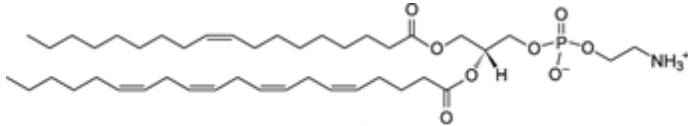
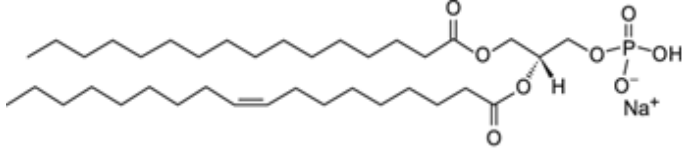
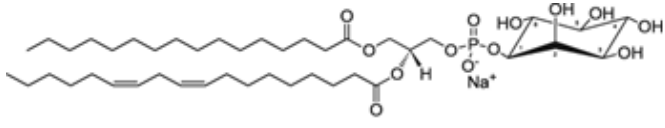
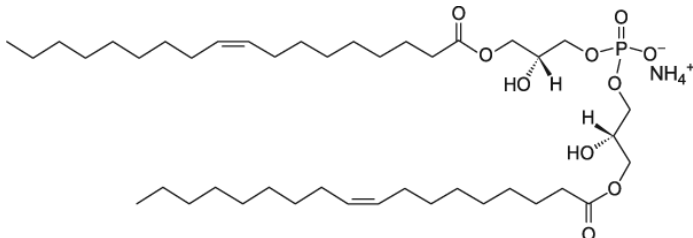
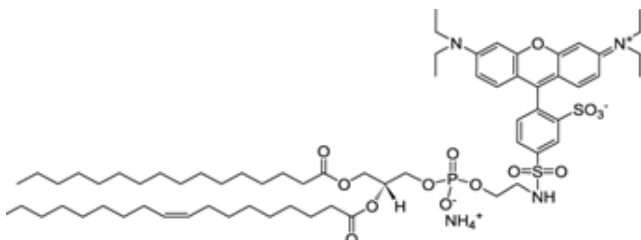
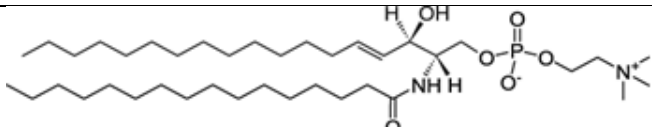
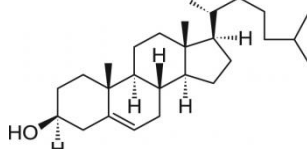
subcellular membranes. The interaction of cholesterol with other lipids and proteins present in the membrane may influence functions of transmembrane proteins.

The lipid composition of membranes has been reported to influence the activity of non-enveloped viral membrane proteins. Echovirus 1 infection was demonstrated to be dependent on cholesterol (Siljamaki *et al.*, 2013). Poliovirus entry has also been shown to be dependent upon cholesterol (Danthi and Chow, 2004). Flock house virus  $\gamma_1$  peptide is lipophilic with membrane permeabilising activity and speculated to play a role in the transmembrane passage of viral RNA.  $\gamma_1$  peptide showed preference for membranes with negatively charged headgroups, 1-palmitoyl-2-oleoyl-*sn*-glycero-3-phosphoglycerol (POPG) over membranes with zwitterionic lipids, 1-Palmitoyl-2-oleoyl-*sn*-glycero-3-phosphocholine (POPC) (Bong *et al.*, 2000). A decrease in dye release induced by  $\gamma_1$  peptide was observed from liposomes enriched in cholesterol (Maia *et al.*, 2006).

In addition to non-enveloped viruses, lipid composition has been reported to influence activity of membrane proteins of enveloped viruses. For instance, HIV-1 group specific antigen (Gag) membrane interactions were reported to be influenced by the phospholipid head groups, cholesterol content and acyl chain unsaturation (Dick *et al.*, 2012). E1 of alphaviruses such as Chikungunya virus, Semliki Forest virus and Sindbis virus fuses with the endosomal membrane during viral entry and this is a cholesterol dependent process (as reviewed in Leung *et al.*, 2011). Dengue fusion occurs only in the late endosome by using anionic lipids like BMP, a lipid specific to the late endosome, as a trigger for fusion of the viral membrane with late endosome membrane (Zaitseva *et al.*, 2010). Therefore, membrane protein function is dependent on membrane composition.

In this study two types of recombinant VP4His were used: myristoylated VP4His (VP4His) and unmyristoylated VP4His ( $\Delta$ VP4His). The generation of VP4His and  $\Delta$ VP4His is described in chapter 3. This chapter describes membrane permeability induced by recombinant VP4 and characterises the effect of VP4 concentration, myristoylation, pH, temperature and membrane composition on the induction of membrane permeability.

Table 4.1 Membrane lipids and their structures. [www.avantilipids.com](http://www.avantilipids.com)

Lipid Name	Structure of predominant lipid species
L- $\alpha$ -phosphatidylcholine (PC)	
L- $\alpha$ -phosphatidylethanolamine (PE)	
L- $\alpha$ -phosphatidic acid (PA)	
L- $\alpha$ -phosphatidylinositol (PI)	
bis(monooleoylglycero)phosphate (BMP)	
L- $\alpha$ -Phosphatidylethanolamine-N-(lissamine rhodamine B sulfonyl) (Rhod-PE)	
Sphingomyelin (SM)	
Cholesterol	

## 4.2 Characterisation of VP4-induced membrane permeability

### 4.2.1 Recombinant VP4 induces membrane permeability in liposomes

VP4 has been shown to partition into membranes and implicated to play a role in facilitating the delivery of the genome into the cytoplasm (section 4.1). Given this proposed role of VP4 in cell entry, VP4His was expected to interact with and permeabilise model membranes.

GST-tagged HRV VP4 has been shown to induce membrane permeability in liposomes without membrane disruption (Davis *et al.*, 2008). GST is a large fusion partner (26 kDa) which may influence the activity of VP4. Therefore, recombinant forms of VP4 that more closely mimicked native VP4, e.g. VP4 with smaller C-terminal tags (e.g. VP4His) were generated (section 3.3).

Lipids were dried, rehydrated in the presence of CF dye and extruded to form liposomes. Liposomes containing CF were purified away from unencapsulated CF by serial pelleting and washing (section 2.22). When liposomes containing self-quenching fluorescent dyes such as CF became permeabilised, CF was released and became unquenched (section 2.23) (Figure 4.1A). The fluorescence was measured at  $\lambda_{\text{ex}}485\text{nm} / \lambda_{\text{em}}520\text{nm}$ .

The membrane permeability assay using liposomes (section 2.23) is a well established approach that has been widely used to study the induction of membrane permeability by a range of different peptides (section 4.1). The real-time nature of the assay enables measurement of induced membrane permeability. Membrane permeability induced by recombinant VP4 was investigated using this membrane permeability assay.

VP4His and  $\Delta$ VP4His were expressed in *E. coli* and purified (section 3.3) to investigate the mechanism of induction of membrane permeability in liposomes. Myristoylated VP4His (VP4His) has been used in this chapter to describe the induction of membrane permeability.

Release of CF contained within liposomes was observed upon addition of VP4His to the membrane permeability assay. An increase in membrane permeability showed a concomitant increase in the release of CF from within liposomes. This was depicted by the increase in relative fluorescence units. This finding demonstrated the functional ability of VP4His to induce membrane permeability. Addition of Triton X-100 to the membrane permeability assay resulted in abrupt and complete CF release as a consequence of lysis of liposome membranes. In contrast, the model pore-forming peptide, melittin, induced controlled CF release from within liposomes. VP4His mediated CF release was similar to that obtained with melittin (Figure 4.1). This finding suggested that VP4-induced membrane permeability involved a mechanism which did not disrupt liposome membranes.

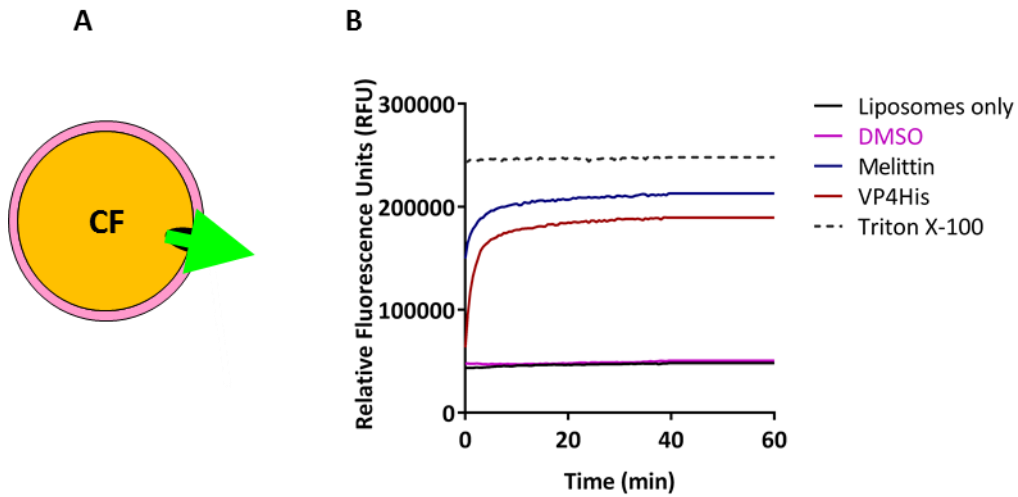


**Figure 4.1 HRV VP4His-mediated membrane permeability.**

**A.** Liposomes containing self-quenching carboxyfluorescein (CF) dye. **B.** VP4His and liposome assay controls (DMSO, melittin and Triton X-100) were incubated with liposomes containing CF. Released CF dye became unquenched and was measured by fluorimetry ( $\lambda_{ex}$  485 nm/  $\lambda_{em}$  520 nm). Dye release was monitored in real-time **with readings recorded every 30 seconds for 1 hr. Liposomes only, liposomes with solvent (5 % v/v DMSO), 10  $\mu$ M melittin, Triton X-100 (5 % v/v), 5  $\mu$ M VP4His** were used to assess the induction of membrane permeability. Background levels of CF release were generated by liposomes only and liposomes with DMSO.

PV VP4His was purified using the same purification method as used for HRV VP4His (described in chapter 3). To rule out the effect of negligible contaminants, bacterial lysate was used as a control sample. Upon incubating PV VP4His with liposomes, CF release observed was similar to that observed with HRV VP4His (Figure 4.2).



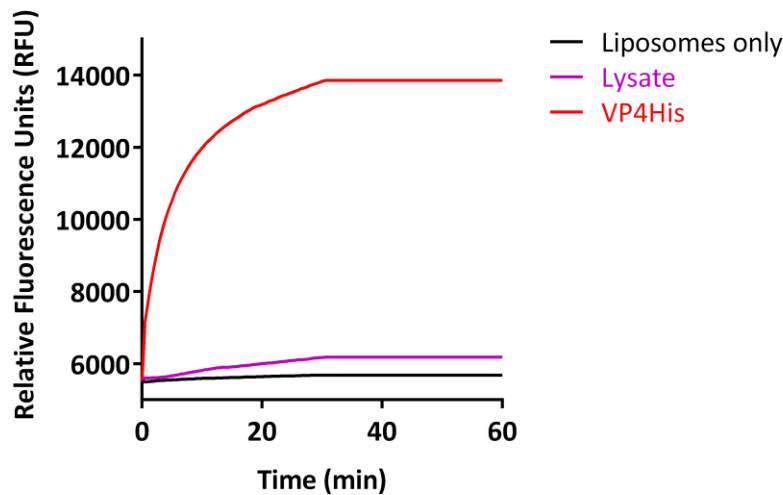


**Figure 4.2 PV VP4His-mediated membrane permeability.**

PV VP4His and liposome assay controls (bacterial lysate) were incubated with liposomes containing CF. Released CF dye became unquenched and was measured by fluorimetry ( $\lambda_{\text{ex}}$  485nm /  $\lambda_{\text{em}}$  520nm). Dye release was monitored in real-time with readings recorded every 30 seconds for 1 hour. Liposomes only, bacterial cell lysate (5 % v/v) and 5  $\mu$ M VP4His were used to assess the induction of membrane permeability. Background levels of CF release were generated by liposomes only and liposomes with bacterial cell lysate. Data shown here is representative of n=2 experiments.

Following the observation of VP4-induced membrane permeability in liposomes (Figures 4.1 and 4.2), the next step was to demonstrate the association of VP4 with liposome membranes. To achieve this, ficoll liposome floatation assays were carried out (section 2.26). Since VP4-induced membrane permeability was demonstrated by CF release, it seemed reasonable to assume that VP4 was associating with membranes. VP4, was therefore, expected to localise with liposomes that floated to the top (or membrane interface) of the ficoll gradient (Figure 4.3A). Liposomes were made fluorescent by including lissamine rhodamine B-labeled phosphatidylethanolamine lipid in their generation. Ficoll gradients were fractionated from the top and liposomes detected by measuring rhodamine fluorescence ( $\lambda_{\text{ex}}$  544 nm /  $\lambda_{\text{em}}$  590 nm) (Figure 4.3B). Eleven fractions of 200  $\mu$ l each were collected and the pellet resuspended in SDS sample loading buffer. Upon analysis by SDS-PAGE and western blot (section 2.3.5), VP4His was detected in the pellet but not in the membrane fractions (Figure 4.3C). Therefore, it was possible that only a proportion of VP4His associated with liposome membranes and was below the detection limit of western blot. The minority of VP4His molecules integrated into liposomes, therefore appeared to be sufficient to induce membrane permeability.

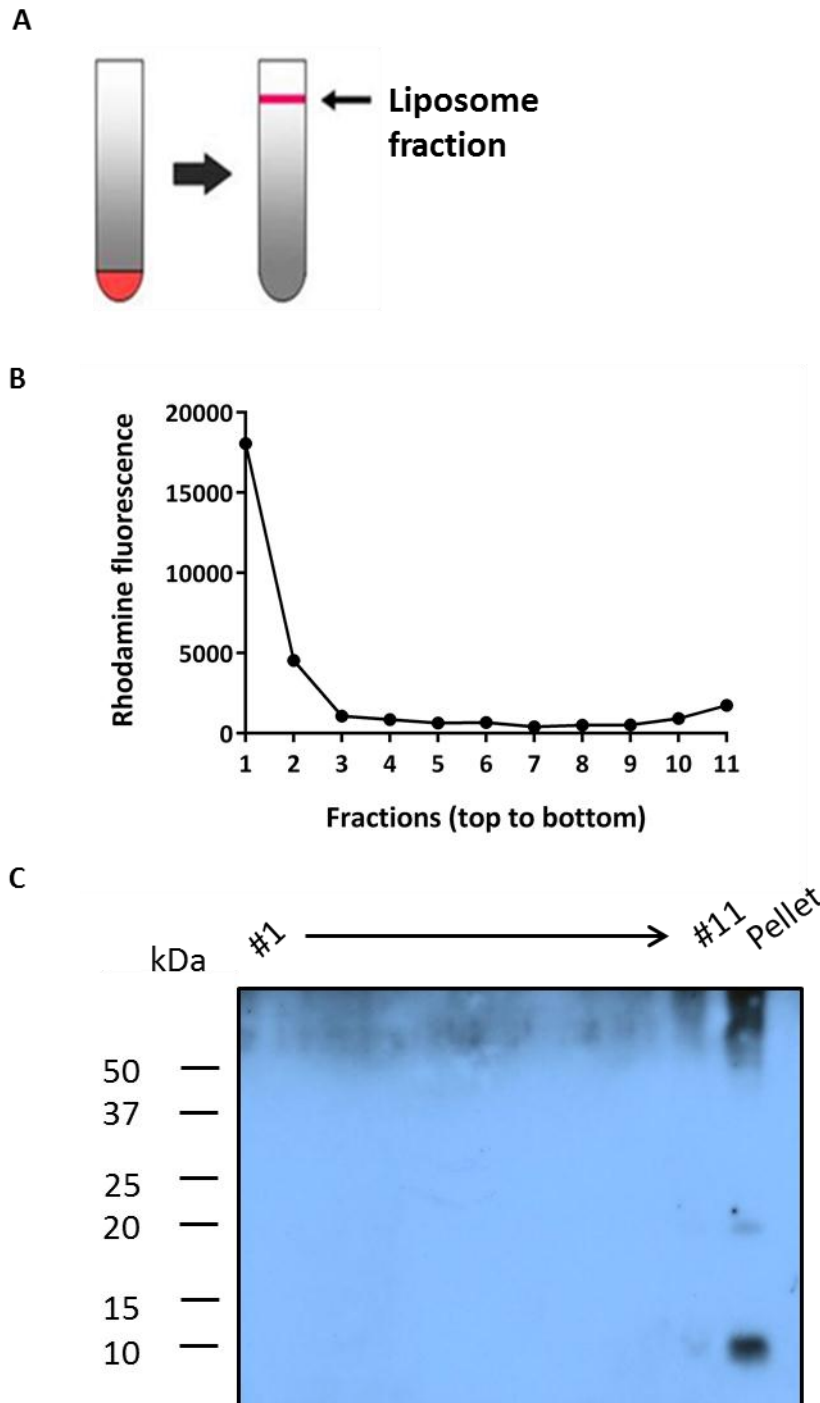


**Figure 4.3 Association of VP4His with liposome membranes.**

VP4His was incubated with liposomes for 30 min prior to layering on a 20 % ficoll discontinuous gradient layered over it. **A.** Pictorial representation of the ficoll liposome floatation assay. **B.** Gradient fractions (top to bottom) were collected post ultracentrifugation and liposome distribution detected by rhodamine fluorescence measured at ( $\lambda_{ex}520\text{ nm} / \lambda_{em}570\text{ nm}$ ). **C.** Samples from each fraction (top to bottom) were separated by SDS-PAGE and VP4His was detected by anti-VP4C-terminus specific western blot. The size of molecular weight markers (kDa) is indicated to the left of the image.

#### 4.2.2 VP4 mediates concentration-dependent release of carboxyfluorescein from liposomes

A range of concentrations of VP4His were used in the membrane permeability assay, in order to determine if VP4His induced membrane permeability in a dose-dependent manner and whether this was related to the increase in the extent and rate of CF release from liposomes. Viral membrane proteins such as HCV p7 (StGelais *et al.*, 2007) and HPV E5 (Wetherill *et al.*, 2012) have been shown to induce concentration-dependent CF release from liposomes. Upon addition of VP4His, membrane permeability was induced and CF release measured by fluorimetry ( $\lambda_{\text{ex}}$  485 nm/ $\lambda_{\text{em}}$  520 nm) (section 2.23). To determine if the nature of CF release was concentration-dependent, increasing concentrations of VP4His (0.3 – 5  $\mu\text{M}$ ) were incubated with CF-containing liposomes. For all the concentrations tested, membrane permeability was observed and an increase in VP4His concentration showed an increase in the observed fluorescence signal. Therefore, with increasing concentration, the rate and extent of permeability increased (Figure 4.4). Maximum membrane permeability observed with 2.5  $\mu\text{M}$  VP4His, at which point, no further significant increase in CF release was observed with increase in VP4His concentration (e.g. 5  $\mu\text{M}$ ).

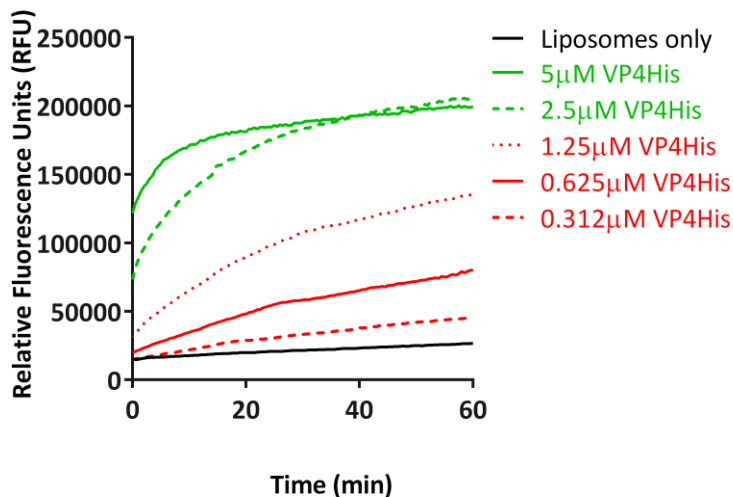


**Figure 4.4 VP4His-induced concentration-dependent CF release from liposomes.**

Increasing concentrations of VP4His were incubated with liposomes and CF release was measured by fluorimetry ( $\lambda_{\text{ex}}$  485 nm/ $\lambda_{\text{em}}$  520 nm) and monitored in real-time. Background levels of CF release were generated by liposomes only.

### 4.2.3 Induction of membrane permeability by VP4 is enhanced by myristoylation and acidic pH conditions

N-terminally myristoylated capsid proteins of non-enveloped viruses such as VP4 of picornaviruses and  $\mu 1$  of reoviruses, are thought to interact with membranes to facilitate delivery of viral genetic material into the cytoplasm (section 1.6.3). To investigate the influence of myristoylation on the ability of VP4 to induce membrane permeability, myristoylated and unmyristoylated forms of VP4His were made. Recombinant VP4His was normally made by co-expressing VP4His with NMT to make myristoylated VP4His (VP4His). In order to make unmyristoylated VP4His ( $\Delta$ VP4His), VP4His was expressed in the absence of NMT (section 3.3).

VP4His or  $\Delta$ VP4His were incubated with liposomes and analysed using the membrane permeability assay (section 2.23). VP4His-induced more extensive CF release as compared to  $\Delta$ VP4His (Figure 4.5).

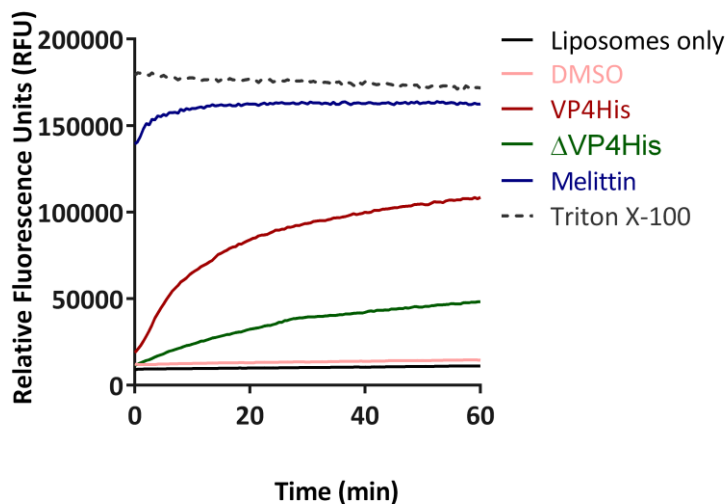


**Figure 4.5 Membrane permeability induced by myristoylated and unmyristoylated VP4.**

VP4His and  $\Delta$ VP4His were incubated with liposomes. CF release was measured by fluorimetry ( $\lambda_{\text{ex}}$  485 nm/ $\lambda_{\text{em}}$  520 nm) and monitored in real-time. Background levels of CF release were generated by liposomes only.

HRVs vary in their dependence on pH to trigger conformational changes. Major group HRV16 shows an absolute dependence on low pH as do minor group human rhinoviruses such as HRV2. In contrast, major group rhinovirus HRV3 is not strictly pH dependent and receptor binding is sufficient to trigger conformational changes for the release of RNA (section 1.6.4.2).

The effect of pH on VP4 function of inducing membrane permeability was studied for two main reasons:

1. There is existing evidence for the requirement of acidic conditions of pH5.5-6.0 for efficient uncoating of receptor primed HRV16 (Nurani *et al.*, 2003). Whether a particular pH is required only for virus uncoating or if VP4 has evolved to require that pH for optimal membrane permeabilising activity, requires investigation.
2. VP4 possesses ionisable residues (Rx2, Hx1, Kx5, Dx4, Ex2). Due to the lack of structural information on membrane associated VP4, the location of these residues in a potential VP4 membrane complex is unknown. Ionisable residues are known to be stably inserted in the membrane and affect TM packing in membranes (Bano-Polo *et al.*, 2012). Therefore, the effect of pH on ionisable residues may influence shape, orientation, proportion and distribution of positive and negative charges, thereby affecting VP4 structure and function.

To investigate the effect of decreasing pH on the ability of VP4 to induce membrane permeability, liposomes were diluted to 50  $\mu$ M lipid content in buffers of varying pH (pH5.5, 6.5, 7.0) in the membrane permeability assay (section 2.23). However, when studies on the effect of pH on VP4 function were initiated, problems with CF fluorescence quenching were encountered. These are described and shown in Figures 4.6 and 4.7.

To confirm the effect of pH on CF fluorescence in the membrane permeability assay, liposomes were diluted to 50  $\mu$ M lipid content in buffers at pH5.5-7.5. Triton X-100 was added to the liposomes and caused membrane disruption at all pH conditions tested. This resulted in the complete release of CF. CF fluorescence was recovered by the addition of 1 M Tris pH7.5, demonstrating that CF fluorescence was quenched by acidic pH (Figure 4.6). Quenching of CF fluorescence by acidic pH prevented the comparison of real-time CF release induced by VP4 at neutral and acidic pH.

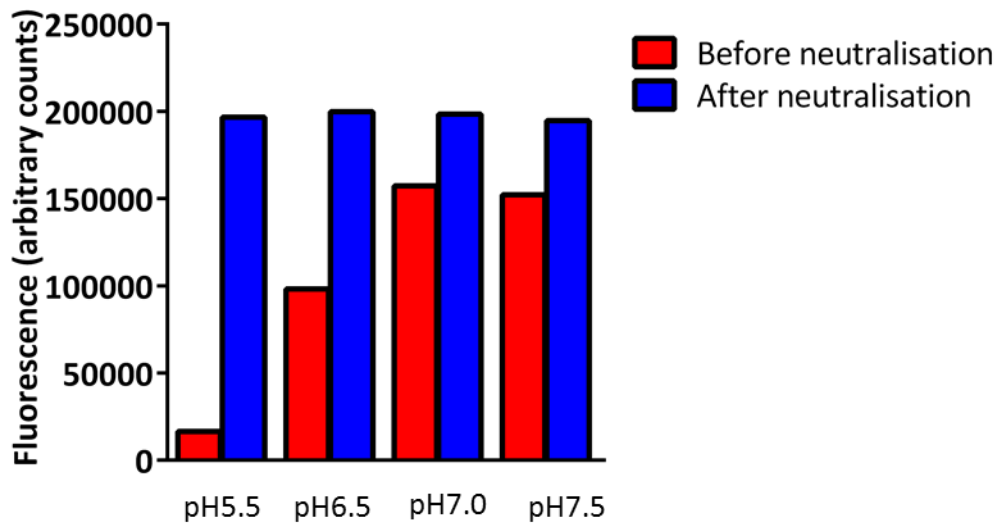


**Figure 4.6 CF fluorescence before and after neutralisation of pH.**

Triton X-100 (5 % v/v) was added to liposomes at pH5.5, 6.5, 7.0 and 7.5. Membrane disruption resulted in the expected complete release of CF at all pH conditions tested. CF fluorescence quenched by low pH (before neutralisation) was recovered by addition of 1 M Tris pH7.5 (after neutralisation).

For the comparison of end point data collected at different pH values, the end point samples were normalised for pH by separating released fluorescence from liposomes and adjusting to the same Triton X-100 and pH conditions as the Triton X-100 released control. However, for the comparison of real-time dye-release at different pH values the membrane permeability data collected had to be normalised differently and is explained below.

In contrast to the pH sensitive pore-forming peptide GALA, melittin (which is a pH independent pore-forming peptide) induced membrane permeability at all pH conditions tested. The fluorescence was reduced at acidic pH compared to that obtained at pH7.0 (Figure 4.7). Therefore, the combination of pH and Triton X-100 had a severe effect on fluorescence. When melittin-induced released fluorescence was separated from liposomes and adjusted to neutral pH, the signal obtained at all pH values was equivalent to the values observe at pH7.0. This confirmed the pH independent induction of membrane permeability by melittin. Thus, dye release data obtained at different pH values was normalised to maximum release by a melittin control at that same pH.

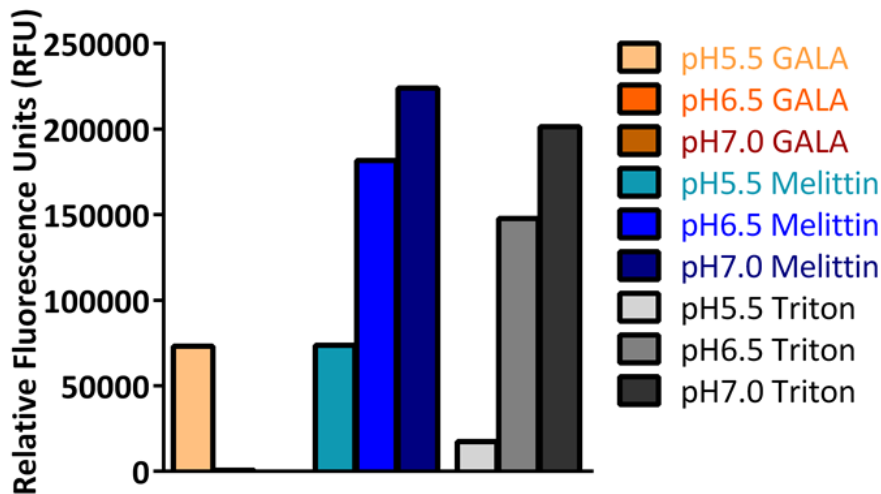


**Figure 4.7 Effect of pH and Triton X-100 on CF fluorescence.**

Triton X-100 (5 % v/v), Melittin (10  $\mu$ M) and GALA (1  $\mu$ M) added to liposomes at pH 5.5, 6.5, 7.0. GALA mediated CF release from liposomes at pH 5.5. Melittin mediated CF release from liposomes at all pH conditions tested. Triton X-100 caused complete CF release at all pH conditions tested. Acidic pH quenched CF fluorescence.

Having identified and resolved the problems with quenching of fluorescence, studies to investigate the effect of pH on VP4 function were undertaken.

The site of HRV16 uncoating is currently unknown. Other major group rhinoviruses such as HRV14 are known to uncoat in the early endosome (Bayer *et al.*, 1999). Therefore, it is possible that HRV16 may also uncoat in the early endosome. However, existing studies have demonstrated the requirement of pH 5.5-6.0 for HRV16 uncoating (Nurani *et al.*, 2003), which is likely to be in the late endosome. Studies to investigate the effect of pH on VP4 permeabilising activity were carried out to determine the optimal pH for VP4 function and, therefore, an indication of the cellular compartment for HRV16 uncoating (release of VP4).

The pH range of 5.5-7.0 was used to mimic the pH conditions likely to be encountered by HRV16 during the cell entry process. The pH of early endosome is predicted to be between pH 5.9 and 6.8 and that of late endosomes pH 4.9 and 6.0 (Maxfield and Yamashiro, 1987). VP4His or  $\Delta$ VP4His (5  $\mu$ M) was added to liposomes at pH 5.5, 6.5 or 7.0 and membrane permeability analysed. GALA (1  $\mu$ M) was used as a positive control for pH as it is known to induce membrane permeability at pH < 6.0 (Figure 4.8A). Both, VP4His and  $\Delta$ VP4His-induced membrane permeability at all pH conditions tested. However, the real-time dye release data showed membrane permeability mediated by VP4His was more extensive than that by  $\Delta$ VP4His. Also, a decrease in pH highlighted an increase in the extent of membrane permeability induced by VP4His and  $\Delta$ VP4His (Figure 4.8C, D). Additionally, the presence of myristoylation and pH 5.5 were shown to be associated with faster initial rates of release

(Figure 4.8F). The above results were summarised as end point fluorescence measurements. Each data point was normalised to end point CF release obtained with 10  $\mu$ M melittin measured at the corresponding pH representative of three experiments. Melittin and GALA were used as positive controls for induction of pH independent and pH dependent membrane permeability, respectively (Figure 4.8A, B). Taken together, both myristoylation and acidic pH conditions were required for the optimal induction of membrane permeability by VP4.



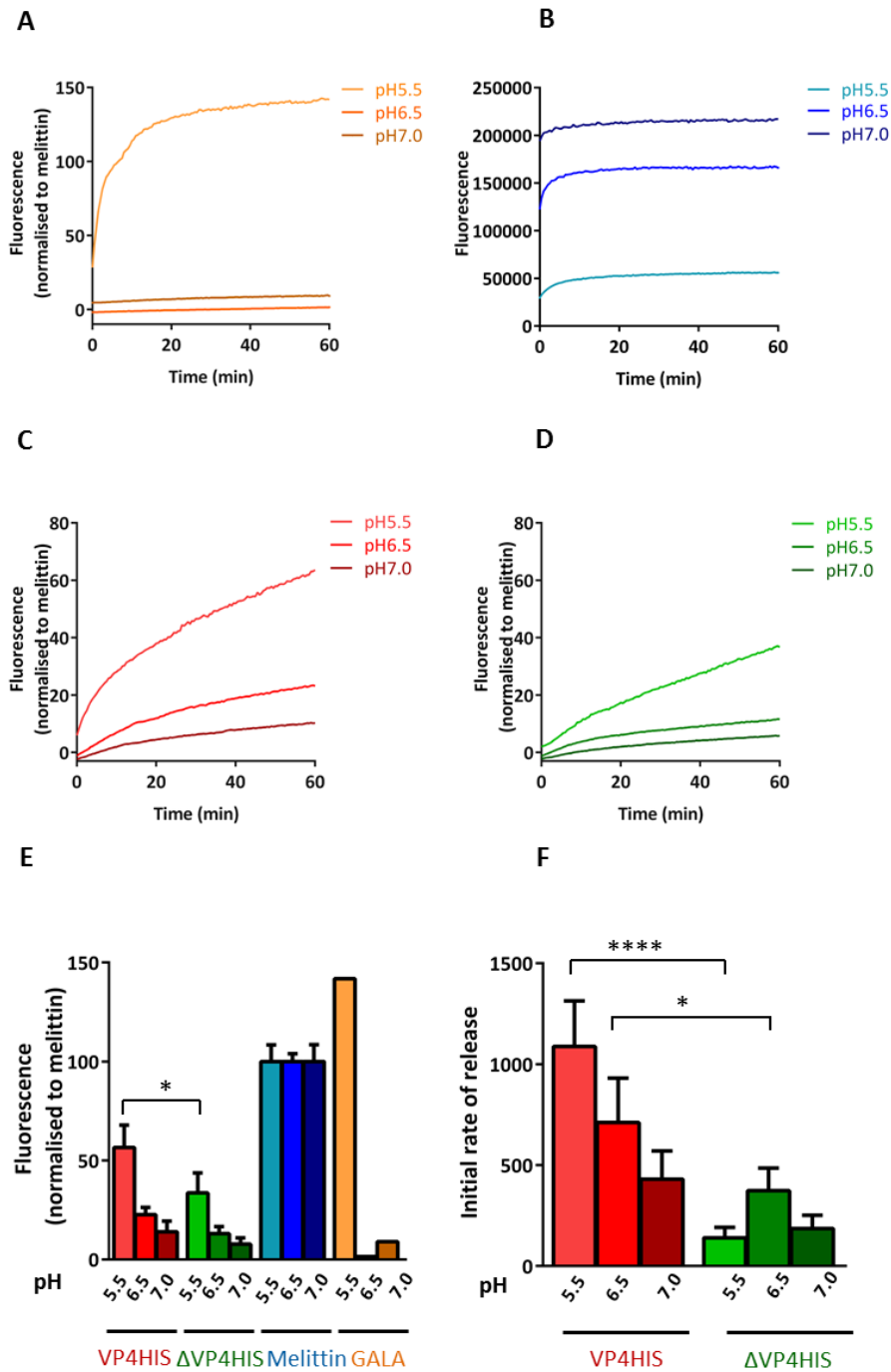


**Figure 4.8 Effect of pH and myristoylation on VP4-induced membrane permeability.** A. GALA. B. Melittin. C. VP4His. D. ΔVP4His added to liposomes at pH5.5, 6.5 and 7.0. CF release was measured by fluorimetry ( $\lambda_{ex}$  485 nm/ $\lambda_{em}$  520 nm) and monitored in real-time. Background levels of CF release were generated by liposomes only and the average CF read subtracted from each data point of GALA, mellitin, VP4His and ΔVP4His mediated CF release. E. End point reads of membrane permeability induced by VP4His, ΔVP4His and the controls melittin and GALA at pH5.5, 6.5 and 7.0. F. Relative initial rates of release for VP4His and ΔVP4His at pH5.5, 6.5 and 7.0 as calculated by fitting a straight line to the initial four data points of the real-time CF release measured at  $\lambda_{ex}$  485 nm/ $\lambda_{em}$  520 nm (experiments n=3). Error bars represent standard deviation of the mean. Statistical significance of difference of membrane permeability induced at different pHs were assessed by one way Anova ( $p^* < 0.05$ ).

#### 4.2.4 Membrane permeability induced by VP4 is influenced by membrane composition

In addition to pH, membrane composition provides cellular compartmentalisation for the uncoating process. Membranes of cellular compartments differ in their lipid composition (van Meer *et al.*, 2008). Cholesterol is a prominent component of membranes which regulates membrane rigidity (section 4.1). As an initial step to study the role of membrane lipid composition in VP4 function, the effect of cholesterol on the ability of VP4His to induce membrane permeability was investigated. Liposomes with or without cholesterol were generated (section 2.22), VP4His or  $\Delta$ VP4His added and membrane permeability analysed (section 2.23). VP4His and  $\Delta$ VP4His induced membrane permeability in both types of liposomes, with more extensive permeability in liposomes devoid of cholesterol (Figure 4.9).

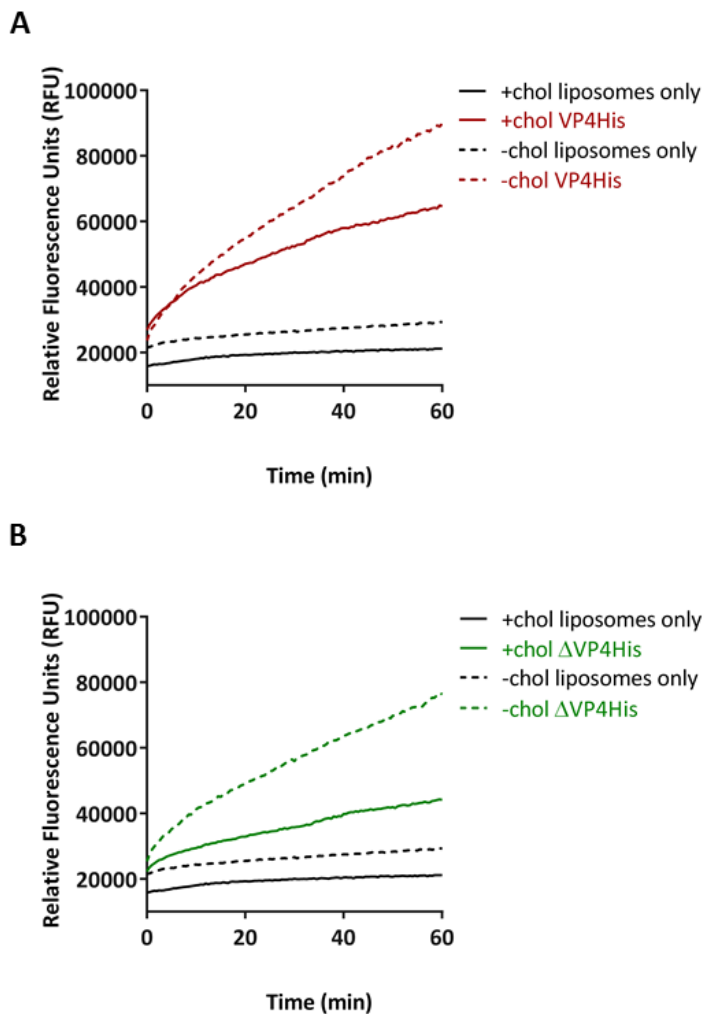


**Figure 4.9 Effect of cholesterol on VP4His-induced membrane permeability.**

**A.** VP4His or **B.**  $\Delta$ VP4His added to liposomes with or without cholesterol. CF release was measured by fluorimetry ( $\lambda_{\text{ex}}$  485 nm/ $\lambda_{\text{em}}$  520 nm) and monitored in real-time. Background levels of CF release were generated by liposomes only.

As mentioned previously, the cellular compartment for HRV16 uncoating has not been identified. HRV16 may uncoat in the early endosome like other major group HRVs. However, the findings observed in Figure 4.8 showed requirement of low pH for optimal VP4 function. This combined with existing studies for the requirement of low pH for HRV16 uncoating (Nurani *et al.*, 2003), suggested the possibility of HRV16 uncoating in the late endosome. Therefore, the effect of pH formed part of the rationale for looking at different compositions of the endocytic pathway.

Early endosomes and late endosomes are composed of different proportion and types of lipids e.g. early endosomes are comprised of PC, PE, SM and cholesterol whereas late endosomes are comprised of PC, PE, cholesterol, PI and BMP (Figure 4.10). In order to compare the effect of membrane composition on VP4-induced membrane permeability, liposomes mimicking the composition of early endosomes (referred to as EE) and late endosomes (referred to as LE) were generated (section 2.22). This comparison would provide fundamental insight by identifying key lipid components likely to influence mechanism of VP4-induced membrane permeability.

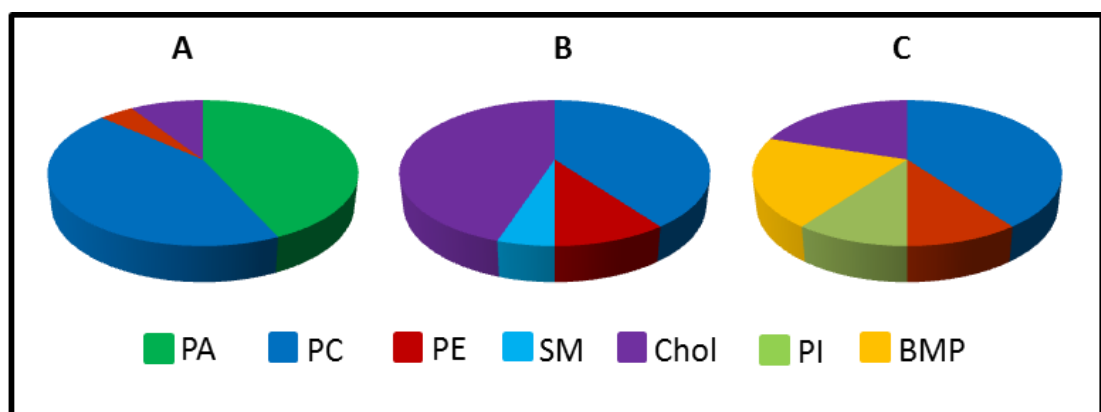


**Figure 4.10 Membrane composition of liposomes.**

Proportion of different lipids in **A**. Standard liposomes. **B**. Liposomes mimicking early endosomes. **C**. Liposomes mimicking late endosomes. PC: dark blue, PE: red, PI: light green, BMP: yellow, cholesterol: purple, PA: dark green, SM: light blue.

Addition of VP4His to standard liposomes or LE showed CF release with characteristics similar to what had been observed with membrane pore forming peptides, such as GALA and melittin in Figure 4.8A, B. In contrast, a clear difference in the nature of CF released from EE and LE was observed (Figure 4.11). VP4His induced abrupt and complete release of CF from EE. This was characteristic of previously observed CF release obtained with Triton X-100 from standard liposomes, as shown in Figure 4.1.

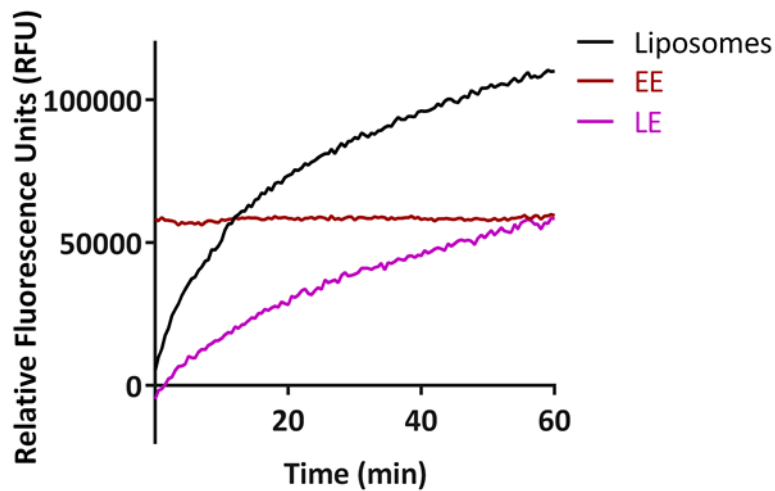


**Figure 4.11 VP4His-induced membrane permeability in liposomes mimicking composition of early or late endosomes.**

VP4His added to standard liposomes or EE or LE. CF release measured by fluorimetry ( $\lambda_{ex}$  485 nm/ $\lambda_{em}$  520 nm) and monitored in real-time. Background levels of CF release were generated by liposomes only. Background levels have been subtracted for clarity.

If membrane composition of early endosomes was more susceptible to permeabilisation by VP4His, it was possible that a vast excess of VP4His was being used in the membrane permeability assay, resulting in the abrupt and complete release of CF from EE. To determine if this was the case, a twofold dilution of VP4His was carried out. VP4His (5  $\mu$ M or 2.5  $\mu$ M) was added to standard liposomes, EE or LE and membrane permeability analysed. Real-time CF release showed that with a decrease in concentration of VP4His, a decrease in the extent of permeability induced was observed in all three types of liposomes (Figure 4.12). This was in agreement with previously observed dose-dependent induction of membrane permeability observed in Figure 4.4. In EE, VP4His appeared to induce either abrupt and complete or no membrane permeability (Figure 4.12B). The membrane permeability observed in EE, confirmed that the observed abrupt and complete CF release was not due to using excessive concentrations of VP4.

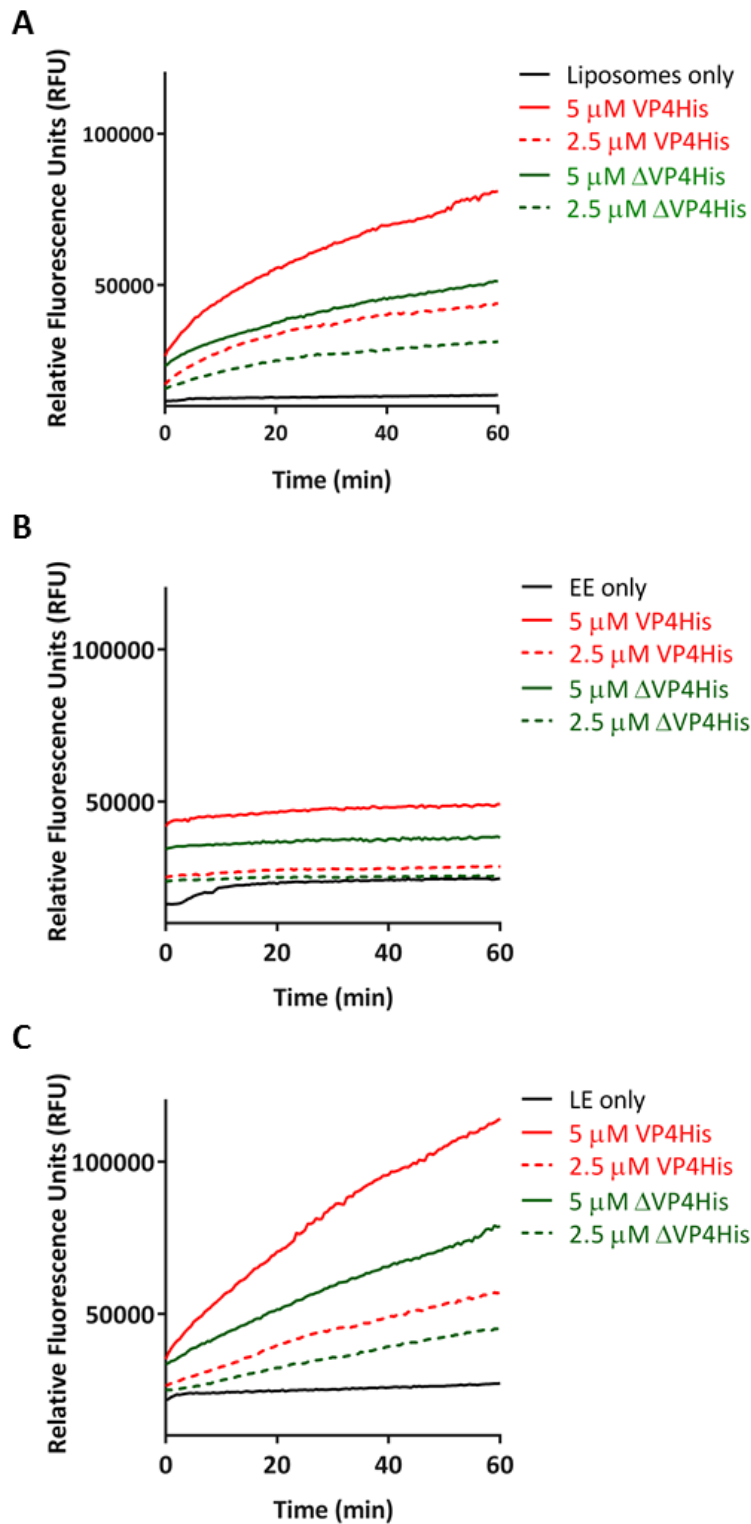


**Figure 4.12 Effect of membrane composition on VP4-induced membrane permeability.**

Two concentrations of myristoylated VP4His (VP4His) and unmyristoylated VP4His ( $\Delta$ VP4His) were incubated with **A**. Standard liposomes or **B**. Liposomes mimicking the composition of early endosomes (EE) or **C**. Liposomes mimicking the composition of late endosomes (LE). CF release was monitored in real-time and measured by fluorimetry ( $\lambda_{\text{ex}}$  485 nm/ $\lambda_{\text{em}}$  520 nm). Background levels of CF release were generated by liposomes only.

The observed difference in VP4-mediated membrane permeability induced in EE or LE (Figure 4.12B and C), led to the investigation of specific lipids influencing VP4-mediated membrane permeability. As a starting point, cholesterol and sphingomyelin membrane components of EE were investigated. EE were generated without cholesterol (referred to as EE-chol) or without sphingomyelin (referred to as EE-SM). Upon addition of VP4His to EE-Chol, membrane permeability was induced with CF release similar to that observed with standard liposomes (Figure 4.13A, C). On the other hand, upon addition of VP4His to EE-SM, membrane permeability was induced with CF release similar to that observed with EE. Membrane permeability induced by VP4His in EE-SM was abrupt and complete (Figure 4.13B, D). Therefore, these findings suggested that the presence of high percentage cholesterol in EE probably resulted in the observed abrupt and complete release of CF.

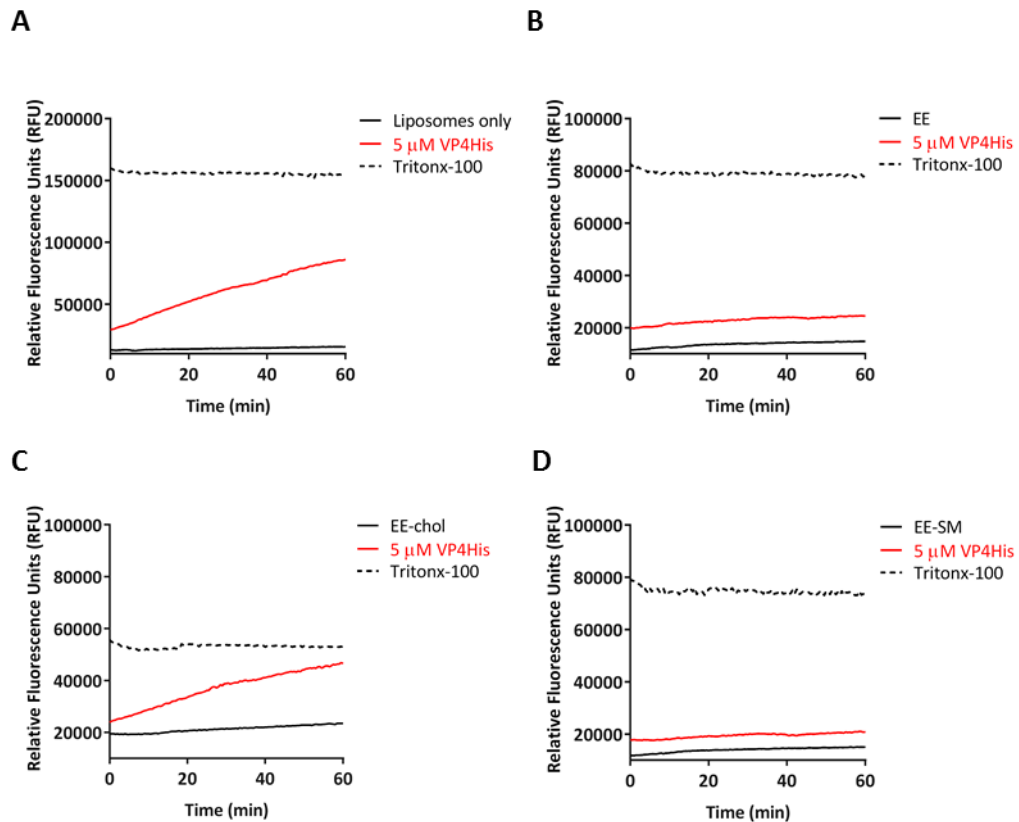


**Figure 4.13 Effect of sphingomyelin and cholesterol in early endosome membrane composition on VP4-induced membrane permeability.**

Myristoylated VP4His (VP4His) was incubated with **A**. Standard liposomes. **B**. Liposomes mimicking the composition of early endosomes (EE). **C**. EE without cholesterol (EE-chol). **D**. EE without sphingomyelin (EE-SM). VP4His-mediated CF release was monitored in real-time and measured by fluorimetry ( $\lambda_{ex}$  485 nm/ $\lambda_{em}$  520 nm). Background levels of CF release were generated by liposomes, EE, EE-chol or EE-SM only.

#### 4.2.5 VP4His-induced membrane permeability is not temperature dependent

Receptor mediated HRV16 uncoating has been demonstrated to occur efficiently at temperatures above 30°C (Casasnovas and Springer, 1994; Hooverlitty and Greve, 1993). The internal capsid protein VP4 and the N-terminus of VP1 become exposed when the capsids of picornaviruses including PV and HRV14 breathe at physiological temperature (Fricks and Hogle, 1990; Lewis *et al.*, 1998). HRV16 uncoating was shown to be both temperature and pH dependent. When HRV16 was bound to its receptor ICAM-1 at 20°C, uncoating was prevented even after the virus-receptor complex was exposed to low pH and higher temperatures (Nurani *et al.*, 2003).

The temperature required to induce a change in the physical state of the lipid from an ordered gel phase to a disordered fluid phase is referred to as the phase transition temperature. In the gel phase the lipid hydrocarbon chains are tightly packed whereas in the fluid phase the hydrocarbon chains are randomly oriented and lipids can diffuse freely inside the lipid bilayer. The transition temperature of lipid components in standard liposomes was estimated to be above the temperatures used in the experiments (25°C and 37°C). Therefore, membrane fluidity was not expected to be significantly affected at 25°C or 37°C.

Towards determining if HRV16 induced more extensive membrane permeability at physiological temperature than at room temperature, HRV16 was incubated with liposomes at 37°C or 25°C. At 37°C, HRV16 induced membrane permeability to a greater extent and with a faster initial rate of release than that induced by HRV16 at 25°C (Figure 4.14A). To investigate if VP4His membrane activity was influenced by temperature, VP4His was added to liposomes and membrane permeability assay carried out at 25°C or 37°C (section 2.23). Liposomes used for studying membrane permeability induced at 37°C were pre-warmed at 37°C. The nature and extent of membrane permeability induced by VP4His at 25°C and 37°C were similar (Figure 4.14B).

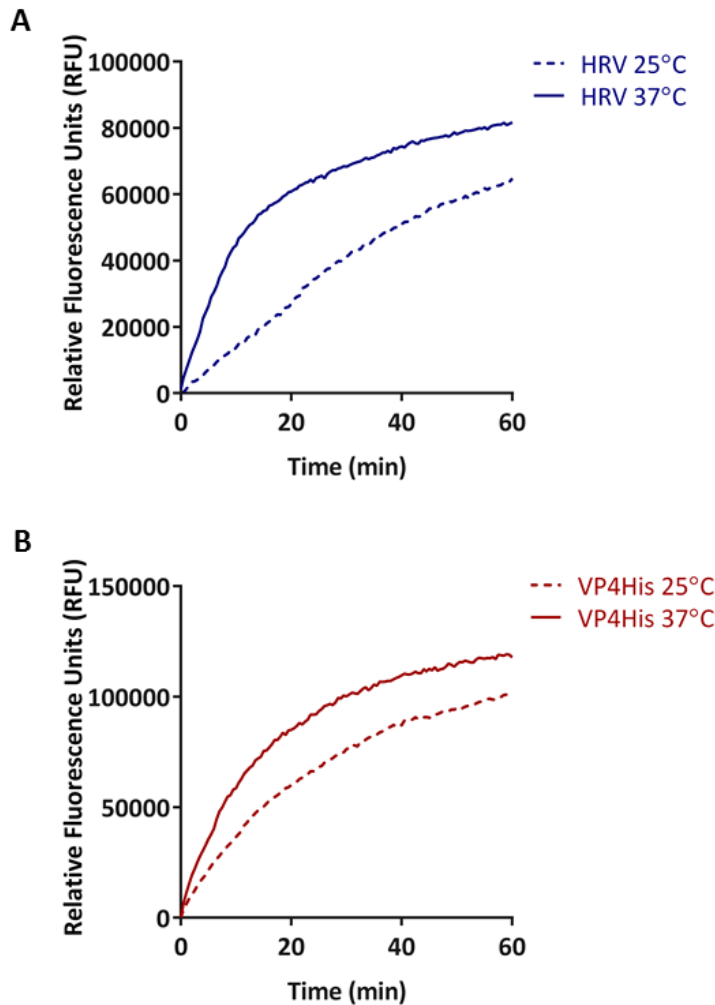


**Figure 4.14 Effect of temperature on HRV and VP4His-induced membrane permeability.**

**A.** HRV16 or **B.** VP4His was incubated with liposomes at 25°C or 37°C. Released CF was measured by fluorimetry ( $\lambda_{\text{ex}}$  485 nm/ $\lambda_{\text{em}}$  520 nm) and kinetics monitored in real-time. Background levels of CF release were generated by liposomes only. For clarity, liposomes only baseline has been subtracted from CF fluorescence measurements obtained from HRV16 and VP4His-mediated CF release at 25°C and 37°C. Data shown here is representative of multiple experiments (n=3).

### 4.3 Discussion and future work

Picornavirus VP4 has been implicated to play a role in the cell entry process (section 4.1). However, the mechanism for VP4-induced membrane permeability remains to be defined. In this chapter, membrane permeability mediated by recombinant VP4 in model membranes was demonstrated and conditions influencing membrane permeability were characterised. VP4His and  $\Delta$ VP4His-mediated membrane permeability were broadly similar to that observed with the model membrane pore forming peptide, melittin. VP4His-induced permeability was dependent on membrane composition but independent of temperature. VP4His and  $\Delta$ VP4His activity was shown to be dose-dependent and enhanced at acidic pH. Additionally, the presence of



myristoylation increased the extent of induced membrane permeability relative to unmyristoylated VP4.

VP4 is released from the virus and is known to partition into cellular membranes during infection (section 1.6.4.4) and recombinant VP4 (VP4His and  $\Delta$ VP4His) was observed to induce permeability in model membranes (Figure 4.5). It was, therefore, reasonable to assume association or binding of VP4His with liposome membranes. Indeed, GST-tagged VP4 had previously been demonstrated to associate with liposome membranes (Davis *et al.*, 2008). In order to demonstrate a membrane association with VP4His, liposome floatation assays were carried out. Based on the analysis of ficoll gradient fractions by western blot, VP4His was not detected in membrane fractions but was clearly detected in the pellet (Figure 4.3C). This may indicate that only a small proportion of VP4 was integrating into membranes and was below the detection limits of subsequent western blot. One possible explanation for the observation of GST-tagged VP4 in liposome membranes but not that of VP4His is that GST-tagged VP4 may be less efficient at inducing membrane permeability than VP4His and, therefore, a greater number of GST-tagged VP4 molecules may be required for the induction of membrane permeability. This concentration of GST-tagged VP4 associated with liposome membranes could be detected by western blot. GST-tagged VP4 was a soluble form of VP4 whereas VP4His was largely insoluble and majority observed in the pellet. It was possible that majority of VP4His did not participate in the induction of membrane permeability. Therefore, VP4His may be more efficient at inducing membrane permeability and the number of VP4His molecules integrated with liposome membranes was below the detection limit of western blot.

VP4His membrane permeability and lipid floatation assays used 8-80 times more protein than that used in similar membrane permeability and liposome floatation studies using GST-tagged VP4 reported by Davis *et al.*, 2008. Although a higher amount of VP4His was used, VP4His was largely insoluble, and it was likely that only a small proportion of VP4His participated to form functional membrane pores.

When virus VP4 is released in the absence of membrane it appears to precipitate, as shown by the cpm in the pellet when pre-heated HRV was purified on a sucrose gradient (section 3.5). However, when VP4 is released in the presence of membranes, VP4 partitions into membranes. Thus, during infection the virus capsid is likely to be held close to the membrane, possibly by the N-terminus of VP1, and this proximity to membrane would facilitate the released VP4 to insert directly into the membrane and induce membrane permeability. We are aware that the model system described here, does not entirely mimic HRV entry as VP4His is in DMSO which is then added to liposomes.

Two other scenarios could explain the clear observation of VP4His in the pellet and not in association with liposome membranes. The first possible scenario is that VP4 had inserted and permeabilised membranes, following which VP4 detached from membranes and was detected in the pellet. However, this was an unlikely event as it would be energetically unfavourable for a viral protein to insert into membrane and then disengage from it. The second possible scenario is that VP4 molecules inserted into membranes but not all of them multimerised to form a functional VP4-membrane pore. This proportion of VP4 which does not participate in forming the pore may have detached from membranes and as a result observed in the insoluble pellet.

As outlined below, VP4His : liposomes ratio was calculated to determine the number of VP4His molecules in the reaction.

$$\begin{aligned}\text{Surface area of liposomes} &= 4\pi r^2 \\ &= 4 \times 22 / 7 \times (200)^2 \\ &= 502655 \text{ nm}^2\end{aligned}$$

$$\text{Approximate surface area per lipid head group} = 0.7 \text{ nm}^2$$

$$\begin{aligned}\text{Lipid in one layer of liposome} &= 502655 / 0.7 \\ &= 718079\end{aligned}$$

$$\begin{aligned}\text{Therefore, lipid per liposome} &= 2 \times 718079 \\ &= 1436157\end{aligned}$$

$$\begin{aligned}\text{Lipid concentration per liposome} &= 50 \text{ }\mu\text{M} \\ &= 50 \times 10^{-6} \text{ moles/ litre}\end{aligned}$$

$$\text{Lipid content in reaction} = 5 \times 10^{-9} \text{ moles / 100 }\mu\text{l}$$

$$\begin{aligned}\text{Number of liposomes in 100 }\mu\text{l} &= 5 \times 10^{-9} \times 6 \times 10^{23} \text{ (Avogadro's number) / 1436157} \\ &= 2.08 \times 10^9\end{aligned}$$

$$1 \text{ M of VP4His} = 8000 \text{ g/L}$$

Therefore, 5  $\mu\text{l}$  of VP4His at a typical concentration of 0.8 mg/ml in 100  $\mu\text{l}$  reaction is approximately 5  $\mu\text{M}$

$$\begin{aligned}\text{Number of VP4 molecules in } 100 \mu\text{l} &= 5.0 \times 10^{-10} \times 6 \times 10^{23} \text{ (Avogadro's number)} \\ &= 3 \times 10^{14}\end{aligned}$$

$$\begin{aligned}\text{Therefore, VP4His : liposome} &= 3 \times 10^{14} : 2.08 \times 10^9 \\ &= \sim 145,000 : 1\end{aligned}$$

It was not possible to estimate the proportion of input VP4His molecules associated with liposome membranes as VP4His could not be detected in the fractions of the liposome floatation assay by anti VP4 C-terminus western blot (Figure 4.3). In addition, only a small proportion of these inserted VP4His molecules may be involved in forming functional membrane pores. Therefore, only a fraction of 145,000 VP4 molecules would be involved in the formation of the VP4-membrane pore complex. The VP4His:liposome ratio required for membrane permeabilisation could not be determined. Despite the difficulties with quantifying and determining the proportion of VP4His that was associated with membranes, our model system using VP4His was valid for investigating VP4 because functional consequences of different assay conditions were readily detectable.

Unsurprisingly, initial rate and extent of release induced by VP4His were dependent upon the concentration of VP4His added to the liposomes in the membrane permeability assay (Figure 4.4). Similar findings of dose-dependent activity have been made with other membrane proteins such as GALA (Kuehne and Murphy, 2001).

In order to determine if myristoylation influenced the induction of membrane permeability by VP4, myristoylated (VP4His) and unmyristoylated ( $\Delta$ VP4His) forms of VP4 were expressed and used in membrane permeability assays. Our findings showed that myristoylation was not essential for the induction of membrane permeability by recombinant VP4. However, myristoylation contributed to faster and more extensive induction of membrane permeability (section 4.2.3). These findings with VP4His are consistent with previously reported observations with myristoylated and unmyristoylated GST-tagged HRV VP4. Both forms of GST-tagged VP4 induced membrane permeability, however, myristoylated form of the protein induced more extensive membrane permeability compared to its unmyristoylated form (Davis *et al.*, 2008). The increase in membrane permeability observed with VP4His (Figure 4.5), was not unexpected as the myristate group constitutes a signal for incorporation into membranes and has been noted to be one of the common features of non-enveloped virus penetration proteins (Chandran *et al.*, 2002; Corcoran *et al.*, 2004). The myristate group has been shown to be sufficient for membrane binding by a chimeric protein comprised of the first nine amino

acids from the N-terminus of PV VP4 fused to GFP. The nine amino acids conferred N-terminal myristoylation and membrane binding to the GFP chimera (Martin-Belmonte *et al.*, 2000). Alternatively, reports have shown the myristate group alone cannot confer membrane attachment and the cooperation of other factors such as clusters of basic residues to facilitate interactions with headgroups of anionic lipids is required (Murray *et al.*, 1998) and (as reviewed in Yalovsky *et al.*, 1999). The hydrophobicity of VP4 is not sufficient for it to be expected to target membranes (Grand average of hydropathicity scores HRV VP4 is -0.16, hepatitis C virus p7 is 1.2, GALA is 0.77, melittin is 0.3 <http://web.expasy.org/cgi-bin/protparam/protparam>) and does not have a cluster of basic residues. Thus, the factors in addition to myristoylation which may contribute to membrane binding of VP4 are unclear.

Members of the picornavirus family vary in their dependence on receptor binding and pH for the initiation of conformational changes in their capsids necessary for the delivery of RNA into the cytoplasm. Although HRVs are phylogenetically closely related their pH dependence for uncoating is variable. Minor group HRVs like HRV2 have an absolute dependence on low pH for uncoating (Brabec *et al.*, 2003) whereas major group human rhinoviruses depend on receptor binding and/or low pH. pH dependence of major group rhinoviruses ranges from none to complete as was demonstrated by the treatment of cells with bafilomycin and ammonium chloride. HRV16 infection of HeLa cells in the presence of bafilomycin inhibited uncoating completely whereas HRV3 uncoating was partially reduced (Nurani *et al.*, 2003) and (as reviewed in Fuchs and Blaas, 2012). Therefore, the observation of increased induction of membrane permeability by VP4His at pH5.5 is in agreement with existing evidence for acidic pH requirement for efficient HRV16 uncoating in HeLa cells. Further evidence in support of a requirement for acidic pH for HRV16 uncoating is suggested by a study showing that HRV16 interacts only weakly with ICAM-1 compared with HRV14, as shown by cryo-EM reconstructions and functional binding studies (Xiao *et al.*, 2004). This relatively low efficiency of HRV16 binding to ICAM-1 may be compensated by greater efficiency at the stage of HRV16 uncoating at acidic pH in the endosome. The pocket factor present in the crystal structure of HRV16 but absent in HRV14 and HRV3 (Hadfield *et al.*, 1999; Rossmann *et al.*, 1985; Zhao *et al.*, 1996) may contribute to increased stability of HRV16. These reasons may explain the requirement for exposure of the ICAM-1 bound HRV16 complex to low pH to release the pocket factor present which decreases virus stability to facilitate conformational changes. It is possible that HRV16 uncoats close to pH5.5 which was observed to be the most favourable for VP4His-mediated membrane permeability (section 4.2.3).

It is also possible that VP4 may have evolved to function optimally at pH5.5 to match the uncoating environment of HRV16. Future experiments comparing VP4 from picornaviruses

dependent on pH for uncoating (e.g. HRV2, FMDV) and others that are pH independent (e.g. HRV3, PV) should be carried out to help verify if VP4 has evolved differently in different picornaviruses to match their respective uncoating environments or if it is an artefact of the assay that favours low pH for optimal VP4 function. A counter argument to VP4 evolving to function at a pH optimal for HRV uncoating is that of HRV adapting to the pH of the environment it is infecting at. For example, major group rhinovirus HRV89 was reported to depend on low pH for uncoating when infecting COS-7 cells which lack ICAM-1 expression. As suggested in the same report, HRV particles needed to be more unstable when infecting cells devoid of ICAM-1 as uncoating could only be achieved by the acidic pH in the endosome (Vlasak *et al.*, 2005). The location and nature of mutations rendering the HRV particle less stable were not investigated. This may have included a mutation in VP4 that enabled HRV89 uncoating to match its environment.

The investigation of the effect of temperature on the induction of membrane permeability by HRV16 showed that HRV16 induced more extensive membrane permeability at 37°C than at 25°C. This was in contrast with VP4His which induced membrane permeability to largely the same extent at both 25°C and 37°C (Figure 4.14). The observed increase in induced membrane permeability by HRV at 37°C compared to 25°C could be explained by the phenomenon of increased capsid breathing at 37°C. Capsid breathing at 37°C resulted in increased exposure of VP4 and N-terminus of VP1 compared to 25°C (Katpally *et al.*, 2009; Li *et al.*, 1994). The enhanced externalisation of these membrane active peptides likely contributed to the increased induced membrane permeability at 37°C. Membrane permeability was induced by HRV16 at both 25°C and 37°C (Figure 4.14A) as the capsid also breathes at 25°C, although less efficiently. One possible explanation for the observed difference in temperature dependence between HRV16 and VP4His could be because uncoating is a stepwise process and 37°C is required to maximise capsid breathing, however, 37°C may not be crucial for the membrane permeabilising function of VP4. Therefore, temperature dependence was not observed when analysing the permeabilising activity of VP4His in liposome membranes.

Priming of pH independent picornaviruses such as PV by Ig-like receptors may be temperature dependent. However, for picornaviruses dependent on low pH for the triggering of conformational changes in the capsid may be less dependent on temperature. Although, in this study, experiments have not included the use of ICAM-1 decorated liposomes, virus breathing and induction of membrane permeability in naked liposomes triggers conformational changes akin to those triggered in ICAM-1 bound virus complexes. Membrane permeability was induced at physiological temperature by PV native particles and receptor modified “A” particles in lipid bilayers devoid of receptors (Tosteson and Chow, 1997). Also, PV and FMDV

particles have been shown to interact with naked liposome membranes, resulting in induction of permeability and the release of RNA (unpublished work carried out at The Pirbright Institute).

The effect of pH on VP4-induced membrane permeability was carried out at 25°C. A clear preference for acidic pH was observed for VP4-mediated membrane permeabilisation at 25°C (Figure 4.8). In the future, it would be interesting to see if breathing observed at higher temperature is influenced by pH. Studying effects of temperature in combination with pH will help determine if lower pH can compensate for lower temperature and induce as efficient membrane permeability as that observed at 37°C.

VP4His and  $\Delta$ VP4His-induced more extensive permeability in liposomes devoid of cholesterol (Figure 4.9) which was unsurprising as cholesterol is known to increase membrane rigidity (see section 4.1). Presence of cholesterol in the membrane has been reported to reduce permeability induced by peptides such as GALA (Nicol *et al.*, 2000) and viruses such as PV (see section 4.1). The difference in the extents of membrane permeability induced by  $\Delta$ VP4His in liposomes with or without cholesterol was much greater than the difference observed with VP4His (Figure 4.9). This suggested that VP4His and  $\Delta$ VP4His could permeabilise both types of liposomes, however, the presence of myristate group in VP4 perhaps somehow compensated and resulted in a less pronounced difference between extents of permeability induced in membranes with or without cholesterol.

Upon incubating VP4His with liposome with early endosome composition, complete and abrupt membrane permeability was induced. In contrast, VP4His-induced membrane permeability in liposomes with late endosome composition showed CF release similar to that observed with melittin in standard liposomes (Figure 4.12). The difference in the nature of CF release may suggest VP4His employs a different mechanism to induce membrane permeability in EE and LE. Standard liposomes contained 10 % cholesterol, while LE was 5 % and EE was 45 %. Since the main difference between EE and LE lipid composition was cholesterol and sphingomyelin, these two lipids were investigated as a starting point to determine the effect of membrane composition on the mechanism of action of VP4His. Investigation of cholesterol in EE showed that VP4His-induced abrupt release of CF from EE containing cholesterol and as expected, VP4-induced more extensive permeability in EE not containing cholesterol. Membrane permeability induced by VP4His in EE not containing cholesterol was similar to that induced by VP4His in standard liposomes. EE with or without sphingomyelin induced similar extents of membrane permeability (Figure 4.13). Therefore, this suggested the high percentage of cholesterol (45 %) in EE and not sphingomyelin contributed to the abrupt nature of membrane permeability induction by VP4His. Other lipid components such as BMP, PI and a

range of cholesterol concentrations need to be further investigated to identify lipid components contributing to abrupt membrane permeability. These experiments using VP4 and other membrane pore forming proteins such as melittin and GALA will help determine whether this nature of abrupt membrane permeability is specific to VP4.

VP4His-induced similar membrane permeability in standard liposomes and LE (Figure 4.12). The nature of dye release observed was typical of that expected from pore forming peptides like melittin and not membrane lytic agents like Triton X-100. Therefore, VP4His may be mediating CF release from LE as would be expected from the formation of membrane pores. The attraction between VP4 and membrane would be affected by charge present on lipid headgroups. This was likely to influence membrane permeability induced by VP4. The data described above indicate that VP4 may have a preference for late endosomal membranes due to the presence of anionic lipids such as PI and BMP. These key lipid determinants may prevent premature activation of VP4-induced membrane permeabilisation by acidic pH in the absence of the target membrane. Lipid dependence has been observed with other viral proteins such as dengue virus E fusion protein. Dengue virus fusion required the anionic lipid BMP as a cofactor during low pH induced fusion for the opening of the fusion pore to transfer RNA from endosome to cytoplasm. This dependence on BMP ensured dengue virus fusion in the LE (Zaitseva *et al.*, 2010). Therefore, like dengue virus, HRV16 may use lipid dependency as an additional control for ensuring uncoating occurs in the appropriate compartment.

HRV14 uncoats in early endosomes (Bayer *et al.*, 1999) and other enteroviruses such as PV release their RNA very close (100-200 nm) to the plasma membrane (Brandenburg *et al.*, 2007). However, the site of HRV16 uncoating has not been demonstrated. As described previously, there are differences in pH dependence of major group HRV to trigger uncoating (Nurani *et al.*, 2003). VP4His was shown to induce efficient membrane permeability at pH5.5 (section 4.2.3) which matches the pH reported for efficient uncoating of HRV16. Moreover, the observed membrane permeability induced by VP4His in LE was broadly characteristic of that induced by pore forming peptides in standard liposomes. This combined evidence indicated late endosomes as a possible site of HRV16 uncoating and VP4-membrane pore formation.

# **Chapter 5**

## **VP4 forms a size-selective multimeric pore**



## 5.1 Introduction

### Site of RNA exit

Since the first structures of PV and HRV were determined, openings at the capsid fivefold axis were identified. This led to the “fivefold” model to explain RNA egress. It was tempting to think that VP1, VP4 and RNA exited from the fivefold axis as it was possible to envisage five receptor molecules at the base of the canyon and five copies of VP1 and/or VP4 exiting at the fivefold axis directed onto the membrane. However, studies over the last few years have contradicted the above fivefold RNA exit model. These studies have suggested openings at the twofold axis, large enough for the passage of unwound ssRNA (< 2 nm), as the site for RNA egress (described in section 1.6.4.3).

### Site of VP1 N-terminus externalisation

Structural studies with PV “A” particles showed that a VP3 plug remained in place at the fivefold axis during conversion from PV native particles (160S) to “A” particles (135S) and therefore there was insufficient room to contain the externalised capsid subunits, VP1 N-terminus and VP4 at the fivefold axis (Bubeck *et al.*, 2005). The site of VP1 N-terminus externalisation during capsid breathing was subsequently demonstrated to be at the twofold axis whereas in the PV “A” particles VP1 N-terminal was externalised at the propeller tip (Lin *et al.*, 2012) (described in section 1.6.4.2). More recently, cryo-tomography of PV uncoating in the presence of model membranes showed an umbilicus linking the virus surface near an opening at the quasi threefold axis to the membrane. The umbilicus was hypothesised to comprise the VP1 N-terminus and VP4 to shield the RNA from enzymatic degradation during RNA delivery into the cytoplasm (Strauss *et al.*, 2013).

### Nature of HRV mediated membrane permeability

During virus infection in cell culture under conditions that prevented uncoating, HRV14 was shown to be associated with endosomes whereas when uncoating was triggered the proportion of free HRV14 particles increased with the simultaneous disappearance of virus associated endosomal peaks. This was indicative of disruption of the endosomal membrane by HRV14, resulting in the release of genetic material into the cytoplasm. In contrast, HRV2 was found associated with endosomes under conditions that both allowed or prevented uncoating. This suggested that HRV2 delivered its RNA across the endosomal membrane into the cytoplasm without disrupting the membrane and the empty capsids were subsequently degraded in lysosomes (Schober *et al.*, 1998). HRV2 (Brabec *et al.*, 2005; Schober *et al.*, 1998) and HRV2 VP1 peptide (Prchla *et al.*, 1995) induced membrane permeability by formation of size-selective membrane pores as determined by the selective release of dextrans of increasing

molecular weights. These studies demonstrated that HRV14 permeabilised membranes by disruption and HRV2 by pore formation.

The real time CF release induced by HRV16 VP4 had characteristics similar to that obtained with melittin when used at a concentration which induced membrane permeability by pore formation (Davis *et al.*, 2008) and (section 4.2.1). To establish that permeability was due to pore formation and not non-specific loss of membrane integrity, it was important to determine pore size-selectivity. Further, it was useful to determine pore dimensions as a first step towards understanding the structure and function of such pores.

### **Multimerisation of VP4**

VP4 has been shown to partition into cellular membranes during infection (Danthi *et al.*, 2003), associate with and induce membrane permeability in liposomal membranes (Tuthill *et al.*, 2006), however, the mechanism for this is not known. In a previously published study by Katpally *et al.*, 2009, under conditions that allowed capsid breathing (37°C), HRV14 with VP4 N-terminus bearing cysteine mutations formed disulphide linked dimers. Similar VP4 dimerisation was not observed at 4°C. This finding showed that capsid breathing was required for VP4 to be externalised and form dimers. Also, the observation that all of the VP4 dimerised, indicated a specific rather than stochastic interaction of extruded VP4 (Katpally *et al.*, 2009). This provided evidence for VP4 multimerisation during picornavirus capsid breathing, however, to date there is no existing evidence for VP4 multimerisation in the presence of membranes. The requirement for a lipidic environment for VP4 multimerisation was therefore investigated here.

The information provided in this section highlighted that although there is some evidence to support parts of the picornavirus cell entry model, the mechanism of how the membrane is permeabilised to facilitate RNA delivery lacks experimental evidence.

This chapter presents evidence for VP4 multimerisation resulting in the formation of a size-selective VP4 membrane pore with dimensions consistent with those required for the release of RNA.

## **5.2 VP4 forms a pentameric or hexameric multimer**

VP4 has been shown to permeabilise membranes, yet the mechanism by which VP4 induces membrane permeability is unknown. Towards determining if VP4-mediated membrane permeability involved the formation of a pore, the multimeric state of VP4His was investigated.

Native PAGE is a technique used to determine the migration of protein complexes in their native state by subjecting them to electrophoresis under non-denaturing conditions.

Therefore, protein migration is dependent on proteins size, shape and intrinsic charge. The pH at which protein carries no net electrical charge is defined as its isoelectric point (pI). The predicted isoelectric point for VP4His is 6.8. Native PAGE was performed at pH 8.3, thereby giving VP4His an overall negative charge which would give an expected electrophoretic migration of VP4His in PAGE. The formation of higher order structures was observed when VP4His was premixed with liposomes (50  $\mu$ M lipid content) or DHPC (300 mM), and analysed by native PAGE (section 2.3.2) and silver staining (section 2.3.4.2). However, VP4His alone (5  $\mu$ g) was not observed to migrate into the native polyacrylamide gel (Figure 5.1A). One possible explanation for this observation was that the interaction of VP4His (in the absence of DHPC or liposomes) with the polypropylene tubes used in sample preparation caused VP4His to adhere to the plasticware. This may have contributed to the failure to load the VP4 sample and analyse VP4His migration by native PAGE and silver staining. Following loading of samples from the tubes onto the native polyacrylamide gel, SDS-PAGE loading buffer was added to the “apparently empty tubes” and heated to 96°C. This treatment was expected to break up potential VP4 aggregates and resuspend VP4His adhering to the polypropylene tubes. Analysis of the contents of the “apparently empty tubes” revealed VP4His present in the tube that had contained VP4His (in the absence of DHPC or liposomes) when analysed by SDS-PAGE (section 2.3.1) and silver staining (section 2.3.4.2) whereas only a small proportion of VP4His adhered to polypropylene tubes in the presence of DHPC or liposomes (Figure 5.1B). Therefore, the concern of VP4His adhering to polypropylene tubes in the absence of a lipidic environment was confirmed. Consequently, it was not possible to confirm if migration and formation of VP4 protein complexes required a lipidic environment, using this approach.

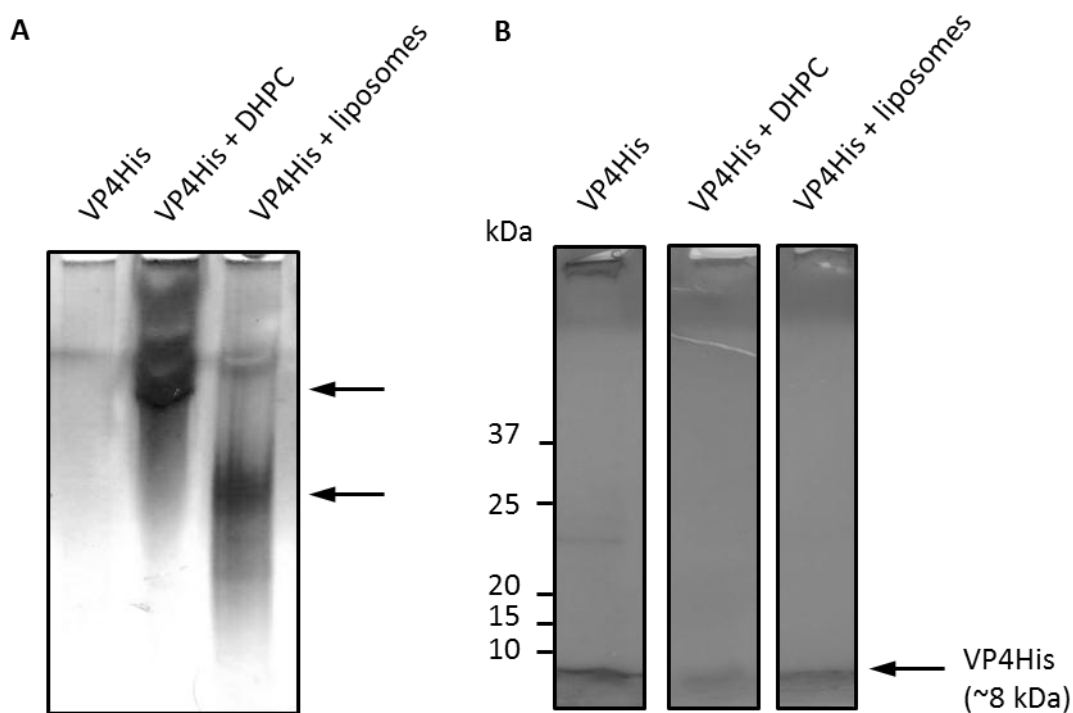


**Figure 5.1 VP4His forms higher order structures in a favourable environment.**

**A.** VP4His premixed with DHPC or liposomes and analysed by 4-20 % tris-glycine gradient native PAGE and silver staining. Black arrows indicate the observed higher order structures of VP4His. **B.** Analysis of material potentially adhered to polypropylene tubes by 4-20 % tris-glycine gradient SDS-PAGE and silver staining. Black arrow indicates VP4 at the expected apparent molecular weight of ~8 kDa. The size of molecular weight markers (kDa) is indicated to the left of the image.

Native PAGE was not suitable for accurate molecular weight determination due to absence of uniform charge on protein molecular weight markers. An alternative way of looking at VP4His multimerisation was by chemical crosslinking. Subjecting VP4His treated with chemical crosslinkers to denaturing gel electrophoresis was carried out to estimate the size of the oligomers formed. Uncrosslinked VP4His would be expected to migrate as a monomer on SDS-PAGE.

A range of crosslinkers reactive towards different protein functional groups were tested to investigate the multimeric state of VP4. The chemical crosslinkers tested included water soluble and membrane permeable crosslinkers with different spacer arm lengths. SDS-PAGE analysis of VP4His treated with chemical crosslinkers would determine the molecular weight of the observed VP4His multimers. Glutaraldehyde (used for membrane proteins, membrane associated proteins and soluble proteins, spacer arm length of 5 Å) dithiobis (succinimidylpropionate) [(DSP), membrane permeable, spacer arm length of 12 Å], 1,5-difluoro-2,4-dinitrobenzene [(DFDNB), membrane permeable, spacer arm length of 3 Å],

dithiobis (sulfosuccinimidylpropionate) [(DTSSP), water soluble, spacer arm length of 12 Å], dimethyl adipimidate [(DMA), water soluble, spacer arm length of 8.6 Å] were the chemical crosslinking reagents used to investigate VP4His multimerisation.

Preliminary studies in the project used PV VP4His. PV VP4His was expressed, purified (section 3.3) and treated with the crosslinker, glutaraldehyde (section 2.3.8.2). PV VP4His (5 µg) was treated with 0.1 % glutaraldehyde either in the presence or absence of liposomes. When treated in the presence of liposomes and analysed by SDS-PAGE (section 2.3.1) and anti-His western blot (section 2.3.5), multimers consistent with the molecular weight of PV VP4His pentamers (~40 kDa) were observed. When treated in the absence of liposomes, the formation of PV VP4His multimers consistent with the molecular weight of PV VP4His dimers (~15 kDa) and trimers (~25 kDa) were observed (Figure 5.2).

Due to the higher expression levels observed with HRV VP4His compared to PV or FMDV VP4His (section 3.3), further studies were carried out using HRV VP4His.

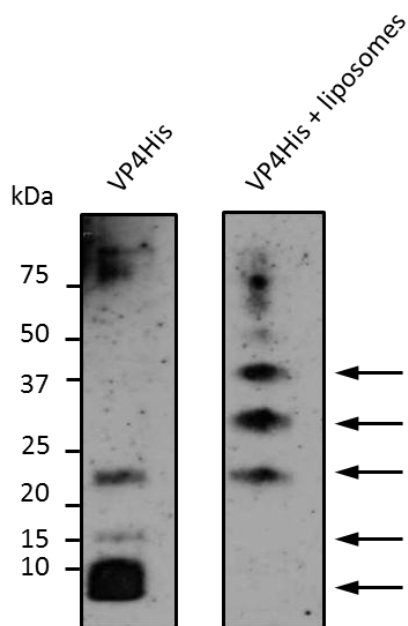


**Figure 5.2 Multimerisation of PV VP4His in the presence or absence of liposomes.**

PV VP4His pre-mixed with or without liposomes and treated with glutaraldehyde. The treated samples containing PV VP4His multimeric species were analysed by 16.5 % tris-tricine SDS-PAGE and anti-His western blot. Middle lanes on the gel are removed for clarity. Arrows indicate observed migration of PV VP4His monomer, dimer, trimer, tetramer and pentamer. The size of molecular weight markers (kDa) is indicated to the left of the image.

The only other chemical crosslinker that yielded VP4His multimers was DSP and this was taken forward. DSP is a chemical crosslinker containing an amine reactive N-hydroxysuccinimide (NHS) ester at each end of an eight carbon spacer arm. HRVVP4His was expressed in *E. coli* and purified under denaturing conditions (sections 2.11 and 2.13). Following treatment of VP4His with DSP in the presence or absence of liposomes (section 2.3.8.1), potential VP4His multimers were subjected to denaturing SDS-PAGE (section 2.3.1) and detected by anti-VP4 C-terminus western blot (section 2.3.5).

$\alpha$ -lactalbumin was used as a control for the crosslinking of VP4His with DSP. VP4His (~8 kDa) and  $\alpha$ -lactalbumin (~15 kDa) contain 4 and 12 primary amines, respectively. Treatment of  $\alpha$ -lactalbumin (1  $\mu$ g) with DSP did not result in the formation of multimers and only monomers were observed (Figure 5.3A) whereas treatment of VP4His (5  $\mu$ g) with DSP yielded VP4His multimers (Figure 5.3B). This demonstrated that crosslinking with DSP was protein specific. Treatment of VP4His in the presence or absence of liposomes (50  $\mu$ M lipid content) resulted in the detection of a ladder of bands, corresponding in size to VP4His monomer (~8 kDa) and VP4His multimers in increasing numbers, up to a VP4His multimeric complex with a molecular weight ~50 kDa, indicative of VP4His hexamers (Figure 5.3B). The detection of VP4His species with uniform and incremental increase in apparent molecular weight equal to the addition of a VP4His monomer, suggested multimerisation of VP4His monomers rather than random aggregation. VP4His multimers observed in the absence of liposomes were similar to those obtained in the presence of liposomes (Figure 5.3B). The observation of VP4His multimerisation in the absence of liposomes suggested that the presence of a lipid membrane for VP4His multimerisation was not critical. This finding raised the question of VP4 multimerisation occurring before or after insertion into the endosomal membrane. When crosslinking of VP4His with DSP was reversed by the addition of DTT, the intensity of the multimeric species decreased and that of monomeric VP4His increased (Figure 5.3B). Similarly, densitometry analysis (section 2.3.6) of the products of VP4His crosslinked with DSP showed a decrease in the proportion of VP4His monomer with a concomitant increase in VP4His multimers upon treatment of VP4His with DSP (Figure 5.3C). The above observations suggested that the multimeric protein complexes were indeed comprised of monomeric VP4His. Interestingly, multimers of VP4His were also observed in the absence of treatment with DSP. These observed intermediate multimers made up of an intermediate number of VP4 molecules were diminished in intensity, similar to those observed upon reversal of crosslinking. However, VP4His dimers and hexamers were clearly detected with and without treatment with DSP and also upon reversed crosslinking (Figure 5.3B). This likely indicated that VP4His dimers and hexamers were more stable than the other VP4His intermediate species.

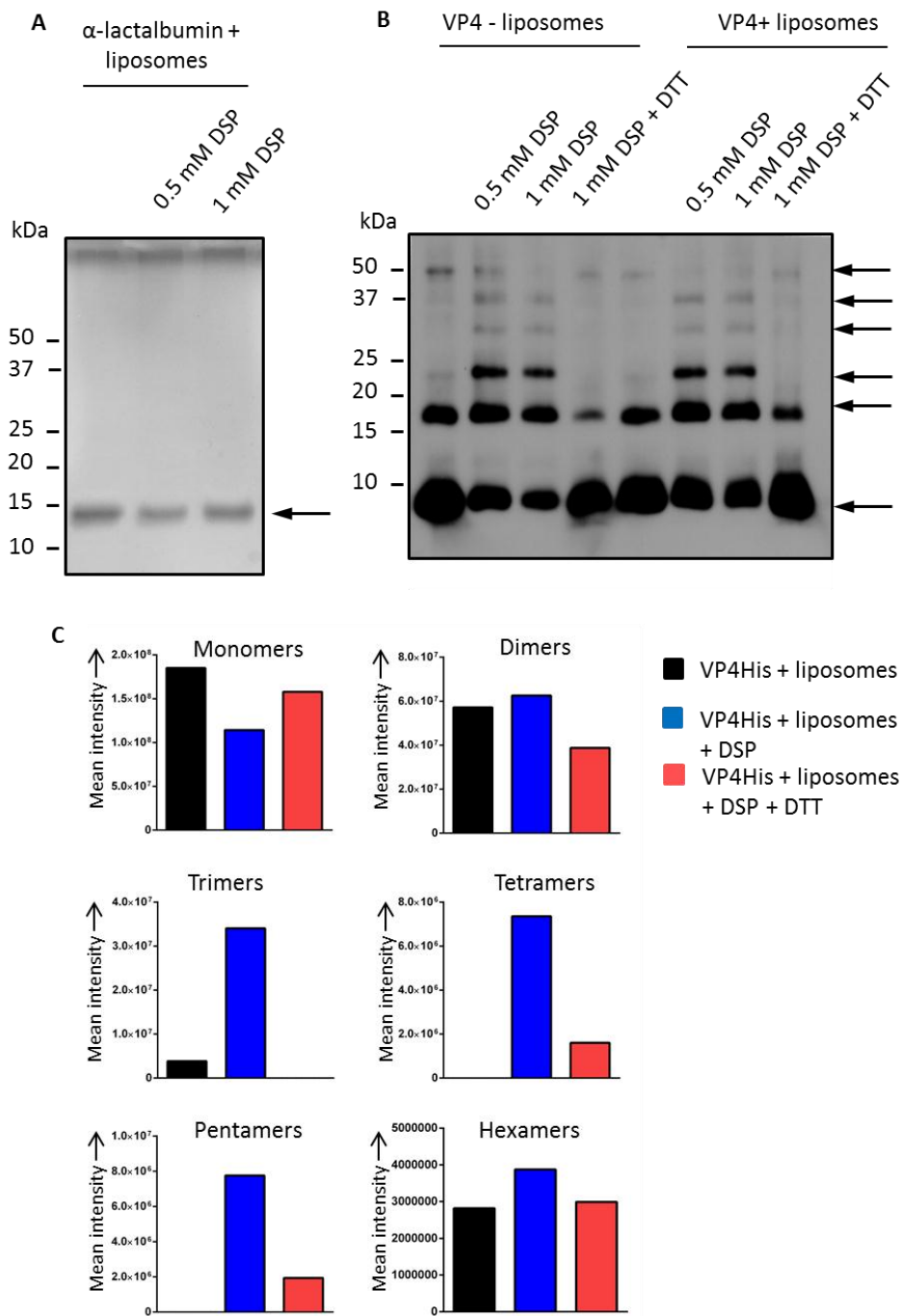


**Figure 5.3 Multimerisation of VP4His in the presence or absence of liposomes.**

**A.**  $\alpha$ -lactalbumin crosslinked with DSP in the presence of liposomes. Samples were separated by 16.5 % tris-tricine SDS-PAGE and analysed by silver staining. Black arrow indicates  $\alpha$ -lactalbumin monomer observed at the expected molecular weight ( $\sim$ 15 kDa). **B.** VP4His crosslinked with DSP in the presence or absence of liposomes. Samples were separated by 16.5 % tris-tricine SDS-PAGE and VP4His detected by anti-VP4 C-terminus western blot. Black arrows indicate the observed migration of VP4His at the expected apparent molecular weights for monomer, dimer, trimer, tetramer, pentamer and hexamer. **C.** Densitometry analysis of the distribution of VP4His monomeric and multimeric species in the presence of liposomes. The net intensity was calculated for each band using Kodak Molecular Imaging Carestream MI NE programme.

### 5.3 VP4 forms a size-selective pore

During infection of cells, minor group rhinovirus HRV2 was demonstrated to form size-selective membrane pores whereas HRV14 was shown to induce membrane permeability by membrane disruption as demonstrated by the release of FITC labelled dextrans of a range of molecular weights (section 5.1). HRV2 VP1 peptides showed the induction of membrane permeability by forming size-selective pores (Prchla *et al.*, 1995). Mutations in PV VP1 affected kinetics of RNA delivery during infection (Kirkegaard, 1990). Therefore, there is evidence for VP1 being involved in membrane binding and playing a role in transfer of RNA across the membrane (described in section 1.6.4.4). Mutations in PV VP4 were correlated with the delay or prevention in genome delivery, suggesting VP4 was likely to be involved in forming a channel for the transfer of RNA into the cytoplasm (Danthi *et al.*, 2003). GST-tagged VP4 of major group HRV16 was shown to induce membrane permeability through intact membranes (Davis *et al.*, 2008). Furthermore, membrane permeability induced by VP4His shared characteristics with that induced by the model pore forming peptide, melittin. This suggested that VP4His did not disrupt liposomes to release their contents (section 4.2.1.). The possibility of pore formation by VP4His was investigated by gauging the dimensions of the molecules that could pass through and those that were retained within the membrane. A standard approach for characterising membrane permeability induced by pore forming peptides and viral proteins was used. For this, liposomes containing FITC labelled dextrans (FD) of different sizes 4 kDa, 10 kDa, 70 kDa, 250 kDa and correspondingly different stokes radii 1.4 nm, 2.3 nm, 6 nm, stokes radius undetermined for FD250, were prepared and purified (section 2.22). The non-selective release of FDs from within liposomes would indicate large scale membrane disruption whereas release of only low molecular weight FDs would indicate formation of a size-restrictive pore.

Melittin is a well characterised membrane pore forming peptide and has been shown to form a membrane pore of defined diameter of 2.5 - 3 nm (Ladokhin *et al.*, 1997). Melittin was used as a positive control in the studies to determine size-selectivity of the membrane pore formed by VP4His. Melittin or VP4His were incubated with liposomes containing FD and membrane permeability analysed (section 2.24). When liposomes were incubated with 10  $\mu$ M melittin, efficient release of FD4 (stokes radius 1.4 nm) was observed which was consistent with the expected pore size formed by melittin. Minimal release of FD10, FD70 and FD250 was observed (Figure 5.4A). In comparison, VP4His (5  $\mu$ M) induced the release of FD4 and FD10 but significantly lower extents of release for FD70 and FD250 (Figure 5.4B). The selective release of FD from within liposomes, as induced by VP4His, indicated that VP4His formed size-selective membrane pores.



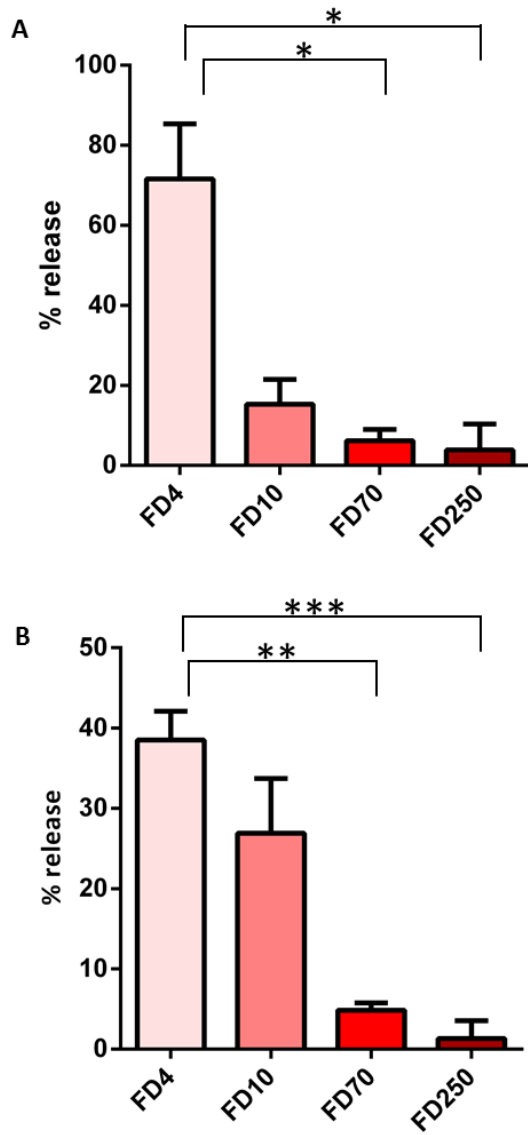


**Figure 5.4 VP4His forms size-selective membrane pores.**

The release of FDs of different molecular weights (4 kDa, 10 kDa, 70 kDa, 250 kDa) contained within liposomes, induced by **A.** Melittin. **B.** VP4His. (Experiments  $n=2$  for panel A and  $n=4$  for panel B). Error bars represent standard deviation of the mean. Statistical significance was calculated by one way Anova ( $p^* < 0.05$ ).

## 5.4 Visualising the VP4-membrane pore complex

The information gained from models for picornavirus cell entry combined with biochemical and structural studies (sections 1.5 and 1.6.4.3) will contribute towards the understanding of the mechanism of membrane permeabilisation that facilitates RNA transfer across the membrane.

Following the observation of VP4-mediated CF release similar to membrane pore forming peptides (section 4.2.3), higher order structures of VP4His by native PAGE and VP4His hexamers by crosslinking studies (section 5.2), and selective dextran release indicating size-restrictive pore formed by VP4His (section 5.3), the next step was the visualisation of the VP4-membrane pore complex.

Transmission electron microscopy (TEM) uses a beam of electrons to create an image of the specimen. TEM has higher resolving power and magnifications compared to light microscopy. This enables detailed visualisation of smaller objects. Negative staining is a technique used in EM, in which stain surrounds the sample and is excluded from the area occupied by the sample. As a result, deflection of the introduced electron beam is higher through stain-rich regions of the carbon grid compared to the protein sample. This generates high contrast but includes drawbacks such as particle distortion as part of the drying step used during the staining procedure.

Negative staining has been used previously to visualise channels formed by viral membrane proteins of sizes similar to VP4His by TEM. Due to resolution limits of TEM, the approaches have relied on the use of tags such as GST and FLAG to enable visualisation of the membrane pore complexes. These include visualising membrane channels formed by E5 of HPV (Wetherill *et al.*, 2012), p7 of HCV (Clarke *et al.*, 2006) and SH of RSV (Carter *et al.*, 2010).

In order to study the native state of membrane proteins, they must be placed in environments that mimic natural conditions. There is no structural data for the visualisation of free VP4 or VP4 inserted in membranes. The approach for visualising the VP4 membrane pore complex by negative stain TEM included the use of VP4 (section 3.4) and GST-tagged VP4 (section 3.2); liposomes (section 2.22) and detergent micelles as favourable environments for protein reconstitution.

Attempts at visualising VP4 in liposomes were unsuccessful due to the size limits required for high resolution images of protein complexes using TEM. Therefore, VP4ThGST was reconstituted in liposomes for the visualisation of the VP4 membrane pore complex. Although pore complexes formed by VP4ThGST multimers in liposomal membranes were expected to be

visualised, the negative staining procedure involved drying which resulted in the collapse of liposomes. This made the identification of pore complexes formed by VP4ThGST in liposome membranes very difficult. An alternative and established approach to reconstitute VP4 and VP4ThGST in detergent micelles was used.

Membrane proteins naturally occur in a complex mosaic bilayer. It is difficult to mimic the exact native environment of membrane proteins, however, the use of detergent micelles for the reconstitution of proteins in their native state is standard practice. Detergents are amphipathic molecules containing a polar head group and a hydrophobic tail and spontaneously form spherical micelles in aqueous solutions. Detergents are classified into three classes based on charge: ionic (anionic, cationic and bile acid salts), non-ionic and zwitterionic. Detergents serve to mimic the lipid bilayer environment membrane proteins are naturally found in (Seddon *et al.*, 2004). Reconstitution of proteins in detergent micelles to determine structures of proteins in their native state has been reported for a number of viral membrane binding proteins including M2 of influenza A virus (Schnell and Chou, 2008) and p7 of HCV (Cook and Opella, 2011).

To determine which detergent would be optimal for VP4 reconstitution, a range of detergents were tested (Table 5.1). An approach using recommended detergent critical micellar concentrations (CMC) (by members of the Chou lab, Harvard Medical School, USA) under different pH conditions of 5.5-8.0 was used to reconstitute VP4 (section 2.16).

**Table 5.1 Range of detergents used for the optimisation of conditions for the reconstitution of VP4. Sodium acetate (NaAc) pH5.5, sodium phosphate (NaPO<sub>4</sub>) pH7.0 or 7.5, 4-(2-hydroxyethyl)-1-piperazineethanesulfonic acid (HEPES) pH8.0.**

Name of detergent	Type of detergent	CMC (mM)	Buffers	pH
CHAPSO	zwitterionic	10, 25	NaAc, Hepes	5.5, 8.0
LDAO	zwitterionic	10, 25	NaAc, Hepes	5.5, 8.0
DPC (FOS-12)	zwitterionic	25, 100	NaAc, NaPO <sub>4</sub>	5.5, 7.5, 7.0
FOS-9	zwitterionic	25, 100	NaAc, NaPO <sub>4</sub>	5.5, 7.5, 7.0
FOS-14	zwitterionic	25, 100	NaAc, NaPO <sub>4</sub>	5.5, 7.5, 7.0
OG	Non-ionic	25, 100	NaAc, NaPO <sub>4</sub>	5.5, 7.5, 7.0
DHPC(hexa)	zwitterionic	25, 100	NaAc, NaPO <sub>4</sub>	5.5, 7.5, 7.0
DHPC (hepta)	zwitterionic	25, 100	NaAc, NaPO <sub>4</sub>	5.5, 7.5, 7.0
LMPG	anionic	25, 100	NaAc, NaPO <sub>4</sub>	5.5, 7.5, 7.0
DDM	Non-ionic	25, 100	NaAc, NaPO <sub>4</sub>	5.5, 7.5, 7.0
LAPAO	zwitterionic	25, 100	NaAc, NaPO <sub>4</sub>	5.5, 7.5, 7.0
SDS	anionic	10, 25, 100	NaAc, NaPO <sub>4</sub>	5.5, 7.5, 7.0

Optimal detergent conditions to reconstitute VP4 (0.1 mg) were identified by mixing VP4 with a range of detergents at different CMCs and pH conditions, followed by clarification using centrifugation. At each stage reconstituted VP4 was checked for visible precipitation. To confirm the incorporation of protein in detergent micelles, reconstituted protein was subjected to size exclusion chromatography (section 2.16). Calibration experiments had previously been carried out on the size exclusion columns (Superdex 200 10/300 or Superose 6 10/300 GL), according to manufacturer's instructions. This enabled determination of void volumes and molecular weight estimations of populations obtained in the elution peaks. VP4 eluted as aggregates with most of the detergents tested, however, VP4 reconstituted in DPC or LMPG in NaAc buffer at pH5.5, gave an optimal elution profile (Figure 5.5). Protein aggregates and empty DPC or LMPG detergent micelles eluted under ~10 ml and above ~22 ml, respectively. A clear peak was observed in the elution profile at ~15 ml (red arrow, Figure 5.5) which indicated 35000-13600 Da for VP4 in DPC or LMPG micelles. A proportion of protein eluted before or after ~15 ml (indicated by blue arrows, Figure 5.5), suggesting there might be a mixed population including VP4 monomers and multimers incorporated into the detergent micelles. Clearly, the majority of VP4 was successfully reconstituted in DPC or LMPG micelles,

in NaAc buffer at pH5.5. This amount of reconstituted VP4 (~ 0.015 mM) could be used for visualising potential structures of VP4 membrane pore complex by TEM (described further in this section), for the determination of secondary structure of VP4 in a lipid environment using CD (described in Chapter 6) and for obtaining 1D NMR spectra (described in Chapter 6). However, 2D heteronuclear single-quantum correlation (HSQC) NMR studies required 0.5-1 mM of reconstituted VP4. Therefore, a higher amount of VP4 (1 mg) was reconstituted in DPC, LMPG and SDS. Upon scaling up, VP4 remained reconstituted in LMPG and SDS, with elution profiles similar to those shown in Figure 5.5. However, VP4 precipitated when its reconstitution was attempted in DPC. The majority of the protein appeared to have aggregated and therefore eluted at ~1 ml (blue arrow, Figure 5.6) and only a proportion of VP4 incorporated in DPC micelles eluted at ~15 ml (red arrow, Figure 5.6). <sup>15</sup>N labelled VP4 was similarly reconstituted in SDS or LMPG micelles and used to acquire 2D NMR spectra of VP4 in detergent micelles and is described in Chapter 6.

VP4ThGST (0.1 mg) reconstituted in DPC showed a clear peak in the elution profile at ~15 ml (red arrow, Figure 5.7), which indicated 67000-13700 Da for VP4ThGST in DPC micelles. A proportion of protein eluted after ~15 ml (indicated by blue arrow, Figure 5.7), which suggested there might be a mixed population of VP4ThGST multimers incorporated into DPC micelles.

Therefore, Figures 5.5 and 5.7 demonstrated successful reconstitution of VP4 and VP4ThGST in detergent micelles which could be taken forward for visualisation by EM and other structural studies such as CD and preliminary NMR.

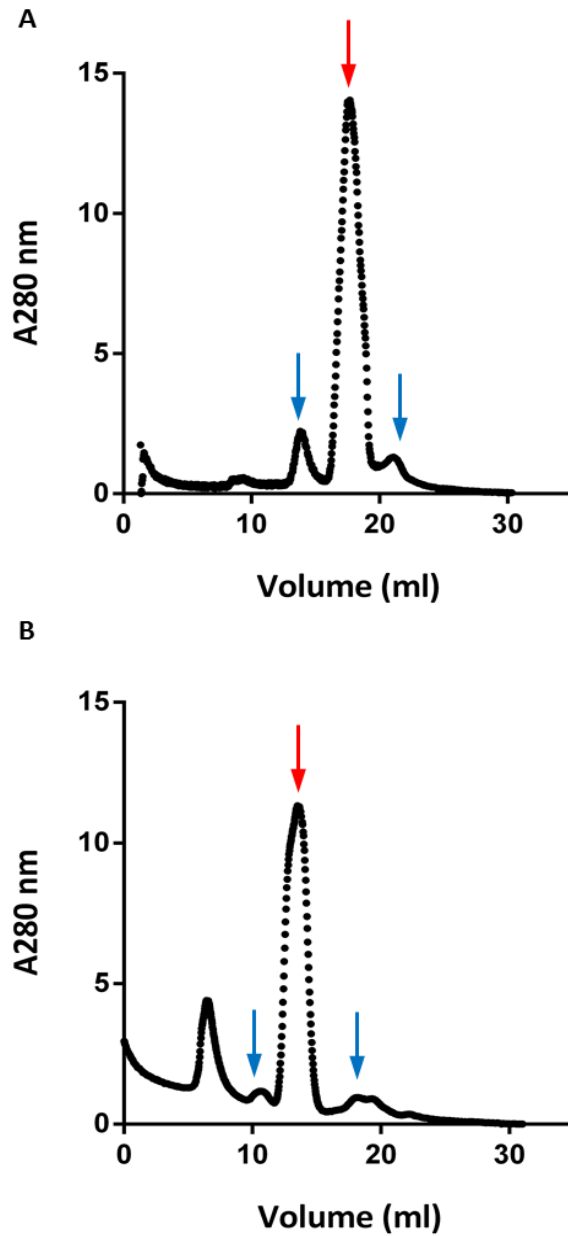


**Figure 5.5 Reconstitution of VP4 in detergent micelles.**

Size exclusion chromatography elution profiles by measuring absorbance at 280 nm of **A.** VP4 reconstituted in DPC. **B.** VP4 reconstituted in LMPG. Red arrows indicate elution volume at ~15 ml for VP4 incorporated in DPC or LMPG micelles. Blue arrows indicate secondary peaks in the elution profile.

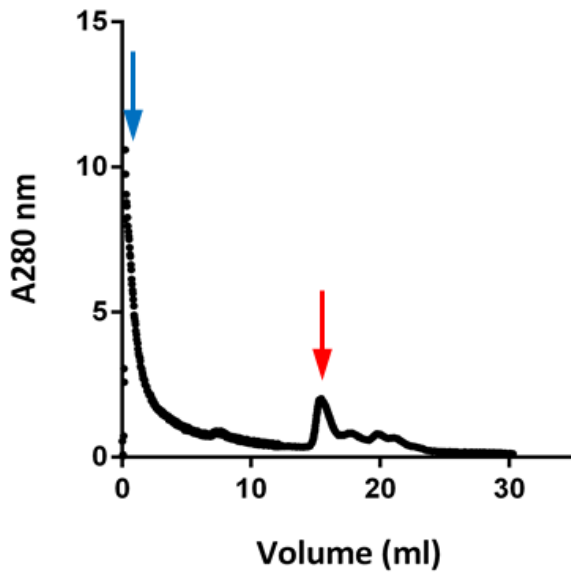


**Figure 5.6 Reconstitution of VP4 in DPC micelles.**

Size exclusion chromatography elution profiles by measuring absorbance at 280 nm of VP4 (1 mg) reconstituted in DPC micelles. Red arrow indicates elution volume at ~15 ml for VP4 incorporated in DPC micelles. Blue arrow indicates aggregated VP4.

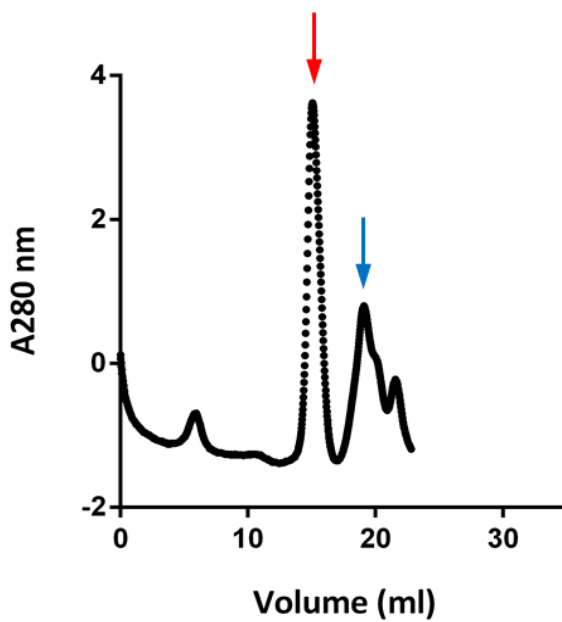


**Figure 5.7 Reconstitution of VP4ThGST in DPC detergent micelles.**

Size exclusion chromatography elution profiles by measuring absorbance at 280 nm of VP4ThGST in DPC. Red arrow indicates elution volume at ~15 ml for VP4ThGST incorporated in DPC micelles. Blue arrow indicates mixed population of VP4ThGST monomers or multimers incorporated in DPC micelles.

Due to the small size of VP4 and associated low resolution by TEM, VP4 incorporated in detergent micelles could not be used to determine the structure of the VP4 membrane pore complex using TEM. To overcome this problem, VP4 with a larger GST-tag (VP4ThGST) was used. VP4ThGST has been functionally characterised in dye release studies (Davis *et al.*, 2008). TEM was used to determine whether recombinant VP4ThGST formed oligomeric structures in a micellar environment and provide information towards determining pore dimensions of the VP4 membrane pore. Uranyl formate has a smaller grain size and better contrast than uranyl acetate (Booth *et al.*, 2011). Therefore, uranyl formate and was used as the negative stain of choice for visualising the VP4ThGST membrane pore complex by TEM.

A sample of VP4ThGST incorporated in DPC micelles and purified by size exclusion chromatography (red peak, Figure 5.7) was stained with uranyl formate and analysed by TEM (section 2.19). Aggregates were observed when an undiluted sample was visualised by TEM (Figure 5.8A). Sample dilutions of 1:100, 1:500 and 1:1000 were tested to determine the optimal dilution for observing individual VP4ThGST oligomeric complexes. With increasing sample dilution, individual VP4ThGST oligomeric ring-like structures became increasingly easier to visualise (Figure 5.8A-D). Upon 1:1000 dilution, individual VP4ThGST ring-like structures were readily observed as “top-down” views of multimeric pores (Figure 5.8D). A set of oligomers were selected to give a more detailed view of the ring-like arrangement (Figure 5.9A, B). Similar oligomeric structures were observed in other regions of the grid. Some of these structures appeared as single individual ring-like structures and others as a pair of ring-like structures (Figure 5.9A, B). The carbon grid alone or stained with uranyl formate or with DPC adsorbed and stained with uranyl formate were used as controls for the experiment and did not show the presence of ring-like structures (Figure 5.9C, D, E). The VP4ThGST ring-like structures were observed to have a lumen diameter of ~5 nm, in agreement with the dextran release studies, suggesting a VP4 pore size cut-off between 4.6 nm - 12 nm (section 5.3). This is the first reported observation of VP4 oligomeric ring-like structures.



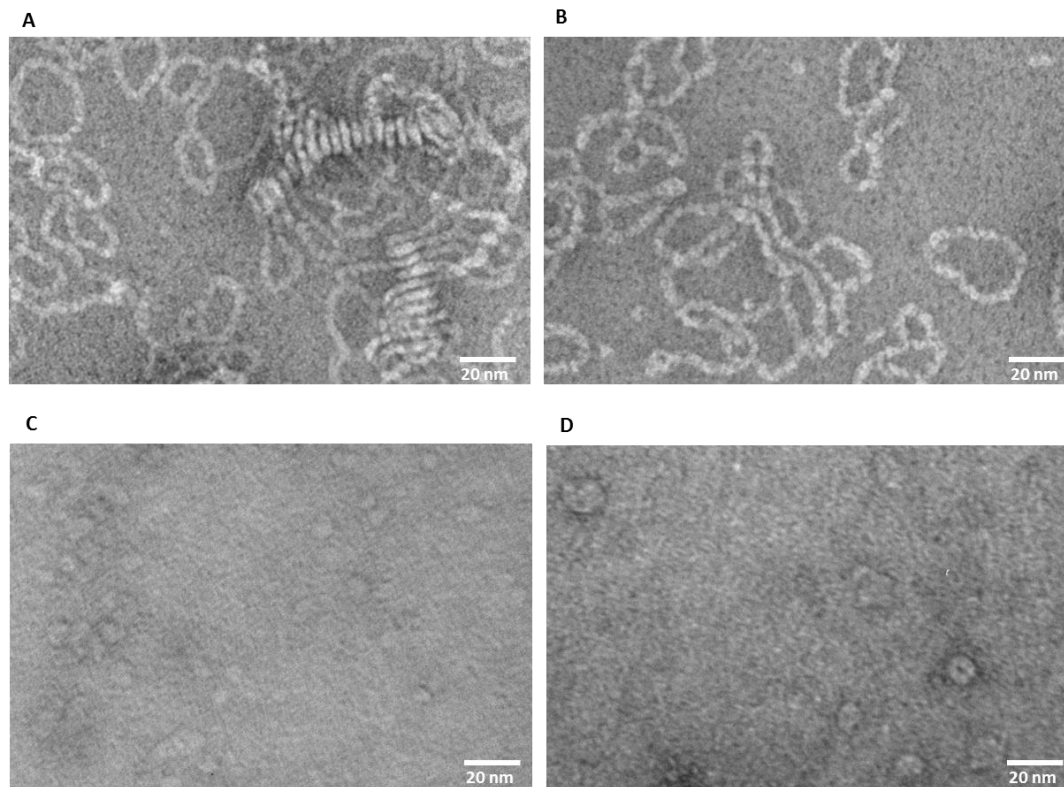


**Figure 5.8 Sample optimisation for the visualisation of VP4ThGST oligomeric structures by TEM.**

A-D show increasing dilution of VP4ThGST reconstituted in DPC micelles **A.** neat sample. **B.** 1:100 **C.** 1:500 **D.** 1:1000. TEM images visualised at 100 000 X magnification.

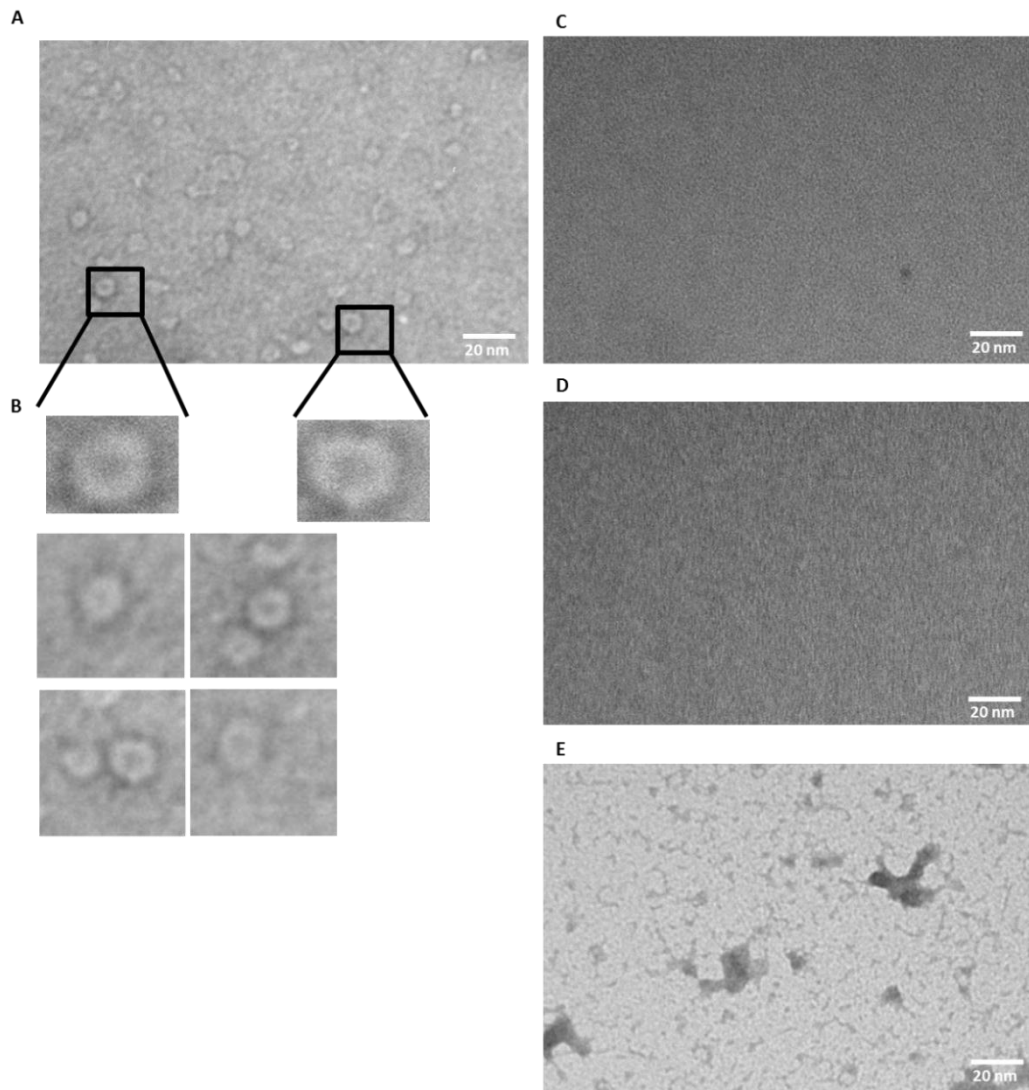


**Figure 5.9 Visualisation of VP4ThGST oligomeric structures by TEM.**

TEM image of VP4ThGST reconstituted in DPC micelles **A**. 1:500 dilution of VP4ThGST reconstituted in DPC micelles to visualise VP4ThGST oligomers. **B**. A set of oligomers were selected (highlighted in black boxes in panel A) to give a more detailed view of the potential ring-like arrangement. C-E controls for TEM. **C**. Carbon grid only. **D**. Carbon grid stained with uranyl formate. **E**. Carbon grid with DPC and stained with uranyl formate. TEM images in panels A, C, D, E visualised at 100 000 X magnification.

## 5.5 Discussion and Future Work

Picornavirus VP4 has been suggested to contribute to the transfer of viral RNA across the cellular membrane and into the cytoplasm (section 1.6.4.4). VP4His was shown to permeabilise membranes and the conditions influencing it characterised in Chapter 4. The mechanism for VP4-mediated membrane permeabilisation was explored in this chapter. The results in this chapter showed that VP4His induced size-selective membrane permeability. VP4His was shown to form a multimeric complex composed of five to six copies of VP4His. Recombinant VP4 was successfully reconstituted in a lipid-mimetic environment (detergents) which enabled visualisation of the VP4 membrane pore complex for the first time, demonstrating pore dimensions, consistent with dextran release studies and with a pore size required for the release of ssRNA. The combination of biochemical multimerisation data and analysis of TEM image suggested a VP4 pore comprising of 5 or 6 copies of VP4.

VP4 was unlikely to form a functional pore with only one copy of VP4, therefore, VP4 multimerisation was expected for the formation of a membrane pore with appropriate dimensions required for the transfer of RNA across the membrane. Two scenarios for VP4 multimerisation are possible. The first scenario is that VP4 multimerises to form an oligomeric complex prior to membrane insertion or the second scenario where VP4 inserts into the membrane and multimerisation follows, leading to the formation of a membrane pore. Whether VP4 multimerisation occurred prior to or following membrane insertion was investigated by treatment of VP4His with chemical crosslinkers, analysed by SDS-PAGE and western blot; or by pre-mixing VP4His with liposomes (or DHPC) and analysed by native PAGE and silver staining (section 5.2). VP4His multimers were formed upon crosslinking VP4His with DSP, both in the presence and absence of liposomes (Figure 5.3B). This suggested that lipid membrane was not critical for VP4His multimerisation. In the context of VP4 released from virus, contributing to pore formation for the transfer of RNA across the membrane, this makes the scenario of VP4 multimerisation before inserting into the lipid membrane, plausible. However, the observation on native-PAGE wherein VP4His did not form detectable higher order structures as those formed in the presence of DHPC or liposomes (Figure 5.1A) suggested the requirement for a lipidic environment. VP4His was not observed as an aggregate in the stacking gel nor did it enter the gel (Figure 5.1A). In the absence of a lipidic environment VP4His was confirmed to adhere to polypropylene tubes used in sample preparation (Figure 5.1B). Thus, it was unclear if VP4 multimerisation was lipid dependent.

The importance of the presence of membranes, for capsid proteins such as picornavirus VP4 and rotavirus VP5\* is discussed in section 1.6.3. In contrast, VP4 was shown to dimerise upon extrusion from the capsid during breathing at physiological temperature (Katpally *et al.*, 2009),

which demonstrated that lipid was not critical for the dimerisation of VP4. When visualised by TEM, recombinant VP4 formed oligomeric ring-like structures only in the presence of DPC micelles, a lipid-mimetic environment (section 5.5). This requirement for a lipidic environment for VP4 multimerisation was consistent with the membrane requirement in the formation of the “umbilicus” connecting the PV “A” particles to the liposome membrane. The “umbilicus” was hypothesised for the transfer of RNA across the membrane (Strauss *et al.*, 2013). These findings suggested the potential significant role of lipid membrane in VP4 multimerisation. This led to the hypothesis of VP4 released from the capsid inserting into the membrane, reaching a critical concentration with VP4 molecules in the appropriate proximity to each other and then multimerising to form a pore which facilitates the transfer of RNA across the membrane. Both VP1 N-terminus and VP4 may be required for the transfer of RNA across the membrane and this is discussed further in Chapter 7.

As shown in section 5.2 chemical crosslinking was used to determine the multimeric state of VP4His. It was important to bear in mind that this was carried out using recombinant VP4 in a cell free system and, thus, was devoid of complete infectious virus and membranes containing both lipid and protein. The advantages of using liposomes included tighter experimental control of liposome membrane composition, pH conditions, temperature and VP4His concentration. Hence, crosslinking studies were carried out with VP4His in the presence of liposomes. Crosslinking of virus with cell membranes will be a useful experiment to undertake to confirm findings of VP4His multimerisation in the presence of liposomes.

The empirical treatment of VP4His with a range of crosslinking reagents such as DFDNB, DTSSP and DMA did not yield any observable VP4His multimers whereas treatment with DSP yielded multimers comprised of five or six copies of VP4 (section 5.2). This observed difference following treatment of VP4His with different crosslinkers could be due to variable spacer arm lengths of the crosslinkers, proximity of VP4His molecules to each other, presence of different functional reactive moieties carried by the crosslinker molecule and accessibility of reactive groups of VP4His residues to the crosslinkers. It is possible that the number of crosslinks obtained experimentally using DSP may be different to that observed in the structure of the VP4 multimeric complex when inserted into the endosomal membrane. Chemical crosslinking of scrambled VP4 sequences can be carried out to confirm the specificity of these interactions. DSP reacts with primary amines of amino acids such as lysines and the residue at the N-terminus of the polypeptide to form stable amide bonds at pH 7-9. VP4His activity was shown to be optimal at pH5.5 (section 4.2.3) and in liposomes with a membrane composition mimicking that of late endosomes (section 4.2.4). Therefore, future work should include treatment of VP4His with crosslinkers compatible with low pH and using liposomes with a

composition mimicking that of late endosomes, thereby investigating VP4His multimerisation under conditions optimal for VP4 function.

Preliminary studies with PV VP4His showed that PV VP4His multimerisation with glutaraldehyde, generated multimers up to a pentamer (Figure 5.2) whereas crosslinking of HRV VP4His with glutaraldehyde, resulted in the absence of detectable multimerisation. However, HRV VP4His crosslinked with DSP generated multimers up to a pentamer or hexamer (Figure 5.3B). Treatment of PV VP4His with DSP was not carried out. Both DSP and glutaraldehyde are amine dependent crosslinkers. PV VP4 and HRV VP4 contain 5 and 4 lysines, respectively. Therefore, the difference in the observed PV and HRV VP4 multimeric species generated upon treatment with different crosslinkers may be due to differences in spacer arm lengths of the crosslinkers (5 Å for glutaraldehyde and 12 Å for DSP) or amino acid differences and accessibility of reactive groups in PV and HRV VP4 residues to the crosslinker. Furthermore, treatment of PV VP4His with glutaraldehyde resulted in the complete disappearance of monomeric and dimeric species of PV VP4His (Figure 5.2). This could be due to glutaraldehyde being a more effective crosslinker than DSP.

In the absence of treatment with DSP, VP4His hexamers were also observed on SDS-PAGE (Figure 5.3B). One possible explanation for this observation is that the VP4His hexamer was the more readily formed multimeric species of VP4His and other intermediate multimers were only observed when VP4His was multimerised using chemical crosslinkers. This was not an unprecedented finding as p7 of HCV also formed higher order structures in the absence of lipid or crosslinkers when electrophoresed on SDS-PAGE (PhD thesis, Toshana Foster, University of Leeds, 2010). It was therefore possible that SDS offered a micellar environment for the multimerisation of VP4His. This was supported by the detection of VP4His hexamers both in the presence and absence of liposomes and DSP, and when analysed by SDS-PAGE and western blot (Figure 5.3B). Further, SDS-resistant multimers have been reported in the past for other viral membrane proteins including those of E5 of HPV (PhD thesis, Laura Wetherill, University of Leeds, 2012), p7 of HCV (Clarke *et al.*, 2006) and other membrane pore forming proteins such as 2B of poliovirus (Agirre *et al.*, 2002) and M glycoprotein of avian coronavirus (Weisz *et al.*, 1993). Until the last decade models for picornavirus entry followed a 'fivefold' model (section 1.6.4.3) where it was tempting to speculate that five copies of VP4 and VP1 N-terminus would exit at the fivefold axis and insert into the membrane to form a pore for the egress of RNA. However, evidence for VP4His multimers comprised of up to six copies of VP4His upon crosslinking with DSP (Figure 5.3B) was not consistent with the 'fivefold' model. However, recent studies have suggested the capsid twofold symmetry axis faced the membrane and RNA was likely to be released from the capsid near the two fold axis (Bostina *et*

*al.*, 2011; Levy *et al.*, 2010). Therefore, it could be envisaged that six copies of VP4 formed the membrane pore for the egress of RNA from the viral capsid through its membrane facing twofold axis.

Despite the key roles played by membrane proteins in pathological and physiological processes, the forces that determine their structure and dynamics in the lipid bilayer are poorly understood. Detergent micelles are used as membrane-like environments to produce homogenous, stable and structurally relevant samples of membrane bound peptides and proteins (Baleja, 2001; Fernandez and Wuthrich, 2003). In this study, different classes of detergents were tested as shown in Table 5.1. Size exclusion elution profile showed successful incorporation of VP4 in DPC and LMPG micelles (Figure 5.5) and VP4ThGST in DPC micelles (Figure 5.7). Size exclusion chromatography cannot be used to determine the number of copies of VP4 or VP4ThGST present in detergent micelles. This is because protein-detergent complex shows anomalous behaviour when subjected to size exclusion chromatography, thereby presenting a challenge in the determination of molar mass and oligomeric state of the protein. Other techniques such as multiple angle light scattering (MALS) are available for determining the number of copies of VP4 contained in micelles. Unfortunately, the detergents successfully used for VP4 reconstitution, were not compatible with MALS. However, successful reconstitution of VP4 and VP4ThGST in detergent micelles enabled further studies to understand the structure of the VP4 membrane pore complex.

Oligomeric ring-like structures formed by VP4ThGST reconstituted in DPC micelles were clearly visualised by negative stain TEM (Figures 5.8D and 5.9). The negative staining process may have caused particle distortion, possible chemical interactions and given rise to artefacts. Therefore, immunogold labelling should be carried out in the future to confirm the number of VP4 molecules forming the multimeric complex. Further, 2D crystallography can be carried out to potentially yield a high resolution structure of the VP4-membrane pore complex.

Previously, GST-tagged VP4 was shown to induce membrane permeability whereas GST-tag was shown not to associate with or induce membrane permeability in liposomes (Davis *et al.*, 2008). Due to this prior knowledge, we considered it not critical to test GST incorporation and oligomerisation in DPC micelles by EM.

The secondary structure of RNA may influence the directional exit of the viral RNA from the capsid. The 3' end of viral RNA has less secondary structure compared to the 5' end. RNA exit studies from HRV2 suggested RNA partially released from the capsid lacked secondary structure but completely released RNA had some secondary structure similar to the clover leaf

structure of the IRES present at the 5' end of RNA (Kienberger *et al.*, 2004). A recent study showed that RNA egress of HRV2 began with its 3' end (Harutyunyan *et al.*, 2013).

The release of dextrans contained within liposomes to investigate the nature of membrane permeability is a well established approach and has been used in several studies to determine membrane-pore size formed by adenovirus, HRV2, HRV2 VP1 and  $\mu$ 1 of reovirus (Brabec *et al.*, 2005; Prchla *et al.*, 1995; Zhang *et al.*, 2009). Co-internalisation of HRV2 with FD10 and FD70 resulted in virus mediated endosomal release of FD10 but not of FD70 (Brabec *et al.*, 2005). The diameter of RNA is 1-1.5 nm (Kienberger *et al.*, 2004). The inferred lumen diameter from the FD release studies was between 4.6 nm and 12 nm (section 5.3) and the oligomeric ring-like structures visualised by TEM revealed a pore diameter of approximately 5 nm (Figures 5.8D and 5.9A). Both these findings are in agreement with the pore dimensions required for the release of RNA that has lost some of its secondary structure. There are limitations to the use of dextrans in determining the size cut-off of membrane pores. Dextrans are linear, flexible, long chain glucose polysaccharides and of limited use as they are different to RNA with secondary structure. It would be possible to refine the assay by using globular protein molecules or single stranded nucleic acids of a range of lengths and extents of secondary structure mimicking the exiting viral RNA. The use of such molecular size probes would complement the experimental results obtained with FDs of different sizes and begin to answer the question of effect of RNA secondary structure on genome delivery.

## **Chapter 6**

# **Structural analysis of VP4: Bioinformatics predictions and characterisation using biophysical techniques**



## 6.1 Introduction

Picornaviruses undergo structural changes upon receiving the appropriate trigger such as receptor binding and/or exposure to low pH. These structural changes include the externalisation of the N-terminus of VP1 and the release of VP4. Capsid alterations are required for the release of RNA from an enclosed vesicle such as the early endosome, into the cytoplasm for replication. Although much information has been gathered about the structural changes in the capsid, little is known regarding the mechanism of transfer of RNA across the membrane. VP1 and VP4 have been implicated in the cell entry process (section 1.6.4.4). The structure of free VP4 upon release from the virus particle or upon membrane insertion is entirely unknown. Despite this lack of structural information, there is sufficient evidence including VP4-mediated membrane permeabilisation (section 4.2.1) and formation of a size-selective pore (sections 5.2, 5.3 and 5.4), to predict VP4 to be a membrane binding protein.

### Structure of VP4

Determining the alterations in VP4 conformation upon externalisation from the virus particle and membrane interaction is crucial for a better understanding of the picornavirus cell entry process.

VP4 is not in a membrane when part of the virus particle. Due to the separate functions of VP4 when part of the virus (section 1.3.1.1) and when released from the virus (section 1.6.4.4.), VP4 structure is likely to be different in order to contribute effectively to the two separate roles of VP4 in virus stability and cell entry, respectively. When VP4 is present as part of the capsid, it is likely to be structurally constrained due to its interactions with other proteins whereas similar constraints would not be present when VP4 is released from the capsid and inserted into the endosomal membrane.

In the context of virus structures determined by X-ray crystallography, in some picornaviruses such as PV3 (Filman *et al.*, 1989), HRV2 (Verdaguer *et al.*, 2000) and HRV16 (Hadfield *et al.*, 1997), a small portion of the N-terminus of VP4 was observed to have an anti-parallel beta strand structure. Whereas VP4 N-terminus was observed to be disordered in other picornavirus structures such as HRV14 (Arnold and Rossmann, 1990) and HRV3 (Zhao *et al.*, 1996). Overall, picornavirus VP4 has little regular structure. However, the conformation that VP4 adopts after release from the capsid and upon binding to the endosomal membrane and the structure of the VP4 membrane pore complex are not known. Therefore, in the absence of any structural information, bioinformatics tools were employed in attempts to predict VP4 protein properties and structure.

**Bioinformatics predictions of VP4**

Structure prediction programmes are used for determining sequence similarities, predicting accessibility of protein residues to solvents, protein secondary structure, transmembrane domains and domains likely to have signal peptides. Protein structures cannot be determined solely based on computational predictions, however, they can provide a useful starting point for protein characterisation and complementary information about protein structure and function.

Computational predictions have their limitations as they predict models based on proteins with similar sequences of known structures in the existing database (Zhang, 2008). As a general limitation, bioinformatics predictions use a reference database which is mainly comprised of soluble globular proteins. The prediction tools have to include a model of the protein environment. A homogeneous and isotropic environment is simpler and therefore, an aqueous environment is used to model the protein environment. Features of a lipid bilayer including the parallel orientation of lipid chains to maximise their interactions, are likely to enforce constraints on the protein arrangement in the bilayer. Therefore, an aqueous environment is a potential problem when predicting structures of insoluble membrane proteins (Chen and Rost, 2002; Wallace *et al.*, 2003). VP4 structure is likely to be different in an aqueous versus lipid or lipid mimetic environment. Therefore, bioinformatics predictions for VP4 structure must be used with caution.

**Circular dichroism spectroscopy to determine protein secondary structure**

Circular dichroism (CD) spectroscopy is a valuable and well established technique for the determination of protein secondary structure. CD spectroscopy measures the difference in the absorption of left and right handed circularly polarised light. The peptide bond is the main chromophore in the far UV spectral region (190-260 nm). A signal is detected when the protein is folded in the provided environment. The characteristic shape and magnitude of the CD spectrum generated provides information on protein secondary structure as alpha helical, beta sheet or random coil (Kelly and Price, 2000; Wallace *et al.*, 2003).

Similar to the problems with bioinformatics predictions, the CD spectra generated depends on spectral reference datasets of proteins with known structures. This data set is mainly comprised of globular soluble proteins and works well for soluble proteins. In order to determine the secondary structure of a membrane protein, it has to be provided with the right environment for it to be properly folded. This membranous environment is provided by lipid or detergent micelles. The difference between a good correlation between calculated structures for soluble proteins and CD data for soluble proteins and not for membrane proteins may be due to the difference in dielectric constants of the membrane-like environment relative to that

of water surrounding soluble proteins (Evans *et al.*, 2007; Wallace *et al.*, 2003). Therefore, CD spectra of membrane proteins should be interpreted with caution.

Horse myoglobin (Mb) is a soluble protein and mechanosensitive channel (MscL) from *Mycobacteria tuberculosis* is a membrane protein. Both proteins have known predominant alpha helical content. Comparison of CD spectra for Mb in deionised water and MscL in detergent (n-Dodecyl- $\beta$ -D-maltoside) micelles, showed that although the magnitude of the peaks differed between soluble and membrane proteins, both types of proteins generated far UV spectra with similar shaped curves. Both proteins gave negative peaks at 222 nm and 208 nm and positive peaks at 192 nm, consistent with the presence of alpha helices (Figure 6.1) (Wallace *et al.*, 2003).

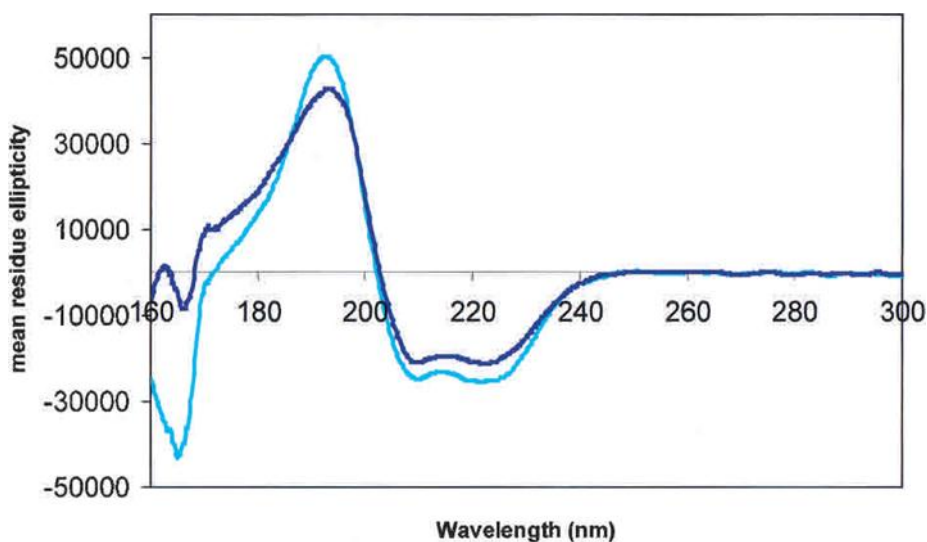


**Figure 6.1 Far UV CD spectra of soluble and membrane proteins.**

Horse myoglobin, Mb (light blue) and mechanosensitive channel, MscL (dark blue) are soluble and membrane proteins respectively. CD spectra indicating both have high alpha helical content with similar shaped curves. Figure adapted from (Wallace *et al.*, 2003).

CD spectra have been used to determine the secondary structure of non-enveloped virus proteins with membrane binding properties. Examples include  $\gamma_1$  peptide of flock house virus and p14 of reovirus.  $\gamma_1$  peptide of the non-enveloped flock house virus contains the N-terminal 21 residues of the  $\gamma$  peptide.  $\gamma_1$  peptide has membrane binding properties and has been implicated to play a role in the process of viral RNA transfer across the endosomal membrane. CD spectroscopy showed that  $\gamma_1$  adopted a predominantly alpha helical conformation in hydrophobic environments of SDS or liposomes but had random coil when in water (Bong *et al.*, 2000; Maia *et al.*, 2006). Another example is that of the N-terminus of p14 fusion-associated small transmembrane (FAST) protein of reptilian reovirus. p14 is known to facilitate cell to cell fusion aiding syncytia formation to increase virus spread. Analysis of the CD spectra

suggested the structural plasticity of the N-terminus of p14 as it was capable of adopting alpha helical or beta turns in a hydrophobic environment but was disordered when in an aqueous solution (Corcoran *et al.*, 2004).

Although CD spectroscopy gives reliable information on the overall alpha or beta secondary structure content, it does not indicate which regions of the protein are of which structural type (Greenfield, 2006; Kelly and Price, 2000). Therefore, techniques such as X-ray crystallography or nuclear magnetic resonance spectroscopy are required to obtain high resolution structures that provide residue specific information.

### **Nuclear magnetic resonance spectroscopy to determine protein structure**

Nuclear magnetic resonance (NMR) is a powerful and versatile biophysical technique used to determine atomic resolution structures and conformational dynamics of proteins and their complexes. NMR has the advantage of measurements being made under potentially physiological conditions. Therefore, NMR is a highly suitable technique for studying the structure of VP4 in a membrane-like environment.

NMR has been used to determine the structure of a number of viral membrane proteins. These include M2 of influenza A virus (Schnell and Chou, 2008), viral protein R (Vpr) of HIV-1 (Morellet *et al.*, 2003) and p7 of Hepatitis C virus (HCV) (Montserret *et al.*, 2010). These proteins are known to multimerise in membranes to form channels or pores that facilitate the transfer of ions, viral genome or subviral particles, across the membrane. All of these viral membrane proteins are small, consisting of approximately 100 residues and contain at least one transmembrane domain. Some of these features are shared by VP4.

A major factor limiting the determination of protein structure by NMR is the tumbling rate of the protein. An increase in molecular weight causes slower tumbling of the molecule in solution which decreases the efficiency of magnetisation transfer through bonds. Reconstitution of proteins in lipid or detergent micelles inevitably increases the size of the complex but one of the challenges is to reconstitute the protein in an appropriate lipid-like environment that will not lead to slow tumbling in solution. Therefore, the size limit of molecules that can be used for structural determination by solution NMR is ~35 kDa (Iwai and Zuger, 2007). In order to study membrane protein structure by NMR spectroscopy, membrane proteins are required to be reconstituted in a suitable lipidic or lipid-mimetic environment. Membrane proteins are found in a complex lipid bilayer (section 5.4) and a suitable substitute such as detergent micelles have to be employed for structural determination of membrane proteins using NMR. Liposomes are avoided as their use results in a drastic increase in size and hence slow tumbling. The membrane mimetic environments most commonly used for solution

NMR include micelles of SDS, DPC or DHPC; bicelles and small unilamellar vesicles (Wang, 2008) and <http://www.drorlist.com/nmr/MPNMR.html>

In an ideal scenario, reconstituted protein would be expected to adopt its native, biologically active conformation. This can be challenging as the protein is only reconstituted and correctly folded in a select few detergents at a given pH and temperature. Therefore, finding the right detergent or lipid environment requires the screening of several reconstitution conditions which is time consuming. VP4 was successfully reconstituted in DPC, LMPG and SDS detergent micelles (described in section 5.4).

## 6.2 Prediction of VP4 structure and topology

Due to the lack of available information on VP4 when it is released from the capsid or when it is inserted into membranes, bioinformatics predictions were used to predict folding and structure of VP4.

Many membrane proteins have a high alpha helical content and contain both hydrophobic and hydrophilic regions, known as amphipathic helices. Amphipathic helices are often associated with proteins that interact with membranes and form pores, such that the hydrophobic side interacts with the membrane lipid and the hydrophilic side points towards the pore lumen.

A helical wheel projection allows the visualisation of the helix showing hydrophobic residues on one side of the helical wheel and hydrophilic residues on the other side. Melittin is a well-characterised pore-forming peptide (sections 4.1 and 5.3) and its helical projection is shown in Figure 6.2A. The thickness of a cellular lipid bilayer is about 30 Å, which would take a helix comprised of ~20 amino acids to span. Therefore, helical wheel projection analysis of VP4 was carried out using a length of approximately 20 amino acids starting from the N-terminus of VP4. The helical wheel projection of the model membrane pore-forming peptide, melittin, showed that hydrophilic residues were concentrated on one side of the helical wheel, while hydrophobic residues showed a higher frequency on the other side of the helical wheel projection (Figure 6.2A). In contrast, a sliding window analysis along the residues of VP4 did not show such a clear difference in the distribution of hydrophilic and hydrophobic residues and some of the examples of this analysis are shown in Figure 6.2B-D.

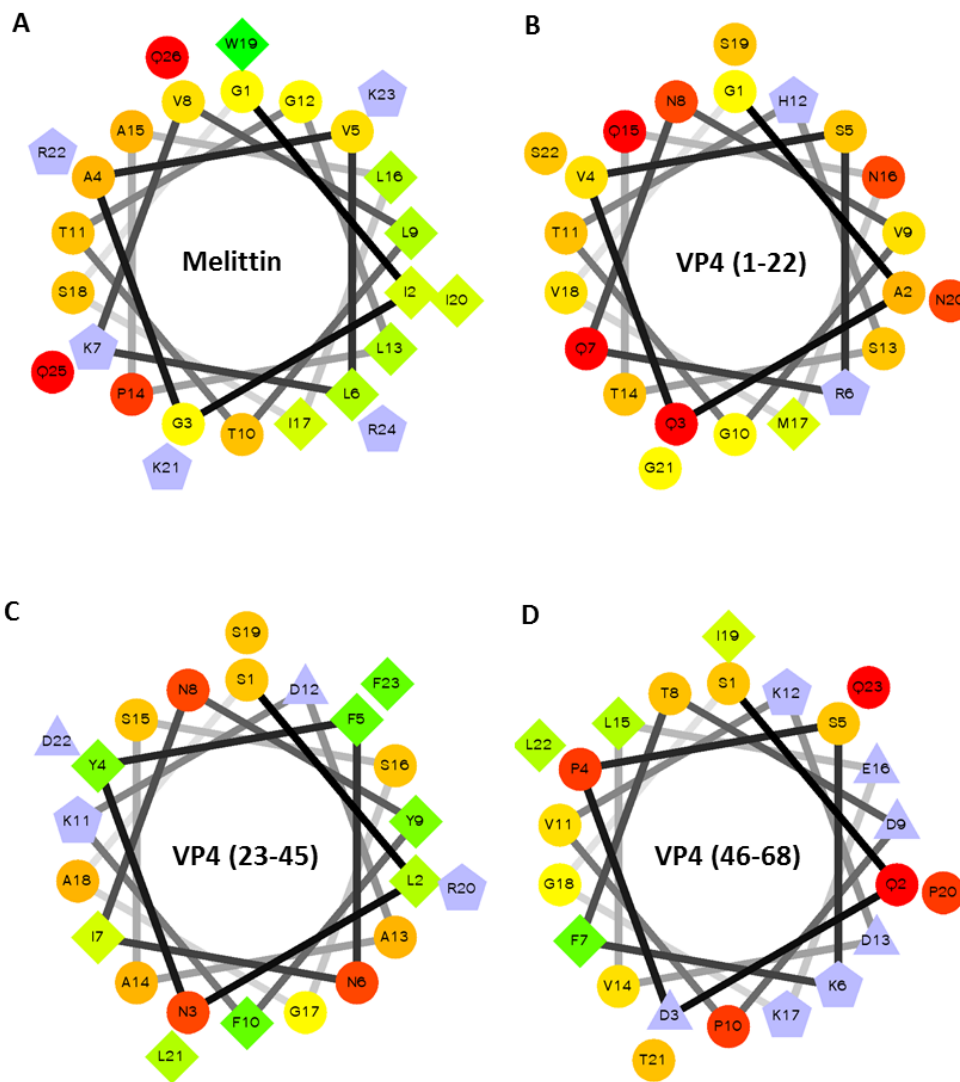


**Figure 6.2 Helical wheel projection for viral membrane proteins.**

**A.** Helical wheel projection for melittin. **B.** Helical wheel projections for VP4 residues 1-22. **C.** Helical wheel projections for VP4 residues 23-45. **D.** Helical wheel projections for VP4 residues 46-68. Helical wheel projections were generated by submitting amino acid sequences into the helical wheel projection program <http://rzlab.ucr.edu/scripts/wheel/wheel.cgi>. The most hydrophobic residues are shown in green, with least hydrophobic residues in yellow. Hydrophilic residues are shown in red. The amount of red decreases proportionally with hydrophilicity. Potentially charged residues are shown in purple.

VP4 was also analysed using hydrophobicity plots, transmembrane (TM) tendency, alpha helical and beta sheet predictions (<http://web.expasy.org/protscale>). This analysis predicted VP4 to contain alpha helical and beta sheet structure with no clear indication of the location of the TM domain (Figure 6.3A). In contrast, using the same bioinformatics prediction tools, the HCV p7 was predicted to contain two TM domains (Figure 6.3B), consistent with its NMR structure (Montserret *et al.*, 2010). Therefore, relative to p7, the predictions for VP4 were not clear.

The protein topology predictor SPLIT 4.0 is used to predict sequence location of beta structures and amphipathic helical content in the protein sequence through an automatic selection of optimal amino acid residues (<http://split4.pmfst.hr>). VP4 structural prediction using SPLIT 4.0 indicated some beta structure throughout the VP4 sequence. VP4 showed a TM helix preference between residues 1-10, 20-30 and 64-69 (Figure 6.4).

The amphipathic helical content of VP4 was also predicted using HeliQuest programme. Based on the primary amino acid sequence of the protein, HeliQuest programme computes physicochemical properties of the protein. The results are then used to screen the databank to identify protein segments with similar properties (Gautier *et al.*, 2008). When a sliding window analysis of VP4 was carried out using HeliQuest, hydrophobic regions were predicted throughout VP4. However, preference for amphipathic regions were not identified (<http://heliquet.ipmc.cnrs.fr/cgi-bin/ComputParamsV2.py>).

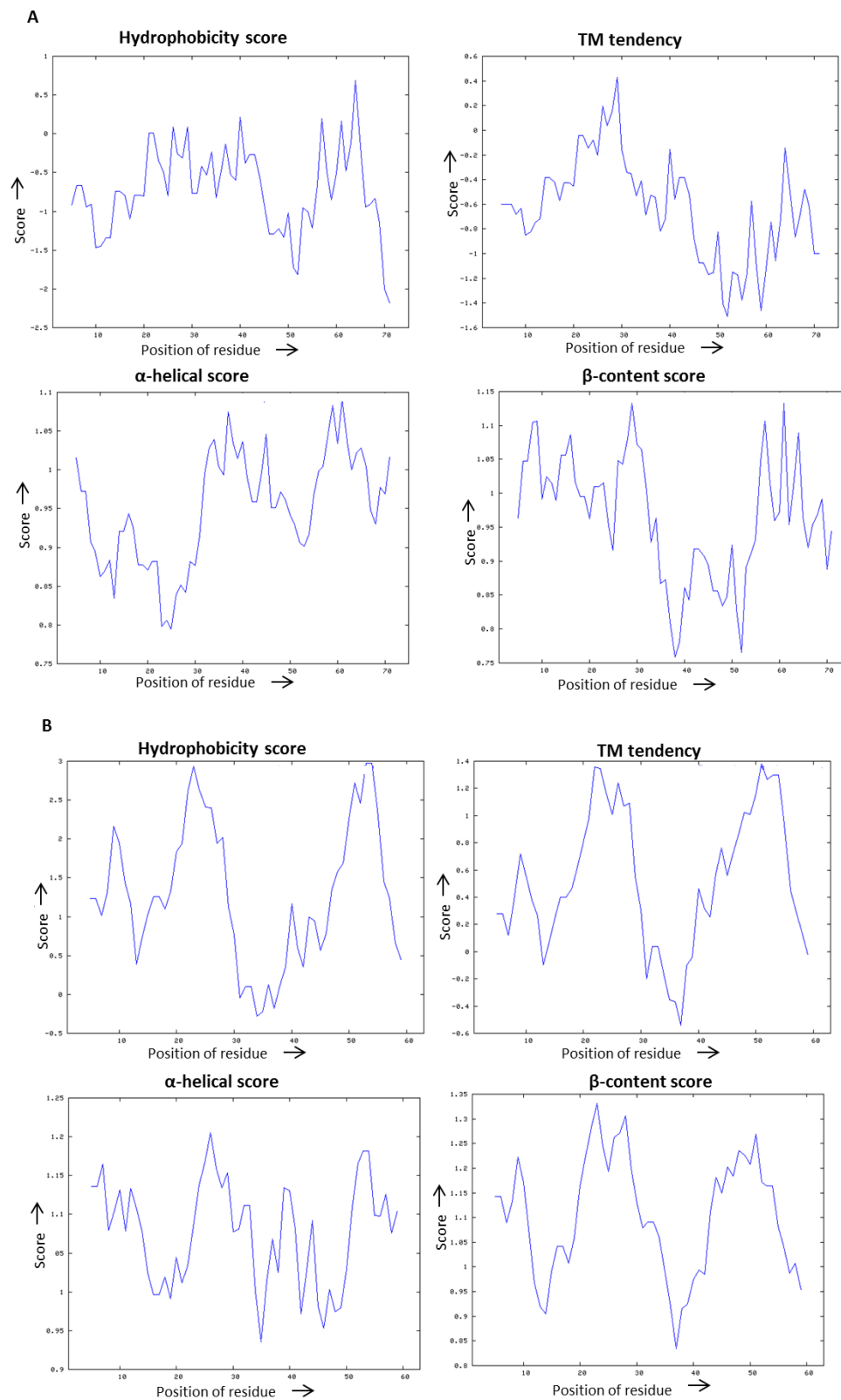


**Figure 6.3 Bioinformatics predictions for VP4 and p7.**

Hydrophobicity score, transmembrane tendency,  $\alpha$ -helical content and  $\beta$ -content for **A.** HRV16 VP4. **B.** HCV p7. Plots were generated by submitting amino acid sequences into the prediction programme <http://web.expasy.org/protscale>.



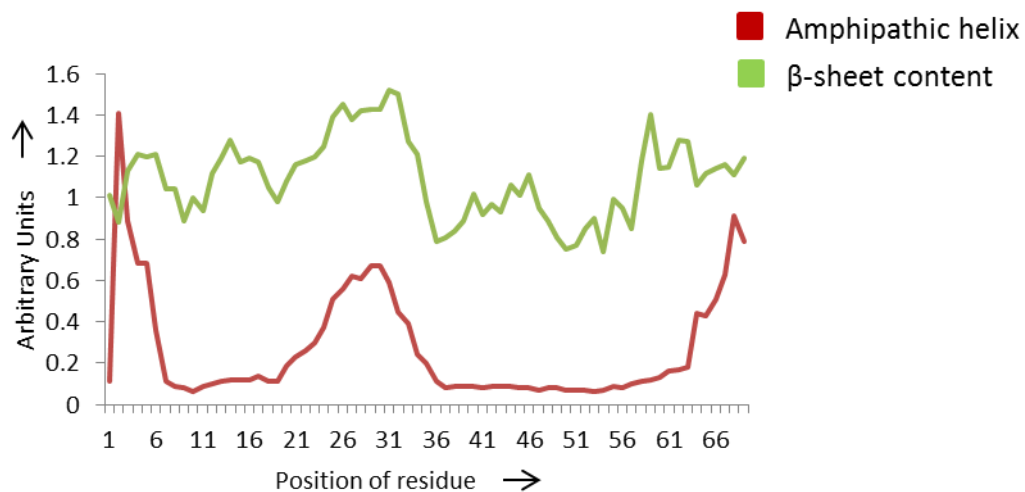


**Figure 6.4 Prediction of VP4 amphipathic helical and β-sheet content.**

Amphipathic helix and β-sheet content of VP4 was predicted by submitting the VP4 amino acid sequence into the prediction programme <http://split4.pmfst.hr>.

Protein TM prediction based on primary amino acid sequence can be carried out using bioinformatics programmes such as membrane protein structure and topology (MEMSAT3) and support vector machine (MEMSAT-SVM) based predictions. MEMSAT3 predicts secondary structure and topology of helical integral membrane proteins. It uses a neural network that has been trained on a set of 184 TM proteins to determine which residues constitute the TM helices and which residues are on the cytoplasmic side (Jones, 2007). MEMSAT-SVM prediction is based on a set of protein sequences with known X-ray crystal structures. It is used for the prediction of signal peptides and alpha helices (Nugent and Jones, 2009). MEMSAT3 predicted the location of a TM domain in the N-terminus whereas MEMSAT-SVM predicted it to be in the C-terminus of VP4 (Figure 6.5).

Taken together, bioinformatics predictions did not clearly illustrate the location of amphipathic helices and TM domain(s) in VP4.

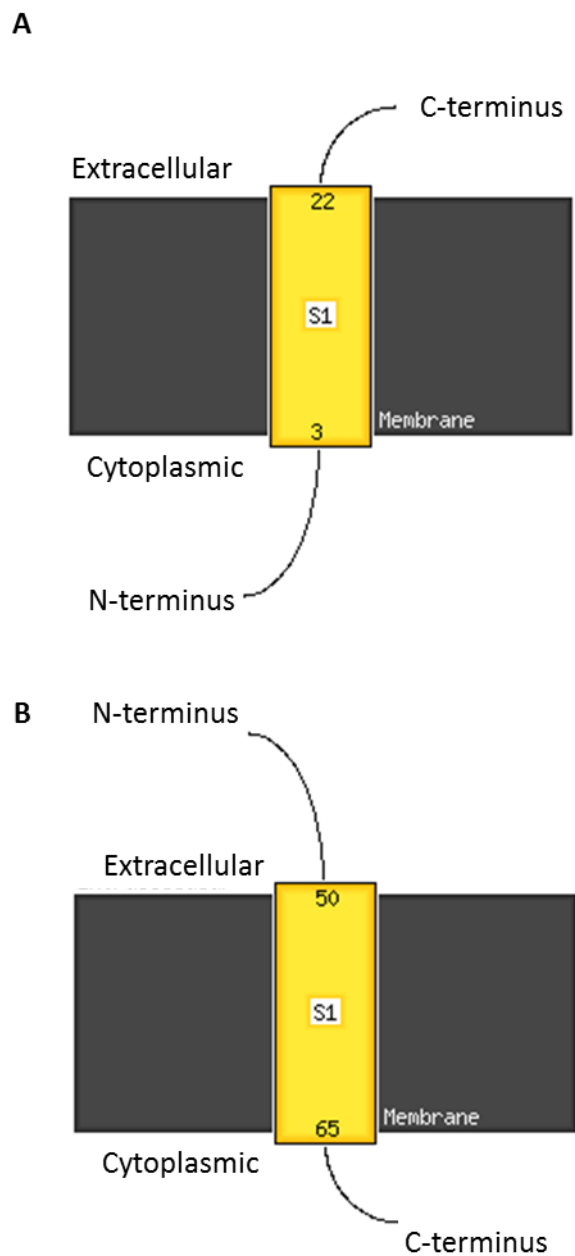


**Figure 6.5 Location of TM domain in VP4.**

**A.** VP4 N-terminus (residues 3-22) predicted to constitute the TM domain by MEMSAT3. **B.** VP4 C-terminus (residues 50-65) predicted to constitute the TM domain by MEMSAT-SVM. Predictions were generated by submitting VP4 amino acid sequence into the prediction programme <http://bioinf.cs.ucl.ac.uk/psipred>.

### 6.3 Circular dichroism spectroscopy to investigate VP4 secondary structure

VP4 has been demonstrated to associate with and permeabilise membranes (section 1.6.4.4 and 4.2.1). VP4 is likely to undergo structural changes upon membrane insertion and adopt a conformation distinct from that when it is a viral capsid protein. Membrane insertion of VP4 may lead to a final protein conformation facilitating membrane pore-formation required for the transfer of RNA across the membrane.

Recombinant untagged VP4 was expressed and purified from inclusion bodies (section 3.4), followed by reconstitution in a membrane-mimetic environment. A range of detergents were screened for VP4 reconstitution (Table 5.1) and VP4 (1 mg) was successfully reconstituted in LMPG and SDS, as demonstrated by size exclusion chromatography (section 5.4).

CD spectroscopy is a technique used to determine protein secondary structure (section 6.1). VP4 reconstituted in detergent (SDS or LMPG) micelles was subjected to CD to investigate VP4 structure in a membrane-mimetic environment (section 2.18). Pilot studies were carried out to determine VP4 concentration, buffer and salt conditions for obtaining optimal CD spectra. Liposomes (section 2.22) were not used as they were too large to be subjected to size exclusion chromatography which was used to demonstrate VP4 reconstitution. A further problem was introduced as liposomes were prepared in 10 mM HEPES buffer (section 2.22) which was suboptimal for use in CD as HEPES absorbs wavelengths in the far UV range (190-260 nm). Liposomes can also cause scattering of light, resulting in signal loss. Therefore, detergent micelles were used to provide a membrane-like environment.

In the absence of a lipid-mimetic environment VP4 did not yield a CD spectrum, most likely due to precipitation of VP4. In contrast, VP4 reconstituted in LMPG micelles exhibited a CD spectrum typical of  $\alpha$ -helical conformation with a maximum at 192 nm and two minima at 208 nm and 222 nm (Figure 6.6A). VP4 was used at 17.5  $\mu$ M or 9  $\mu$ M in 12.5 mM LMPG. At these two concentrations, the maxima and minima of the magnitude spectra showed subtle differences but the overall shape was typical of  $\alpha$ -helix conformation (Figure 6.6A). A similar spectrum was obtained with VP4 (12.5  $\mu$ M) reconstituted in SDS (8 mM) micelles with a maximum at 192 nm and two minima at 208 nm and 215 nm (Figure 6.6B). CDSSTR algorithm (section 2.18) was used to estimate protein secondary structure of VP4 reconstituted in LMPG or SDS. This showed VP4 reconstituted in LMPG had 45% alpha helical content and 12% beta strand content. VP4 in reconstituted SDS showed 37% alpha helical content and 17% beta strand content. Therefore, VP4 reconstituted in a membrane-like environment had a

predominantly alpha helical content. The estimation of protein secondary structure was kindly carried out by Franz Hagn (Harvard Medical School).

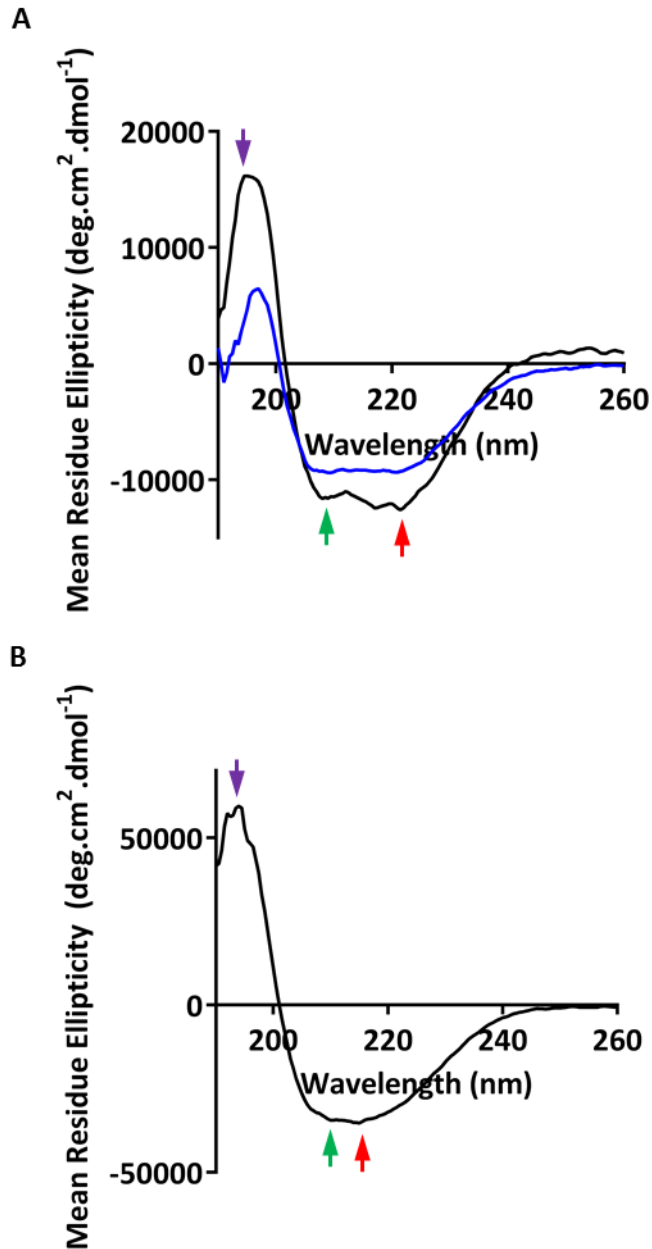


**Figure 6.6 Far UV CD analysis of VP4 reconstituted in detergent micelles.**

Far UV CD spectra of VP4 reconstituted in detergent micelles and recorded in the 190-260 nm wavelength range at 25°C. CD spectra demonstrating secondary structure of **A.** VP4 reconstituted in LMPG. CD spectra obtained with 17.5  $\mu\text{M}$  VP4 in 12.5 mM LMPG shown in blue and 9  $\mu\text{M}$  VP4 in 12.5 mM LMPG shown in black. Both spectra showed minima at 208 nm (green arrow) and 222 nm (red arrow) and a peak at 192 nm (purple arrow). **B.** VP4 reconstituted in SDS (12.5  $\mu\text{M}$  VP4 in 8mM SDS). Spectrum showed minima at 208 nm (green arrow) and 215 nm (red arrow) and a peak at 192 nm (purple arrow).

## 6.4 NMR to investigate VP4 membrane pore complex structure

Recombinant VP4 was shown to multimerise in a hydrophobic environment to form a multimeric size-selective pore which was visualised by TEM (section 5.4). A step forward from the visualisation of the VP4 oligomeric ring-like structure by TEM, would be the determination of the atomic structure of the VP4 membrane pore complex. NMR spectroscopy, has been used to determine the structure of several viral membrane proteins that share characteristics with VP4 (section 6.1), therefore, this technique was used to investigate and determine the structure of the VP4 membrane pore complex.

Solution NMR methods are suitable for the investigation of the structure of proteins and their complexes in solution, with some limitations. Membrane proteins embedded in a lipid bilayer are not amenable to structural determinations using solution NMR mainly due to slow tumbling rates of protein-lipid complexes. Slow tumbling leads to broad NMR signals, which lowers spectral resolution and dramatically reduces the signal to noise ratio. However, solution NMR can be used to investigate the structure of membrane proteins that have been extracted from their host membrane and reconstituted in other membrane-like environments. Detergent micelles do not truly represent the complex lipid environment that membrane proteins are naturally found in. However, detergent micelles tumble quickly and provide well resolved NMR spectra. Detergent micelles serve as lipid mimetic reagents and can be appropriate substitutes of the lipid bilayer. For a number of membrane binding peptides, evidence for the use of detergents as suitable substitutes for membrane bilayers was provided by the observation that a number of them adopted similar NMR structures when reconstituted in lipid bilayers (anionic phosphatidylglycerols) or in detergent micelles (SDS micelles) (Li *et al.*, 2006; Wang *et al.*, 2003). The solution NMR structure of influenza haemagglutinin also showed similar structures in lipid bilayers (POPC) and detergent micelles (DPC) (Han *et al.*, 2001). Therefore, there was existing evidence to show that detergent micelles could be used to mimic membrane environments. Hence,  $^{15}\text{N}$ -VP4 (section 3.4.3) was reconstituted in detergent micelles and used towards determining the structure of the VP4 membrane pore complex.

In addition to screening of detergents for the reconstitution of VP4 (section 5.4), bicelles were tested. Bicelles are a mix of long and short chain lipids. The long chain phospholipid forms the central bilayer while the short chain phospholipid shields the bilayer from the surrounding aqueous medium. Long chain:short chain ratio ( $q$ ) is used to control the size of bicelles (Whiles *et al.*, 2002). This ratio is crucial as high values of  $q$  give rise to slow tumbling. At low values of  $q$ , bicelles tumble quickly, thereby giving well resolved NMR spectra. Bicelles with  $q \leq 0.5$  are generally amenable to solution NMR. However, the 1,2-Dimyristoyl-sn-Glycero-3-Phosphocholine:1,2-Dihexanoyl-sn-Glycero-3-Phosphocholine (DMPC:DHPC) ratio

corresponding to the long chain:short chain phospholipids ratio which successfully reconstituted VP4 was high ( $q=1$ ) and expected to give slow tumbling. Therefore, VP4 reconstituted in bicelles was considered unsuitable for solution NMR.

Pilot studies aimed to find optimal reconstitution conditions were carried out using 0.1 mg of  $^{15}\text{N}$ -VP4. At a concentration of 0.042 mM,  $^{15}\text{N}$ -VP4 was successfully reconstituted in 100 mM DPC and LMPG (section 5.4). Typically, using current NMR instrumentation approximately 0.05 and 0.2 mM of protein is required for carrying out 1D and 2D heteronuclear single-quantum correlation (HSQC) NMR experiments, respectively. Upon increasing the concentration of  $^{15}\text{N}$ -VP4 to 0.42 mM, reconstituted in 100 mM SDS, LMPG or DPC,  $^{15}\text{N}$ -VP4 precipitated from DPC micelles but continued to be reconstituted in SDS and LMPG micelles (section 5.4).

1D NMR spectra of  $^{15}\text{N}$ -VP4 reconstituted in SDS or LMPG detergent micelles (in NaAc buffer, pH5.5) were collected to provide initial information on the folded state of the protein. This would serve to guide subsequent NMR structural determination studies. Thirty two scans were used to acquire 1D spectra of  $^{15}\text{N}$ -VP4 (~0.05 mM) in SDS or LMPG (100 mM) at 25°C at 600 MHz (section 2.17). The spectra of well folded proteins contain sharp and narrow peaks which are well dispersed, whereas spectra of unfolded proteins are broad and less well dispersed. The 1D spectra of reconstituted VP4 showed well dispersed narrow peaks and some regions with overlapping peaks. More information on the VP4 residues could be obtained by introducing an additional spectral dimension. Therefore, the next step was to obtain 2D HSQC NMR spectra on  $^{15}\text{N}$ -VP4. This experiment correlates the chemical shift of protons with the chemical shift of a directly bonded nitrogen atom, in proteins typically from peptide H-N bonds and  $\text{NH}_2$  side chain of glutamine and asparagine. The spectra acquired from this experiment would provide information on the conformation of the protein and help determine if the conditions used for VP4 reconstitution are amenable to 3D NMR structural determination studies. Each peak in the spectrum is derived from a proton attached to a nitrogen atom and can be mapped to a single amide bond in an amino acid (No peaks are observed for the first amino acid and proline residues due to the absence of a free amide group).

$^{15}\text{N}$ -VP4 (0.42 mM) reconstituted in SDS or LMPG were used for the 2D HSQC experiments. 300 scans were recorded at 700MHz, 25°C (section 2.17). VP4 is comprised of 68 residues, 3 of which are prolines, and the first residue of the protein is not detected, therefore 64 peaks would be expected to be detected. In the 2D HSQC spectra of VP4 in SDS, 61 residues (depicted as purple peaks, Figure 6.7) are clearly observed. Approximately 60 residues in the 2D HSQC spectra of VP4 in LMPG were observed, although with less sharp peaks (depicted as red peaks, Figure 6.7). The peak positions observed in the 2D HSQC spectra of VP4 reconstituted in LMPG or SDS could be used initially to assess the changes in protein folding

when reconstituted in different detergents. The peaks of VP4 when reconstituted in LMPG or SDS were well dispersed signifying protein folding. The peaks observed with VP4 reconstituted in LMPG were broader, less well resolved (red peaks, Figure 6.7) and had moved significantly when compared to the peaks obtained with VP4 reconstituted in SDS (purple peaks, Figure 6.7). Although the influence of different detergents on the spectral properties of a protein could be significant, this change in the spectra between VP4 reconstituted in LMPG or SDS could also indicate that VP4 adopted a different conformation or aggregation number in LMPG compared to SDS. There are NMR structures of membrane proteins solved in SDS micelles. However, SDS is usually known as a protein denaturant and therefore, VP4 may be more likely to adopt its native conformation when reconstituted in LMPG. 1D and 2D NMR spectra were acquired and Figure 6.7 kindly generated by Dr Fu and Dr Brüeschweiler (Chou lab, Harvard Medical School).

In summary, our preliminary studies showed a good spectrum allowing the observation of resolved peaks representing majority of the VP4 residues using 2D HSQC NMR. Based on 1D and 2D spectra we can say that VP4 reconstituted in LMPG or SDS is folded at least to some extent. Therefore, VP4 reconstitution conditions amenable to future 3D NMR studies of the VP4 membrane pore complex were successfully identified.

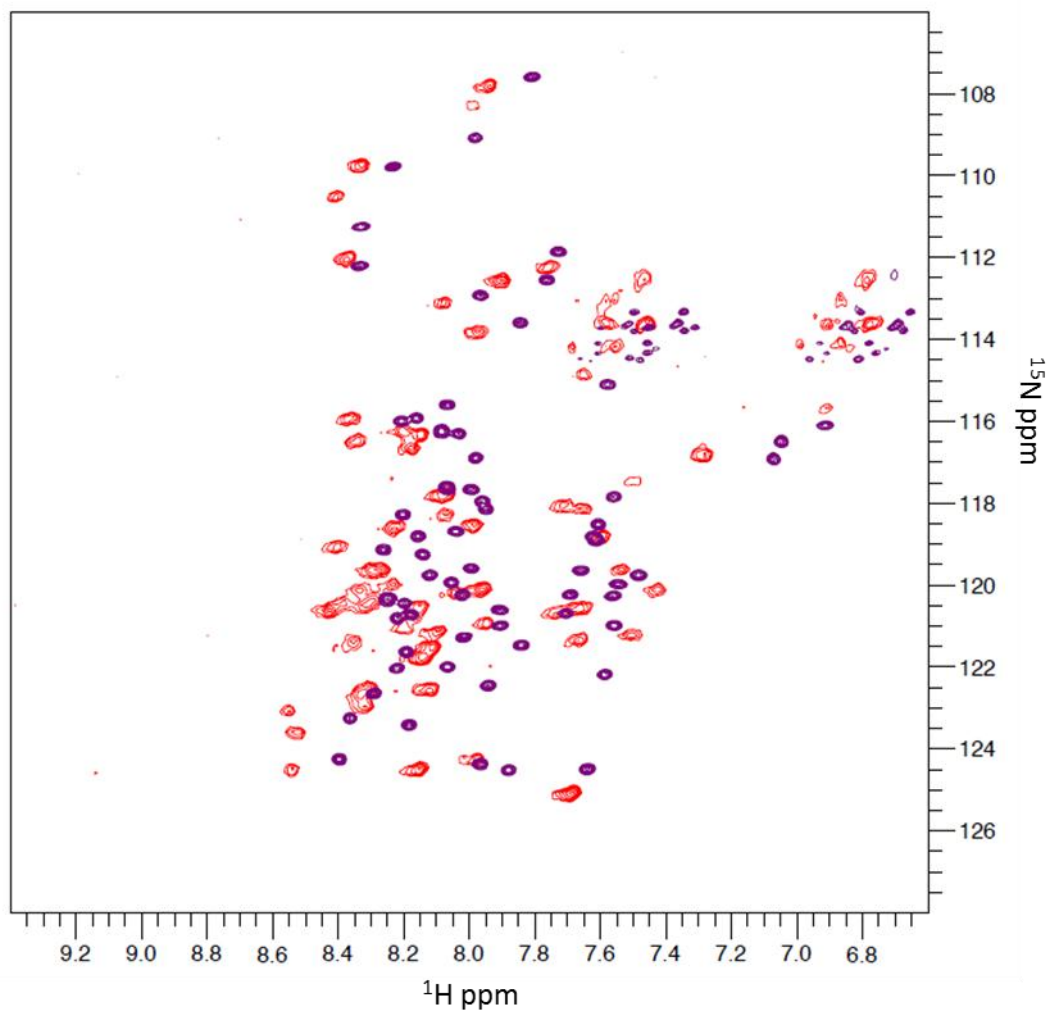


**Figure 6.7** Overlay of 2D HSQC spectra of  $^{15}\text{N}$ -VP4 reconstituted in LMPG or SDS micelles. Peaks representing VP4 residues for  $^{15}\text{N}$ -VP4 reconstituted in LMPG (red) or in SDS (purple). ppm: parts per million. Plot generated by Dr Brüeschweiler using NMR pipe and NMR draw.

## 6.5 Discussion and future work

VP4 is a membrane protein implicated in the cell entry process. VP4 is known to partition into liposome and cellular membranes and induce permeability. Existing evidence suggested VP4 contributed to the formation of channels in membranes which facilitated the delivery of viral RNA across the membrane (section 1.6.4.4). VP4His was shown to induce membrane permeability similar to those induced by the membrane pore-forming peptide, melittin (section 4.2.1). Recombinant VP4 was shown to multimerise to form a size-selective membrane pore which was visualised by TEM (sections 5.2, 5.3 and 5.4). However, the structure adopted by VP4 upon binding membranes was unknown. In this chapter, several bioinformatics predictions were used to provide information on VP4 properties and structure.



Circular dichroism and NMR spectroscopy were used to investigate the structure of VP4 in a membrane-like environment.

Overall, prediction models based on VP4 primary amino acid sequence did not give a clear prediction for where the TM domain may be present. This was in contrast to the clear prediction observed for other viral membrane proteins such as p7 (Figure 6.3B). Structural studies on VP4 reconstituted in detergent micelles demonstrated a predominantly alpha helical content by far UV CD spectroscopy (Figure 6.6) which was consistent with observations of secondary structure for a number of proteins with TM domains. The well resolved 2D HSQC spectra (Figure 6.7) demonstrated the suitability of reconstituted VP4 for future structure determination of the VP4 membrane pore complex by 3D NMR.

In the absence of existing structural information on VP4, bioinformatics predictions were used to gain information on protein properties and indications of protein structure. The helical wheel projection did not clearly show if VP4 was likely to contain an amphipathic helix because no preference was shown for hydrophobic residues being located on one side of the helical wheel (Figure 6.2). Additional bioinformatics predictions indicated alpha helical and beta sheet content of VP4 but did not suggest clear and distinct regions that were likely to form the VP4 TM domain (Figure 6.3A). In addition to the above bioinformatics prediction tools, SPLIT 4.0 and Heliquist were used. The SPLIT server showed only a slight preference of the N-terminal region for containing an amphipathic helix (Figure 6.4). While SPLIT 4.0 is indeed a dedicated tool for predicting sequence segments likely to interact with membrane, like other existing bioinformatics predictions, it does not take into account the attachment of a fatty acid such as myristic acid, to the peptide sequence. VP4 is N-terminally myristoylated and attachment of fatty acids such as myristic acid can influence protein affinity for membranes (section 4.1). Thus, the presence of the myristic acid at the N-terminus of VP4 is likely to increase the membrane affinity of the indicated N-terminal amphipathic helix in Figure 6.4. The structural predictions using VP4 primary sequence by SPLIT 4.0, heliquist and <http://web.expasy.org/protscale>, indicated a large alpha helical content (Figures 6.3A and 6.4). However, the regions with alpha helical content as predicted by different bioinformatics prediction tools showed slight variation. This was likely due to the differences in reference datasets and algorithms used in the different prediction programmes. The predominantly alpha helical content of VP4 was in agreement with protein secondary structure predictions for TM proteins. Although, the secondary structure predictions were carried out without considering the effect of the environment on protein structure, the predominantly alpha helical content prediction was in agreement with the observed CD spectra of VP4 reconstituted in a membrane-mimetic environment of SDS or LMPG micelles (Figure 6.6).

Structures of membrane proteins are often determined by reconstitution in a membrane-like environment. Membrane proteins are known to behave differently in different detergents due to the inherent differences in protein stability and structure. The ideal detergent of choice for membrane protein reconstitution should be gentle to prevent protein denaturation, yet strong enough to prevent protein aggregation. A range of different detergents were screened for reconstitution of VP4 (Table 5.1). DPC, LMPG and SDS were the detergents in which VP4 did not precipitate and remained reconstituted as evidenced by size exclusion chromatography (section 5.4). A large proportion of VP4 precipitated upon increasing the concentration of VP4 in DPC micelles (figure 5.6). Therefore, preparations of VP4 incorporated in DPC micelles could not be used for obtaining 2D HSQC NMR spectra. Attempts at VP4 reconstitution at 100 mM in SDS or LMPG micelles were successful and well resolved 2D HSQC spectra acquired (Figure 6.7).

Analysis of far UV CD spectra showed that VP4 reconstituted in LMPG gave characteristic positive and negative peaks as expected of a protein with alpha helical secondary structure. Interestingly, VP4 reconstituted in SDS showed similar CD spectra (section 6.3). Although, clearly indicating that VP4 reconstituted in SDS contained alpha helical secondary structure, VP4 may be monomeric in SDS micelles as SDS is a strong anionic detergent and therefore, less likely to permit formation of VP4 multimers. However, it was also possible that SDS provided a micellar environment which permitted VP4 multimerisation and this would be in agreement with the VP4 hexamers observed in the absence of treatment with DSP and liposomes, when analysed by SDS-PAGE (Figure 5.3B).

To further investigate protein folding, the process towards determining solution NMR structure of the VP4 membrane pore complex was initiated. Although the spectrum of VP4 reconstituted in LMPG showed good dispersion, NMR signals on the spectrum of VP4 reconstituted in SDS showed sharper peaks. This could be indicative of differences in conformation adopted by or aggregation number of VP4 when reconstituted in SDS or LMPG (Krueger-Koplin *et al.*, 2004). LMPG is a milder detergent and less likely to cause protein denaturation compared to SDS. Peak overlap in 2D HSQC spectra is often observed in membrane proteins due to the hydrophobic residues contained within alpha helical regions (Reckel *et al.*, 2008). The observation of spectral overlap in the 2D HSQC spectra of VP4 reconstituted in LMPG (Figure 7.7) was encouraging as it indicated possible TM region(s) in VP4. LMPG has previously been used as a medium for the structural determination of membrane proteins such as T-cell receptor zeta chain (Duchardt *et al.*, 2007), human Potassium voltage-gated channel subfamily E member 1, KCNE1 (Kang *et al.*, 2008), *E. coli* histidine kinase receptors (Maslennikov *et al.*, 2010). Therefore, the knowledge of the above

structures determined in LMPG, in combination with the 2D HSQC NMR spectra acquired for VP4 reconstituted in LMPG (Figure 6.7), provides confidence that a structure of the VP4 membrane pore complex using 3D NMR is achievable with VP4 reconstituted in LMPG. VP4 is relatively well conserved among picornaviruses, is essential for viral infectivity and stability and, therefore, presents an excellent target for antiviral drugs. 3D structural determination of the biological process of VP4 multimerisation would aid the development of antivirals and small molecule inhibitors to block virus infection at the early stage of virus cell entry.

The X-ray crystal structure of HRV16 showed VP4 residues 1-7 and 23-44 form beta strands and the remaining residues are either disordered or not visible (Hadfield *et al.*, 1997). Bringing together the structural information of HRV16 VP4 when present in the virus and when reconstituted in membrane-like environments, it can be hypothesised that VP4 adopts an alpha helical structure upon inserting into the membrane, at the appropriate concentration when VP4 molecules are at the right proximity to each other, VP4 multimerises to form a pore, through which RNA is delivered across the membrane into the cytoplasm. This is supported by the observation that recombinant VP4 and VP4 released from the virus are insoluble in aqueous solution and require the presence of a membrane to be functional. Furthermore, VP4 multimeric pore was observed by TEM when in the presence of a membrane-like environment (section 5.4). In conclusion, there is a clear indication for the requirement of a membrane-like environment for VP4 to be functional.

The presence of myristic acid at the N-terminus of VP4 suggested that this end of the protein would be directly involved in membrane interactions. Studies with peptides corresponding to the N or C-terminal halves of VP4 (described in Chapter 7) showed that a much lower concentration of VP4 N-terminal peptide was required to induce membrane permeability, relative to VP4 C-terminal peptide, indicating that the N-terminus is perhaps more likely to contain a TM domain. However, bioinformatics predictions described in this chapter, suggested that N and/or C-termini could contain the TM domain, therefore, the possibility of both N and C-termini inducing membrane permeability cannot be ruled out.

# **Chapter 7**

## **Towards mapping the function of VP4 and the role of VP1 by use of synthetic peptides**

## 7.1 Introduction

### **Evidence for VP4 and N-terminus of VP1 in membrane interactions**

VP4 and the N-terminus of VP1 have been implicated in membrane interactions to facilitate the transfer of RNA across the membrane (described in section 1.6.4.4). Additional evidence supporting a role for VP4-mediated membrane permeability during viral entry has been demonstrated elsewhere in this thesis. For example VP4-induced membrane permeability (Chapter 4), VP4 multimerisation to form a size-selective pore (Chapter 5), reconstitution and structural studies on VP4 in a lipid-mimetic environment (Chapter 6).

Although VP4 has been shown to interact with membranes, there is little evidence regarding which region of VP4 is directly involved. During HRV capsid breathing, there is evidence that the N-terminus of VP4 is transiently externalised (Katpally *et al.*, 2009), suggesting that the N-terminus leaves the capsid and becomes available for membrane interactions before the remainder of the protein. In addition, the N-terminus of VP4 is myristoylated which is likely to be involved in targeting VP4 to membranes (section 4.1). Therefore, limited information available appears to favour the involvement of the VP4 N-terminus in membrane interactions.

### **Identification of the membrane active terminus**

In general, the N and/or C termini of proteins identified as being responsible for membrane binding and permeabilisation have hydrophobic domains able to form an amphipathic alpha helix, or may possess myristoylation or palmitoylation, or may be products of cleavage of a precursor protein and contain a motif of polybasic residues (Bordag and Keller, 2010). Some examples of such membrane binding proteins of non-enveloped viruses include the following: adenovirus protein VI (Maier and Wiethoff, 2010),  $\gamma$ 1 of flock house virus (Maia *et al.*, 2006),  $\mu$ 1 of reoviruses (Zhang *et al.*, 2006) (described in section 1.6.3). These properties of membrane binding proteins can be identified by bioinformatics prediction programs. Such predictions were used for VP4 and defined regions with high alpha helical content and domains likely to form transmembrane regions were not clearly identified (section 6.2). In contrast, for viral proteins such as p7 of HCV, defined common hydrophobic regions with alpha helical content were predicted which clearly correlated with regions predicted to contain TM domains (section 6.2) and which were confirmed by NMR (Montserret *et al.*, 2010).

This chapter investigates if one or both termini of VP4 are involved in mediating membrane permeability and if the N-terminus of VP1 may modulate VP4-induced membrane permeability.

## **7.2 VP4 N-terminus induces more extensive membrane permeability than VP4 C-terminus or VP1 N-terminus peptides**

The structure of VP4 in the presence of membranes is unknown and bioinformatics prediction tools did not clearly indicate regions containing potential TM domains (section 6.2), therefore, mapping of the function of VP4 was initiated with the synthesis of peptides corresponding to the N or C-terminal halves of VP4. Myristoylated VP4 N-terminus specific peptide will be referred to as VP4N (52mer) and VP4 C-terminus specific peptide as VP4C (51mer).

In addition to the release of VP4, the conformational changes in the capsid during transition from native to “A” particles includes the irreversible externalisation of the VP1 N-terminus, which has been shown to associate with membranes (section 1.6.4.4). In order to investigate the potential involvement of the VP1 N-terminus in modulating VP4-induced membrane permeability, a peptide corresponding to the N-terminus of VP1 was also synthesised. VP1 N-terminus peptide will be referred to as VP1N (30mer).

Six lysine residues were added to the C-terminus of each of the peptides to facilitate solubility. The addition of lysine residues is a standard approach for increasing peptide solubility (Kato *et al.*, 2007; Torres *et al.*, 2007; Yang *et al.*, 2004). The peptides were resuspended in aqueous solution and dissolved readily. Membrane permeability induced by VP4N, VP4C and VP1N was investigated using the membrane permeability assay (section 2.23).

VP4His and  $\Delta$ VP4His (2.5  $\mu$ M) were mixed with liposomes (50  $\mu$ M) and both forms of recombinant VP4-induced membrane permeability (Figure 7.1), consistent with previous findings (Figure 4.5). The model pore forming peptide, melittin (10  $\mu$ M and 1  $\mu$ M) was used as the positive control. Melittin induced expected membrane permeability, characteristic of pore forming peptides. VP4C (5  $\mu$ M) and VP1N (5  $\mu$ M) induced membrane permeability broadly similar to that induced by melittin. Membrane permeability induced by VP4C was more extensive than that induced by VP1N. In contrast, the VP4N-induced membrane permeability appeared dramatically different to that induced by any of the other proteins or peptides, producing an abrupt and more extensive permeability (Figure 7.1). This suggested that VP4N was able to induce membrane permeability by a different mechanism when used at 5  $\mu$ M.

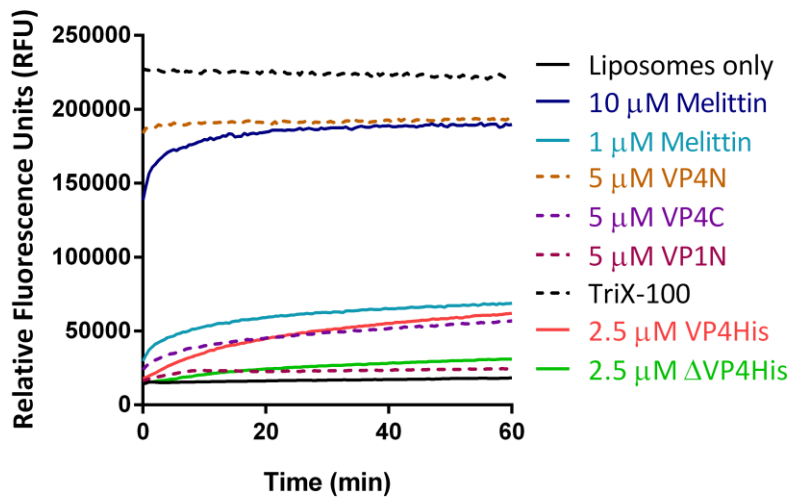


**Figure 7.1 Membrane permeability induced by VP4 and VP1 peptides.**

VP4 N and C-terminus peptides, VP1 N-terminus peptide, VP4His or  $\Delta$ VP4His was incubated with liposomes. Released CF dye was measured by fluorimetry ( $\lambda_{\text{exc}}$  485 nm/ $\lambda_{\text{em}}$  520 nm) and CF release monitored in real time. Negligible levels of CF release were recorded from liposomes in the absence of protein or peptide (Liposomes only). Data shown here is representative of multiple experiments.

In order to determine the effect of peptides at different concentrations and confirm whether the rapid VP4N-induced permeability a real effect (and not an artefact of using excessive amounts of peptide), a twofold dilution series of VP4N, VP4C or VP1N were incubated with liposomes and membrane permeability analysed (Figure 7.2).

VP4C and VP4N induced dose-dependent release from liposomes and at each peptide concentration tested, membrane permeability induced by VP4C (10  $\mu$ M, 5  $\mu$ M, 2.5  $\mu$ M, 1.25  $\mu$ M, 0.625  $\mu$ M) was more extensive than VP1N (10  $\mu$ M, 5  $\mu$ M, 2.5  $\mu$ M, 1.25  $\mu$ M, 0.625  $\mu$ M, 0.32  $\mu$ M) (Figure 7.2B, C). Membrane permeability mediated by VP4C and VP1N was broadly similar to that observed with melittin. However, when VP4N (5  $\mu$ M, 2.5  $\mu$ M, 1.25  $\mu$ M) was incubated with liposomes, abrupt and complete release of CF was observed as before. Despite using a twofold dilution of 5  $\mu$ M VP4, there was no observed difference in the nature of membrane permeability induced with these peptide concentrations (Figure 7.2A). With further twofold dilutions of VP4N (1.25  $\mu$ M, 0.625  $\mu$ M, 0.32  $\mu$ M, 0.16  $\mu$ M), a dose-dependent effect was observed but the membrane permeability induced continued to be rapid and extensive. VP4N induced extensive permeability at 0.32  $\mu$ M but relatively minimal membrane permeability at 0.16  $\mu$ M (Figure 7.2A). The large increase in relative extents of VP4N activity between 0.16  $\mu$ M and 0.32  $\mu$ M, suggested a threshold for VP4N acting with a potentially different mechanism at the concentrations above 0.32  $\mu$ M.

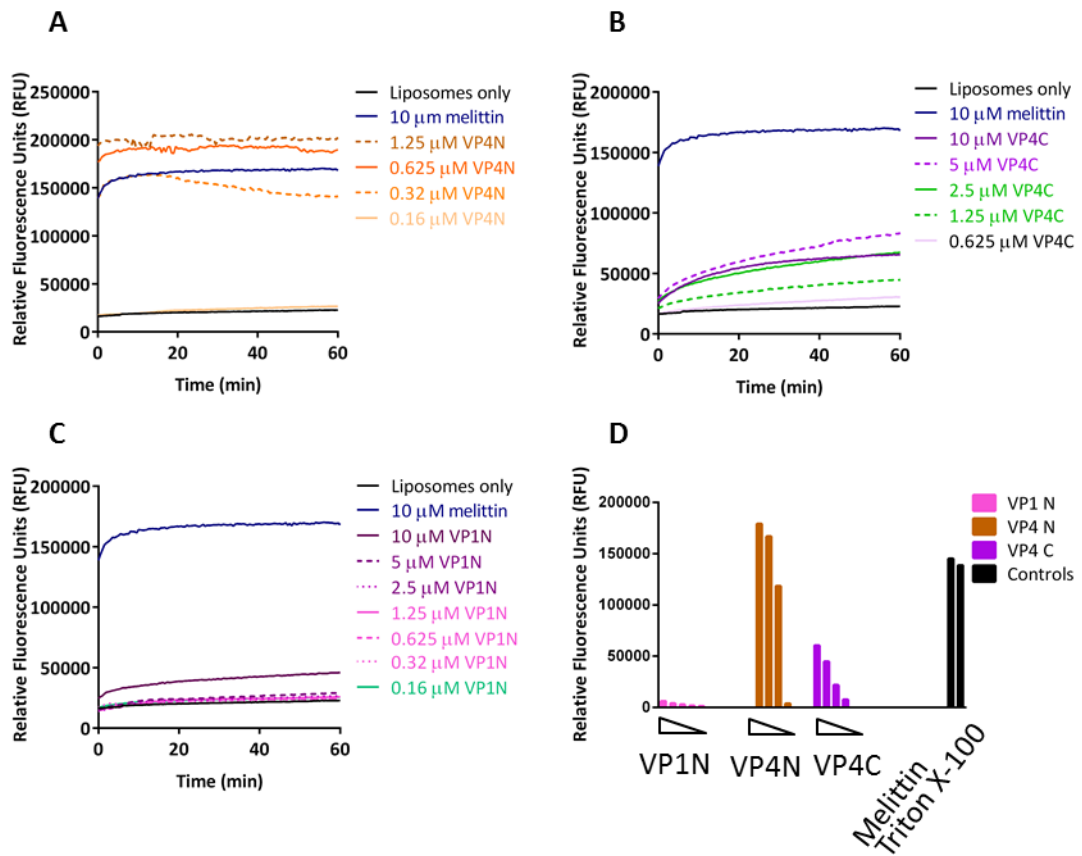


**Figure 7.2 Membrane permeability induced by dilution series of VP4 and VP1 peptides.**

Twofold dilutions of peptides were incubated with liposomes and released CF dye was measured by fluorimetry ( $\lambda_{ex}$  485 nm/ $\lambda_{em}$  520 nm). **A.** VP4 N-terminus peptide. **B.** VP4 C-terminus peptide. **C.** VP1 N-terminus peptide. **D.** Comparison of end point fluorescence measurements of membrane permeability induced by VP4 and VP1 peptides from panels A-C. Data shown here is representative of multiple experiments. Background levels of CF release were generated by liposomes only. Data shown here is representative of multiple experiments.

In order to further compare the peptides with recombinant proteins, peptide concentrations were chosen by comparing data in Figures 7.1 and 7.2, 5  $\mu$ M VP1N, 0.16  $\mu$ M VP4N, 0.625  $\mu$ M VP4C were chosen as concentrations as they induced levels of membrane permeability relatively similar to that observed with 2.5  $\mu$ M  $\Delta$ VP4His. Similarly, 10  $\mu$ M VP1N, 2.5  $\mu$ M VP4C and 0.16  $\mu$ M VP4N were chosen for inducing release relative to VP4His.

Comparison of concentrations of each peptide required to yield CF release similar to that obtained with  $\Delta$ VP4His, demonstrated the requirement of low concentration VP4N (0.16  $\mu$ M), whereas VP4C and VP1N required higher concentrations of 0.625  $\mu$ M and 5  $\mu$ M, respectively (Figure 7.3A). When attempting to compare membrane permeability induced by peptides with VP4His, VP4N used at 0.32  $\mu$ M was observed to induce membrane permeability that was more extensive than that induced by VP4His whereas VP4N at 0.16  $\mu$ M induced permeability



relatively lower compared to VP4His. VP4C (2.5  $\mu\text{M}$ ) and VP1N (10  $\mu\text{M}$ ) were observed to induce membrane permeability comparable to that induced by VP4His (Figure 7.3B).

These observations demonstrated that VP4N was able to induce membrane permeability comparable to that induced by recombinant forms of VP4 at a lower concentration than VP4C or VP1N. In comparison to the membrane permeability induced by peptides similar to  $\Delta\text{VP4His}$ , twofold more of VP1N (10  $\mu\text{M}$ ) and fourfold more of VP4C (2.5  $\mu\text{M}$ ) were required to induce membrane permeability similar to VP4His (Figure 7.3).

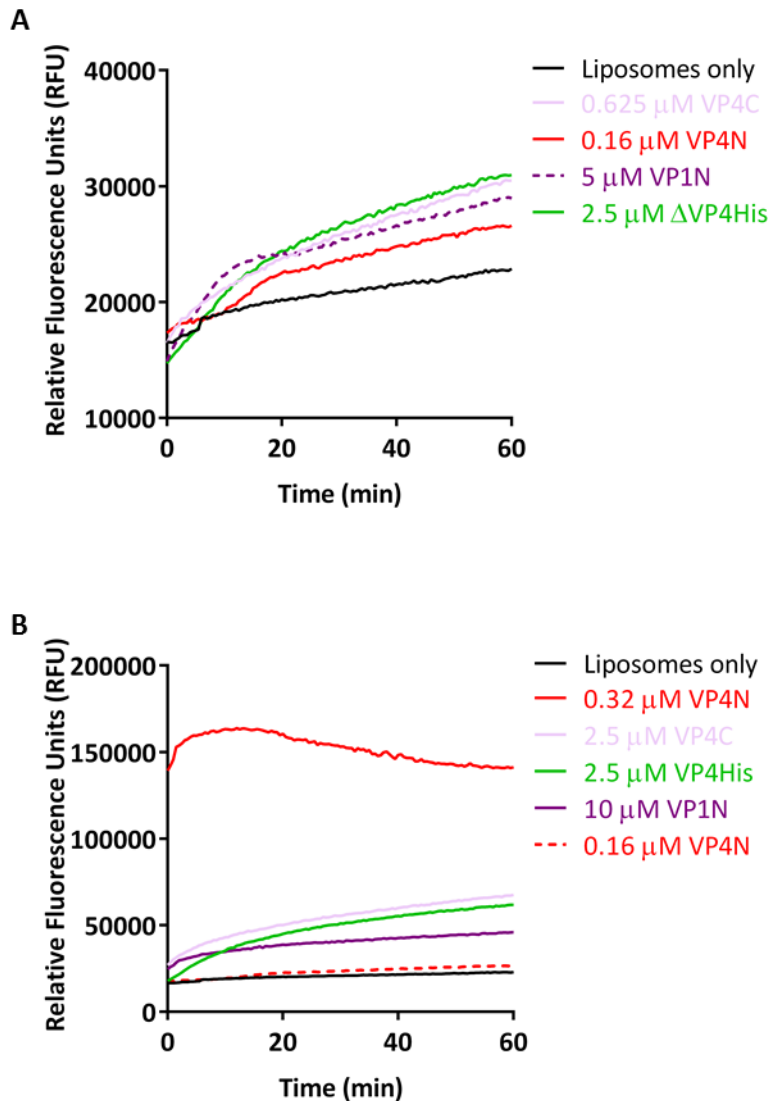


**Figure 7.3 Comparison of membrane permeability induced by VP4 and VP1 peptides, VP4His and  $\Delta\text{VP4His}$ .**

VP4N or C-terminus or VP1 N-terminus specific peptides were incubated with liposomes and membrane permeability analysed. Peptide mediated membrane permeability compared to **A.**  $\Delta\text{VP4His}$  and **B.** VP4His. Released CF dye was measured by fluorimetry ( $\lambda_{\text{ex}}$  485 nm/ $\lambda_{\text{em}}$  520 nm) and CF release monitored in real time. Background levels of CF release were generated by liposomes only.

### **7.3 VP1N-terminus and VP4 act synergistically to induce membrane permeability**

VP4 and the N-terminus of VP1 have been shown to be involved in membrane permeability (section 1.6.4.4). Whether membrane permeability is induced by VP4, VP1 N-terminus or by VP4 in concert with VP1 N-terminus has been a long standing subject of debate but remains unknown.

In order to investigate if VP4-induced membrane permeability was modulated by VP1, VP4 and VP1N were added in combination to liposomes and membrane permeability analysed. For initial experiments, VP4N and VP4C values were chosen based on comparative analysis carried out with VP4His (Figure 7.3) and a standard concentration of VP1N was added to determine the effect of VP1N on membrane permeability induced by VP4N, VP4C and VP4His. Upon incubating VP4N (0.16  $\mu\text{M}$ ) and VP1N (2.5  $\mu\text{M}$ ) with liposomes, membrane permeability was induced by both peptides individually. This was consistent with previous observations shown in Figures 7.2 and 7.3. The combined effect of VP4N and VP1N on the induction of membrane permeability was dramatic, becoming more rapid and extensive than the individual effects of each peptide (Figure 7.4A). Therefore, the combination of VP4N and VP1N showed a synergistic effect on the induction of membrane permeability.

Upon incubating VP4C (2.5  $\mu\text{M}$ ) with liposomes, moderate membrane permeability was induced. However, in contrast to the increase in membrane permeability observed with combined VP4N and VP1N, the combined effect of VP4C and VP1N, decreased the extent of induced membrane permeability (Figure 7.4B). Although, the concentration of VP4C was fifteen-fold higher than VP4N, the permeability induced by VP4N was more extensive than that induced by VP4C.

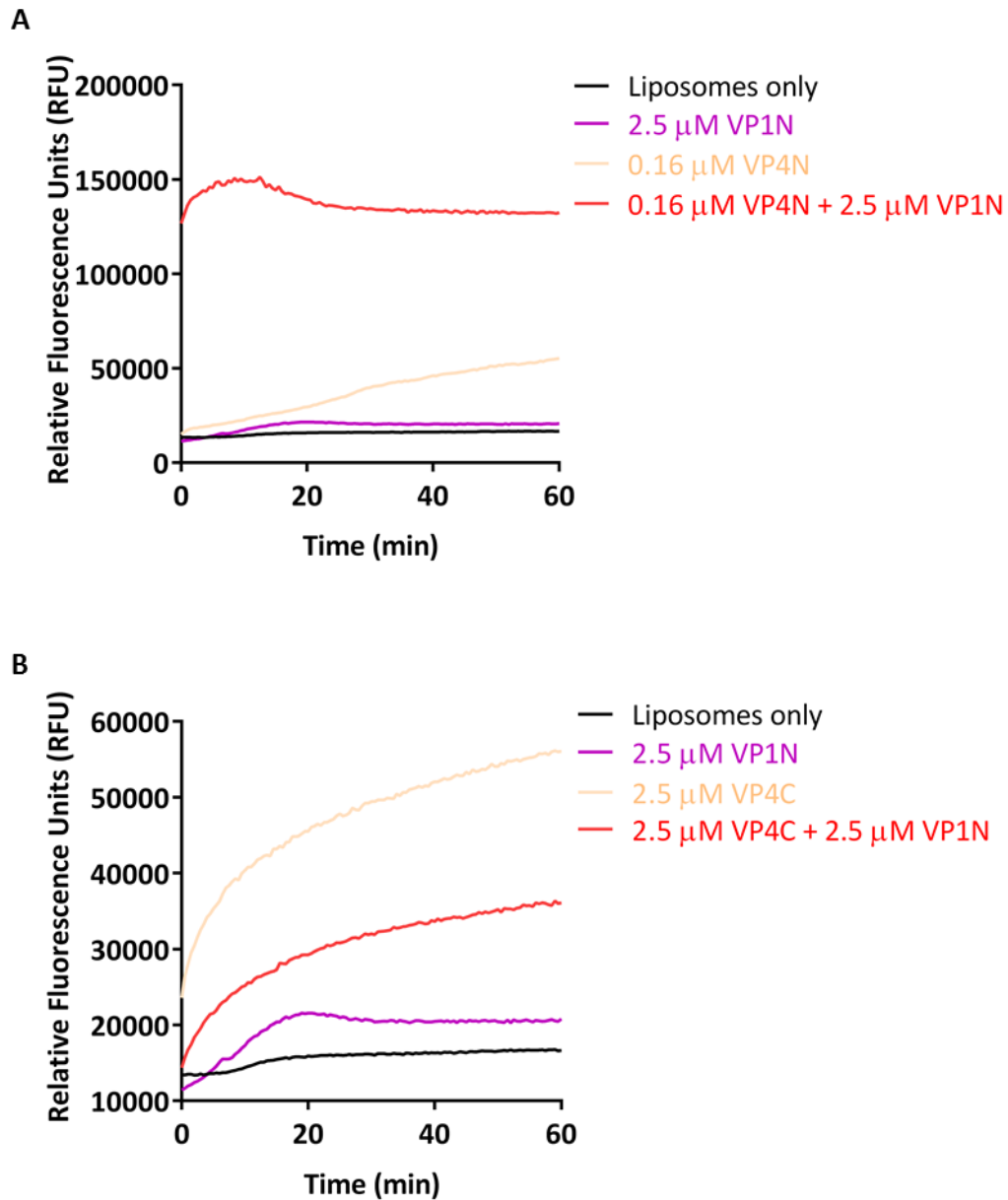


**Figure 7.4 Combined effect of VP4 and VP1 peptides on the induction of membrane permeability.**

**A.** VP4 N-terminus with VP1 N-terminus peptides were incubated with liposomes. **B.** VP4 C-terminus with VP1 N-terminus peptides were incubated with liposomes and membrane permeability analysed. Released CF dye was measured by fluorimetry ( $\lambda_{\text{ex}}$  485 nm/ $\lambda_{\text{em}}$  520 nm) and CF release monitored in real time. Background levels of CF release were generated by liposomes only.

The next step was to determine if VP1N modulated VP4His induced membrane permeability in a similar way as observed with VP4N induced membrane permeability (Figure 7.4). Towards achieving this, 2.5  $\mu\text{M}$  VP4His was incubated with a range of VP1N concentrations (5  $\mu\text{M}$ , 2.5  $\mu\text{M}$ , 1.25  $\mu\text{M}$ ) and membrane permeability analysed.

As previously observed, VP4His and VP1N individually induced membrane permeability at all the concentrations tested. For a given VP4His concentration of 2.5  $\mu\text{M}$ , the extent of membrane permeability induced by VP4His and VP1N was greater than that induced individually by VP4His or VP1N (Figure 7.5). This study showed that when combined with VP1N, the extent of membrane permeability induced by VP4His was enhanced. Interestingly, the greatest enhancement of VP4His activity was observed at a VP1N concentration of 2.5  $\mu\text{M}$  while VP1N concentrations either side of this (5  $\mu\text{M}$  and 1.25  $\mu\text{M}$ ) showed reduced enhancing effect (Figure 7.5). This finding suggested the requirement of an optimal concentration of VP4N and VP1N to permeabilise membranes most efficiently.

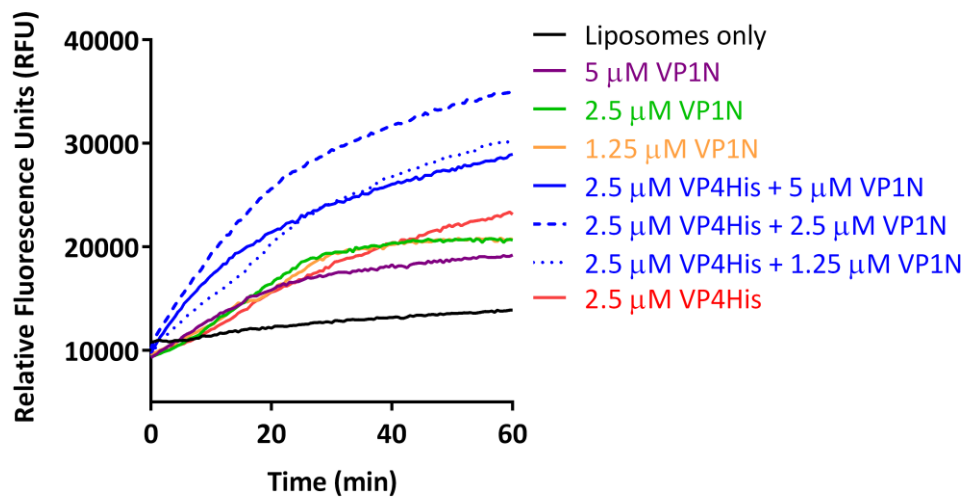


**Figure 7.5 Combined effect of VP4His and VP1 N-terminus peptide on the induction of membrane permeability.**

VP4His (2.5  $\mu\text{M}$ ) and VP1 N-terminus peptide (5  $\mu\text{M}$ , 2.5  $\mu\text{M}$  and 1.25  $\mu\text{M}$ ) were incubated with liposomes and membrane permeability analysed. Released CF dye was measured by fluorimetry ( $\lambda_{\text{ex}}$  485 nm/ $\lambda_{\text{em}}$  520 nm) and CF release monitored in real time. Background levels of CF release were generated by liposomes only.

## **7.4 Comparison of membrane permeability induced by recombinant VP4 and virus**

Membrane permeability induced by either recombinant VP4 (VP4His) or a peptide corresponding to the N-terminus of VP4 (VP4N) was enhanced by the addition of VP1N (Figures 7.4A, 7.5). It was important to relate the membrane permeabilising activity of recombinant VP4 with virus. To achieve this, HRV (1 µg) or VP4His (5 µM) was incubated with liposomes and membrane permeability analysed. Consistent with previous observations (Figure 4.14), membrane permeability was induced by HRV and VP4His at both 25°C and 37°C. VP4His induced similar extents of membrane permeability at 25°C and 37°C (Figure 7.6), in agreement with a previously demonstrated lack of effect of temperature on the induction of membrane permeability by VP4His (Figure 4.14B). In contrast, HRV-induced membrane permeability was enhanced at 37°C compared to 25°C (Figure 7.6). This was not unexpected as HRV capsid breathing would be expected to be taking place more efficiently at 37°C. Samples of HRV which had been pre-heated (to convert virus to empty particles) (1 µg) gave minimal CF release upon incubation with liposomes at either 25°C or 37°C (Figure 7.6).

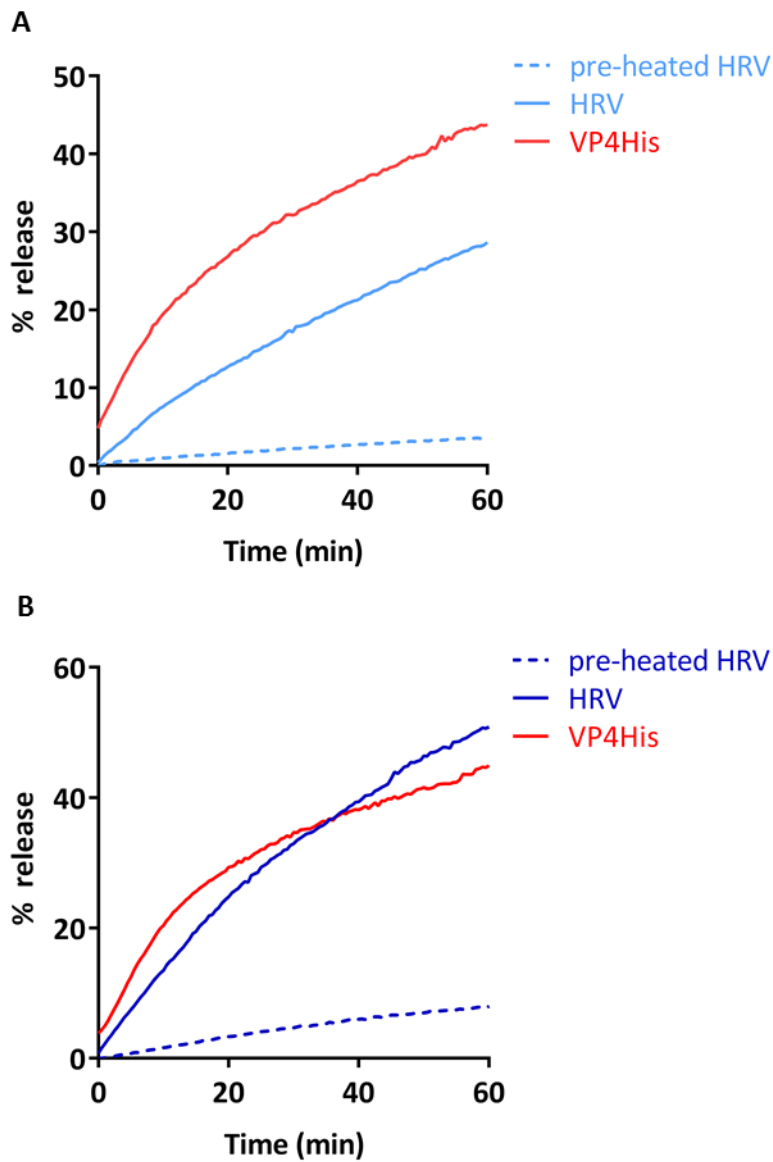


**Figure 7.6 HRV and VP4His induced membrane permeability.**

HRV (1  $\mu\text{g}$ ), pre-heated HRV (1  $\mu\text{g}$ ) or VP4His (5  $\mu\text{M}$ ) were incubated with liposomes at **A.** 25°C and **B.** 37°C. Released CF dye was measured by fluorimetry ( $\lambda_{\text{ex}}$  485 nm/ $\lambda_{\text{em}}$  520 nm) and CF release monitored in real time. Background levels of CF release were generated by liposomes only and subtracted from fluorimetry measurements generated by HRV, pre-heated HRV and VP4His.

## 7.5 Discussion and future Work

Synthetic peptides were used to map the function of VP4. We hoped to use bioinformatics predictions of hydrophobic regions in VP4 containing TM domains/amphipathic helices to determine the design of peptides. However, the predictions obtained did not clearly define these features (section 6.2). Therefore, VP4 peptides of specific sequence length based on the predicted location of TM domains could not be synthesised. As an alternative, peptides corresponding to the N-terminus (VP4N) and the C-terminus of VP4 (VP4C) were synthesised to carry out experiments with the aim of beginning to map the function of VP4. In addition to VP4, the VP1 N-terminus has been implicated in the cell entry process of picornaviruses. Thus, a peptide corresponding to the first 24 amino acids at the VP1 N-terminus (VP1N) was synthesised to investigate its role in the induction of membrane permeability. VP4N, VP4C and VP1N induced permeability in liposome membranes with VP4N being markedly more active than the other peptides. To investigate if either of the VP4 termini acted in combination with VP1 N-terminus, VP1N was used together with VP4N or VP4C or VP4His. The addition of VP1N to VP4N or VP4His resulted in the enhancement of induced membrane permeability, but a similar effect was not observed when VP1N was used together with VP4C. Membrane permeability induced by VP4His was compared with permeability induced by virus. VP4His induced permeability was not affected by temperature, whereas HRV induced more extensive permeability at 37°C than at 25°C.

All three peptides, VP4N, VP4C and VP1N induced membrane permeability. The nature and extents of membrane permeability induced differed between peptides. At relatively high concentration (5  $\mu\text{M}$ ) VP4N induced abrupt and extensive CF release, and which therefore seemed to suggest this peptide may be acting by inducing membrane disruption. This was in contrast to the CF release induced by VP4C and VP1N which were similar to that observed with VP4His and the model pore forming peptide, melittin (Figure 7.1).

Analysis of CF release showed that VP4N, at 0.16  $\mu\text{M}$  and 0.32  $\mu\text{M}$ , induced membrane permeability with CF release characteristics broadly similar to that observed with VP4His or melittin. There was a large increase in relative levels of permeability between VP4N concentrations of 0.16  $\mu\text{M}$  and 0.32  $\mu\text{M}$  (Figure 7.2), suggesting a threshold for VP4N activity with a different mechanism of membrane permeability induction at higher concentrations.

A low concentration of VP4N was required to induce robust membrane permeability, whereas a higher concentration of VP4C was required to induce similar extents of permeability. VP4N induced more extensive permeability than VP4C even when thirtyfold greater amounts of VP4C was used in the membrane permeability assay (Figure 7.2). Therefore, VP4N seemed to

be the more active peptide and a possible reason for this was the presence of the myristate group at the N-terminus of VP4 which was likely to target membranes and facilitate VP4 membrane permeabilising activity. The presence of N-terminal myristoylation is a common feature of a number of viral proteins such as  $\mu 1$  of reoviruses and Nef of HIV-1 which are known to interact with membranes (section 4.1). The findings in Figures 7.2 and 7.3, indicated that the N-terminus of VP4 was the most membrane-active region of the protein. VP4N may be acting by two different mechanisms depending on its concentration in the membrane. It is conceivable that when VP4N was used at a concentration above the threshold of  $0.32 \mu\text{M}$ , CF release was induced by membrane disruption. But when VP4N was used at a concentration at or below  $0.32 \mu\text{M}$ , CF release was induced by membrane pore formation. Future work could confirm this hypothesis, by determining CF release induced by VP4N when used at concentrations in the range between  $0.16 \mu\text{M}$  and  $0.32 \mu\text{M}$ .

Several findings have indicated the N-terminus may be the region of VP4 with the ability to induce membrane permeability during picornavirus cell entry. For example, presence of the myristate group at the N-terminus of VP4, mutations in threonine at position 28 showed that it was critical for channel formation and RNA delivery during infection (Danthi *et al.*, 2003), evidence that the N-terminus of VP4 emerges first during capsid breathing was provided by the dimerisation of the N-terminus of HRV VP4 (Katpally *et al.*, 2009). In addition to the above studies, the findings described here show that more extensive membrane permeability was induced by VP4N compared to VP4C (section 7.2), thereby adding weight towards the evidence for N-terminus of VP4 functioning as the membrane active region of the protein.

Membrane permeability induced by VP4His was enhanced by the addition of VP1N. VP4His and VP1N appeared to have a synergistic effect on the induction of membrane permeability (Figure 7.4). There appeared to be an optimal ratio of VP4His:VP1N for maximum synergistic effect and if peptide or recombinant protein concentration was changed to alter this ratio, permeability decreased (Figure 7.5).

The peptides used in these studies appeared to be highly soluble in aqueous solution and it was therefore assumed that majority of peptide molecules were available to take part in membrane interactions. In contrast, as VP4His was largely insoluble, only a small proportion of VP4His molecules were likely to participate in the membrane interaction and formation of the membrane pore but this proportion of membrane active VP4His molecules could not be accurately determined (section 4.3). Nevertheless, it was possible to estimate that if for example, 10% of VP4His molecules were participating in membrane interactions, a VP4His:VP1N of 1:10 would be required for membrane permeabilisation and if 1% of VP4His molecules were participating then a VP4His:VP1N of 1:100 would be required.



Similar to the observations made with VP4His, membrane permeability induced by VP4N also increased upon the addition of VP1N. The extent of membrane permeability induced was greater than the sum of the extents of permeability induced by VP4N or VP1N individually (Figure 7.4A). This suggested that VP4N and VP1N acted synergistically to induce membrane permeability. In contrast, membrane permeability induced by VP4C decreased upon addition of VP1 N-terminus peptide (Figure 7.4B). Thus, synergy was observed with VP1N and VP4N and VP4His. This suggested that VP4 and the N-terminus of VP1 acted in concert with each other. However, it should be noted that these were preliminary studies.

VP4N and VP1N were soluble peptides and it was therefore possible to calculate VP4N:VP1N ratio. The experiments in which maximum synergy between VP4N and VP1N was observed (Figure 7.4) used a VP4N:VP1N ratio determined as 1:15. Therefore, for the experiments with peptide or protein in which synergistic effects were observed, the ratios of VP4N:VP1N and estimated ratio VP4His:VP1N were broadly similar.

It is important to remember that the peptides (VP4N, VP4C and VP1N) have six lysine residues at the C-terminus to increase their solubility which may inadvertently affect biophysical properties of VP4 such as membrane affinity and insertion, consequently impacting the resulting peptide topology. To confirm membrane targeting and induction of permeability was not due to the presence of polybasic residues, a non-membrane permeabilising peptide with six lysines could be included as a control. Also, the lysine residues render the peptides soluble and, therefore, do not entirely reflect the native viral capsid proteins VP1 and VP4.

As mentioned previously, there is no evidence to show a direct contribution of VP4 at the stage of virus entry where the altered particle is tethered to the membrane. The findings in Figures 7.4 and 7.5 provide the strongest evidence to date that the membrane permeabilisation machinery is likely to involve concerted actions of VP4 and N-terminus of VP1. These findings for the involvement of VP4 and VP1 N-terminus, support various iterations of picornavirus entry models that have proposed the involvement of VP4 and VP1 N-terminus in membrane interactions and induction of membrane permeability, and the transfer of RNA across the membrane (section 1.6.4).

In the context of the virus, it is possible that VP4 N-terminus contains the membrane interacting domains but VP4 C-terminus may or may not be required at the stage of genome transfer. Possibilities of whether VP4 C-terminus is redundant at this stage of virus entry or is required for the function of VP1 N-terminus, requires further investigation.

Permeability induced by recombinant VP4His and permeability induced by virus were compared. Exposing enteroviruses to elevated temperatures (~60°C) results in the formation

of empty particles (80S) (Breindl, 1971; Schober *et al.*, 1998). HRV particles induced membrane permeability but empty particles induced minimal membrane permeability (Figure 7.6). This was expected as empty particles have lost the majority of VP4 during the conversion from virus. In addition, they may possibly not contain externalised VP1 N-terminus in a form primed to bind membranes and therefore, empty particles might not even be able to bind membranes. However, it is also possible that not all copies of VP4 are lost from the empty particle as some VP4 has been detected in or associated with HRV empty particles (Greve *et al.*, 1991; Hooverlitty and Greve, 1993). The X-ray structure of HRV14 identified missing or disordered density corresponding to VP4 and VP1 N-terminus in the empty particles compared to the native particles. It is, therefore possible that residual VP4 in empty particles may have contributed to the observed low level membrane permeability (Figure 7.6). The observed extensive membrane permeability mediated by HRV and low level membrane permeability mediated by pre-heated HRV particles, provided further weight to the contribution of VP4 and N-terminus of VP1 in the induction of membrane permeability, thereby implying the importance of the capsid proteins, VP4 and VP1, in facilitating genome transfer across the membrane.

Membrane permeability induced by VP4His (5 µg) was more extensive than that observed with HRV (1 µg) at 25°C (Figure 7.6). This may have resulted from the possibility that a greater number of VP4His molecules were available for membrane insertion compared to the number of native VP4 molecules released from HRV and available for membrane insertion. Due to the low solubility of VP4His, it was not possible to quantify the number of VP4 molecules inserting into membranes and forming pores resulting in the release of CF from within liposomes (section 4.3). The low solubility of VP4His made it likely that only a proportion of VP4His took part in the formation of functional membrane pores. If this active proportion was 10% of the total (5 µg), this would be equivalent to 500 ng and if it was 1% of the total, it would be 50 ng of active VP4His per assay. 50 ng is approximately equal to the amount of native VP4 in 1 µg of virus.

Membrane permeability induced by HRV was more extensive at 37°C than at 25°C. This was consistent with the expectation of increased virus breathing at 37°C compared to 25°C (Figure 7.6). Breathing involves the transient externalisation of hydrophobic membrane binding capsid proteins VP4 and N-terminus of VP1. Presumably, interaction of these transiently exposed capsid proteins with membranes triggers particle alterations and leads to membrane permeabilisation. This observation of increased permeability due to externalisation of VP4 and VP1 was in agreement with findings of HRV breathing at room temperature (Lewis *et al.*, 1998) and uncoating being more efficient at temperature above 25°C (Nurani *et al.*, 2003).

PV and FMDV have been shown to induce liposome permeability and release RNA at room temperature and in the absence of receptors or low pH (The Pirbright Institute and Jim Hogle's lab, Harvard Medical School, USA, personal communication). Therefore, it seems that changes in particle conformation can be triggered by interaction with model membranes at room temperature and without the trigger normally required for uncoating. This was likely due to the differences between the nature of cell membranes and model membranes. Virus particles could bind naked membranes and undergo conformational alterations. However, due to the presence of different phospholipids and proteins present in the cell membrane, receptors are required to act as "hooks" which concentrate the virus on the surface.

The experiments described in this chapter have identified the N-terminus of VP4 as the region of VP4 most likely responsible for the induction of membrane permeability or the "business end" of VP4. In the future, a sliding window analysis of VP4 could be carried out and the corresponding proteins expressed and purified from *E.coli* or synthesised as peptides, which would help facilitate determining the minimal functional regions of VP4. In PV, mutations of threonine (amino acid 28) have shown that this amino acid at this position is critical for PV infection (Danthi *et al.*, 2003). Future studies of PV VP4 wild type and PV VP4 mutant proteins, and their HRV equivalents will help shed light on the importance of this position or of the nature of the residue at this position for picornavirus VP4 membrane interactions during the cell entry process.

Further work needs to be carried out to determine if membrane permeability induced by VP4N, VP4C, VP1N and HRV16 is by the formation of size-selective pores comparable to that formed by recombinant VP4 (sections 5.2, 5.3 and 5.4). Accompanying this, future studies could be carried out to characterise membrane pores formed by the different peptides (VP4N, VP4C, VP1N), recombinant VP4His and virus (HRV16).

The findings in Figure 7.5 demonstrated an increase in the extent permeability induced by VP4His upon addition of VP1 N-terminus specific peptide at pH 7.4. Bearing in mind the reported findings of HRV16 uncoating at acidic pH (Nurani *et al.*, 2003) and the observations where VP4His and  $\Delta$ VP4His induced enhanced membrane permeability at pH 5.5 (section 4.2.3), future studies should be carried out to study the effect of pH on VP1 N-terminus modulated membrane permeability induced by VP4N. This will help further our understanding of the factors contributing to the optimal conditions under which membrane pore formation occurs.

# **Chapter 8**

## **Concluding remarks and future perspectives**

## 8.1 Concluding remarks and future perspectives

A fundamental step in the process of viral infection is the delivery of the virus genome across the host cell membrane to the site of replication. This step is well understood for enveloped viruses which use fusion of the virus membrane with the host cell membrane to transfer their genetic material to the cytoplasm. However, non-enveloped viruses lack a membrane and therefore must employ an alternative mechanism for delivery of their genetic material to the cytoplasm. Although studies of several non-enveloped viruses including poliovirus, reovirus and flock house virus have suggested the involvement of capsid proteins mediating membrane penetration for genome delivery (described in sections 1.6.3 and 1.6.4.2), the mechanism of this process remains to be understood. The work described in this thesis sought to further our understanding of the role played by the internal capsid protein VP4 in picornavirus cell entry.

In this thesis, recombinant VP4 was generated and its interaction with membranes characterised. Recombinant VP4 interacted with and permeabilised membranes by a multimeric, size-selective pore (sections 5.2, 5.3, 5.4). At physiological temperature, membrane permeability induced by VP4His was similar to that observed with infectious virus (section 7.4), suggesting that the membrane pore formed by recombinant VP4 mimics that formed by the virus. This could be investigated further by characterising virus-derived pores in studies similar to those carried out with VP4His (section 5.3). In the future, the dextran dye release assay could be refined by using synthetic single stranded nucleic acids which more closely match the structure of RNA exiting from the membrane pore, as this will begin to answer the question of the effect of RNA structure on genome delivery.

Chemical crosslinking and SDS-PAGE showed that recombinant VP4 formed a homo-multimeric complex comprised of five to six copies of VP4. The multimeric complex was visualised by TEM as a pore structure. The pore lumen diameter of approximately 5 nm, as suggested by dextran dye release studies and as visualised by TEM, is expected to be sufficient to allow the transfer of RNA across the membrane and into the cytoplasm. The site of exit of RNA from the capsid has long been debated. The RNA exit site was believed to be at the fivefold axis. However, recent research has led to the picornavirus cell entry model being updated and the evidence now suggests an opening at the twofold axis as the site of RNA exit (section 1.6.4.3). The site on the capsid from which VP4 is released is yet to be determined.

Membrane permeability was enhanced at an acidic pH of 5.5 and the presence of N-terminal myristoylation (section 4.2.3). Although the exact site for HRV16 uncoating is not known, findings from *in-vitro* studies of the effect of pH on VP4-induced membrane permeability (section 4.2.3) is consistent with the pH in late endosomes. This is also consistent with previous studies showing the requirement of acidic pH for HRV16 uncoating (Nurani *et al.*, 2003). Therefore, the combined evidence suggests the late endosome as a likely site for virus uncoating and formation of the VP4-membrane pore complex.

During virus entry, both VP4 and the N-terminus of VP1 are exposed and are known to interact with membranes. Preliminary studies using synthetic peptides showed that membrane permeability induced by recombinant VP4 was enhanced by the addition of a peptide corresponding to the N-terminus of VP1 (section 7.3). Future work should be carried out to determine the interaction of VP1 N-terminus with VP4 to modulate VP4-mediated membrane permeability. It would be interesting to determine and compare the stoichiometry of the pore complexes formed by VP4, VP4 with VP1 N-terminus, and the native virus. A range of methods such as chemical crosslinking and SDS-PAGE, proteolysis followed by mass spectrometry to identify residual protein components embedded in the membrane, could be employed to identify the pore components and determine if VP1 N-terminus is required for recombinant VP4 to form a membrane-pore complex mimicking that formed by native virus. Extending this work to other species of the picornavirus family will help determine if VP4 from different picornaviruses form similar membrane pores by following similar mechanisms of membrane permeabilisation.

Circular dichroism (CD) spectroscopy analysis of VP4 reconstituted in detergent micelles showed VP4 had a high alpha helical content, a feature typical of membrane binding proteins (section 6.3). 2D nuclear magnetic resonance (NMR) spectra acquired for reconstituted VP4, suggested VP4 to be a potential membrane binding protein (section 6.4). The 2D NMR spectra demonstrated the suitability of reconstituted VP4 for future structure determination of the VP4-membrane pore complex by 3D NMR. Similar structural studies carried out with myristoylated VP4 would closely mimic the uncoating process occurring *in vivo*. Furthermore, comparative NMR studies of the VP4-membrane pore complex and the VP4-membrane pore complex bound to potential entry inhibitors may facilitate understanding of the mechanism of inhibition of picornavirus uncoating.

Membrane permeability induced by peptides corresponding to the N or C-terminus of VP4, showed that the N-terminus of VP4 was more active than the C-terminus, suggesting that the N-terminus was likely to be the “business end” of the protein. This would be in agreement with the transient externalisation of the N-terminus of VP4 observed during capsid breathing

(Katpally *et al.*, 2009) and the fact that VP4 is N-terminally myristoylated which would contribute to targeting of VP4 to the membrane (section 4.1). Future mutagenesis studies should be carried out to map VP4 function by analysing the effect of mutations on VP4-induced membrane permeability, multimerisation and pore size-selectivity.

HRV VP4 is conserved across the approximately 150 virus serotypes and VP4 entry inhibitors therefore have the potential to be cross-protective. Thus, one obvious area of future focus should be on investigating VP4 as a candidate for the development of vaccines and antiviral drugs.

The potential mechanism of VP4-induced membrane permeability was the formation of a size-selective multimeric membrane pore, as shown by biochemical and structural approaches. Also, the conditions influencing VP4-induced membrane permeability were characterised. These findings have contributed to further our understanding of the role of VP4 in facilitating the transfer of RNA across the membrane and into the cytoplasm. This has highlighted a possible mechanism that may be used by several other non-enveloped viruses that have capsid proteins with characteristics similar to VP4 (section 1.6.3). It would be useful to extend these studies with HRV16 VP4 to other medically important members of the picornavirus family such as poliovirus and enterovirus 71, the causative agents of poliomyelitis and hand, foot and mouth disease, respectively.

Bringing together the existing evidence for picornavirus cell entry and the findings described in this thesis, the following cell entry mechanism can be hypothesised. After receptor binding and/or exposure to acidic pH, the VP1 N-terminus is released at or near the twofold symmetry axis and the first 30 residues predicted to form an amphipathic helix insert into the membrane to anchor the virus. The remaining residues may contribute to form the umbilicus connecting the virus particle to the membrane. VP4 is also released, inserts into the membrane to form a pore comprising of five to six copies of VP4. RNA is released from the capsid from an opening at the twofold symmetry axis closest to the membrane, and may exit with its less structured 3' end first. As the RNA passes through the umbilicus (RNA may be shielded from enzymatic degradation by VP1 and/or VP4 forming the umbilicus) in a ratchet-like movement, it becomes unwound and once in the cytoplasm it regains its structure. Upon delivery into the cytoplasm the RNA is likely to refold, for the process of translation to begin.

# Chapter 9

# References



- Abrams, C.C., King, A.M.Q. and Belsham, G.J. (1995).** Assembly of Foot-and-Mouth-Disease Virus Empty Capsids Synthesized by a Vaccinia Virus Expression System. *Journal of General Virology* **76**, 3089-3098.
- Acharya, R., Fry, E., Stuart, D., Fox, G., Rowlands, D. and Brown, F. (1989).** The Three-Dimensional Structure of Foot-and-Mouth Disease Virus at 2.9. Å Resolution. *First Congress, European Society for Veterinary Virology, Liege, Belgium, 6-7 April, 1989 Abstracts.*
- Adams, M.J. and Carstens, E.B. (2012).** Ratification Vote on Taxonomic Proposals to the International Committee on Taxonomy of Viruses (2012). *Archives of Virology* **157**, 1411-1422.
- Adams, M.J., King, A.M.Q. and Carstens, E.B. (2013).** Ratification Vote on Taxonomic Proposals to the International Committee on Taxonomy of Viruses (2013). *Archives of virology* **158**, 2023-2030.
- Adams, P., Lea, S., Newman, J., Blakemore, W., King, A., Stuart, D. and Fry, E. (2010).** 2wzr: The Structure of Foot and Mouth Disease Virus Serotype Sat1. *Protein Data Bank.*
- Agirre, A., Barco, A., Carrasco, L. and Nieva, J.L. (2002).** Viroporin-Mediated Membrane Permeabilization - Pore Formation by Nonstructural Poliovirus 2b Protein. *Journal of Biological Chemistry* **277**, 40434-40441.
- Alexander, L.N., Seward, J.F., Santibanez, T.A., Pallansch, M.A., Kew, O.M., Prevots, D.R., Strebel, P.M., Cono, J., Wharton, M., Orenstein, W.A. and Sutter, R.W. (2004).** Vaccine Policy Changes and Epidemiology of Poliomyelitis in the United States. *Jama-Journal of the American Medical Association* **292**, 1696-1701.
- Ambros, V. and Baltimore, D. (1978).** Protein Is Linked to 5' End of Poliovirus Rna by a Phosphodiester Linkage to Tyrosine. *Journal of Biological Chemistry* **253**, 5263-5266.
- Andino, R., Rieckhof, G.E. and Baltimore, D. (1990).** A Functional Ribonucleoprotein Complex Forms around the 5' End of Poliovirus Rna. *Cell* **63**, 369-380.
- Andino, R., Boddeker, N. and Gamarnik, A.V. (1999).** Intracellular Determinants of Picornavirus Replication. *Trends in Microbiology* **7**, 76-82.
- Angov, E. (2011).** Codon Usage: Nature's Roadmap to Expression and Folding of Proteins. *Biotechnology Journal* **6**, 650-659.
- Ansardi, D.C., Porter, D.C. and Morrow, C.D. (1992).** Myristylation of Poliovirus Capsid Precursor-P1 Is Required for Assembly of Subviral Particles. *Journal of Virology* **66**, 4556-4563.
- Ansardi, D.C. and Morrow, C.D. (1995).** Amino-Acid Substitutions in the Poliovirus Maturation Cleavage Site Affect Assembly and Result in Accumulation of Provirions. *Journal of Virology* **69**, 1540-1547.
- Armer, H., Moffat, K., Wileman, T., Belsham, G.J., Jackson, T., Duprex, W.P., Ryan, M. and Monaghan, P. (2008).** Foot-and-Mouth Disease Virus, but Not Bovine Enterovirus, Targets the Host Cell Cytoskeleton Via the Nonstructural Protein 3c(Pro). *Journal of Virology* **82**, 10556-10566.
- Arnold, E. and Rossmann, M.G. (1990).** Analysis of the Structure of a Common Cold Virus, Human Rhinovirus-14, Refined at a Resolution of 3.0-Å. *Journal of Molecular Biology* **211**, 763-801.
- Back, S.H., Kim, Y.K., Kim, W.J., Cho, S., Oh, H.R., Kim, J.E. and Jang, S.K. (2002).** Translation of Polioviral Mrna Is Inhibited by Cleavage of Polypyrimidine Tract-Binding Proteins Executed by Polioviral 3c(Pro). *Journal of Virology* **76**, 2529-2542.
- Baleja, J.D. (2001).** Structure Determination of Membrane-Associated Proteins from Nuclear Magnetic Resonance Data. *Analytical Biochemistry* **288**, 1-15.
- Balinda, S.N., Tjornehoj, K., Muwanika, V.B., Sangula, A.K., Mwiine, F.N., Ayebazibwe, C., Masembe, C., Siegismund, H.R. and Alexandersen, S. (2009).** Prevalence Estimates of Antibodies Towards Foot-and-Mouth Disease Virus in Small Ruminants in Uganda. *Transboundary and Emerging Diseases* **56**, 362-371.
- Baltimore, D., Girard, M. and Darnell, J.E. (1966).** Aspects of Synthesis of Poliovirus Rna and Formation of Virus Particles. *Virology* **29**, 179-&.

- Banerjee, M., Khayat, R., Walukiewicz, H.E., Odegard, A.L., Schneemann, A. and Johnson, J.E. (2009).** Dissecting the Functional Domains of a Nonenveloped Virus Membrane Penetration Peptide. *Journal of Virology* **83**, 6929-6933.
- Banerjee, R. and Dasgupta, A. (2001).** Interaction of Picornavirus 2c Polypeptide with the Viral Negative-Strand Rna. *Journal of General Virology* **82**, 2621-2627.
- Bano-Polo, M., Baeza-Delgado, C., Orzaez, M., Marti-Renom, M.A., Abad, C. and Mingarro, I. (2012).** Polar/Ionizable Residues in Transmembrane Segments: Effects on Helix-Helix Packing. *PLoS One* **7**.
- Basavappa, R., Syed, R., Flore, O., Icenogle, J.P., Filman, D.J. and Hogle, J.M. (1994).** Role and Mechanism of the Maturation Cleavage of Vpo in Poliovirus Assembly - Structure of the Empty Capsid Assembly Intermediate at 2.9-Angstrom Resolution. *Protein Science* **3**, 1651-1669.
- Basavappa, R., Gomez-Yafal, A. and Hogle, J.M. (1998).** The Poliovirus Empty Capsid Specifically Recognizes the Poliovirus Receptor and Undergoes Some, but Not All, of the Transitions Associated with Cell Entry. *Journal of Virology* **72**, 7551-7556.
- Bastiaanse, E.M.L., Hold, K.M. and VanderLaarse, A. (1997).** The Effect of Membrane Cholesterol Content on Ion Transport Processes in Plasma Membranes. *Cardiovascular Research* **33**, 272-283.
- Baxter, N.J., Roetzer, A., Liebig, H.D., Sedelnikova, S.E., Hounslow, A.M., Skern, T. and Waltho, J.P. (2006).** Structure and Dynamics of Coxsackievirus B4 2a Proteinase, an Enzyme Involved in the Etiology of Heart Disease. *Journal of Virology* **80**, 1451-1462.
- Bayer, N., Prchla, E., Schwab, M., Blaas, D. and Fuchs, R. (1999).** Human Rhinovirus Hrv14 Uncoats from Early Endosomes in the Presence of Bafilomycin. *FEBS Letters* **463**, 175-178.
- Belnap, D.M., Filman, D.J., Trus, B.L., Cheng, N.Q., Booy, F.P., Conway, J.F., Curry, S., Hiremath, C.N., Tsang, S.K., Steven, A.C. and Hogle, J.M. (2000a).** Molecular Tectonic Model of Virus Structural Transitions: The Putative Cell Entry States of Poliovirus. *Journal of Virology* **74**, 1342-1354.
- Belnap, D.M., McDermott, B.M., Filman, D.J., Cheng, N.Q., Trus, B.L., Zuccola, H.J., Racaniello, V.R., Hogle, J.M. and Steven, A.C. (2000b).** Three-Dimensional Structure of Poliovirus Receptor Bound to Poliovirus. *Proceedings of the National Academy of Sciences of the United States of America* **97**, 73-78.
- Belsham, G.J., McInerney, G.M. and Ross-Smith, N. (2000).** Foot-and-Mouth Disease Virus 3c Protease Induces Cleavage of Translation Initiation Factors Eif4a and Eif4g within Infected Cells. *Journal of Virology* **74**, 272-280.
- Belsham, G.J. (2013).** Influence of the Leader Protein Coding Region of Foot-and-Mouth Disease Virus on Virus Replication. *The Journal of general virology* **94**, 1486-1495.
- Bergelson, J.M., Shepley, M.P., Chan, B.M.C., Hemler, M.E. and Finberg, R.W. (1992).** Identification of the Integrin  $\alpha$ 5 $\beta$ 1 as a Receptor for Echovirus-1. *Science* **255**, 1718-1720.
- Bergelson, J.M., Cunningham, J.A., Droguett, G., KurtJones, E.A., Krithivas, A., Hong, J.S., Horwitz, M.S., Crowell, R.L. and Finberg, R.W. (1997).** Isolation of a Common Receptor for Coxsackie B Viruses and Adenoviruses 2 and 5. *Science* **275**, 1320-1323.
- Berryman, S., Clark, S., Monaghan, P. and Jackson, T. (2005).** Early Events in Integrin  $\alpha$ 5 $\beta$ 1-Mediated Cell Entry of Foot-and-Mouth Disease Virus. *Journal of Virology* **79**, 8519-8534.
- Bienz, K., Egger, D., Troxler, M. and Pasamontes, L. (1990).** Structural Organization of Poliovirus Rna Replication Is Mediated by Viral-Proteins of the P2 Genomic Region. *Journal of Virology* **64**, 1156-1163.
- Birtley, J.R., Knox, S.R., Jaulent, A.M., Brick, P., Leatherbarrow, R.J. and Curry, S. (2005).** Crystal Structure of Foot-and-Mouth Disease Virus 3c Protease. *Journal of Biological Chemistry* **280**, 11520-11527.
- Bizzintino, J., Lee, W.M., Laing, I.A., Vang, F., Pappas, T., Zhang, G., Martin, A.C., Khoo, S.K., Cox, D.W., Geelhoed, G.C., McMinne, P.C., Goldblatt, J., Gern, J.E. and Le Soue, P.N. (2011).** Association between Human Rhinovirus C and Severity of Acute Asthma in Children. *European Respiratory Journal* **37**, 1037-1042.

- Blair, W.S., Li, X.Y. and Semler, B.L. (1993). *3cd Cleavage of the Poliovirus P1 Precursor - a Model for Complex Proteinase Substrate Interactions.*
- Blomqvist, S., Roivainen, M., Puhakka, T., Kleemola, M. and Hovi, T. (2002).** Virological and Serological Analysis of Rhinovirus Infections During the First Two Years of Life in a Cohort of Children. *Journal of Medical Virology* **66**, 263-268.
- Blyn, L.B., Towner, J.S., Semler, B.L. and Ehrenfeld, E. (1997).** Requirement of Poly(Rc) Binding Protein 2 for Translation of Poliovirus Rna. *Journal of Virology* **71**, 6243-6246.
- Boisson, B. and Meinel, T. (2003).** A Continuous Assay of Myristoyl-Coa : Protein N-Myristoyltransferase for Proteomic Analysis. *Analytical Biochemistry* **322**, 116-123.
- Bong, D.T., Steinem, C., Janshoff, A., Johnson, J.E. and Ghadiri, M.R. (1999).** A Highly Membrane-Active Peptide in Flock House Virus: Implications for the Mechanism of Nodavirus Infection. *Chemistry & Biology* **6**, 473-481.
- Bong, D.T., Janshoff, A., Steinem, C. and Ghadiri, M.R. (2000).** Membrane Partitioning of the Cleavage Peptide in Flock House Virus. *Biophysical Journal* **78**, 839-845.
- Booth, D.S., Avila-Sakar, A. and Cheng, Y. (2011).** Visualizing Proteins and Macromolecular Complexes by Negative Stain Em: From Grid Preparation to Image Acquisition. *Journal of visualized experiments : JoVE*.
- Bordag, N. and Keller, S. (2010).** Alpha-Helical Transmembrane Peptides: A "Divide and Conquer" Approach to Membrane Proteins. *Chemistry and Physics of Lipids* **163**, 1-26.
- Bostina, M., Levy, H., Filman, D.J. and Hogle, J.M. (2011).** Poliovirus Rna Is Released from the Capsid near a Twofold Symmetry Axis. *Journal of Virology* **85**, 776-783.
- Brabec, M., Baravalle, G., Baas, D. and Fuchs, R. (2003).** Conformational Changes, Plasma Membrane Penetration, and Infection by Human Rhinovirus Type 2: Role of Receptors and Low Ph. *Journal of Virology* **77**, 5370-5377.
- Brabec, M., Schober, D., Wagner, E., Bayer, N., Murphy, R.F., Blaas, D. and Fuchs, R. (2005).** Opening of Size-Selective Pores in Endosomes During Human Rhinovirus Serotype 2 in Vivo Uncoating Monitored by Single-Organelle Flow Analysis. *Journal of Virology* **79**, 1008-1016.
- Brandenburg, B., Lee, L.Y., Lakadamyali, M., Rust, M.J., Zhuang, X. and Hogle, J.M. (2007).** Imaging Poliovirus Entry in Live Cells. *Plos Biology* **5**, 1543-1555.
- Breindl, M. (1971).** Structure of Heated Poliovirus Particles. *Journal of General Virology* **11**, 147-&.
- Bubeck, D., Filman, D.J., Cheng, N.Q., Steven, A.C., Hogle, J.M. and Belnap, D.M. (2005).** The Structure of the Poliovirus 135s Cell Entry Intermediate at 10-Angstrom Resolution Reveals the Location of an Externalized Polypeptide That Binds to Membranes. *Journal of Virology* **79**, 7745-7755.
- Bunch, T., Rieder, E. and Mason, P. (1994).** Sequence of the S-Fragment of Foot-and-Mouth-Disease Virus Type a(12). *Virus Genes* **8**, 173-175.
- Burckhardt, C.J., Suomalainen, M., Schoenenberger, P., Boucke, K., Hemmi, S. and Greber, U.F. (2011).** Drifting Motions of the Adenovirus Receptor Car and Immobile Integrins Initiate Virus Uncoating and Membrane Lytic Protein Exposure. *Cell Host & Microbe* **10**, 105-117.
- Campanella, M., de Jong, A.S., Lanke, K.W.H., Melchers, W.J.G., Willems, P., Pinton, P., Rizzuto, R. and van Kuppeveld, F.J.M. (2004).** The Coxsackievirus 2b Protein Suppresses Apoptotic Host Cell Responses by Manipulating Intracellular Ca<sup>2+</sup> Homeostasis. *Journal of Biological Chemistry* **279**, 18440-18450.
- Carter, S.D., Dent, K.C., Atkins, E., Foster, T.L., Verow, M., Gorny, P., Harris, M., Hiscox, J.A., Ranson, N.A., Griffin, S. and Barr, J.N. (2010).** Direct Visualization of the Small Hydrophobic Protein of Human Respiratory Syncytial Virus Reveals the Structural Basis for Membrane Permeability. *Febs Letters* **584**, 2786-2790.
- Casasnovas, J.M. and Springer, T.A. (1994).** Pathway of Rhinovirus Disruption by Soluble Intercellular-Adhesion Molecule-1 (Icam-1) - an Intermediate in Which Icam-1 Is Bound and Rna Is Released. *Journal of Virology* **68**, 5882-5889.

- Castello, A., Alvarez, E. and Carrasco, L. (2011).** The Multifaceted Poliovirus 2a Protease: Regulation of Gene Expression by Picornavirus Proteases. *Journal of Biomedicine and Biotechnology*.
- Chan, D.C. and Kim, P.S. (1998).** Hiv Entry and Its Inhibition. *Cell* **93**, 681-684.
- Chandran, K., Farsetta, D.L. and Nibert, M.L. (2002).** Strategy for Nonenveloped Virus Entry: A Hydrophobic Conformer of the Reovirus Membrane Penetration Protein Mu 1 Mediates Membrane Disruption. *Journal of Virology* **76**, 9920-9933.
- Chase, A.J. and Semler, B.L. (2012).** Viral Subversion of Host Functions for Picornavirus Translation and Rna Replication. *Future Virology* **7**, 179-191.
- Chejanovsky, N. and Loyter, A. (1985).** Fusion between Sendai Virus Envelopes and Biological-Membranes - the Use of Fluorescent-Probes for Quantitative Estimation of Virus-Membrane Fusion. *Journal of Biological Chemistry* **260**, 7911-7918.
- Chen, C.P. and Rost, B. (2002).** State-of-the-Art in Membrane Protein Prediction. *Applied bioinformatics* **1**, 21-35.
- Chen, D. and Texada, D.E. (2006).** Low-Usage Codons and Rare Codons of Escherichia Coli. *Gene Therapy and Molecular Biology* **10A**, 1-12.
- Chen, Z.G., Stauffacher, C., Li, Y.G., Schmidt, T., Wu, B.M., Kamer, G., Shanks, M., Lomonosoff, G. and Johnson, J.E. (1989).** Protein-Rna Interactions in an Icosahedral Virus at 3.0-Å Resolution. *Science* **245**, 154-159.
- Chevallet, M., Luche, S. and Rabilloud, T. (2006).** Silver Staining of Proteins in Polyacrylamide Gels. *Nature Protocols* **1**, 1852-1858.
- Chow, M., Newman, J.F.E., Filman, D., Hogle, J.M., Rowlands, D.J. and Brown, F. (1987).** Myristylation of Picornavirus Capsid Protein Vp4 and Its Structural Significance. *Nature, UK* **237**, 482-486.
- Clarke, B.E., Sangar, D.V., Burroughs, J.N., Newton, S.E., Carroll, A.R. and Rowlands, D.J. (1985).** 2 Initiation Sites for Foot-and-Mouth-Disease Virus Polyprotein In Vivo. *Journal of General Virology* **66**, 2615-2626.
- Clarke, D., Griffin, S., Beales, L., Gelais, C.S., Burgess, S., Harris, M. and Rowlands, D. (2006).** Evidence for the Formation of a Heptameric Ion Channel Complex by the Hepatitis C Virus P7 Protein in Vitro. *Journal of Biological Chemistry* **281**, 37057-37068.
- Clavijo, A., Wright, P. and Kitching, P. (2004).** Developments in Diagnostic Techniques for Differentiating Infection from Vaccination in Foot-and-Mouth Disease. *Veterinary Journal* **167**, 9-22.
- Cohen, L., Benichou, D. and Martin, A. (2002).** Analysis of Deletion Mutants Indicates That the 2a Polypeptide of Hepatitis a Virus Participates in Virion Morphogenesis. *Journal of Virology* **76**, 7495-7505.
- Compton, S.J. and Jones, C.G. (1985).** Mechanism of Dye Response and Interference in the Bradford Protein Assay. *Analytical Biochemistry* **151**, 369-374.
- Cook, G.A. and Opella, S.J. (2011).** Secondary Structure, Dynamics, and Architecture of the P7 Membrane Protein from Hepatitis C Virus by Nmr Spectroscopy. *Biochimica Et Biophysica Acta-Biomembranes* **1808**, 1448-1453.
- Corcoran, J.A., Syvitski, R., Top, D., Epand, R.M., Epand, R.F., Jakeman, D. and Duncan, R. (2004).** Myristoylation, a Protruding Loop, and Structural Plasticity Are Essential Features of a Nonenveloped Virus Fusion Peptide Motif. *Journal of Biological Chemistry* **279**, 51386-51394.
- Cuconati, A., Molla, A. and Wimmer, E. (1998).** Brefeldin a Inhibits Cell-Free, De Novo Synthesis of Poliovirus. *Journal of Virology* **72**, 6456-6464.
- Curry, S., Chow, M. and Hogle, J.M. (1996).** The Poliovirus 135s Particle Is Infectious. *Journal of Virology* **70**, 7125-7131.
- Curry, S., Fry, E., Blakemore, W., Abu-Ghazaleh, R., Jackson, T., King, A., Lea, S., Newman, J. and Stuart, D. (1997).** Dissecting the Roles of Vp0 Cleavage and Rna Packaging in Picornavirus Capsid Stabilization: The Structure of Empty Capsids of Foot-and-Mouth Disease Virus. *J Virol* **71**, 9743-9752.

- Danthi, P., Tosteson, M., Li, Q.H. and Chow, M. (2003).** Genome Delivery and Ion Channel Properties Are Altered in Vp4 Mutants of Poliovirus. *Journal of Virology* **77**, 5266-5274.
- Danthi, P. and Chow, M. (2004).** Cholesterol Removal by Methyl-Beta-Cyclodextrin Inhibits Poliovirus Entry. *Journal of Virology* **78**, 33-41.
- Davis, M.P., Bottley, G., Beales, L.P., Killington, R.A., Rowlands, D.J. and Tuthill, T.J. (2008).** Recombinant Vp4 of Human Rhinovirus Induces Permeability in Model Membranes. *Journal of Virology* **82**, 4169-4174.
- de Jong, A.S., de Mattia, F., Van Dommelen, M.M., Lanke, K., Melchers, W.J.G., Willems, P.H.G.M. and van Kuppeveld, F.J.M. (2008).** Functional Analysis of Picornavirus 2b Proteins: Effects on Calcium Homeostasis and Intracellular Protein Trafficking. *Journal of Virology* **82**, 3782-3790.
- De Palma, A.M., Vliegen, I., De Clercq, E. and Neyts, J. (2008).** Selective Inhibitors of Picornavirus Replication. *Medicinal Research Reviews* **28**, 823-884.
- Debernardezclark, E. and Georgiou, G. (1991).** Inclusion-Bodies and Recovery of Proteins from the Aggregated State. *Acs Symposium Series* **470**, 1-20.
- Denisova, E., Dowling, W., LaMonica, R., Shaw, R., Scarlata, S., Ruggeri, F. and Mackow, E.R. (1999).** Rotavirus Capsid Protein Vp5\* Permeabilizes Membranes. *Journal of Virology* **73**, 3147-3153.
- Dick, R.A., Goh, S.L., Feigenson, G.W. and Vogt, V.M. (2012).** Hiv-1 Gag Protein Can Sense the Cholesterol and Acyl Chain Environment in Model Membranes. *Proceedings of the National Academy of Sciences of the United States of America* **109**, 18761-18766.
- Doedens, J.R., Giddings, T.H. and Kirkegaard, K. (1997).** Inhibition of Endoplasmic Reticulum-to-Golgi Traffic by Poliovirus Protein 3a: Genetic and Ultrastructural Analysis. *Journal of Virology* **71**, 9054-9064.
- Donnelly, M.L.L., Gani, D., Flint, M., Monaghan, S. and Ryan, M.D. (1997).** The Cleavage Activities of Aphthovirus and Cardiovirus 2a Proteins. *Journal of General Virology* **78**, 13-21.
- Donnelly, M.L.L., Luke, G., Mehrotra, A., Li, X.J., Hughes, L.E., Gani, D. and Ryan, M.D. (2001).** Analysis of the Aphthovirus 2a/2b Polyprotein 'Cleavage' Mechanism Indicates Not a Proteolytic Reaction, but a Novel Translational Effect: A Putative Ribosomal 'Skip'. *Journal of General Virology* **82**, 1013-1025.
- Dougherty, R.H. and Fahy, J.V. (2009).** Acute Exacerbations of Asthma: Epidemiology, Biology and the Exacerbation-Prone Phenotype. *Clinical and Experimental Allergy* **39**, 193-202.
- Dowling, W., Denisova, E., LaMonica, R. and Mackow, E.R. (2000).** Selective Membrane Permeabilization by the Rotavirus Vp5\*Protein Is Abrogated by Mutations in an Internal Hydrophobic Domain. *Journal of Virology* **74**, 6368-6376.
- Duchardt, E., Sigalov, A.B., Aivazian, D., Stern, L.J. and Schwalbe, H. (2007).** Structure Induction of the T-Cell Receptor Zeta-Chain Upon Lipid Binding Investigated by Nmr Spectroscopy. *ChemBiochem* **8**, 820-827.
- Duff, K.C. and Ashley, R.H. (1992).** The Transmembrane Domain of Influenza-a M2 Protein Forms Amantadine-Sensitive Proton Channels in Planar Lipid Bilayers. *Virology* **190**, 485-489.
- Duronio, R.J., Jacksonmachelski, E., Heuckeroth, R.O., Olins, P.O., Devine, C.S., Yonemoto, W., Slice, L.W., Taylor, S.S. and Gordon, J.I. (1990).** Protein N-Myristoylation in Escherichia-Coli - Reconstitution of a Eukaryotic Protein Modification in Bacteria. *Proceedings of the National Academy of Sciences of the United States of America* **87**, 1506-1510.
- Dvorak, C.M.T., Hall, D.J., Hill, M., Riddle, M., Pranter, A., Dillman, J., Deibel, M. and Palmenberg, A.C. (2001).** Leader Protein of Encephalomyocarditis Virus Binds Zinc, Is Phosphorylated During Viral Infection, and Affects the Efficiency of Genome Translation. *Virology* **290**, 261-271.
- Ehrenfeld, E., Domingo, E. and Roos, R.P. (2010). Genome Organization and Encoded Proteins. In *The Picornaviruses*, pp. 3-17. Edited by E. Ehrenfeld, E. Domingo & R. P. Roos.
- Engel, S., Heger, T., Mancini, R., Herzog, F., Kartenbeck, J., Hayer, A. and Helenius, A. (2011).** Role of Endosomes in Simian Virus 40 Entry and Infection. *Journal of Virology* **85**, 4198-4211.
- Evans, D.J. and Almond, J.W. (1998).** Cell Receptors for Picornaviruses as Determinants of Cell Tropism and Pathogenesis. *Trends in Microbiology* **6**, 198-202.

- Evans, P., Bateman, O.A., Slingsby, C. and Wallace, B.A. (2007).** A Reference Dataset for Circular Dichroism Spectroscopy Tailored for the Beta Gamma-Crystallin Lens Proteins. *Experimental Eye Research* **84**, 1001-1008.
- Farazi, T.A., Waksman, G. and Gordon, J.I. (2001).** The Biology and Enzymology of Protein N-Myristoylation. *Journal of Biological Chemistry* **276**, 39501-39504.
- Fernandez, C. and Wuthrich, K. (2003).** Nmr Solution Structure Determination of Membrane Proteins Reconstituted in Detergent Micelles. *Febs Letters* **555**, 144-150.
- Filman, D.J., Syed, R., Chow, M., Macadam, A.J., Minor, P.D. and Hogle, J.M. (1989).** Structural Factors That Control Conformational Transitions and Serotype Specificity in Type-3 Poliovirus. *Embo Journal* **8**, 1567-1579.
- Fitzgerald, K.D. and Semler, B.L. (2011).** Re-Localization of Cellular Protein Srp20 During Poliovirus Infection: Bridging a Viral Ires to the Host Cell Translation Apparatus. *PLoS pathogens* **7**, e1002127-e1002127.
- Forss, S. and Schaller, H. (1982).** A Tandem Repeat Gene in a Picornavirus. *Nucleic Acids Research* **10**, 6441-6450.
- Fricks, C.E. and Hogle, J.M. (1990).** Cell-Induced Conformational Change in Poliovirus - Externalization of the Amino Terminus of Vp1 Is Responsible for Liposome Binding. *Journal of Virology* **64**, 1934-1945.
- Frottin, F., Martinez, A., Peynot, P., Mitra, S., Holz, R.C., Giglione, C. and Meinnel, T. (2006).** The Proteomics of N-Terminal Methionine Cleavage. *Molecular & Cellular Proteomics* **5**, 2336-2349.
- Fry, E.E., Newman, J.W., Curry, S., Najjam, S., Jackson, T., Blakemore, W., Lea, S.M., Miller, L., Burman, A., King, A.M. and Stuart, D.I. (2005a).** 1zbe: Foot-and Mouth Disease Virus Serotype A1061. *Protein Data Bank* **3.1**.
- Fry, E.E., Newman, J.W., Curry, S., Najjam, S., Jackson, T., Blakemore, W., Lea, S.M., Miller, L., Burman, A., King, A.M. and Stuart, D.I. (2005b).** 1zba: Foot-and-Mouth Disease Virus Serotype A1061 Complexed with Oligosaccharide Receptor. *Protein Data Bank* **3.1**.
- Fuchs, R. and Blaas, D. (2010).** Uncoating of Human Rhinoviruses. *Reviews in Medical Virology* **20**, 281-297.
- Fuchs, R. and Blaas, D. (2012).** Productive Entry Pathways of Human Rhinoviruses. *Advances in virology* **2012**, 826301-826301.
- Gallwitz, M., Enoksson, M., Thorpe, M. and Hellman, L. (2012).** The Extended Cleavage Specificity of Human Thrombin. *Plos One* **7**.
- Gamarnik, A.V. and Andino, R. (1998).** Switch from Translation to Rna Replication in a Positive-Stranded Rna Virus. *Genes & Development* **12**, 2293-2304.
- Gan, S.W., Ng, L., Lin, X., Gong, X. and Torres, J. (2008).** Structure and Ion Channel Activity of the Human Respiratory Syncytial Virus (Hrsv) Small Hydrophobic Protein Transmembrane Domain. *Protein Science* **17**, 813-820.
- Garriga, D., Pickl-Herk, A., Luque, D., Wruss, J., Caston, J.R., Blaas, D. and Verdaguer, N. (2012).** Insights into Minor Group Rhinovirus Uncoating: The X-Ray Structure of the Hrv2 Empty Capsid. *Plos Pathogens* **8**.
- Gautier, R., Douguet, D., Antonny, B. and Drin, G. (2008).** Heliquet: A Web Server to Screen Sequences with Specific Alpha-Helical Properties. *Bioinformatics* **24**, 2101-2102.
- Gazina, E.V., Mackenzie, J.M., Gorrell, R.J. and Anderson, D.A. (2002).** Differential Requirements for Copi Coats in Formation of Replication Complexes among Three Genera of Picornaviridae. *Journal of Virology* **76**, 11113-11122.
- Geller, R., Vignuzzi, M., Andino, R. and Frydman, J. (2007).** Evolutionary Constraints on Chaperone-Mediated Folding Provide an Antiviral Approach Refractory to Development of Drug Resistance. *Genes & Development* **21**, 195-205.
- Georgiou, C.D., Grintzalis, K., Zervoudakis, G. and Papapostolou, I. (2008).** Mechanism of Coomassie Brilliant Blue G-250 Binding to Proteins: A Hydrophobic Assay for Nanogram Quantities of Proteins. *Analytical and Bioanalytical Chemistry* **391**, 391-403.

- Gerber, K., Wimmer, E. and Paul, A.V. (2001).** Biochemical and Genetic Studies of the Initiation of Human Rhinovirus 2 Rna Replication: Purification and Enzymatic Analysis of the Rna-Dependent Rna Polymerase 3d(Pol). *Journal of Virology* **75**, 10969-10978.
- Gingras, A.C., Raught, B. and Sonenberg, N. (1999).** Eif4 Initiation Factors: Effectors of Mrna Recruitment to Ribosomes and Regulators of Translation. *Annual Review of Biochemistry* **68**, 913-963.
- Glueck, J.M., Hoffmann, S., Koenig, B.W. and Willbold, D. (2010).** Single Vector System for Efficient N-Myristoylation of Recombinant Proteins in E. Coli. *Plos One* **5**.
- Goodfellow, I., Chaudhry, Y., Richardson, A., Meredith, J., Almond, J.W., Barclay, W. and Evans, D.J. (2000).** Identification of a Cis-Acting Replication Element within the Poliovirus Coding Region. *Journal of Virology* **74**, 4590-4600.
- Goodfellow, I.G., Kerrigan, D. and Evans, D.J. (2003).** Structure and Function Analysis of the Poliovirus Cis-Acting Replication Element (Cre). *Rna-a Publication of the Rna Society* **9**, 124-137.
- Goodwin, S., Tuthill, T.J., Arias, A., Killington, R.A. and Rowlands, D.J. (2009).** Foot-and-Mouth Disease Virus Assembly: Processing of Recombinant Capsid Precursor by Exogenous Protease Induces Self-Assembly of Pentamers in Vitro in a Myristoylation-Dependent Manner. *Journal of Virology* **83**, 11275-11282.
- Greenfield, N.J. (2006).** Using Circular Dichroism Spectra to Estimate Protein Secondary Structure. *Nature Protocols* **1**, 2876-2890.
- Greninger, A.L., Knudsen, G.M., Betegon, M., Burlingame, A.L. and DeRisi, J.L. (2012).** The 3a Protein from Multiple Picornaviruses Utilizes the Golgi Adaptor Protein Acbd3 to Recruit Pi4kiii Beta. *Journal of Virology* **86**, 3605-3616.
- Greve, J.M., Forte, C.P., Marlor, C.W., Meyer, A.M., Hooverlitty, H., Wunderlich, D. and McClelland, A. (1991).** Mechanisms of Receptor-Mediated Rhinovirus Neutralization Defined by 2 Soluble Forms of Icam-1. *Journal of Virology* **65**, 6015-6023.
- Grubman, M.J. and Baxt, B. (2004).** Foot-and-Mouth Disease. *Clinical Microbiology Reviews* **17**, 465-+.
- Guarne, A., Tormo, J., Kirchweger, R., Pfistermueller, D., Fita, I. and Skern, T. (1998).** Structure of the Foot-and-Mouth Disease Virus Leader Protease: A Papain-Like Fold Adapted for Self-Processing and Eif4g Recognition. *Embo Journal* **17**, 7469-7479.
- Guglielmi, K.M., Johnson, E.M., Stehle, T. and Dermody, T.S. (2006).** Attachment and Cell Entry of Mammalian Orthoreovirus. *Reoviruses: Entry, Assembly and Morphogenesis* **309**, 1-38.
- Gustafsson, C., Govindarajan, S. and Minshull, J. (2004).** Codon Bias and Heterologous Protein Expression. *Trends in Biotechnology* **22**, 346-353.
- Hadfield, A.T., Lee, W.M., Zhao, R., Oliveira, M.A., Minor, I., Rueckert, R.R. and Rossmann, M.G. (1997).** The Refined Structure of Human Rhinovirus 16 at 2.15 Angstrom Resolution: Implications for the Viral Life Cycle. *Structure* **5**, 427-441.
- Hadfield, A.T., Diana, G.D. and Rossmann, M.G. (1999).** Analysis of Three Structurally Related Antiviral Compounds in Complex with Human Rhinovirus 16. *Proceedings of the National Academy of Sciences of the United States of America* **96**, 14730-14735.
- Hambidge, S.J. and Sarnow, P. (1992).** Translational Enhancement of the Poliovirus 5' Noncoding Region Mediated by Virus-Encoded Polypeptide-2a. *Proceedings of the National Academy of Sciences of the United States of America* **89**, 10272-10276.
- Han, X., Bushweller, J.H., Cafiso, D.S. and Tamm, L.K. (2001).** Membrane Structure and Fusion-Triggering Conformational Change of the Fusion Domain from Influenza Hemagglutinin. *Nature Structural Biology* **8**, 715-720.
- Harutyunyan, S., Kumar, M., Sedivy, A., Subirats, X., Kowalski, H., Kohler, G. and Blaas, D. (2013).** Viral Uncoating Is Directional: Exit of the Genomic Rna in a Common Cold Virus Starts with the Poly-(a) Tail at the 3'-End. *PLoS pathogens* **9**, e1003270-e1003270.
- Hato, S.V., Ricour, C., Schulte, B.M., Lanke, K.H.W., de Bruijini, M., Zoll, J., Melchers, W.J.G., Michiels, T. and van Kuppeveld, F.J.M. (2007).** The Mengovirus Leader Protein Blocks Interferon-

- Alpha/Beta Gene Transcription and Inhibits Activation of Interferon Regulatory Factor 3. *Cellular Microbiology* **9**, 2921-2930.
- He, Y.N., Mueller, S., Chipman, P.R., Bator, C.M., Peng, X.Z., Bowman, V.D., Mukhopadhyay, S., Wimmer, E., Kuhn, R.J. and Rossmann, M.G. (2003).** Complexes of Poliovirus Serotypes with Their Common Cellular Receptor, Cd155. *Journal of Virology* **77**, 4827-4835.
- Hellen, C.U.T. and Sarnow, P. (2001).** Internal Ribosome Entry Sites in Eukaryotic Mrna Molecules. *Genes & Development* **15**, 1593-1612.
- Herold, J. and Andino, R. (2001).** Poliovirus Rna Replication Requires Genome Circularization through a Protein-Protein Bridge. *Molecular Cell* **7**, 581-591.
- Hertzler, S., Luo, M. and Lipton, H.L. (2000).** Mutation of Predicted Virion Pit Residues Alters Binding of Theiler's Murine Encephalomyelitis Virus to Bhk-21 Cells. *Journal of Virology* **74**, 1994-2004.
- Hewat, E.A., Neumann, E., Conway, J.F., Moser, R., Ronacher, B., Marlovits, T.C. and Blaas, D. (2000).** The Cellular Receptor to Human Rhinovirus 2 Binds around the 5-Fold Axis and Not in the Canyon: A Structural View. *Embo Journal* **19**, 6317-6325.
- Hewat, E.A., Neumann, E. and Blaas, D. (2002).** The Concerted Conformational Changes During Human Rhinovirus 2 Uncoating. *Molecular Cell* **10**, 317-326.
- Hewat, E.A. and Blaas, D. (2004).** Cryoelectron Microscopy Analysis of the Structural Changes Associated with Human Rhinovirus Type 14 Uncoating. *Journal of Virology* **78**, 2935-2942.
- Hicks, A.L. and Duffy, S. (2011).** Genus-Specific Substitution Rate Variability among Picornaviruses. *Journal of Virology* **85**, 7942-7947.
- Hindiyeh, M., Li, Q.H., Basavappa, R., Hogle, J.M. and Chow, M. (1999).** Poliovirus Mutants at Histidine 195 of Vp2 Do Not Cleave Vp0 into Vp2 and Vp4. *Journal of Virology* **73**, 9072-9079.
- Hofer, F., Gruenberger, M., Kowalski, H., Machat, H., Huettinger, M., Kuechler, E. and Blaas, D. (1994).** Members of the Low-Density-Lipoprotein Receptor Family Mediate Cell Entry of a Minor-Group Common Cold Virus. *Proceedings of the National Academy of Sciences of the United States of America* **91**, 1839-1842.
- Hogle, J.M., Chow, M. and Filman, D.J. (1985).** 3-Dimensional Structure of Poliovirus at 2.9 a Resolution. *Science* **229**, 1358-1365.
- Hogle, J.M. (2002).** Poliovirus Cell Entry: Common Structural Themes in Viral Cell Entry Pathways. *Annual Review of Microbiology* **56**, 677-702.
- Hooverlitty, H. and Greve, J.M. (1993).** Formation of Rhinovirus-Soluble Icam-1 Complexes and Conformational-Changes in the Virion. *Journal of Virology* **67**, 390-397.
- Hope, D.A., Diamond, S.E. and Kirkegaard, K. (1997).** Genetic Dissection of Interaction between Poliovirus 3d Polymerase and Viral Protein 3ab. *Journal of Virology* **71**, 9490-9498.
- Hsu, N.-Y., Ilnytska, O., Belov, G., Santiana, M., Chen, Y.-H., Takvorian, P.M., Pau, C., van der Schaar, H., Kaushik-Basu, N., Balla, T., Cameron, C.E., Ehrenfeld, E., van Kuppeveld, F.J.M. and Altan-Bonnet, N. (2010).** Viral Reorganization of the Secretory Pathway Generates Distinct Organelles for Rna Replication. *Cell* **141**, 799-811.
- Ikemura, T. (1985).** Codon Usage and Transfer-Rna Content in Unicellular and Multicellular Organisms. *Molecular Biology and Evolution* **2**, 13-34.
- Iruzun, A., Perez, L. and Carrasco, L. (1992).** Involvement of Membrane Traffic in the Replication of Poliovirus Genomes - Effects of Brefeldin-A. *Virology* **191**, 166-175.
- Ivanovic, T., Agosto, M.A., Zhang, L., Chandran, K., Harrison, S.C. and Nibert, M.L. (2008).** Peptides Released from Reovirus Outer Capsid Form Membrane Pores That Recruit Virus Particles. *Embo Journal* **27**, 1289-1298.
- Iwai, H. and Zuger, S. (2007).** Protein Ligation: Applications in Nmr Studies of Proteins. *Biotechnology & genetic engineering reviews* **24**, 129-145.
- Jackson, R.J., Hunt, S.L., Gibbs, C.L. and Kaminski, A. (1994).** Internal Initiation of Translation of Picornavirus Rnas. *Molecular Biology Reports* **19**, 147-159.
- Jackson, T., Ellard, F.M., Ghazaleh, R.A., Brookes, S.M., Blakemore, W.E., Corteyn, A.H., Stuart, D.I., Newman, J.W. and King, A.M.Q. (1996).** Efficient Infection of Cells in Culture by Type O Foot-and-



- Mouth Disease Virus Requires Binding to Cell Surface Heparan Sulfate. *Journal of Virology* **70**, 5282-5287.
- Jackson, T., Sharma, A., AbuGhazaleh, R., Blakemore, W.E., Ellard, F.M., Simmons, D.L., Newman, J.W.I., Stuart, D.I. and King, A.M.Q. (1997).** Arginine-Glycine Aspartic Acid-Specific Binding by Foot-and-Mouth Disease Viruses to the Purified Integrin Alpha V Beta 3 in Vitro. *Journal of Virology* **71**, 8357-8361.
- Jackson, T., King, A.M.Q., Stuart, D.I. and Fry, E. (2003).** Structure and Receptor Binding. *Virus Research* **91**, 33-46.
- Joachims, M., Van Breugel, P.C. and Lloyd, R.E. (1999).** Cleavage of Poly(a)-Binding Protein by Enterovirus Proteases Concurrent with Inhibition of Translation in Vitro. *Journal of Virology* **73**, 718-727.
- Jones, D.T. (2007).** Improving the Accuracy of Transmembrane Protein Topology Prediction Using Evolutionary Information. *Bioinformatics* **23**, 538-544.
- Jones, K.L., Smyth, R.P., Pereira, C.F., Cameron, P.U., Lewin, S.R., Jaworowski, A. and Mak, J. (2011).** Early Events of Hiv-1 Infection: Can Signaling Be the Next Therapeutic Target? *Journal of Neuroimmune Pharmacology* **6**, 269-283.
- Kang, C., Tian, C., Soennichsen, F.D., Smith, J.A., Meiler, J., George, A.L., Jr., Vanoye, C.G., Kim, H.J. and Sanders, C.R. (2008).** Structure of Kcne1 and Implications for How It Modulates the Kcnq1 Potassium Channel. *Biochemistry* **47**, 7999-8006.
- Kato, A., Maki, K., Ebina, T., Kuwajima, K., Soda, K. and Kuroda, Y. (2007).** Mutational Analysis of Protein Solubility Enhancement Using Short Peptide Tags. *Biopolymers* **85**, 12-18.
- Katpally, U., Fu, T.M., Freed, D.C., Casimiro, D.R. and Smith, T.J. (2009).** Antibodies to the Buried N Terminus of Rhinovirus Vp4 Exhibit Cross-Serotypic Neutralization. *Journal of Virology* **83**, 7040-7048.
- Kelly, S.M. and Price, N.C. (2000).** The Use of Circular Dichroism in the Investigation of Protein Structure and Function. *Current Protein & Peptide Science* **1**, 349-384.
- Kerkvliet, J., Edukulla, R. and Rodriguez, M. (2010).** Novel Roles of the Picornaviral 3d Polymerase in Viral Pathogenesis. *Advances in Virology* **2010**, 368068-Article ID 368068.
- Kew, O.M., Sutter, R.W., de Gourville, E.M., Dowdle, W.R. and Pallansch, M.A. (2005). Vaccine-Derived Polioviruses and the Endgame Strategy for Global Polio Eradication. In *Annual Review of Microbiology*, pp. 587-635.
- Kielian, M., Chanel-Vos, C. and Liao, M. (2010).** Alphavirus Entry and Membrane Fusion. *Viruses-Basel* **2**, 796-825.
- Kienberger, F., Zhu, R., Moser, R., Blaas, D. and Hinterdorfer, P. (2004).** Monitoring Rna Release from Human Rhinovirus by Dynamic Force Microscopy. *Journal of Virology* **78**, 3203-3209.
- Kirkegaard, K. (1990).** Mutations in Vp1 of Poliovirus Specifically Affect Both Encapsidation and Release of Viral-Rna. *Journal of Virology* **64**, 195-206.
- Kolatkar, P.R., Bella, J., Olson, N.H., Bator, C.M., Baker, T.S. and Rossmann, M.G. (1999).** Structural Studies of Two Rhinovirus Serotypes Complexed with Fragments of Their Cellular Receptor. *Embo Journal* **18**, 6249-6259.
- Krausslich, H.G., Nicklin, M.J.H., Toyoda, H., Etchison, D. and Wimmer, E. (1987).** Poliovirus Proteinase-2a Induces Cleavage of Eukaryotic Initiation Factor-4f Polypeptide-P220. *Journal of Virology* **61**, 2711-2718.
- Krueger-Koplin, R.D., Sorgen, P.L., Krueger-Koplin, S.T., Rivera-Torres, A.O., Cahill, S.M., Hicks, D.B., Grinius, L., Krulwich, T.A. and Girvin, M.E. (2004).** An Evaluation of Detergents for Nmr Structural Studies of Membrane Proteins. *Journal of Biomolecular Nmr* **28**, 43-57.
- Kuehne, J. and Murphy, R.M. (2001).** Synthesis and Characterization of Membrane-Active Gala-Okt9 Conjugates. *Bioconjugate Chemistry* **12**, 742-749.
- Ladokhin, A.S., Selsted, M.E. and White, S.H. (1997).** Sizing Membrane Pores in Lipid Vesicles by Leakage of Co-Encapsulated Markers: Pore Formation by Melittin. *Biophysical Journal* **72**, 1762-1766.

- Lama, J., Paul, A.V., Harris, K.S. and Wimmer, E. (1994).** Properties of Purified Recombinant Poliovirus Protein 3ab as Substrate for Viral Proteinases and as Cofactor for Rna-Polymerase 3d(Pol). *Journal of Biological Chemistry* **269**, 66-70.
- Lentz, K. and Arnold, E. (1998).** 1eah: Pv2I Complexed with Antiviral Agent Sch48973. *Protein Data Bank*.
- Lentz, K.N., Smith, A.D., Geisler, S.C., Cox, S., Buontempo, P., Skelton, A., DeMartino, J., Rozhon, E., Schwartz, J., Girijavallabhan, V., Oconnell, J. and Arnold, E. (1997).** Structure of Poliovirus Type 2 Lansing Complexed with Antiviral Agent Sch48973: Comparison of the Structural and Biological Properties of the Three Poliovirus Serotypes. *Structure* **5**, 961-978.
- Leung, J.Y.-S., Ng, M.M.-L. and Chu, J.J.H. (2011).** Replication of Alphaviruses: A Review on the Entry Process of Alphaviruses into Cells. *Advances in virology* **2011**, 249640-249640.
- Levy, H.C., Bostina, M., Filman, D.J. and Hogle, J.M. (2010).** Catching a Virus in the Act of Rna Release: A Novel Poliovirus Uncoating Intermediate Characterized by Cryo-Electron Microscopy. *Journal of Virology* **84**, 4426-4441.
- Lewis, J.K., Bothner, B., Smith, T.J. and Siuzdak, G. (1998).** Antiviral Agent Blocks Breathing of the Common Cold Virus. *Proceedings of the National Academy of Sciences of the United States of America* **95**, 6774-6778.
- Li, Q.H., Yafal, A.G., Lee, Y.M.H., Hogle, J. and Chow, M. (1994).** Poliovirus Neutralization by Antibodies to Internal Epitopes of Vp4 and Vp1 Results from Reversible Exposure of These Sequences at Physiological Temperature. *Journal of Virology* **68**, 3965-3970.
- Li, X., Li, Y.F., Han, H.Y., Miller, D.W. and Wang, G.S. (2006).** Solution Structures of Human LI-37 Fragments and Nmr-Based Identification of a Minimal Membrane-Targeting Antimicrobial and Anticancer Region. *Journal of the American Chemical Society* **128**, 5776-5785.
- Lin, J., Lee, L.Y., Roivainen, M., Filman, D.J., Hogle, J.M. and Belnap, D.M. (2012).** Structure of the Fab-Labeled "Breathing" State of Native Poliovirus. *Journal of Virology* **86**, 5959-5962.
- Lin, S.-H. and Guidotti, G. (2009). Purification of Membrane Proteins. In *Guide to Protein Purification, Second Edition*, pp. 619-629. Edited by R. R. Burgess & M. P. Deutscher.
- Ludert, J.E., Feng, N.G., Yu, J.H., Broome, R.L., Hoshino, Y. and Greenberg, H.B. (1996).** Genetic Mapping Indicates That Vp4 Is the Rotavirus Cell Attachment Protein in Vitro and in Vivo. *Journal of Virology* **70**, 487-493.
- Luo, J., Xu, X., Hall, H., Hyland, E.M., Boeke, J.D., Hazbun, T. and Kuo, M.-H. (2010).** Histone H3 Exerts a Key Function in Mitotic Checkpoint Control. *Molecular and Cellular Biology* **30**, 537-549.
- Luo, M., Vriend, G., Kamer, G., Minor, I., Arnold, E., Rossmann, M.G., Boege, U., Scraba, D.G., Duke, G.M. and Palmenberg, A.C. (1987).** The Atomic-Structure of Mengo-Virus at 3.0-Å Resolution. *Science* **235**, 182-191.
- Ma, C., Polishchuk, A.L., Ohigashi, Y., Stouffer, A.L., Schoen, A., Magavern, E., Jing, X., Lear, J.D., Freire, E., Lamb, R.A., DeGrado, W.F. and Pinto, L.H. (2009).** Identification of the Functional Core of the Influenza A Virus A/M2 Proton-Selective Ion Channel. *Proceedings of the National Academy of Sciences of the United States of America* **106**, 12283-12288.
- Madan, V., Sanchez-Martinez, S., Vedovato, N., Rispoli, G., Carrasco, L. and Nieva, J.L. (2007).** Plasma Membrane-Porating Domain in Poliovirus 2b Protein. A Short Peptide Mimics Viroporin Activity. *Journal of Molecular Biology* **374**, 951-964.
- Mahy, B.W.J. (2005).** Introduction and History of Foot-and-Mouth Disease Virus. *Foot and Mouth Disease Virus* **288**, 1-8.
- Maia, L.F., Soares, M.R., Valente, A.P., Almeida, F.C.L., Oliveira, A.C., Gomes, A.M.O., Freitas, M.S., Schneemann, A., Johnson, J.E. and Silva, J.L. (2006).** Structure of a Membrane-Binding Domain from a Non-Enveloped Animal Virus - Insights into the Mechanism of Membrane Permeability and Cellular Entry. *Journal of Biological Chemistry* **281**, 29278-29286.
- Maier, O., Galan, D.L., Wodrich, H. and Wiethoff, C.M. (2010).** An N-Terminal Domain of Adenovirus Protein Vi Fragments Membranes by Inducing Positive Membrane Curvature. *Virology* **402**, 11-19.

- Maier, O. and Wiethoff, C.M. (2010).** N-Terminal Alpha-Helix-Independent Membrane Interactions Facilitate Adenovirus Protein Vi Induction of Membrane Tubule Formation. *Virology* **408**, 31-38.
- Makela, M.J., Puhakka, T., Ruuskanen, O., Leinonen, M., Saikku, P., Kimpimaki, M., Blomqvist, S., Hyypia, T. and Arstila, P. (1998).** Viruses and Bacteria in the Etiology of the Common Cold. *Journal of Clinical Microbiology* **36**, 539-542.
- Marc, D., Masson, G., Girard, M. and Vanderwerf, S. (1990).** Lack of Myristoylation of Poliovirus Capsid Polypeptide Vp0 Prevents the Formation of Virions or Results in the Assembly of Noninfectious Virus-Particles. *Journal of Virology* **64**, 4099-4107.
- Marcotte, L.L., Wass, A.B., Gohara, D.W., Pathak, H.B., Arnold, J.J., Filman, D.J., Cameron, C.E. and Hogle, J.M. (2007).** Crystal Structure of Poliovirus 3cd Protein: Virally Encoded Protease and Precursor to the Rna-Dependent Rna Polymerase. *Journal of Virology* **81**, 3583-3596.
- Marongiu, M.E., Pani, A., Corrias, M.V., Sau, M. and Lacolla, P. (1981).** Poliovirus Morphogenesis .1. Identification of 80s Dissociable Particles and Evidence for the Artifacts Production of Procapsids. *Journal of Virology* **39**, 341-347.
- Martin-Belmonte, F., Lopez-Guerrero, J.A., Carrasco, L. and Alonso, M.A. (2000).** The Amino-Terminal Nine Amino Acid Sequence of Poliovirus Capsid Vp4 Protein Is Sufficient to Confer N-Myristoylation and Targeting to Detergent-Insoluble Membranes. *Biochemistry* **39**, 1083-1090.
- Martinez-Gil, L., Sauri, A., Marti-Renom, M.A. and Mingarro, I. (2011).** Membrane Protein Integration into the Endoplasmic Reticulum. *Febs Journal* **278**, 3846-3858.
- Marvil, P., Knowles, N.J., Mockett, A.P.A., Britton, P., Brown, T.D.K. and Cavanagh, D. (1999).** Avian Encephalomyelitis Virus Is a Picornavirus and Is Most Closely Related to Hepatitis a Virus. *Journal of General Virology* **80**, 653-662.
- Maslennikov, I., Klammt, C., Hwang, E., Kefala, G., Okamura, M., Esquivies, L., Moers, K., Glaubitz, C., Kwiatkowski, W., Jeon, Y.H. and Choe, S. (2010).** Membrane Domain Structures of Three Classes of Histidine Kinase Receptors by Cell-Free Expression and Rapid Nmr Analysis. *Proceedings of the National Academy of Sciences of the United States of America* **107**, 10902-10907.
- Mason, P.W., Baxt, B., Brown, F., Harber, J., Murdin, A. and Wimmer, E. (1993).** Antibody-Complexed Foot-and-Mouth-Disease Virus, but Not Poliovirus, Can Infect Normally Unsusceptible Cells Via the Fc Receptor. *Virology* **192**, 568-577.
- Mason, P.W., Rieder, E. and Baxt, B. (1994).** Rgd Sequence of Foot-and-Mouth-Disease Virus Is Essential for Infecting Cells Via the Natural Receptor but Can Be Bypassed by an Antibody-Dependent Enhancement Pathway. *Proceedings of the National Academy of Sciences of the United States of America* **91**, 1932-1936.
- Mason, P.W., Bezborodova, S.V. and Henry, T.M. (2002).** Identification and Characterization of a Cis-Acting Replication Element (Cre) Adjacent to the Internal Ribosome Entry Site of Foot-and-Mouth Disease Virus. *Journal of Virology* **76**, 9686-9694.
- Mateu, M.G. (2011).** Virus Engineering: Functionalization and Stabilization. *Protein Engineering Design & Selection* **24**, 53-63.
- Matsubara, M., Tao, J., Kawamura, K., Shimojo, N., Titani, K., Hashimoto, K. and Hayashi, N. (2005).** Myristoyl Moiety of Hiv Nef Is Involved in Regulation of the Interaction with Calmodulin in Vivo. *Protein Science* **14**, 494-503.
- Matthews, D., Smith, W.W., Ferre, R.A., Condon, B., Budahazi, G., Sisson, W., Villafranca, J.E., Janson, C., McElroy, H., Gribskov, C. and Worland, S. (1994).** Crystal Structure of Human Rhinovirus Type 14 3c Protease. *Journal of Cellular Biochemistry Supplement* **0**, 170-170.
- Maxfield, F.R. and Yamashiro, D.J. (1987).** Endosome Acidification and the Pathways of Receptor-Mediated Endocytosis. *Advances in experimental medicine and biology* **225**, 189-198.
- Maxfield, F.R. and Wustner, D. (2002).** Intracellular Cholesterol Transport. *Journal of Clinical Investigation* **110**, 891-898.
- McGregor, S., Hall, L. and Rueckert, R.R. (1975).** Evidence for Existence of Protomers in Assembly of Encephalomyocarditis Virus. *Journal of Virology* **15**, 1107-1120.

- McGregor, S. and Rueckert, R.R. (1977).** Picornaviral Capsid Assembly - Similarity of Rhinovirus and Enterovirus Precursor Subunits. *Journal of Virology* **21**, 548-553.
- McKnight, K.L. and Lemon, S.M. (1998).** The Rhinovirus Type 14 Genome Contains an Internally Located Rna Structure That Is Required for Viral Replication. *Rna-a Publication of the Rna Society* **4**, 1569-1584.
- Medina, M., Domingo, E., Brangwyn, J.K. and Belsham, G.J. (1993).** The 2 Species of the Foot-and-Mouth-Disease Virus Leader Protein, Expressed Individually, Exhibit the Same Activities. *Virology* **194**, 355-359.
- Meier, O. and Greber, U.F. (2004).** Adenovirus Endocytosis. *Journal of Gene Medicine* **6**, S152-S163.
- Merril, C.R., Bisher, M.E., Harrington, M. and Steven, A.C. (1988).** Coloration of Silver-Stained Protein Bands in Polyacrylamide Gels Is Caused by Light-Scattering from Silver Grains of Characteristic Sizes. *Proceedings of the National Academy of Sciences of the United States of America* **85**, 453-457.
- Moffat, K., Howell, G., Knox, C., Belsham, G.J., Monaghan, P., Ryan, M.D. and Wileman, T. (2005).** Effects of Foot-and-Mouth Disease Virus Nonstructural Proteins on the Structure and Function of the Early Secretory Pathway: 2bc but Not 3a Blocks Endoplasmic Reticulum-to-Golgi Transport. *Journal of Virology* **79**, 4382-4395.
- Moffat, K., Knox, C., Howell, G., Clark, S.J., Yang, H., Belsham, G.J., Ryan, M. and Wileman, T. (2007).** Inhibition of the Secretory Pathway by Foot-and-Mouth Disease Virus 2bc Protein Is Reproduced by Coexpression of 2b with 2c, and the Site of Inhibition Is Determined by the Subcellular Location of 2c. *Journal of Virology* **81**, 1129-1139.
- Monaghan, P., Gold, S., Simpson, J., Zhang, Z.D., Weinreb, P.H., Violette, S.M., Alexandersen, S. and Jackson, T. (2005).** The Alpha V Beta 6 Integrin Receptor for Foot-and-Mouth Disease Virus Is Expressed Constitutively on the Epithelial Cells Targeted in Cattle. *Journal of General Virology* **86**, 2769-2780.
- Montserret, R., Saint, N., Vanbelle, C., Salvay, A.G., Simorre, J.-P., Ebel, C., Sapay, N., Renisio, J.-G., Boeckmann, A., Steinmann, E., Pietschmann, T., Dubuisson, J., Chipot, C. and Penin, F. (2010).** Nmr Structure and Ion Channel Activity of the P7 Protein from Hepatitis C Virus. *Journal of Biological Chemistry* **285**, 31446-31461.
- Morellet, N., Bouaziz, S., Petitjean, P. and Roques, B.P. (2003).** Nmr Structure of the Hiv-1 Regulatory Protein Vpr. *Journal of Molecular Biology* **327**, 215-227.
- Moscufo, N., Simons, J. and Chow, M. (1991).** Myristoylation Is Important at Multiple Stages in Poliovirus Assembly. *Journal of Virology* **65**, 2372-2380.
- Moscufo, N. and Chow, M. (1992).** Myristate-Protein Interactions in Poliovirus - Interactions of Vp4 Threonine-28 Contribute to the Structural Conformation of Assembly Intermediates and the Stability of Assembled Virions. *Journal of Virology* **66**, 6849-6857.
- Mosimann, S.C., Cherney, M.M., Sia, S., Plotch, S. and James, M.N.G. (1997).** Refined X-Ray Crystallographic Structure of the Poliovirus 3c Gene Product. *Journal of Molecular Biology* **273**, 1032-1047.
- Moyer, C.L., Wiethoff, C.M., Maier, O., Smith, J.G. and Nemerow, G.R. (2011).** Functional Genetic and Biophysical Analyses of Membrane Disruption by Human Adenovirus. *Journal of Virology* **85**, 2631-2641.
- Muckelbauer, J.K., Kremer, M., Minor, I., Diana, G., Dutko, F.J., Groarke, J., Pevear, D.C. and Rossmann, M.G. (1995).** The Structure of Coxsackievirus B3 at 3.5 Angstrom Resolution. *Structure* **3**, 653-667.
- Murray, D., Matsumoto, L.H., Buser, C.A., Tsang, J., Sigal, C.T., Ben-Tal, N., Honig, B., Resh, M.D. and McLaughlin, S. (1998).** Electrostatics and the Membrane Association of Src: Theory and Experiment. *Biochemistry* **37**, 2145-2159.
- Murray, K.E. and Barton, D.J. (2003).** Poliovirus Cre-Dependent Vpg Uridylylation Is Required for Positive-Strand Rna Synthesis but Not for Negative-Strand Rna Synthesis. *Journal of Virology* **77**, 4739-4750.

- Nathanson, N. (2008). The Pathogenesis of Poliomyelitis: What We Don't Know. In *Advances in Virus Research, Vol 71*, pp. 1-50. Edited by K. Maramorosch, A. J. Shatkin & F. A. Murphy.
- Nayak, A., Goodfellow, I.G. and Belsham, G.J. (2005).** Factors Required for the Uridylylation of the Foot-and-Mouth Disease Virus 3b1, 3b2, and 3b3 Peptides by the Rna-Dependent Rna Polymerase (3d(Pol)) in Vitro. *Journal of Virology* **79**, 7698-7706.
- Nayak, A., Goodfellow, I.G., Woolaway, K.E., Birtley, J., Curry, S. and Belsham, G.J. (2006).** Role of Rna Structure and Rna Binding Activity of Foot-and-Mouth Disease Virus 3c Protein in Vpg Uridylylation and Virus Replication. *Journal of Virology* **80**, 9865-9875.
- Newton, S.E., Carroll, A.R., Campbell, R.O., Clarke, B.E. and Rowlands, D.J. (1985).** The Sequence of Foot-and-Mouth-Disease Virus-Rna to the 5' Side of the Poly(C) Tract. *Gene* **40**, 331-336.
- Nicol, F., Nir, S. and Szoka, F.C. (1996).** Effect of Cholesterol and Charge on Pore Formation in Bilayer Vesicles by a Ph-Sensitive Peptide. *Biophysical Journal* **71**, 3288-3301.
- Nicol, F., Nir, S. and Szoka, F.C. (2000).** Effect of Phospholipid Composition on an Amphipathic Peptide-Mediated Pore Formation in Bilayer Vesicles. *Biophysical Journal* **78**, 818-829.
- Nielsen, B.L. and Brown, L.R. (1984).** The Basis for Colored Silver Protein Complex-Formation in Stained Polyacrylamide Gels. *Analytical Biochemistry* **141**, 311-315.
- Nishimura, Y. and Shimizu, H. (2009).** Identification of P-Selectin Glycoprotein Ligand-1 as One of the Cellular Receptors for Enterovirus 71. *Uirusu* **59**, 195-203.
- Nugent, C.I., Johnson, K.L., Sarnow, P. and Kirkegaard, K. (1999).** Functional Coupling between Replication and Packaging of Poliovirus Replicon Rna. *Journal of Virology* **73**, 427-435.
- Nugent, T. and Jones, D.T. (2009).** Transmembrane Protein Topology Prediction Using Support Vector Machines. *Bmc Bioinformatics* **10**.
- Nurani, G., Lindqvist, B. and Casasnovas, J.M. (2003).** Receptor Priming of Major Group Human Rhinoviruses for Uncoating and Entry at Mild Low-Ph Environments. *Journal of Virology* **77**, 11985-11991.
- O'Donnell, V., LaRocco, M. and Baxt, B. (2008).** Heparan Sulfate-Binding Foot-and-Mouth Disease Virus Enters Cells Via Caveola-Mediated Endocytosis. *Journal of Virology* **82**, 9075-9085.
- Odegard, A.L., Chandran, K., Zhang, X., Parker, J.S.L., Baker, T.S. and Nibert, M.L. (2004).** Putative Autocleavage of Outer Capsid Protein Mu 1, Allowing Release of Myristoylated Peptide Mu 1n During Particle Uncoating, Is Critical for Cell Entry by Reovirus. *Journal of Virology* **78**, 8732-8745.
- Olson, N.H., Kolatkar, P.R., Oliveira, M.A., Cheng, R.H., Greve, J.M., McClelland, A., Baker, T.S. and Rossmann, M.G. (1993).** Structure of a Human Rhinovirus Complexed with Its Receptor Molecule. *Proceedings of the National Academy of Sciences of the United States of America* **90**, 507-511.
- Palmenberg, A.C., Spiro, D., Kuzmickas, R., Wang, S., Djikeng, A., Rathe, J.A., Fraser-Liggett, C.M. and Liggett, S.B. (2009).** Sequencing and Analyses of All Known Human Rhinovirus Genomes Reveal Structure and Evolution. *Science* **324**, 55-59.
- Parente, R.A., Nir, S. and Szoka, F.C. (1990).** Mechanism of Leakage of Phospholipid Vesicle Contents Induced by the Peptide Gala. *Biochemistry* **29**, 8720-8728.
- Parsley, T.B., Towner, J.S., Blyn, L.B., Ehrenfeld, E. and Semler, B.L. (1997).** Poly (Rc) Binding Protein 2 Forms a Ternary Complex with the 5'-Terminal Sequences of Poliovirus Rna and the Viral 3cd Proteinase. *Rna-a Publication of the Rna Society* **3**, 1124-1134.
- Pathak, H.B., Oh, H.S., Goodfellow, I.G., Arnold, J.J. and Cameron, C.E. (2008).** Picornavirus Genome Replication: Roles of Precursor Proteins and Rate-Limiting Steps in Orii-Dependent Vpg Uridylylation. *The Journal of biological chemistry* **283**, 30677-30688.
- Paul, A.V., Cao, X.M., Harris, K.S., Lama, J. and Wimmer, E. (1994).** Studies with Poliovirus Polymerase 3d(Pol) - Stimulation of Poly(U) Synthesis in-Vitro by Purified Poliovirus Protein 3ab. *Journal of Biological Chemistry* **269**, 29173-29181.
- Perera, R., Daijogo, S., Walter, B.L., Nguyen, J.H.C. and Semler, B.L. (2007).** Cellular Protein Modification by Poliovirus: The Two Faces of Poly(Rc)-Binding Protein. *Journal of Virology* **81**, 8919-8932.

- Petersen, J.F.W., Cherney, M.M., Liebig, H.D., Skern, T., Kuechler, E. and James, M.N.G. (1999).** The Structure of the 2a Proteinase from a Common Cold Virus: A Proteinase Responsible for the Shut-Off of Host-Cell Protein Synthesis. *Embo Journal* **18**, 5463-5475.
- Plempner, R.K. (2011).** Cell Entry of Enveloped Viruses. *Current Opinion in Virology* **1**, 92-100.
- Plevka, P., Perera, R., Yap, M.L., Cardosa, J., Kuhn, R.J. and Rossmann, M.G. (2013).** Structure of Human Enterovirus 71 in Complex with a Capsid-Binding Inhibitor. *Proceedings of the National Academy of Sciences of the United States of America* **110**, 5463-5467.
- Porta, C., Kotecha, A., Burman, A., Jackson, T., Ren, J., Loureiro, S., Jones, I.M., Fry, E.E., Stuart, D.I. and Charleston, B. (2013).** Rational Engineering of Recombinant Picornavirus Capsids to Produce Safe, Protective Vaccine Antigen. *PLoS pathogens* **9**, e1003255-e1003255.
- Powell, R.M., Schmitt, V., Ward, T., Goodfellow, I., Evans, D.J. and Almond, J.W. (1998).** Characterization of Echoviruses That Bind Decay Accelerating Factor (Cd55): Evidence That Some Haemagglutinating Strains Use More Than One Cellular Receptor. *Journal of General Virology* **79**, 1707-1713.
- Prasad, B.V. and Chiu, W. (1994).** Structure of Rotavirus. *Current topics in microbiology and immunology* **185**, 9-29.
- Prchla, E., Kuechler, E., Blaas, D. and Fuchs, R. (1994).** Uncoating of Human Rhinovirus Serotype-2 from Late Endosomes. *Journal of Virology* **68**, 3713-3723.
- Prchla, E., Plank, C., Wagner, E., Blaas, D. and Fuchs, R. (1995).** Virus-Mediated Release of Endosomal Content in-Vitro - Different Behavior of Adenovirus and Rhinovirus Serotype-2. *Journal of Cell Biology* **131**, 111-123.
- Putnak, J.R. and Phillips, B.A. (1981).** Picornaviral Structure and Assembly. *Microbiological Reviews* **45**, 287-315.
- Racaniello, V.R. (1996).** Early Events in Poliovirus Infection: Virus-Receptor Interactions. *Proceedings of the National Academy of Sciences of the United States of America* **93**, 11378-11381.
- Raghava, S., Giorda, K.M., Romano, F.B., Heuck, A.P. and Hebert, D.N. (2011).** The Sv40 Late Protein Vp4 Is a Viroporin That Forms Pores to Disrupt Membranes for Viral Release. *Plos Pathogens* **7**.
- Reckel, S., Sobhanifar, S., Schneider, B., Junge, F., Schwarz, D., Durst, F., Loehr, F., Guentert, P., Bernhard, F. and Doetsch, V. (2008).** Transmembrane Segment Enhanced Labeling as a Tool for the Backbone Assignment of Alpha-Helical Membrane Proteins. *Proceedings of the National Academy of Sciences of the United States of America* **105**, 8262-8267.
- Resh, M.D. (1999).** Fatty Acylation of Proteins: New Insights into Membrane Targeting of Myristoylated and Palmitoylated Proteins. *Biochimica Et Biophysica Acta-Molecular Cell Research* **1451**, 1-16.
- Rodriguez, L.L. and Gay, C.G. (2011).** Development of Vaccines toward the Global Control and Eradication of Foot-and-Mouth Disease. *Expert Review of Vaccines* **10**, 377-387.
- Rodriguez, P.L. and Carrasco, L. (1993).** Poliovirus Protein-2c Has Atpase and Gtpase Activities. *Journal of Biological Chemistry* **268**, 8105-8110.
- Roivainen, M., Piirainen, L., Rysa, T., Narvanen, A. and Hovi, T. (1993).** An Immunodominant N-Terminal Region of Vp1 Protein of Poliovirion That Is Buried in Crystal-Structure Can Be Exposed in Solution. *Virology* **195**, 762-765.
- Rosenberg, M.R. and Casarotto, M.G. (2010).** Coexistence of Two Adamantane Binding Sites in the Influenza a M2 Ion Channel. *Proceedings of the National Academy of Sciences of the United States of America* **107**, 13866-13871.
- Rossmann, M.G., Arnold, E., Erickson, J.W., Frankenberger, E.A., Griffith, J.P., Hecht, H.J., Johnson, J.E., Kamer, G., Luo, M., Mosser, A.G., Rueckert, R.R., Sherry, B. and Vriend, G. (1985).** Structure of a Human Common Cold Virus and Functional-Relationship to Other Picornaviruses. *Nature* **317**, 145-153.
- Rossmann, M.G. (1994).** Viral Cell Recognition and Entry. *Protein Science* **3**, 1712-1725.

- Rossmann, M.G., Bella, J., Kolatkar, P.R., He, Y.N., Wimmer, E., Kuhn, R.J. and Baker, T.S. (2000). Cell Recognition and Entry by Rhino- and Enteroviruses. *Virology* **269**, 239-247.
- Rossmann, M.G., He, Y.N. and Kuhn, R.J. (2002). Picornavirus-Receptor Interactions. *Trends in Microbiology* **10**, 324-331.
- Rowlands, D., Logan, D., Abu-Ghazaleh, R., Blakemore, W., Curry, S., Jackson, T., King, A., Lea, S., Lewis, R. and Newman, J. (1994). The Structure of an Immunodominant Loop on Foot and Mouth Disease Virus, Serotype O1, Determined under Reducing Conditions. *Archives of virology Supplementum* **9**, 51-58.
- Russell, R.J., Kerry, P.S., Stevens, D.J., Steinhauer, D.A., Martin, S.R., Gamblin, S.J. and Skehel, J.J. (2008). Structure of Influenza Hemagglutinin in Complex with an Inhibitor of Membrane Fusion. *Proceedings of the National Academy of Sciences of the United States of America* **105**, 17736-17741.
- Rust, R.C., Landmann, L., Gosert, R., Tang, B.L., Hong, W.J., Hauri, H.P., Egger, D. and Bienz, K. (2001). Cellular Copii Proteins Are Involved in Production of the Vesicles That Form the Poliovirus Replication Complex. *Journal of Virology* **75**, 9808-9818.
- Ryan, M.D. and Flint, M. (1997). Virus-Encoded Proteinases of the Picornavirus Super-Group. *Journal of General Virology* **78**, 699-723.
- Schlegel, A., Giddings, T.H., Ladinsky, M.S. and Kirkegaard, K. (1996). Cellular Origin and Ultrastructure of Membranes Induced During Poliovirus Infection. *Journal of Virology* **70**, 6576-6588.
- Schnell, J.R. and Chou, J.J. (2008). Structure and Mechanism of the M2 Proton Channel of Influenza a Virus. *Nature* **451**, 591-U512.
- Schober, D., Kronenberger, P., Prchla, E., Blaas, D. and Fuchs, R. (1998). Major and Minor Receptor Group Human Rhinoviruses Penetrate from Endosomes by Different Mechanisms. *J Virol* **72**, 1354-1364.
- Schwarz, G., Zong, R.T. and Popescu, T. (1992). Kinetics of Melittin Induced Pore Formation in the Membrane of Lipid Vesicles. *Biochimica Et Biophysica Acta* **1110**, 97-104.
- Seddon, A.M., Curnow, P. and Booth, P.J. (2004). Membrane Proteins, Lipids and Detergents: Not Just a Soap Opera. *Biochimica Et Biophysica Acta-Biomembranes* **1666**, 105-117.
- Shafren, D.R., Bates, R.C., Agrez, M.V., Herd, R.L., Burns, G.F. and Barry, R.D. (1995). Cocksackieviruses B1, B3, and B5 Use Decay-Accelerating Factor as a Receptor for Cell Attachment. *Journal of Virology* **69**, 3873-3877.
- Shai, Y. (1999). Mechanism of the Binding, Insertion and Destabilization of Phospholipid Bilayer Membranes by Alpha-Helical Antimicrobial and Cell Non-Selective Membrane-Lytic Peptides. *Biochimica Et Biophysica Acta-Biomembranes* **1462**, 55-70.
- Sharp, P.M., Cowe, E., Higgins, D.G., Shields, D.C., Wolfe, K.H. and Wright, F. (1988). Codon Usage Patterns in Escherichia-Coli, Bacillus-Subtilis, Saccharomyces-Cerevisiae, Schizosaccharomyces-Pombe, Drosophila-Melanogaster and Homo-Sapiens - a Review of the Considerable within-Species Diversity. *Nucleic Acids Research* **16**, 8207-8211.
- Siljamaki, E., Rintanen, N., Kirsi, M., Upla, P., Wang, W., Karjalainen, M., Ikonen, E. and Marjomaki, V. (2013). Cholesterol Dependence of Collagen and Echovirus 1 Trafficking Along the Novel Alpha2beta1 Integrin Internalization Pathway. *PLoS one* **8**, e55465-e55465.
- Singh, S.M. and Panda, A.K. (2005). Solubilization and Refolding of Bacterial Inclusion Body Proteins. *Journal of Bioscience and Bioengineering* **99**, 303-310.
- Smyth, M.S. and Martin, J.H. (2002). Picornavirus Uncoating. *Journal of Clinical Pathology-Molecular Pathology* **55**, 214-219.
- Spear, P.G. (2004). Herpes Simplex Virus: Receptors and Ligands for Cell Entry. *Cellular Microbiology* **6**, 401-410.
- Stanway, G. and Hyypia, T. (1999). Parechoviruses. *Journal of Virology* **73**, 5249-5254.
- Steil, B.P. and Barton, D.J. (2009). Cis-Active Rna Elements (Cres) and Picornavirus Rna Replication. *Virus Research* **139**, 240-252.

- StGelais, C., Tuthill, T.J., Clarke, D.S., Rowlands, D.J., Harris, M. and Griffin, S. (2007).** Inhibition of Hepatitis C Virus P7 Membrane Channels in a Liposome-Based Assay System. *Antiviral Research* **76**, 48-58.
- StGelais, C., Foster, T.L., Verow, M., Atkins, E., Fishwick, C.W.G., Rowlands, D., Harris, M. and Griffin, S. (2009).** Determinants of Hepatitis C Virus P7 Ion Channel Function and Drug Sensitivity Identified in Vitro. *Journal of Virology* **83**, 7970-7981.
- Stoscheck, C.M. (1990). Quantitation of Protein. In *Deutscher, M P*, pp. 50-68. Edited by M. P. Deutscher: Academic Press, Inc.
- Strauss, M., Levy, H.C., Bostina, M., Filman, D.J. and Hogle, J.M. (2013).** Rna Transfer from Poliovirus 135s Particles across Membranes Is Mediated by Long Umbilical Connectors. *Journal of virology* **87**, 3903-3914.
- Stuart, A.D., McKee, T.A., Williams, P.A., Harley, C., Shen, S., Stuart, D.I., Brown, T.D.K. and Lea, S.M. (2002).** Determination of the Structure of a Decay Accelerating Factor-Binding Clinical Isolate of Echovirus 11 Allows Mapping of Mutants with Altered Receptor Requirements for Infection. *Journal of Virology* **76**, 7694-7704.
- Suomalainen, M. and Greber, U.F. (2013).** Uncoating of Non-Enveloped Viruses. *Current Opinion in Virology* **3**, 27-33.
- Tal, M., Silberstein, A. and Nusser, E. (1985).** Why Does Coomassie Brilliant Blue-R Interact Differently with Different Proteins - a Partial Answer. *Journal of Biological Chemistry* **260**, 9976-9980.
- Talbot, P., Rowlands, D.J., Burroughs, J., Sangar, D.V. and Brown, F. (1973).** Evidence for a Group Protein in Foot-and-Mouth Disease Virus-Particles. *Journal of General Virology* **19**, 369-380.
- Teterina, N.L., Levenson, E., Rinaudo, M.S., Egger, D., Bienz, K., Gorbalenya, A.E. and Ehrenfeld, E. (2006).** Evidence for Functional Protein Interactions Required for Poliovirus Rna Replication. *Journal of Virology* **80**, 5327-5337.
- Thompson, S.R. (2012).** Tricks an Ires Uses to Enslave Ribosomes. *Trends in Microbiology* **20**, 558-566.
- Todd, S., Towner, J.S., Brown, D.M. and Semler, B.L. (1997).** Replication-Competent Picornaviruses with Complete Genomic Rna 3' Noncoding Region Deletions. *Journal of Virology* **71**, 8868-8874.
- Torres, J., Maheswari, U., Parthasarathy, K., Ng, L., Liu, D.X. and Gong, X. (2007).** Conductance and Amantadine Binding of a Pore Formed by a Lysine-Flanked Transmembrane Domain of Sars Coronavirus Envelope Protein. *Protein Science* **16**, 2065-2071.
- Tosteson, M.T. and Chow, M. (1997).** Characterization of the Ion Channels Formed by Poliovirus in Planar Lipid Membranes. *Journal of Virology* **71**, 507-511.
- Tosteson, M.T., Wang, H., Naumov, A. and Chow, M. (2004).** Poliovirus Binding to Its Receptor in Lipid Bilayers Results in Particle-Specific, Temperature-Sensitive Channels. *Journal of General Virology* **85**, 1581-1589.
- Toyoda, H., Franco, D., Fujita, K., Paul, A.V. and Wimmer, E. (2007).** Replication of Poliovirus Requires Binding of the Poly(Rc) Binding Protein to the Cloverleaf as Well as to the Adjacent C-Rich Spacer Sequence between the Cloverleaf and the Internal Ribosomal Entry Site. *Journal of Virology* **81**, 10017-10028.
- Trask, S.D., Kim, I.S., Harrison, S.C. and Dormitzer, P.R. (2010).** A Rotavirus Spike Protein Conformational Intermediate Binds Lipid Bilayers. *Journal of Virology* **84**, 1764-1770.
- Tsang, S.K., McDermott, B.M., Racaniello, V.R. and Hogle, J.M. (2001).** Kinetic Analysis of the Effect of Poliovirus Receptor on Viral Uncoating: The Receptor as a Catalyst. *Journal of Virology* **75**, 4984-4989.
- Tuthill, T.J., Bubeck, D., Rowlands, D.J. and Hogle, J.M. (2006).** Characterization of Early Steps in the Poliovirus Infection Process: Receptor-Decorated Liposomes Induce Conversion of the Virus to Membrane-Anchored Entry-Intermediate Particles. *Journal of Virology* **80**, 172-180.
- Tuthill, T.J., Harlos, K., Walter, T.S., Knowles, N.J., Gropelli, E., Rowlands, D.J., Stuart, D.I. and Fry, E.E. (2009).** Equine Rhinitis a Virus and Its Low Ph Empty Particle: Clues Towards an Aphthovirus Entry Mechanism? *PLoS Pathog* **5**, e1000620.



- Tuthill, T.J., Gropelli, E., Hogle, J.M. and Rowlands, D.J. (2010).** Picornaviruses. *Curr Top Microbiol Immunol*.
- van Kuppeveld, F.J.M., de Jong, A.S., Melchers, W.J.G. and Willems, P. (2005).** Enterovirus Protein 2b Po(U)Res out the Calcium: A Viral Strategy to Survive? *Trends in Microbiology* **13**, 41-44.
- van Meer, G., Voelker, D.R. and Feigenson, G.W. (2008).** Membrane Lipids: Where They Are and How They Behave. *Nature Reviews Molecular Cell Biology* **9**, 112-124.
- Vance, L.M., Moscufo, N., Chow, M. and Heinz, B.A. (1997).** Poliovirus 2c Region Functions During Encapsidation of Viral Rna. *Journal of Virology* **71**, 8759-8765.
- vanKuppeveld, F.J.M., Galama, J.M.D., Zoll, J., vandenHurk, P. and Melchers, W.J.G. (1996).** Coxsackie B3 Virus Protein 2b Contains a Cationic Amphipathic Helix That Is Required for Viral Rna Replication. *Journal of Virology* **70**, 3876-3886.
- Verdaguer, N., Blaas, D. and Fita, I. (2000).** Structure of Human Rhinovirus Serotype 2 (Hrv2). *Journal of Molecular Biology* **300**, 1179-1194.
- Verlinden, Y., Cuconati, A., Wimmer, E. and Rombaut, B. (2000).** The Antiviral Compound 5-(3,4-Dichlorophenyl) Methylhydantoin Inhibits the Post-Synthetic Cleavages and the Assembly of Poliovirus in a Cell-Free System. *Antiviral Research* **48**, 61-69.
- Vijayvergiya, V., Wilson, R., Chorak, A., Gao, P.F., Cross, T.A. and Busath, D.D. (2004).** Proton Conductance of Influenza Virus M2 Protein in Planar Lipid Bilayers. *Biophysical Journal* **87**, 1697-1704.
- Vlasak, M., Blomqvist, S., Hovi, T., Hewat, E. and Blaas, D. (2003).** Sequence and Structure of Human Rhinoviruses Reveal the Basis of Receptor Discrimination. *Journal of Virology* **77**, 6923-6930.
- Vlasak, M., Goester, I. and Blaas, D. (2005).** Human Rhinovirus Type 89 Variants Use Heparan Sulfate Proteoglycan for Cell Attachment. *Journal of Virology* **79**, 5963-5970.
- Wald, T.G., Shult, P., Krause, P., Miller, B.A., Drinka, P. and Gravenstein, S. (1995).** A Rhinovirus Outbreak among Residents of a Long-Term-Care Facility. *Annals of Internal Medicine* **123**, 588-593.
- Wallace, B.A., Lees, J.G., Orry, A.J.W., Lobley, A. and Janes, R.W. (2003).** Analyses of Circular Dichroism Spectra of Membrane Proteins. *Protein Science* **12**, 875-884.
- Walukiewicz, H.E., Johnson, J.E. and Schneemann, A. (2006).** Morphological Changes in the T=3 Capsid of Flock House Virus During Cell Entry. *Journal of Virology* **80**, 615-622.
- Wang, G. (2008).** Nmr of Membrane-Associated Peptides and Proteins. *Current Protein & Peptide Science* **9**, 50-69.
- Wang, G.S., Keifer, P.A. and Peterkofsky, A. (2003).** Solution Structure of the N-Terminal Amphitropic Domain of Escherichia Coli Glucose-Specific Enzyme Iia in Membrane-Mimetic Micelles. *Protein Science* **12**, 1087-1096.
- Wang, R.Y.L., Kuo, R.-L., Ma, W.-C., Huang, H.-I., Yu, J.-S., Yen, S.-M., Huang, C.-R. and Shih, S.-R. (2013).** Heat Shock Protein-90-Beta Facilitates Enterovirus 71 Viral Particles Assembly. *Virology* **443**, 236-247.
- Wang, X., Peng, W., Ren, J., Hu, Z., Xu, J., Lou, Z., Li, X., Yin, W., Shen, X., Porta, C., Walter, T.S., Evans, G., Axford, D., Owens, R., Rowlands, D.J., Wang, J., Stuart, D.I., Fry, E.E. and Rao, Z. (2012).** A Sensor-Adaptor Mechanism for Enterovirus Uncoating from Structures of Ev71. *Nature Structural & Molecular Biology* **19**, 424-429.
- Ward, T., Pipkin, P.A., Clarkson, N.A., Stone, D.M., Minor, P.D. and Almond, J.W. (1994).** Decay-Accelerating Factor Cd55 Is Identified as the Receptor for Echovirus-7 Using Celics, a Rapid Immune-Focal Cloning Method. *Embo Journal* **13**, 5070-5074.
- Weisz, O.A., Swift, A.M. and Machamer, C.E. (1993).** Oligomerization of a Membrane-Protein Correlates with Its Retention in the Golgi-Complex. *Journal of Cell Biology* **122**, 1185-1196.
- Wetherill, L.F., Holmes, K.K., Verow, M., Mueller, M., Howell, G., Harris, M., Fishwick, C., Stonehouse, N., Foster, R., Blair, G.E., Griffin, S. and Macdonald, A. (2012).** High-Risk Human Papillomavirus E5 Oncoprotein Displays Channel-Forming Activity Sensitive to Small-Molecule Inhibitors. *Journal of Virology* **86**, 5341-5351.

- Whiles, J.A., Deems, R., Vold, R.R. and Dennis, E.A. (2002).** Bicelles in Structure-Function Studies of Membrane-Associated Proteins. *Bioorganic Chemistry* **30**, 431-442.
- Wien, M.W. and Hogle, J.M. (1995).** 1fpt: Three-Dimensional Structure of the Complex between the Fab Fragment of a Neutralizing Antibody for Type 1 Poliovirus and Its Viral Epitope. *Protein Data Bank*.
- Wien, M.W., Chow, M. and Hogle, J.M. (1996).** Poliovirus: New Insights from an Old Paradigm. *Structure* **4**, 763-767.
- Wiethoff, C.M., Wodrich, H., Gerace, L. and Nemerow, G.R. (2005).** Adenovirus Protein Vi Mediates Membrane Disruption Following Capsid Disassembly. *Journal of Virology* **79**, 1992-2000.
- Woo, P.C.Y., Lau, S.K.P., Choi, G.K.Y., Huang, Y., Teng, J.L.L., Tsoi, H.-W., Tse, H., Yeung, M.L., Chan, K.-H., Jin, D.-Y. and Yuen, K.-Y. (2012).** Natural Occurrence and Characterization of Two Internal Ribosome Entry Site Elements in a Novel Virus, Canine Picodistrovirus, in the Picornavirus-Like Superfamily. *Journal of Virology* **86**, 2797-2808.
- Xiao, C., Tuthill, T.J., Kelly, C.M.B., Challinor, L.J., Chipman, P.R., Killington, R.A., Rowlands, D.J., Craig, A. and Rossmann, M.G. (2004).** Discrimination among Rhinovirus Serotypes for a Variant Icam-1 Receptor Molecule. *Journal of Virology* **78**, 10034-10044.
- Xing, L., Huhtala, M., Pietiainen, V., Kapyla, J., Vuorinen, K., Marjomaki, V., Heino, J., Johnson, M.S., Hyypia, T. and Cheng, R.H. (2004).** Structural and Functional Analysis of Integrin Alpha I-2 Domain Interaction with Echovirus 1. *Journal of Biological Chemistry* **279**, 11632-11638.
- Yalovsky, S., Rodriguez-Concepcion, M. and Gruissem, W. (1999).** Lipid Modifications of Proteins - Slipping in and out of Membranes. *Trends in Plant Science* **4**, 439-445.
- Yamashita, T., Ito, M., Kabashima, Y., Tsuzuki, H., Fujiura, A. and Sakae, K. (2003).** Isolation and Characterization of a New Species of Kobuvirus Associated with Cattle. *Journal of General Virology* **84**, 3069-3077.
- Yamayoshi, S., Yamashita, Y., Li, J., Hanagata, N., Minowa, T., Takemura, T. and Koike, S. (2009).** Scavenger Receptor B2 Is a Cellular Receptor for Enterovirus 71. *Nature Medicine* **15**, 798-U715.
- Yang, J., Prorok, M., Castellino, F.J. and Weliky, D.P. (2004).** Oligomeric Beta-Structure of the Membrane-Bound Hiv-1 Fusion Peptide Formed from Soluble Monomers. *Biophysical Journal* **87**, 1951-1963.
- Yang, Y., Rijnbrand, R., McKnight, K.L., Wimmer, E., Paul, A., Martin, A. and Lemon, S.M. (2002).** Sequence Requirements for Viral Rna Replication and Vpg Uridylylation Directed by the Internal Cis-Acting Replication Element (Cre) of Human Rhinovirus Type 14. *Journal of Virology* **76**, 7485-7494.
- Yin, J., Liu, Y., Wimmer, E. and Paul, A.V. (2007).** Complete Protein Linkage Map between the P2 and P3 Non-Structural Proteins of Poliovirus. *Journal of General Virology* **88**, 2259-2267.
- Yu, J.-m., Xu, Z.-q., Li, B.-w., Zhang, Q., Cui, S.-x., Jin, M. and Duan, Z.-j. (2011).** Analysis and Characterization of the Complete Genome of a Member of a New Species of Kobuvirus Associated with Swine. *Archives of Virology* **156**, 747-751.
- Zaitseva, E., Yang, S.-T., Melikov, K., Pourmal, S. and Chernomordik, L.V. (2010).** Dengue Virus Ensures Its Fusion in Late Endosomes Using Compartment-Specific Lipids. *Plos Pathogens* **6**.
- Zautner, A.E., Korner, U., Henke, A., Badorff, C. and Schmidtke, M. (2003).** Heparan Sulfates and Coxsackievirus-Adenovirus Receptor: Each One Mediates Coxsackievirus B3pd Infection. *Journal of Virology* **77**, 10071-10077.
- Zhang, L., Chandran, K., Nibert, M.L. and Harrison, S.C. (2006).** Reovirus Mu 1 Structural Rearrangements That Mediate Membrane Penetration. *Journal of Virology* **80**, 12367-12376.
- Zhang, L., Agosto, M.A., Ivanovic, T., King, D.S., Nibert, M.L. and Harrison, S.C. (2009).** Requirements for the Formation of Membrane Pores by the Reovirus Myristoylated Mu 1n Peptide. *Journal of Virology* **83**, 7004-7014.
- Zhang, P., Mueller, S., Morais, M.C., Bator, C.M., Bowman, V.D., Hafenstein, S., Wimmer, E. and Rossmann, M.G. (2008).** Crystal Structure of Cd155 and Electron Microscopic Studies of Its Complexes with Polioviruses. *Proceedings of the National Academy of Sciences of the United States of America* **105**, 18284-18289.

- Zhang, Y. (2008).** Progress and Challenges in Protein Structure Prediction. *Current Opinion in Structural Biology* **18**, 342-348.
- Zhao, R., Pevear, D.C., Kremer, M.J., Giranda, V.L., Kofron, J.A., Kuhn, R.J. and Rossmann, M.G. (1996).** Human Rhinovirus 3 at 3.0 Angstrom Resolution. *Structure* **4**, 1205-1220.
- Zoll, J., Heus, H.A., van Kuppeveld, F.J.M. and Melchers, W.J.G. (2009).** The Structure-Function Relationship of the Enterovirus 3'-Utr. *Virus Research* **139**, 209-216.